



NOTTINGHAM
TRENT UNIVERSITY

**NOVEL ASSESSMENT OF WALL
INSULATION IN BUILDINGS USING
MATHEMATICAL MODELLING,
INFRARED THERMOGRAPHY AND
ARTIFICIAL INTELLIGENCE**

ARIJIT SEN

BSc.(Engg.), MSc.

A thesis submitted in partial fulfilment of the requirements of Nottingham
Trent University for the Degree of Doctor of Philosophy

JANUARY 27, 2021

Copyright Statement

This work is the intellectual property of the author. You may copy up to 5% of this thesis for private study, or personal, non-commercial research. Any re-use of the information contained within this document should be fully referenced, quoting the author, title, University, degree level and pagination. Queries or requests for any other use, or if a more substantial copy is required, should be directed in the first instance to the author of the Intellectual Property Rights.

Abstract

The high energy consumption for space heating in buildings and the need to reduce carbon emission point out the need for enhancing thermal insulation in buildings. Modern buildings normally have a good standard of insulation and the focus should be given to existing buildings towards enhancing the energy performance via retrofitting of buildings with upgradation of wall insulation. This thesis suggests and examines three different novel approaches towards measuring wall insulation and energy losses as well as estimating the benefits of retrofitting.

The three approaches are:

- Estimating energy losses due to working from home during Covid-19 pandemic and the difference between a poorly insulated house and a modern well-insulated house in terms of energy costings.
- Estimating heat loss through external walls and benefits of retrofitting via the use of infrared thermography and Artificial Neural Networks (ANN).
- Estimating the in-situ U-value of walls using a novel new device which combines infrared thermography with artificial neural networks.

In the first approach, a mathematical model is developed which suggests that energy bills and CO₂ emission during winter will be significantly higher in a poorly insulated house than that in a modern house when working from home due to Covid-19 pandemic situation and the lockdown. The findings also show that a family living in a well-insulated modern house and commute to work would make financial savings due to working from home as the commuting cost will be eliminated and the additional energy cost for heating and other daytime daily requirements will be minimal.

In the second approach, two case studies are presented which demonstrate the suitability of combining ANN with infrared thermography, the optimum ANN architecture and the practical minimum monitoring period required for ANN to predict future heat losses through walls in buildings in quick time with a reasonable accuracy. A mathematical model is also developed to realize the theoretical monitoring period for this purpose.

In the third approach, a novel product has been developed to estimate the in-situ U-value of buildings' walls. The product can be calibrated by training an ANN with temperature profiles generated from infrared images which are obtained from monitoring sample walls under point heat in the laboratory environment. The results of the experimental work show the new device combined with ANN could provide a reasonable estimation of the U value.

In general, the suggested three techniques have been found to be beneficial to estimate energy losses in buildings and evaluate thermal insulation to provide households with estimations of energy savings and payback period towards enhancing sustainability in buildings. In the first approach, heat loss in a building is estimated considering the U-value of walls; in the second approach, the heat loss is estimated from thermography and ANN without considering the U-value of wall; and in the third approach, the U-value of a building's wall is determined with the help of thermography and ANN.

Acknowledgement

At first, I would like to thank Nottingham Trent University for offering the PhD scholarship which allowed me to do this research work; and to be part of the Doctoral Training Alliance for Energy. Next, I would like to express my sincere gratitude to my Director of study, Prof. Amin Al-Habaibeh, for his support, guidance, motivation and advices throughout my PhD journey. I would also like to extend my sincere thanks to Dr Daniel Shin, who was the independent observer and my co-supervisors Prof. Benachir Medjdoub and Dr Adam O'Rourke for their support and advice. In addition, I want to express my appreciation to academic, technical, administrative and library staffs as well as my other colleagues at Nottingham Trent University for their assistance and support throughout my PhD study.

I would like to convey my heartfelt gratitude to my parents for all their blessings and love, and thanks to my younger brother Avijit Sen for taking a lot of family commitments to allow me to complete the PhD study. I would also like to express my gratitude to my parents-in-law for their blessings and good wishes and thanks to my brother-in-law Mr Soumitra Majumdar for his supports towards the fulfilment of much of my family commitments to allow me to focus more on my PhD work.

Finally, my special thanks go to my beloved wife, Sharmila Majumdar; without her support it would be impossible for me to complete the PhD study.

3. Join Dean Jackson on BBC Radio Nottingham, (2021). BBC Radio Nottingham. 8th January.
4. Lee, R. (2020). 'Working from home could cost £45 per month more this winter'. Nottingham Post. 27th December. Available at: <https://www.nottinghampost.com/news/jobs/working-home-could-cost-45-4803800>. (Accessed on: 26/01/2021)
5. Shoffman, M. (2020). 'How to save on energy bills as working from home could cost households an extra £45 a month'. The Sun. 8th December. Available at: <https://www.thesun.co.uk/money/13413917/how-to-save-on-energy-bills-working-from-home/>. (Accessed on: 26/01/2021)

List of Figures

Figure 1.1: The structure of the thesis.....	8
Figure 2.1: HFP01 heat flux meter from Hukseflux (Campbell Scientific, 2012).....	23
Figure 2.2: HT-50 heat flux meter from International thermal Instrument (International Thermal Instrument Company, no date)	24
Figure 2.3: HFS heat flux meter from Omega Engineering. (OMEGA Engineering, no date)	24
Figure 3.1: Schematic representation of the research methodology adopted for this PhD thesis.....	45
Figure 3.2: Schematic representation of the research methodology adopted for this PhD thesis.....	48
Figure 3.3: Relationship between outdoor temperature and external wall temperature	49
Figure 3.4: Schematic diagram of the experimental setup.....	52
Figure 3.5: Schematic representation of the experimental work with the proposed U-value kit.	53
Figure 4.1: Average increase per month in (a) household energy consumption, (b) household energy bills due to working from home in winter.....	62
Figure 4.2: Average household savings per month for a family uses (a)1 car, (b) 2 cars for travelling.	64
Figure 4.3: Average increase in CO ₂ emission per month because of the excess household energy demand during winter.....	65
Figure 4.4: Net change in CO ₂ emission per month per household that uses (a) 1 car for travelling and (b) 2 cars for travelling	66
Figure 5.1: Infrared image of the insulated and the uninsulated house in High Wycombe.	76

Figure 5.2: Temperature profiles generated from infrared images of the insulated and the uninsulated house in High Wycombe.	78
Figure 5.3: Sensitivity of feed forward neural network regarding (a) number of hidden layers and (b) number of neurons in each hidden layer for hourly heat loss prediction (case study 1).	80
Figure 5.4: Architecture of feed forward neural network for hourly average heat loss prediction.....	80
Figure 5.5: Sensitivity of NARnet, NARxnet and LSTM neural network regarding number of neurons in hidden layer for hourly heat loss prediction.....	81
Figure 5.6: Architecture of recurrent neural networks used in this study (a) NARnet (b) NARxnet and (b) LSTM neural network.	82
Figure 5.7: Performance of feed forward neural network to predict hourly heat loss (a) insulated building and (b) uninsulated building.....	84
Figure 5.8: Comparison of performances among feed forward, NARnet, NARxnet and LSTM neural network for hourly heat loss prediction in (a) insulated building and (b) uninsulated building in case study 1.	85
Figure 5.9: Comparison between the calculated heat loss and the ANN (feed forward) predicted heat loss for the years 2012 to 2019.....	86
Figure 5.10: Heatmap representation of average temperature in each month from 2004 to 2019.....	87
Figure 5.11: Sensitivity of feed forward neural network regarding (a) number of hidden layers and (b) number of neurons in each hidden layer for monthly heat loss prediction. ..	88
Figure 5.12: Sensitivity NARnet, NARxnet and LSTM neural network regarding number of neurons in hidden layer for monthly heat loss prediction.	89

Figure 5.13: Comparison of performances among feed forward, NARnet, NARXnet and LSTM neural network for monthly heat loss prediction in (a) insulated building and (b) uninsulated building in case study 1.	90
Figure 5.14: Comparison between the calculated heat loss and the ANN (LSTM) predicted heat loss for the years 2012 to 2019 in case of monthly heat loss prediction.	91
Figure 5.15: Infrared image of the insulated and the uninsulated house in Nottingham	93
Figure 5.16: Temperature profiles generated from infrared images of the insulated and the uninsulated house in Nottingham.	94
Figure 5.17: Sensitivity of feed forward neural network: (a) number of hidden layers and (b) number of neurons in each hidden layer for hourly heat loss prediction in case study 2. ...	95
Figure 5.18: Sensitivity NARnet, NARXnet and LSTM neural network regarding the number of neurons in the hidden layer for hourly heat loss prediction in case study 2.	95
Figure 5.19: Comparison of performances among feed forward, NARnet, NARXnet and LSTM neural networks for hourly heat loss prediction in (a) insulated building and (b) uninsulated building in case study 2.	97
Figure 5.20: Comparison between the calculated heat loss and the ANN (feed forward) predicted heat loss for the years 2012 to 2019 in buildings of second case study.	98
Figure 5.21: Sensitivity of feed forward neural network regarding (a) number of hidden layers and (b) number of neurons in each hidden layer for monthly heat loss prediction in the second case study.	99
Figure 5.22: Sensitivity NARnet, NARxnet and LSTM neural network regarding number of neurons in hidden layer for monthly heat loss prediction in second case study.	100
Figure 5.23: Comparison of performances among feed forward, NARnet, NARxnet and LSTM neural network for monthly heat loss prediction in (a) insulated building and (b) uninsulated building in case study 2.	101

Figure 5.24: Comparison between the calculated monthly heat loss and the ANN (LSTM) predicted monthly heat loss for the years 2012 to 2019 in buildings of second case study.	103
Figure 5.25: Comparison of energy savings among calculated heat loss, feed forward neural network predicted heat and LSTM neural network predicted heat loss: (a) case study 1 and (b) case study 2.....	104
Figure 5.26: Estimation of simple payback period for the retrofitted house in case study 1.	106
Figure 6.1: Schematic model of the proposed U-value kit with its major parts and assembly.	109
Figure 6.2: The test of glow plug performance of with the help of a variable power supply.	110
Figure 6.3: Test of the glow plug heating on MDF board for burning spot.....	111
Figure 6.4: Schematic diagram of (a) sample A (MDF), (b) sample B (MS) and (c) sample C (MS and MDF clamped together).....	111
Figure 6.5: Initial test on (a) sample A (b) sample B.....	113
Figure 6.6: Infrared images of sample A from the initial test.....	114
Figure 6.7: Infrared images of Sample B from the initial test.	115
Figure 6.8: (a) rock wool insulation of aluminium bar and glow plug and (b) the wrapping on the insulation.	115
Figure 6.9: Test on sample A after modification	116
Figure 6.10: Test on sample B after modification.....	116
Figure 6.11: Infrared images of sample A1 and sample A2: (a) after 1 minute, (b) after 10 minutes, (c) after 30 minutes and (d) after 50 minutes.	117
Figure 6.12: Test on sample A3 after modification of test rig.	118

Figure 6.13: infrared image of (a) sample A, (b) sample B and (C) sample C.	119
Figure 6.14: Comparison of temperature profile through a specific point on infrared images of sample A and sample B.	120
Figure 6.15: Comparison of temperature profile through a specific point on infrared images of sample C and sample B.....	120
Figure 6.16: Comparison of temperature profile through a specific point on infrared images of sample A and sample C.	121
Figure 6.17: Neural Network Architecture for the classification of samples A, B and C [Source: generated using Matlab software].....	122
Figure 6.18: Schematic diagram of (a) sample D, (b) sample F (c) sample E and (d) sample G.....	123
Figure 6.19: Experiment on sample D.	124
Figure 6.20: Experiment on sample F.	124
Figure 6.21: Experiment on sample E.....	125
Figure 6.22: Experiment on sample G.	125
Figure 6.23: (a) Temperature profile of sample D and sample E through a specific point, (b) external temperature during the monitoring period of samples D and E.	126
Figure 6.24: The profile T^a through a specific point on sample D and sample E.	128
Figure 6.25: (a) Profiles of T^b and (b) profiles of T^{ab} through a point on a brick wall (sample D) and an insulated brick wall (sample E).	129
Figure 6.26: (a) Five periods moving range of T , (b) five periods moving range of T^a , (c) five periods moving range of T^b , and (d) five periods moving range of T^{ab}	130
Figure 6.27: (a) standard deviation of T , T^a , T^b and T^{ab} (b) standard deviation of five periods moving range of T , T^a , T^b and T^{ab}	130
Figure 6.28: The result of visual inspection.....	131

Figure 6.29: (a) Infrared image of brick wall, (b) infrared image of insulated brick wall, (c) infrared image of brick wall with crop boundary and (d) infrared image of insulated brick wall with crop boundary.....	133
Figure 6.30: Percentage error in categorisation of wall samples (a) profile T^b , (b) standard deviation of profile T^{ab} and (c) standard deviation of profile T^b	135
Figure 7.1: The monitoring of a sample wall in laboratory.	142
Figure 7.2: (a) Location of the building on Google Map (no date). (b) The schematic layout of the flat showing the location of monitoring the walls.	143
Figure 7.3: The experimental setup at one of the locations in the building.....	143
Figure 7.4: Visual inspection of temperature profiles from sample E, H and I.	144
Figure 7.5: The ANN architecture used in this case study [Source: generated using Matlab software].....	145
Figure 7.6: The comparison of training and test performance of the ANN.	146
Figure 7.7: (a) ANN predicted U-values obtained using profiles T , T^a , T^b and T^{ab} as input to the ANN and (b) percentage deviation of ANN predicted U-values.	148

List of Tables

Table 2.1: Heat flux meter and temperature sensors used in the reviewed research work. .	22
Table 4.1: Reference U-values of buildings' wall BRE (2016).	56
Table 4.2: The reference values used in for estimation and their sources.	57
Table 4.3: Increase in heating energy (gas) demand and energy bill per household because of working from home.	59
Table 4.4: Increase in average monthly energy demand of dwellings with solid wall construction (U-value of 1.7 W/m ² K) because of working from home.	61
Table 4.5: Increase in monthly electricity demand, electricity bills and CO ₂ emission per household because of working from home.	61
Table 5.1: Average savings in energy bills per year.	105
Table 6.1: Properties of samples A, B and C	113
Table 6.2: Properties of samples D, E, F and G.	124
Table 7.1: Properties of sample wall used to train and test the ANN	141

Nomenclature

A	Wall surface area exposed external environment
ANN	Artificial Neural Network
APE	Average percentage error.
D	Number of days in a month.
d	Thickness of a layer of wall
e	Error
E	Radiation heat transfer
e _d	Absolute percentage deviation
E _e	Electrical energy consumption
E _h	Heating energy consumption
e _p	Percentage error
H	Hours of operation for an electrical appliance per day
i	Index (x axis)
j	Index (y axis)
k	Stephan Boltzmann's constant
k	Index (z axis)
n	Number of variables
P	Thermal power
P _e	Power required by an electric appliance,
P _m	Monthly total heat loss
Q	Heat loss through wall
q	Heat flux
R	Thermal resistance
R _e	Thermal resistance of air at the external surface
R _i	Thermal resistance of air at the internal surface
T	Temperature
T ^a	Difference between infrared image temperature and external temperature
T ^{ab}	Cumulative gradient of T ^a
T ^b	Cumulative gradient of temperature (T)
T _c	Surrounding temperature
T _{ext}	External environment temperature
T _{in}	Indoor temperature
T _{int}	Internal environment temperature
T _{out}	Outdoor temperature
T _{ref.}	Reflective temperature
T _s	Surface temperature
U	U-value of a wall
U _c	Calculated U-value
U _p	ANN predicted U-value
ε	Emissivity
λ	Thermal conductivity
v	Wind speed

Table of Contents

Abstract	ii
Acknowledgement.....	iv
Publication list.....	v
List of Figures	vii
List of Tables.....	xiii
Nomenclature	xiv
Table of Contents	xv
Chapter 1: Introduction	1
1.1 Background	1
1.2 Research Scope	4
1.3 Aim.....	6
1.4 Objectives.....	6
1.5 Research Questions	7
1.6 Thesis structure	8
1.7 Summary	10
Chapter 2: Literature Review.....	11
2.1 Introduction.....	11
2.2 Insulation in Buildings	11
2.2.1 Impact of wall Insulation in energy consumption.....	13

2.3 Infrared thermography	17
2.4 In-situ U-value Assessment	19
2.4.1 Heat Flux Meter	21
2.4.2 U-value Estimation using HFM Method.....	25
2.4.3 U-value Estimation Using ITT Method	29
2.4.5 Other methods of U-value estimation	34
2.5 Artificial Neural Network (ANN).....	35
2.5.1 Review of ANN’s application.....	39
2.6 Summary	43
Chapter 3: Methodology	44
3.1 Introduction.....	44
3.2 Methodology of the Research	45
3.2.1 Literature Review.....	46
3.2.2 Role of Wall insulation in Energy consumption due to Covid-19 Situation	46
3.2.3 Development of heat loss prediction tool.....	48
3.2.4 Development of U-value Estimation Kit	51
3.3 Potential Contribution to the Knowledge.....	53
3.4 Summary	54
Chapter 4: The Role of Wall Insulation on Household Energy demand, Carbon Emission and Household Budget in English Dwellings due to Covid-19 Lock Down Situation During Winter.....	55
4.1 Introduction.....	55

4.2 Assumptions and reference values	56
4.3 Equation used for the estimation of energy demand.....	57
4.4 Effects on household energy demand and budget:.....	58
4.5 Effects on CO ₂ emission	64
4.6 Conclusion	67
Chapter 5: Development of a Prediction Tool to Estimate Heat loss through walls using Infrared Thermography and Artificial Neural Network.....	69
5.1 Introduction.....	69
5.2 Implemented approach	70
5.2.1 Equations used for the study	70
5.2.2 Assumptions.....	71
5.2.3 Heat loss calculation	71
5.2.4 Mathematical model to determine the optimum monitoring period of a building	72
5.2.5 ANN Prediction.....	74
5.3 Case study 1: Buildings in High Wycombe	76
5.3.1 Infrared image analysis	77
5.3.2 Hourly heat loss prediction:	79
5.3.3 Monthly heat loss prediction.....	88
5.4 Case study 2: Buildings in Nottingham	92
5.4.1 Analysis of infrared image	92
5.4.2 Hourly average heat loss prediction.....	94

5.4.3 Monthly heat loss prediction	99
5.5 Energy savings	103
5.6 Conclusion	106
Chapter 6: Development of U-value Estimation Kit.....	108
6.1 Introduction	108
6.2 Construction of the U-value kit.....	109
6.3 Experiment with the modified test kit.....	115
6.4 Visual analysis of infrared images from samples A, B and C	118
6.5 ANN analysis of data obtained from Samples A, B and C	121
6.6 Experiments on brick and concrete block walls.....	122
6.7 Visual analysis of infrared images obtained from samples D, E, F and G	126
6.7.1 Readjustment of infrared images for accurate comparison.....	132
6.8 Categorisation of wall types using ANN	134
6.9 Conclusion	138
Chapter 7: Experimental Work on Real Building.....	139
7.1 Introduction	139
7.2 Implemented approach	139
7.3 Experimental works	141
7.4 Results and Discussion.....	144
7.4.1 visual inspection of infrared images	144
7.4.2 ANN prediction of U-value.....	145

7.5 Conclusion	150
Chapter 8: Discussion and Conclusion	151
8.1 Introduction	151
8.2 Answer to the research questions with the achievement of the objectives	152
8.3 Contribution to knowledge.....	154
8.4 Key findings	155
8.5 Limitations and Future work	157
8.6 Summary	158
References	159
Appendix: A	180
Appendix: B	184
Appendix: C	188

Chapter 1: Introduction

1.1 Background

The ongoing expansion of market economy is largely responsible for an increase in worldwide energy demand (OECD, 2011). The increased energy demand due to rapid urbanization triggers a massive release of greenhouse gases (Akpan and Akpan, 2012). In spite of significant growth (17%) in the renewable energy sector, the worldwide energy production is still heavily dependent on the use of fossil fuels (BP, 2018). As a result, the energy related greenhouse gas emissions reached the highest point in history in 2018 (IEA, 2019). In order to mitigate the impact of climate change due to global greenhouse gas emission, the Paris Agreement set the target to restrict the increase in global average temperature below 2°C of the pre-industrial level with a further vision to limit the increase in global average temperature within 1.5°C of the average global temperature of the pre-industrial levels (United Nations Framework Convention on Climate Change, 2015). According to the Climate Change Act (2008), the UK Govt. sets the target of reducing greenhouse gas emission to 80% of 1990's level by 2050. The target has been revised to net zero greenhouse gas emission by 2050 (Department for Business Energy & Industrial Strategy, 2019b). Committee on Climate Change (2016) suggested that policies should be taken in order to make new buildings highly energy efficient; and existing buildings should be better insulated to achieve the goal of the climate change act. The built environment is responsible for half of the total greenhouse gas emission in the UK and therefore, the UK Government has adopted a strategy of limiting greenhouse gas emission from built environment to 50% of 1990's level by 2025 in line with the achievement of the climate change act's goal (Construction 2025, 2013). According to the UK Green Building Council (2017), infrastructure industry controls 16% of UK's total carbon emission; and 37% of

UK's total carbon emission is related to the use of infrastructure. In addition, The Sustainable Energy Association ^(b), (2017) estimated that 63% people live in their own house in UK and, around 94% of owner occupied homes have central heating resulting in 37% of UK's total greenhouse gas emission from buildings. Haslett (2016) also added that the energy related CO₂ emission due to the heating of residential buildings in UK is circa 17% of the total CO₂ emissions. Therefore, energy consumption in buildings is responsible for a substantial amount of greenhouse gas release to the environment and reducing energy consumption in buildings will cut down overall greenhouse gas emission. The domestic energy consumption was the second highest in 2017 after the transport sector (Department for Business Energy & Industrial Strategy, 2018) and the trend continued to 2018 as well (Waters, 2019). According to the statistics from the Department for Business Energy & Industrial Strategy, the rise in overall energy consumption by 1.6% in 2016 was largely contributed by the domestic sector with the highest percentage increase of circa 3.1% (Department for Business Energy & Industrial Strategy and Waters, 2017). The major portion of overall household energy demand comprises of energy consumption for space heating and hot water, which is around 80% of overall domestic energy demand (Department for Business Energy & Industrial Strategy and Waters, 2017). The above statistics point out the need for development of strategies in relation to lowering the heating energy consumption in buildings. That would also improve the global carbon footprint as buildings are responsible for consuming circa 20% of overall energy produced in the world (U.S. Energy Information Administration, 2016). Improving the wall insulation of a building could make it more energy efficient and henceforth reduce the energy demand. Considering the impacts on economy and environment, it is more sensible to act for reducing energy demand instead of producing more energy (Adamczyk and Dylewski, 2017). However, it is found from literature that the energy savings due to the enhancement of wall insulation is subject to

many factors such as: local weather, types of insulation and the material used for insulation (Al-Habaibeh, Sen and Chilton, 2020). Biddulph et al. (2014) stated that evaluation of heat loss through external walls would be a key requirement for building energy simulations to enhance the quality of building design. The thermal performance of buildings' wall is evaluated considering the thermal transmittance or U-value. The U-value of an uninsulated wall is higher than the U-value of an insulated wall. According to the building regulations for conservation of fuel and power, the limiting U-value of walls of newly designed buildings should be $0.30 \text{ W/m}^2\text{K}$ ('L1A Conservation of fuel and power in new dwellings', 2014). The U-value threshold for existing buildings' wall is $0.70 \text{ W/m}^2\text{K}$ and the buildings with wall U-values worse than the threshold value should undergo upgradation ('L1B Conservation of fuel and power in existing dwellings', 2015). It is also recommended by the same regulation that U-value after upgradation should be better than $0.30 \text{ W/m}^2\text{K}$ for walls with external or internal insulation and $0.55 \text{ W/m}^2\text{K}$ for walls with cavity insulation. In addition, the payback period of such upgradations should be limited to 15 years or less otherwise the U-value can be compromised up to $0.70 \text{ W/m}^2\text{K}$ for the sake of achieving less than or equal to 15 years payback period ('L1B Conservation of fuel and power in existing dwellings', 2015). Therefore, a prediction tool to rapidly estimate the future heat loss through buildings' wall will help the stakeholders in quick assessment of the future energy savings and determination of the target U-value for such upgradation. Several devices are available for measuring U-value of a test specimen under laboratory condition as well as real buildings' wall; however, Doran (2001) found that existing procedures of calculating U-value used for regulatory purpose in the UK frequently underestimate true heat losses for walls as high as 30% and above. In-situ estimation of U-value can greatly aid in identifying the actual U-value as well as the real energy efficiency of the existing buildings. In-situ U-value of wall refers to the estimated U-value of a wall obtained through a measurement survey. Up to the present date,

significant efforts have been made to estimate U-value under both laboratory condition and in-situ; however, all these methods have some limitations. Many a time, the reliable estimation of in-situ U-value in real buildings is difficult because of some constraints. These constraints are associated with installation of instruments, extended monitoring period, dependency on season, dependency on weather condition and impact of solar irradiation. Furthermore, there are complex and nonlinear relationships exist among these parameters which need to be considered for accurate estimation of U-value. One of the robust technologies for evaluating the thermal performance of buildings is Infrared thermography which can rapidly provide significant information regarding the thermal performance of a building's wall. Artificial intelligence has a wide range of use in buildings' energy performance studies. Therefore, integration of artificial intelligence and infrared thermography could be a novel approach for assessing the performance of wall insulation. The novel approach would overcome the previously mentioned limitations for the prediction of heat loss and estimation of in-situ U-value of walls in a building.

1.2 Research Scope

Building insulation and energy loss is critical to enhance sustainability, and U-value is considered one of the most useful measures to assess wall insulation. Current Covid-19 pandemic situation compelled many people to work from home and there is a scope to conduct research on the role of wall's U-value in the shift in energy demand among different dwelling types because of working from home in winter. The investment on retrofitting a building with improved insulation is recovered from the savings due to post retrofit reduced energy consumption. Simulation of future heat losses through a building's wall would aid to estimate the future energy savings due to retrofitting. There are many simulation software available for this purpose; however it requires extensive computer modelling, high computation power and skilled manpower to operate the software. Infrared thermography

could rapidly generate significant information about the thermal performance of a building's wall and ANN has been successfully used in prediction of energy demand; however, the integration of infrared thermography and ANN is yet to be investigated. U-value is the ratio of heat flux through a wall and the temperature gradient between indoor and outdoor environment. By measuring the heat flux, indoor temperature and outdoor temperature, it is possible to estimate the U-value. In an ideal condition, the U-value of a wall is constant and therefore, the amount of heat passing through the wall should linearly change with the temperature difference between the indoor and the outdoor environments. However, in real life it is not possible to achieve such ideal condition rather a very complex and nonlinear relation exists between the heat flux and the temperature difference. Hence, it requires a significantly high temperature gradient between indoor and outdoor environments to ensure a steady heat flux with a prolonged monitoring period of wall. Because of these, the existing U-value estimation methods are limited to perform in winter only. Applying a point heat from the internal side of a wall could create the temperature gradient required for the accurate measurement of U-value regardless of dependency on winter season. Another key limitation is the prolonged monitoring period. Infrared thermography can be used to overcome that as it is able to provide quick information about the thermal performance of a wall when the wall is exposed to heating from one side. However, there could be subtle variation in thermal responses which are difficult to identify with visual inspection of infrared images. Artificial Neural Network (ANN) is capable of mapping nonlinear and complex relationship among different parameters. However, there is limited information available regarding the use of ANN in combination with thermography to evaluate buildings' thermal performance. As a result, there is a research scope to address the feasibility of combining ANN and infrared thermography with the application of heating from one side of a wall in relation to the estimation of thermal performance of a building's wall as well as to evaluate the performance

of different ANN architecture in this regard. This thesis focuses on three approaches to assess energy losses via buildings' walls and evaluate the financial losses and benefits as a result of that. These include the development of a mathematical model to estimate heat losses in different dwelling types with different U-values of wall and hence analyse its financial implications, and development of a novel use of infrared thermography and neural networks for the same purpose. It also investigates the design and testing of a new device to estimate the in-situ U-value of buildings' walls. The aim and objectives of the research work is discussed in the next sections.

1.3 Aim

To develop novel techniques to evaluate the benefits of thermal insulation in buildings by estimating heat losses and financial costs via mathematical models, artificial intelligence and thermography, and experimental works.

1.4 Objectives

1. To conduct a comprehensive literature review on wall insulation, current U-value measuring systems, infrared thermography and how ANN is used for the evaluation of buildings' energy and thermal performance.
2. To evaluate the role of wall insulation for household energy consumption and carbon emission during winter when people are required to work from home due to the Covid-19 pandemic situation. (This objective has been extended to consider the work from home situation due to Covid-19 pandemic in Summer 2020 with an assumption that work from home situation would continue in future.)
3. To develop a tool for evaluation of buildings' thermal performance in terms of heat loss by combining infrared thermography and ANN.

4. To conduct case study analysis on evaluation of buildings' thermal performance combining infrared thermography and ANN.
5. To design and develop a test rig to monitor specimen walls of different thickness from the internal side using infrared camera with the application of point heat source.
6. To conduct experiments to capture infrared images and sensor signals using the test rig on different wall samples in laboratory environment and analyse the experimental data for categorisation of the test walls using ANN.
7. To conduct experiments for in-situ assessment of the U-value walls in a real building and to analyse the in-situ data using ANN to estimate the U-value of walls in the real building.

1.5 Research Questions

In the previous sections, the background, scope, aim and objectives of the current research work is discussed. To accomplish the aim and objectives, the overall research question to be answered is: Is it possible to develop a system for assessment of wall insulation by combining infrared thermography and ANN? This leads to some specific research questions to be answered by the research work which are:

1. What are the influences of buildings' wall insulation in household energy demand and carbon emission?
2. How ANN can be combined with infrared thermography for the evaluation of heat loss of buildings' walls?
3. What is the monitoring period required to successfully evaluate the future heat losses through a building's wall?
4. What are the suitable ANN architectures required to predict the heat loss through buildings' wall?

5. What are the drawbacks of existing U-value measurement systems and, how infrared thermography and ANN can be used for in-situ U-value estimation of walls in buildings?
6. How to develop a test kit to monitor the thermal performance of a wall using infrared camera with the application of point heat?
7. How to process the infrared data for ANN analysis?
8. What configuration of ANN would be suitable for the U-value estimation?

1.6 Thesis structure

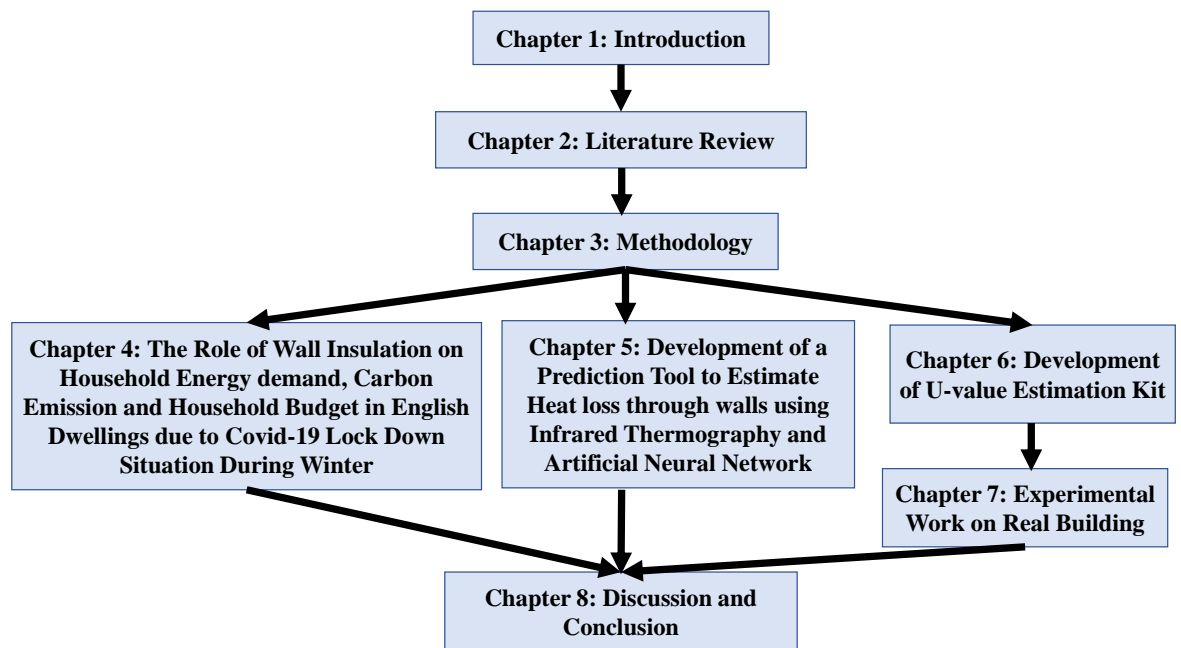


Figure 1.1: The structure of the thesis.

The thesis is organised into eight chapters consisting of introduction, literature review, methodology, influence of wall insulation on the change in energy consumption due to working from home, case studies on combining ANN and infrared thermography to evaluate buildings thermal performances, design and development of a test kit for U-value estimation,

experimental works on a real building's walls with the test kit and conclusion of the thesis. The structure of each chapter is discussed below.

Chapter one: The background of the current research work in relation to need for U-value estimation is discussed at the beginning of the chapter. The research scope with the aim, objectives and the research questions are presented in later section of the chapter.

Chapter two: A comprehensive literature review is conducted on wall insulation and its impact on buildings' energy performance, infrared thermography, methods of existing in-situ U-value estimation, Artificial Neural Network and its application in the evaluation of buildings' energy performance are discussed. The limitations of existing U-value measurement methods are also summarised at the end of relevant sections.

Chapter three: The research methodology adopted for the current PhD research work has been presented in this chapter. The details of the three levels that comprise of the methodology is discussed with graphical representation of relevant flow charts.

Chapter four: This chapter discusses the influence of insulation in the household energy consumption, effect on the household energy bills and net change in carbon emission due to working from during the winter of 2020-21 as a result of Covid-19 pandemic situation.

Chapter five: The development of an evaluation tool to predict heat loss in buildings using a novel approach of integrating infrared thermography and ANN is presented in this chapter. Two case studies are also included in the chapter to demonstrate the application of the novel heat prediction tool.

Chapter six: The development of a novel U-value estimation kit by combining infrared thermography and ANN with the application of a point heat is presented in this chapter. The application of the newly developed kit in categorising wall samples is also included in the chapter.

Chapter seven: This chapter shows the implementation of the novel U-value estimation kit to estimate the in-situ U-value of walls in a real building.

Chapter eight: The conclusion of the thesis is presented in this chapter showing the fulfilment of objectives, the key findings and the contribution to the knowledge made by the current research. The chapter finishes with the recommendation for future research works.

1.7 Summary

This chapter begins with describing the current scenario of the energy consumption in domestic sector in the UK in response to the ambition of the UK Govt. to reduce greenhouse gas emissions. A key strategy in relation to this would be the retrofitting of existing buildings with added wall insulation to minimise the energy consumption for space heating. The need for U-value estimation prior to retrofitting is explained. Addressing to the limitations of existing U-value estimation methods, a novel approach of combining infrared thermography and ANN is proposed. The research scope, the aim and objectives of the thesis, and the research questions to be addressed by the thesis are presented in the later sections. The chapter ends with a brief summary of the structure of this thesis.

Chapter 2: Literature Review

2.1 Introduction

Wall insulation significantly influences the thermal performance of buildings by lowering the U-value of buildings' wall. However, prior to applying insulation on buildings' wall to rectify the U-value of wall, it is necessary to identify the existing level of U-value of the wall. Infrared thermography has been successfully used to evaluate buildings' thermal performance. A number of research works are available regarding the effect of insulation in buildings' thermal performances, use of thermography for the evaluation of buildings' thermal performance as well as measuring the U-value of wall in buildings. Therefore, a comprehensive literature review about the wall insulation, infrared thermography and U-value measurement in buildings are included in next three sections of this chapter. Following to that a detailed literature review about Artificial Neural Network and its use in the prediction of energy demand in buildings are presented.

2.2 Insulation in Buildings

Insulation in buildings broadly refers to the materials applied around a building's envelop to restrict heat flow. Insulation materials are the materials with low thermal conductivity, which are used in buildings' components to restrict heat flow between internal and external environments as well as reduce the U-value and to help maintain stable temperature within the building envelop in spite of fluctuations in external ambient temperature. As a result, it reduces energy consumption for heating and air-conditioning and consequently reduces burning of fossil fuels for electricity generation (Aditya *et al.*, 2017).

There is a diverse range of materials used for insulation these days. Different researchers have attempted to classify the commercially available insulating materials. Among them Papadopoulos, (2005) categorized the insulating materials into four different classes namely:

organic materials, inorganic materials, combined materials and new technology materials. A very similar classification is done by Sadineni, Madala and Boehm, (2011) who also classified insulation materials into four broad classes namely organic materials, inorganic materials, metallic or metalized reflective membranes and advanced materials. Organic and inorganic materials are further grouped into cellular/foamy material and fibrous material (Papadopoulos, 2005; Sadineni, Madala and Boehm, 2011). Tabrizi, Hill and Aitchison, (2017) conducted a hypothetical case study about the impact of energy consumption using six different types of insulation material belonging to the above mentioned organic and inorganic groups namely: Glass Fibre, Expanded Polystyrene (EPS) foam slab (40% and 100% recycled), Cellulose Fibre, Rock Wool and Extruded Polystyrene (XPS). The study was conducted on a multi-storeyed residential building in Sydney and three different thicknesses (30 mm, 60 mm and 90 mm) of insulation layers were considered. The study showed that the variation in cooling energy consumption is only 2% among different samples; however, the heating energy consumption varied by 43% and Extruded Polystyrene showed the best performance in terms of saving heating energy. As a result, selection of right insulation material is necessary to get optimum benefits of energy savings. However, there are other issues such as environmental impact, resistance to sound, moisture and catching fire, that need to be considered as well (Papadopoulos, 2005). Non-recyclable insulation materials commonly used in the market, may lead to release of more greenhouse gas during the disposal process at the end of their life resulting in forfeiting the benefits of the less greenhouse gas emission due to lower energy consumption from improved insulation (Asdrubali, D'Alessandro and Schiavoni, 2015). In a review on unconventional insulation materials, the authors found that recycled polyethylene terephthalate (PET) and recycled textile materials release 1.62-0.99 kg less CO₂ than rock wool and kenaf material per

functional unit; where the functional unit refers to the mass of the insulation material required to attain a thermal resistance of $1 \text{ m}^2\text{K/W}$.

In a building, insulation can be applied on walls, roof, and floor as well. Significant amount of simulation study, experimental work and survey of real buildings show the benefits of wall insulation in terms of energy savings which are discussed in section 2.2.1. Other than wall insulation, floor and loft insulations also contribute to reduce heat loss through building envelop as well as to lower energy consumption for heating and air-conditioning. For example, Hong, Oreszczyn and Ridley, (2006) show that cavity wall and loft insulation could reduce 11% annual fuel consumption for space heating. Staszczuk, Wojciech and Kuczyński, (2017) show that floor insulation significantly reduces the heating energy demand during winter. As the current research is focused on the thermal performance of buildings wall the literature review is limited to explore the energy performance of wall insulation only.

2.2.1 Impact of wall Insulation in energy consumption

Insulation can be applied on both sides of wall. If the insulation is applied on the external surface of a building's wall, it is called external insulation and, if it is applied on the internal surface of a building's wall, it is called internal insulation. The U-value of wall does not depend on whether the insulation is applied internally or externally rather it depends on the thickness of the insulation layer in the wall. However, the thermal performance of buildings' wall after retrofitting with improved insulation vary based on whether they are internally or externally insulated as well as the climatic conditions where the buildings are located. Several studies report the effectiveness of external wall insulation over internal wall insulation while some researchers find internal wall insulation is more effective than external wall insulation. Some literatures are explored below to understand the energy performance of externally and internally insulated buildings' wall as well as the change in energy

performance due to retrofitting buildings' wall with improved insulation in different climatic zones.

Kossecka and Kosny, (2002) conducted a parametric equation-based simulation study to evaluate the energy performance of a residential building with six different combinations of wall insulation considering the metrological data of six cities in USA. The result shows that the model with purely external wall insulation has the least energy demand and the model with purely internal wall insulation has the highest energy demand. The authors further stated that the effectiveness of insulation depends on the climate zone where the house is located. On the contrary, a simulation study about the impact of different levels of external and internal wall insulation on the energy consumption and thermal comfort in a residential building in China showed that the model with purely internal wall insulation has least energy consumption and most thermal comfort hours during winter and summer however, for transitional periods the model with external insulation showed least energy consumption (Wang *et al.*, 2016). Reilly and Kinnane, (2017) also reached to a similar conclusion from their simulation study and reported that an internally insulated buildings envelop consumes 10% less energy than that of an externally insulated building. The authors explain the reason for that as the internal surfaces of building elements themselves absorb energy before reaching in equilibrium with the room temperature. The internal insulation on wall reduces the available indoor space; and therefore, the authors' observation is that the trade-off between space requirement and energy demand reduction often go against the internal insulation. Furthermore, according to Wang *et al.*, (2016), a building with external insulation has better thermal stability than a building with internal insulation. Another simulation study conducted by Kim and Moon, (2009) considering the impact of insulation in American buildings in cold and hot climate zone also showed that external wall insulation can reduce 25.5% energy consumption for space heating in colder climate areas; however, in the warmer

climate areas it could reduce around 0.14% of cooling energy consumption. Another evidence found in the favour of external insulation where the numerical simulation of energy performance in a typical residential building with 80 mm thick Expanded Polystyrene (EPS) insulation showed that the external wall insulation outperformed the internal wall insulation by 4% to 10% (Kolaitis *et al.*, 2013). Although the energy consumption for space cooling with internal insulation is marginally less than that of external insulation, the energy consumption for space heating with internal insulation is substantially larger than that of external insulation. Two climatic conditions were considered: warm Mediterranean climate and moderate Oceanic climate and the result showed that both external and internal insulation drastically reduce the annual heating energy demand, however, there is a slight increase in annual cooling energy demand. Berger *et al.*, (2016) conducted a simulation study about the impact of external insulation on energy consumption for heating and cooling in different types of office buildings at Vienna in Austria. The result shows that additional external insulation slightly increases the cooling energy demand in summer; however, the reduction in heating energy demand in winter is very large in compare to the cooling energy demand. The authors analyse the reason behind that would be the internal heat gain due to the ejected heat from electrical and electronics equipment installed in the buildings and therefore, recommend to use energy efficient electrical equipment to utilise the benefits of wall insulation in terms of energy savings. Lee *et al.*, (2017) draw a similar conclusion on the energy performance of external wall insulation supported by a simulation study in a building in South Korea; however, they recommend to carefully design the wall insulation rather than cutting down internal heat gain by using energy efficient electrical/electronic equipment. On the other hand, a study to assess the energy savings due the external insulation in a residential building in Algeria shows that both the heating and cooling energy consumption are reduced by 20% during the coolest months in winter and 38% during the

hottest months in summer respectively (Derradji *et al.*, 2017). The authors present another interesting finding that the insulated building has more stable room temperature (about 2°C variation) than that of uninsulated buildings in both winter and summer. This fact is also supported by an experimental work to find the impact of external wall insulation on the energy consumption of air-conditioning in tropical climate during summer and the result shows the variation in internal temperatures is around 0.4°C in the insulated building (Fang *et al.*, 2014). The authors also found that an externally insulated building's wall with 30 mm extruded polystyrene could reduce the energy demand for air-conditioning by 23.5% in the tropical climate zone during summer. Byrne *et al.*, (2016) observed the thermal performance of Irish building before and after retrofitting with cavity wall and external insulation. The authors monitored the test buildings three times. Firstly, before retrofitting, secondly, after retrofitting those with cavity wall and finally, after retrofitting them with external insulation. The result shows that the cavity wall reduces heat flux through north and south walls by 52% and 50% respectively. With the addition of external insulation, the heat flux through north and south walls further decreases by 48% and 60% respectively. The authors conclude that as the cavity wall is done before external insulation the sole effect of external insulation may be higher percentage of heat flux reduction than observed in this case.

The above review of literature regarding the performance of wall insulation establishes the fact that buildings' wall insulation significantly contributes to the reduction of energy consumption; however, effectiveness of wall insulation is not consistent throughout different climate zones. Most of the studies found that externally insulated buildings have higher energy savings for space heating than space cooling in cold climatic areas. Some studies have found better energy performance of the internal insulation over the external insulation; however, those studies also point out the limitations of the internal insulation as it occupies some of the available indoor spaces and has poorer thermal stability compared to the external

insulation. External insulation is more expensive and has longer payback period than internal insulation (Kolaitis *et al.*, 2013); however, it significantly reduces the household energy consumption for space heating and consequently improves the quality of inhabitants' life (Adamczyk and Dylewski, 2017). The inconsistency in the energy performance of wall insulation in different climatic regions leads to the fact that it is difficult to generalise a standard for retrofitting buildings with improved wall insulation, rather different standards based on the local climate would be more efficient.

2.3 Infrared thermography

Infrared thermography refers to the technology that involves noncontact temperature measurement of any object by identifying heat radiation from that object. An infrared image could reveal significant information regarding the thermal radiation from different objects in that image. Every object radiates heat energy if that has a higher temperature than the surrounding environment and absorbs heat energy from surroundings if that has a lower temperature than the surrounding environment. This energy radiation occurs because of the continuous vibration of the molecules that constitute the object. When electrons in a molecule are accelerated due to rise in temperature, they release energy in the form of radiation. This exchange of heat energy takes place by the propagation of electromagnetic waves or photons. Within the full spectrum of the electromagnetic waves, the waves with wavelength ranges from 10^{-1} μm to 10^2 μm are responsible for thermal radiation and the thermal radiations that occur from $0.7\mu\text{m}$ to 10^2 μm wavelength range are called infrared thermal radiation (Incropera *et al.*, 2011). The net heat transfer due to infrared radiation can be expressed using Stephan Boltzmann's law as,

$$E = \varepsilon k(T_s^4 - T_c^4) \quad (2.1)$$

Here E represents the net heat transfer, T_s and T_c are the surface temperature and the surrounding temperature, respectively. The symbol k stands for the Stephan Boltzmann's

constant and normally the value of it is considered as $5.67 \times 10^{-8} \text{ W/m}^2\text{K}^4$. The symbol ε represent the emissivity of the object of interest and the value of emissivity is considered equal to 1 for a perfect black body. For a grey body, the emissivity value is less than 1 and it depends on the texture of the object. For instance, the emissivity of a brick wall is between 0.85 to 0.95 (CIBSE, 2006), and the emissivity of low emission glass window would be less than 0.07 (Hartig, K.W., Larson, S.L. and Lingle, P.J., 1996). An infrared camera is constructed with infrared sensitive elements organised as arrays of sensor. These infrared sensitive sensor arrays can measure the intensity of any incidental infrared ray and generate a response accordingly. An infrared image is constructed by combining these responses from the sensor arrays. The intensity of incidental infrared rays on the sensors is proportional to the surface temperature and based on that, the variation on surface temperatures can be clearly differentiated using different colours and intensity of colours with the help of a suitable colour coded scale. The resolution of an infrared camera depends on the number and orientation of arrays containing infrared sensors. Infrared cameras first came on the market in 1956 (Lisowska-Lis, Mitkowski and Augustyn, 2011). Available infrared cameras have a typical working range of $0.7 \mu\text{m}$ to $20 \mu\text{m}$ (Al-Habaibeh et al., 2010). The radiation captured by the sensors in an infrared camera is composed of three different emissions. They are emission from that surface, reflection of the emissions of the surroundings from the surface and emission from the atmosphere. The surface temperature of the object of interest can be obtained from equation 2.2 which combines these three emissions (Usamentiaga *et al.*, 2014).

$$T_s = \sqrt[4]{\frac{W_{tot} - (1 - \varepsilon_s)\tau_{atm}k(T_{ref})^4 - (1 - \tau_{atm})k(T_{atm})^4}{\varepsilon_s\tau_{atm}k}} \quad (2.2)$$

Here T_s represents the surface temperature, W_{tot} represents the total radiation received by the camera, ε_s represents the emissivity of the surface, τ_{atm} represents the transmittance of

the atmosphere and k represents the Stephan Boltzmann's constant. T_{ref} and T_{atm} are the reflective temperature and the atmospheric temperature. The value of τ_{atm} is close to 1, and therefore, the effect of atmospheric temperature is negligible. The infrared radiation from an object could easily propagate through air and that makes infrared thermography an useful tool to measure the surface temperature of buildings' wall in a noncontact way from a short distance (Marino, Muñoz and Thomas, 2017). It is also useful to apply infrared thermography for the estimation of thermal transmittance of buildings' windows (Baldinelli and Bianchi, 2014), heat loss through door openings (Al-Habaibeh, Medjdoub and Pidduck, 2012) and characterisation of the thermal performance of buildings' facade (Bienvenido-Huertas *et al.*, 2019). Moreover, study shows it is convenient to estimate energy savings due to retrofitting a building with improved insulation by comparing the infrared images captured before and after retrofit respectively (Al-Habaibeh and Siena, 2012). O'Grady *et al.* (2017) show that infrared thermography can be used to estimate the heat flow rate through a thermal bridge and Ferrarini *et al.* (2016) show the use of thermography for the estimation of time shift values of temperature in building elements. It could also be used to investigate transient temperature response behaviour over the time (Xie *et al.*, 2019). One of the advantage of using thermography in the field of evaluating buildings' thermal performance is that the infrared images could be upgraded to higher resolution applying different mathematical algorithms to achieve higher precisions for the analysis of infrared data (Baldinelli *et al.*, 2018).

2.4 In-situ U-value Assessment

In general, U-value represents the overall thermal transmittance of an object through its opposite surfaces. Mathematically, U-value is the reciprocal of summation of thermal resistances which represent the overall thermal transmittance of a solid object. Therefore, higher U-value of buildings' walls means higher heat transfer through the walls. The

convention for estimating theoretical U-value or designed U-value of a building's wall is governed by the regulation stated in BS EN ISO 6946 (Anderson, 2006). According to the BS EN ISO 6946, the U-value is represented as the reciprocal of the overall resistance of all layers of the wall (ISO, 2007 in Gaspar, Casals and Gangoellis, 2016) and is expressed as

$$U = \frac{1}{R_T} \quad (2.3)$$

where, $R_T = R_i + \frac{d_1}{\lambda_1} + \frac{d_2}{\lambda_2} + \frac{d_3}{\lambda_3} \dots \dots \dots + R_e$; represents the overall thermal resistance of the wall. Here R_i and R_e are the thermal resistance of air at the internal surface and the external surface, respectively. The parameters $d_1, d_2, d_3 \dots \dots \dots$ and $\lambda_1, \lambda_2, \lambda_3 \dots \dots \dots$, represent the thicknesses and the thermal conductivities of the respective wall layers. The theoretical U-value would be good enough to use for the design purpose of new built buildings; however, to assess the thermal performance of an existing building before or after retrofit it may convey misleading information as the actual U-value a building's wall may change due several reasons such as: degradation of the wall materials due to prolonged exposure to the external environment, presence of void within the wall layers, deviation from the designed thickness due to poor craftsmanship and so on (Evangelisti *et al.*, 2015). A research work comparing the designed U-value and the in-situ U-value among three different types of buildings in Italy, where one was a very old building, another was built in early 1950 and the third one was built in 2000's, shows that the old building has 153% deviation, the early 1950 building has 37% average deviation and the 2000's building has 17% deviation with the designed U-value (Evangelisti *et al.*, 2015). The findings of that research indicate that the material properties of old building would change over time and hence in-situ U-value measurement is necessary especially for old buildings. Furthermore, a field survey in 29 different types of buildings shows that the in-situ U-value is higher than the calculated U-value in most of the cases because the theoretical U-value calculation is based on the ideal

construction condition (Doran, 2001). A later study using data from 277 properties also reveals that the ratio between the in-situ U-value and the calculated U-value ranges between 61% to 134 % depending on the wall types in a building. Rye (2010) conducted a research work to compare the in-situ U-value measured with the theoretical U-value calculated using BuildDesk v3.4 in English Heritage buildings and the result shows that the software overestimates the U-value in 79% cases.

Several research works have been undertaken to measure the in-situ U-value of buildings' walls. Among them, there are two major approaches found namely: Heat Flux Meter Method (HFM) and Infrared Thermovision Technique (ITT). Besides these two, there is a laboratory based method where samples from different layers of a wall are collected by drilling holes and tested in laboratory to determine the actual thermal conductivity which is then used alongside the wall layers' thickness to evaluate the in-situ U-value from equation 2.1 (Ficco *et al.*, 2015). However, it is a destructive process and merely applied in existing buildings. Another approach mentioned by Ficco *et al.*, (2015), is to consider historical data regarding the building characteristics and estimate U-value based on those data. However, the research of Lucchi, (2017) shows that this method tends to overestimate the actual U-value because of the inclusion of safety factors in the standard historical data as well as the change in material property due to aging. Therefore, the author suggests that in-situ U-value measurement is the best among all alternatives. The HFM method uses a heat flux meter in conjunction with temperature sensors and the ITT method uses an infrared camera often accompanied with other temperature sensors.

2.4.1 Heat Flux Meter

Heat flow meter or heat flux meter is a device used to measure heat flux rate through any surface of an object. Heat flux rate refers to the amount of heat energy passing through unit area of a surface per second. In Table 2.1, the specification of heat flux meter in the reviewed

literature is listed and it is found that the most widely used heat flux meter for U-value measurement is HFP01 from Hukseflux. According to the user manual (Campbell Scientific, 2012) the device contains mainly a thermopile, which measures temperature differences across a thin sensor body made of ceramic-plastic composite.

Table 2.1: Heat flux meter and temperature sensors used in the reviewed research work.

Serial No.	Reference	Heat Flux Meter	Temperature Sensor
1	Doran, (2001)	Thermocouple-based heat flux meter	N/A
2	Gong and Huang (2006)	Thermocouple-based heat flow meters and	Thermocouple-based temperature sensors
3	Baker (2008)	Hukseflux HFP01 with Scientific CR1000 data loggers	Campbell Scientific type 107 stainless steel-sheathed thermistors.
4	Rye (2010)	Hukseflux HFP01 with Scientific CR1000 data loggers	Gemini TinyTag Plus 2 TGP-4520 loggers
5	Desogus et al. (2011)	FE01-3B heat flux sensor for measuring heat flux and TGU2 data loggers for recording data.	Resistive temperature detector (RTD)
6	Biddulph et al. (2014)	HuksefluxHFP01 heat flux meter	Thermistor based temperature sensor
7	Li et al. (2015)	HuksefluxHFP01 heat flux meter with Eltek 401 data logger	Thermistor based temperature sensor
8	Hulme and Doran (2015)	HuksefluxHFP01 heat flux meter with Eltek 401 data logger	Thermistor based temperature sensor with Gemini Tinytag data logger
9	Evangelisti et al. (2015)	TESTO 435-2	N/A
10	Gaspar et al. (2016)	HFP01 from Hukseflux.	The inside air temperature was measured using T107 temperature sensor with CR850 acquisition system from Campbell Scientific, Inc. The outside air temperature sensor and its acquisition system used was TF-500 and PCE-T390 from PCE Iberica, SL
11	Lucchi (2017)	HFS series (HFS-3 and HFS-4).	Thermocouple-based temperature sensors

A thermopile is made by connecting several thermocouples either in series connection or in parallel connection. Thermopile converts temperature difference into electric voltage. The temperature difference between two sides of sensor body can be determined from the voltage reading obtained by using a voltmeter. Dividing the temperature difference with thermal conductivity of the sensor body, the heat flux can be obtained. HFP01 is supplied with a sensitivity factor (calibration constant) and the voltage reading divided by that factor directly gives the heat flux in watt per square metre. Figure 2.1 shows a HFP01 heat flux meter from Hukseflux. Other than HFP01, there is HT-50 thermal flux meter from International Thermal Instrument Company. According to their website (International Thermal Instrument Company, no date), the HT-50 thermal flux meter is a flat metallic transducer and able to measure directly the heat flux of the surface where it is placed. The working principle of HT-50 is similar to the working principle of HFP01, i.e. to measure the temperature difference between two surfaces of the sensor using thermopile.

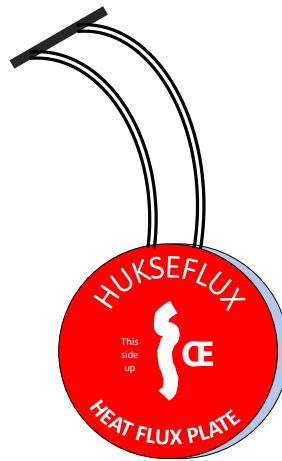


Figure 2.1: HFP01 heat flux meter from Hukseflux (Campbell Scientific, 2012)

The output voltage generated by the thermopile is converted to heat flux by multiplying that with a calibration constant to directly get the heat flux value in BTU/ft²hr. This calibration constant is supplied to consumer with every heat flux meter. Figure 2.2 shows a HT-50 heat flux meter from International thermal Instrument. Furthermore, Omega Engineering

produces heat flux sensor under HFS series (HFS-3 and HFS-4). According to the user guide (OMEGA Engineering, no date), the main part of the HFS Sensors is differential thermocouple. A thin foil containing a thermopile with more than 50 junctions is placed around a thermal barrier of known thermal characteristics.

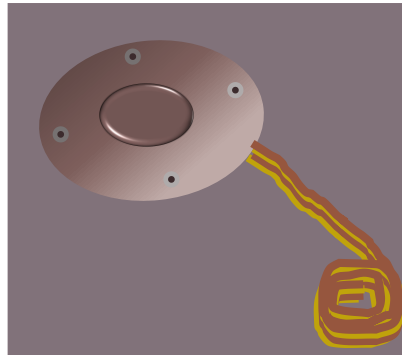


Figure 2.2: HT-50 heat flux meter from International thermal Instrument (International Thermal Instrument Company, no date)

The thermal barrier is made using Kapton (polyimide film) and the junctions are created by combining copper and constantan on both sides of the barrier in series connection. The first junction on the upper surface and the last junction on the lower surface contains the copper outputs leads which can be connected to a voltmeter to get the voltage reading. Dividing the voltage reading by the sensitivity constant of the sensor gives heat flux in $\text{BTU}/\text{ft}^2\text{hr}$. Figure 2.3 shows an HFS series heat flux meter from Omega.

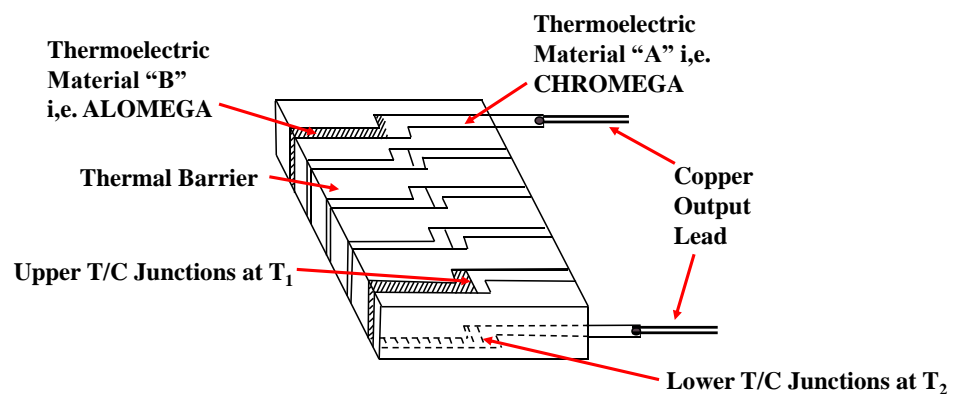


Figure 2.3: HFS heat flux meter from Omega Engineering. (OMEGA Engineering, no date)

2.4.2 U-value Estimation using HFM Method

The standard guideline for HFM method is described in ISO 9869 Part 1 (ISO, 2014). According to the guideline the U-value is ratio of total heat flux with temperature gradient between indoor and outdoor environment and can be represented using equation 2.4 (Gaspar, Casals and Gangoellis, 2016).

$$U = \frac{\sum_{j=1}^n q_j}{\sum_{j=1}^n (T_{ij} - T_{ej})} \quad (2.4)$$

Here U represents the estimated U-value, q is the heat flux rate in watt per square meter, T_i and T_e are the inner and outer temperatures in degree Kelvin respectively. The recommended duration for data acquisition in ISO 9869 guideline is at least 72 hours (Gaspar, Casals and Gangoellis, 2018). However, analysis of survey data conducted by Doran (2001) demonstrates that to get a reliable estimation of U-value in HFM method, at least more than 5 days observation is required and U-values measured over five days result in standard deviations ranging from 10% to 25% depending on the thickness of walls. Similar survey works have been carried out by Baker (2008) in a project for the Centre for Research on Indoor Climate & Health, Glasgow Caledonian University (GCU) to measure the U-value of 20 different types of walls in Scottish Buildings. The result shows that at least one week's observation is required to limit the variation in the in-situ U-value within $\pm 5\%$ of the average value and it is recommended to have around 27 days data to determine the final value. In a more comprehensive survey containing data from 277 properties, Hulme and Doran (2015) recommend that the duration for the measurement of temperature should be for at least two weeks to get an accurate result. The research of Gaspar, Casals and Gangoellis, (2018) also shows that it is not possible to get a stable result in 72 hours as guided by ISO 9869 and two out of three case studies conducted by the author show that it requires more than 96 hours of observation to reach to a stable result.

Desogus et al. (2011) conducted research to observe the effect of temperature gradient between indoor and outdoor temperature in the estimation of U-values by using Heat Flux Meter (HFM) technique and endoscopic or destructive sampling method in a wall between two rooms of Architecture Department building in Cagliari, Italy. Two series of measurements were carried out by the author with 10°C difference between internal and external environment temperature in the first case and 7°C in difference between internal and external environment temperature the second case. The result showed that the U-value measured at 10°C temperature gradient using HFM methods had less than 10% uncertainty on the other hand U-value measured using destructive method had about 16% uncertainty. U-value measured using HFM method at 7°C temperature gradient had uncertainty of 13.5% and therefore the author concluded that measuring U-value using HFM method would be ideal for assessment of buildings' wall thermal performance if that is performed in correct environment. Ficco *et al.* (2015) conducted a field investigation to evaluate in-situ U-value of seven different building components using four commercial heat flux meters. The comparison of the field investigation results with U-value obtained using design data and the U-value obtained from endoscopic sampling show that low temperature difference (less than 10°C) and consequently low heat flow rate lead to unacceptable uncertainty in the U-value estimation. The same authors also demonstrate that during summer, when the heat flow is reversed, the uncertainty in the estimated in-situ U-value goes as high as 50%; while during winter, when the temperature difference is more than 10°C between indoor and outdoor environments, the uncertainty in the estimated in-situ U-value drops to 8%. Gaspar, Casals and Gangolells (2016) also notice significant deviation in measured U-value if the temperature difference between indoor and outdoor environments drops below 10°C and the authors termed it as nonoptimal condition for in-situ U-value measurement. However, by adopting dynamic methods of calculation described in ISO 9869-1 (ISO, 2014 in Gaspar,

Casals and Gangolells, 2016), which consider temperature derivatives of all previous time steps could produce better estimation in case of nonoptimal conditions. In a comparative study between the average method and the dynamic method of in-situ U-value measurement using HFM method it is found that the difference in theoretical and in-situ U-value is less than 5% for average method and less than 1% for dynamic method in optimal condition (the average temperature difference between indoor and outdoor is higher than 10°C); however, in non-optimal condition, the difference between theoretical and in-situ U-values goes up to 20% for average method and 10% for dynamic method respectively (Gaspar, Casals and Gangolells, 2016). The authors conclude that dynamic method of calculation should be adopted as it produces more precise estimation and a later study by the same authors also support the fact by achieving around 50% more precision with dynamic method of calculation than with average method of calculation (Gaspar, Casals and Gangolells, 2018). Gong and Huang (2006) attempted to improve the precision of the dynamic analysis method of U-value calculation described in ISO 6946 with Z-transfer function of discrete time series model used in dynamic calculation method and the result shows this approach reduces the estimation errors from 1.18% to 0.89%. Aiming to shorten the measurement period and reduce the influence of less than 10°C difference between indoor and outdoor temperature in HFM method, Biddulph et al. (2014) propose to add a thermal mass parameter and use Bayesian statistical analysis for deriving estimated U-value. The authors show that addition of a single thermal mass parameter reduces the time required to stabilize the fluctuations in the measurement of U-value from 10 days to 3 days. Considering the stability in the estimated U-values the authors expect that the method could provide benefits in measuring U-value in non-optimal condition as well. Li et al. (2015) apply the model developed by Biddulph et al. (2014) to compare the in-situ U-values of solid walls with the U-values of solid walls quoted by the Chartered Institute of Building Service Engineers (CIBSE) and

reach to a similar conclusion as Biddulph et al. (2014) made regarding the time required to get a reliable estimation of in-situ U-value in HFM method. The authors also state that U-value measurement in occupied houses using heat flux sensor under predicts the U-value because of lack of good thermal contact between the solid wall and the heat flux sensor, difficulty in positioning the sensor at a suitable place on the wall and thermal bridge among adjacent partition walls; however, by using thermal mass model with Bayesian statistical analysis all these problem could be minimised to some extent. Gori et al. (2017) further extended the research of Biddulph et al. (2014) by adding two thermal masses instead of one and use two heat flux meters in internal and external surface of a wall respectively. The authors achieved further precision than that of Biddulph et al. (2014) and believe that their model could be useful in estimating U-values in summer condition as well. However, none of the above-mentioned authors attempt to verify the performance of their models in the summer condition. Sassine (2016) used Fourier series and Laplace transform to improve the accuracy of HFM estimation and the result of the experimental works conducted in laboratory showed that the deviation drops below 4%; however, the time required for the measurement is around six days and the method is not tested on real buildings.

Therefore, from the above discussion the limitations of the HFM method can be summarised as:

1. HFM method could not produce good result if the temperature difference between the internal and external environment is less than 10°C due to lack of adequate heat flow.
2. HFM method does not produce good result if the heat flow is reversed i.e., under summer condition.
3. HFM method needs at least 72 hours reading to estimate U-value.

2.4.3 U-value Estimation Using ITT Method

The guidelines for ITT method is described in ISO 9869 Part 2 (ISO, 2018). The basic theory behind the U-value calculation in ITT method is similar to that of HFM method and can be expressed as,

$$U = \frac{P}{T_{int}-T_{ext}} \quad (2.5)$$

Here U represents the estimated U-value, P is the total thermal power, T_{int} , represents internal environment temperature and T_{ext} represents external environment temperature. The thermal power represents the total heat passing through the wall from internal environment by conduction and dissipating to the external environment by radiation and convection. The radiation heat transfer can be explained with equation 2.1 and the convection heat transfer can be estimated from the temperature difference between the wall surface and the external environment multiplied by a constant called coefficient of convection (Hoyano, Asano and Kanamaru, 1999). Equation 2.6 express the quantification of convection heat.

$$H = \alpha_c(T_s - T_{ext}) \quad (2.6)$$

Here H represent the amount of heat transfer due to convection, α_c is the coefficient of convection heat transfer, T_s is the wall surface temperature and T_{ext} is the environmental temperature. By combining equation 2.1 and equation 2.6 thermal power can be calculated. Different researchers attempt to quantify thermal power by combining radiation heat flux and convection heat flux with slight modification based on some assumptions. For instance, Madding (Madding 2008 in Nardi et al. 2016) used the following equation 2.7 to estimate thermal power and replace surrounding temperature with the reflective temperature and consider the third power of mean of the wall surface temperature and reflective temperature for the radiative part heat flux part.

$$P = 4\varepsilon\sigma T_m^3(T_s - T_{ref}) + \alpha_c(T_s - T_{int}) \quad (2.7)$$

Where, $T_m = \frac{T_s + T_{ref}}{2}$ is the mean temperature of T_s and T_{ref} . It is also noted that the author considers internal environment temperature in the convective heat flux part instead of external environment temperature. On the other hand, Albatici and Tonelli (2010) replaced the coefficient of convection heat flux with wind speed applying Jurges' equation and consider Stephen Boltzmann's law for grey body radiation for the radiative part of heat flux to estimate the thermal power which is presented in equation (2.8)

$$P = 5.67\varepsilon_{tot} \left(\left(\frac{T_s}{100} \right)^4 - \left(\frac{T_{ext}}{100} \right)^4 \right) + 3.8054v(T_s - T_{ext}) \quad (2.8)$$

Here, ε_{tot} is the emissivity on the entire spectrum, v is the wind speed. However, in a later study (Albatici, Tonelli and Chiogna, 2015) the emissivity consideration has been conserved to the spectral range of the thermal camera rather than the entire spectrum. The initial study by Albatici and Tonelli (2010) shows that the U-value estimated by ITT method is 31% higher than the theoretical U-value whereas the U-value estimated by HFM method is 59% higher than the theoretical U-value. The author attributed some causes behind such high deviations in the result and commented that ITT method is much faster and accurate than HFM method, but it is limited to perform after sunset with overcast sky preferable to avoid the effect of solar reflection. Also, it is necessary to maintain more than 10°C temperature difference between indoor and outdoor. Nardi et al. (2014) conducted an experimental study to measure U-value using ITT method based on the work of Albatici and Tonelli (2010) and compared the result with designed U-value and U-value measured using HFM method. The result shows that the U-values measured using HFM method have deviations from 11% to 29% with design value and the U-values measured with Infrared thermography have deviation from 16% to 29% with the designed value which refers that HFM and ITT produce similar sort of outcome. Furthermore, regarding the influence of solar radiation on the U-

value in the same study it is found that U-value measured on a cloudy day has less than 2% deviation with HFM method U-value measured in a sunny day has 37% with HFM method. In a later comparison with the use of guarded hot box within laboratory environment by Nardi et al. (2015), it is found that the deviation between theoretical U-value and the U-value measured following HFM method is 10.71%, whereas the deviation between theoretical U-value and the U-value measured following ITT method ranges from 3% to 7%. Albatici et al. (2015) conducted extensive experimental work on 10 different walls based on the theory developed in the previous research (Albatici and Tonelli 2010) to further verify the sensitivity of different parameters. The result of the study shows that the light walls have higher standard deviation (about 35% to 50%) than the heavier wall (about 10% to 18%) and therefore it could be concluded that the result's accuracy depends on mass per unit area of the walls. The authors also find that the south facades walls which are more exposed to solar irradiation than the north facades have higher dispersion in the estimated U-values. In terms of the sensitivity of parameters such as wind speed, internal environment temperature, external environment temperature and external wall surface temperature, wind speed has the lowest sensitivity, which is 9%; however, low wind speed (less than 0.5 m/s) is preferable high wind speed could result in excess convective heat loss. The internal environment temperature has maximum sensitivity of 27% much lower compared with the external environment temperature sensitivity, which is about 50% for heavy walls and about 350% for light walls. Therefore, the authors suggest that the weather condition and the time of performing measurement play an important role in the deviation of U-value and overcast sky with a temperature difference of above 10°C between indoor and outdoor would minimize the deviation. Fokaides and Kalogirou (2011) use Madding's (2008) equation for thermal power calculation in their study measure U-value using ITT method, however, they consider the third power of surface temperature instead of mean temperature used by Madding (2008).

The result of the study shows the percentage deviation between the theoretical U-value and U-value measured using ITT method is in the range of 10% to 20% which is higher than the deviation in U-value measured using HFM method. However, the authors argued that ITT result might be more accurate as this method considers the radiation effects that are ignored by other methods. Dall'O', Sarto and Panza, (2013) simplified Albatici and Tonelli (2010)'s equation for calculating thermal power by neglecting the effect of radiative heat flux with the assumption that the outdoor air is in steady temperature with the wall surface and hence considers only the convective heat flux. The results of the study show a good agreement with the theoretical U-value of solid walls in old buildings'; however, for the modern building with well insulated wall the deviation tends to be above 50%. The authors attributed the reasons behind such deviation in well insulated wall to the low thermal inertia of the walls which leads to a small heat flux difference and argued in favour of ITT method that it produces overall closer estimation to the theoretical U-value compared to the HFM result which shows around 65% deviation from the theoretical values. Nardi et al. (2016) experimentally compared the theories developed by Madding (2008), Fokaides and Kalogirou (2011), Dall'O' et al. (2013) and Albatici et al (2015) within the laboratory environment using guarded hot box. The designed or theoretical U-value measured according to ISO 6946 and U-value measured using HFM method according to ISO 9869 are considered as the benchmark for the comparison. The results show that the U-values calculated using the equations developed by Madding (2008) and Fokaides and Kalogirou (2011) exhibit similar trend under various internal and external temperature differences as well as variation in reflected temperatures. It is also found that these two U-values are very close the theoretical U-value with around 2% deviation. On the other hand, the U-value calculated using the equations developed by Dall'O' et al. (2013) and Albatici et al (2015) exhibit similarity in trend under different variation of indoor and outdoor temperature. The

U-values calculated using the equation developed by Albatici et al (2015) have proximity to the U-value calculated using HFM method with around 12% deviation. The U-value calculated using equation developed by Dall'O' et al. (2013) shows the worst performance because it is heavily dependent on the convective mode of heat transfer but inside the laboratory heat convection is limited due to stagnant air. The similarities in trend in the outcomes of the experiments are fairly expected as the equation developed by Fokaides and Kalogirou (2011) is based on the work of Madding's work and the equation developed by Dall'O' et al. (2013) is the modification of the work of Albatici and Tonelli (2010) with some assumptions. The difference between indoor and outdoor temperature has a significant impact on the result and it is found at 16°C temperature difference the variation among the U-values is 30% while at 20°C temperature difference the variation drops to 20%. The reflective temperature also has an important influence in the result; as the reflective temperature increases, the dispersion in U-values also increases. And this fact points out to the preference of overcast weather when the measurement is taken place. Tzifa et al. (2017) attempt to see the influence of thermal camera on the U-value estimation with using different thermal cameras for the U-value measurement of same wall, where the U-value calculated in HFM method and the theoretical U-value are considered as the benchmark for comparison. The result shows that change in thermal camera does not influence the U-value as long as the camera is accurately calibrated, and all the temperatures are measured with same camera. Danielski & Fröling (2015) combined HFM and ITT methods where the coefficient of heat convection is estimated from the total heat flux through a small sample wall measured using HFM method and the U-value of actual building is estimated using ITT method considering coefficient of heat convection obtained from the test on small wall. The authors validated the ITT result with the HFM result for both the small and the large wall and finds that the deviations between HFM and ITT results range from 4% to 11%; and

hence, the authors conclude in favour of ITT method because of its versatility in use for measuring large building area as well as the capability to point out imperfect areas on the wall and thermal bridges.

ITT method could be considered as the cheapest and quickest technique for in-situ U-value estimation of a building's wall (Nardi *et al.*, 2018); however, the above literature review points out some limitations of it. These are:

1. To get a reliable U-value, the temperature difference between internal and external environment should be more than 10°C and some researchers argue that it should be more 15°C.
2. To avoid reflection of solar radiation overcast condition is better for measurement and the readings are preferred to be taken before sunrise as walls gain heat due to solar exposure during the daytime.
3. The wind speed is preferred to be less than 0.5 m/s to avoid heat loss due to convection.
4. The deviation in the result varies with thickness of wall. Heavier walls used to produce less variation than lighter walls as the mass per unit area is higher in heavier walls.
5. ITT method is not proven to work well under summer condition.

2.4.5 Other methods of U-value estimation

Sørensen (2010) developed a heat-loss measuring device called U-value meter that considers both conduction and radiation heat loss through the facades. The U-value meter consists of a copper plate, which works as a heat absorption sensor, and it is covered with highly insulating material to keep it separate from surrounding environment. A small air gap keeps the copper plate apart from the test wall surface and in that gap the heat emitted from the wall due to radiation as well as convection is trapped. That trapped heat in the gap is

conducted in the copper plate resulting in the change of temperature in the copper plate. The temperature of copper plate is measured continuously to obtain the energy change and thereby from the relative change of energy the U-value is calculated. A reflective foil behind the copper plate was used to reflect any radiation escaping from the copper plate. For data acquisition, the meter needs to be taken inside and outside the building. One of the limitations is that it requires some time to acclimatize. The other limitations are the effects of wind speed, solar radiation in the facades and the moisture content in the wall material. The author presented some example of data acquired by the U-value meter in Sørensen (2013) and the data was collected over three days from Energy Technological Development and Demonstration Program (EUDP) in typical residential houses built between 1960 and 1970 in Denmark. The result shows that the average U-value has around 2.5% deviation from the theoretical U-value. It is also found from the results that the U-value meter is suitable for measuring light building materials and heavy walls do not show good results due to the unsteady nature of heat transfer process in the heavy walls. A further development of HFM method is made by Greentag AG (GreenTEG AG, 2019) with a software containing a comprehensive building catalogue that facilitates to estimate U-value in about an hour; however, it is still required to satisfy other conditions of HFM method. Another U-value measurement device is developed by TESTO that is able to determine the in-situ U-value from indoor temperature, outdoor temperature and wall surface temperature on three points on a wall using a dedicated software from the company (TESTO, no date). This method requires over 15°C temperature difference between indoor and outdoor environments, and it is recommended to conduct measurement for one day.

2.5 Artificial Neural Network (ANN)

Development of Artificial Neural Network (ANN) is a milestone in the history of artificial intelligence. In 1943 McCulloch and Pitts first develop the idea of initial neural network

which was extended by Hebb and Rosenblatt (Lippmann, 1987). ANN is a mathematical model used for information processing which mimics the work process of the biological nervous system. This system is very effective in understanding nonlinear behaviour between and a set of inputs and outputs. To solve a problem a neural network is initially trained with a training data set where the known outputs are set as the targets for the ANN to attain from the features of input data set. The nonlinearity between the input and the output values are learned by the network and these learned features are used later to estimate the unknown output from the similar input data set. As like human brain, the network in ANN is composed of several neurons arranged in different layers. A simplest ANN contains at least three layers namely: input layer, hidden layer and output layer; however, in complex ANNs the hidden layer portion could be composed of multiple layers. The ANNs with multiple hidden layers are called Deep Learning Neural Network. Input layer is the first layer which receives inputs, and the output layer is the final layer that delivers the outputs. The hidden layer(s) are mainly responsible for learning the characteristics of input data and the relationship between inputs and outputs. The neurons in a layer parallelly process data and pass the processed data to the next layer. Usually, each neuron of one layer is connected with every neuron of the next layer except the first and the final layers. Inside a neuron, there are three functional transformations that occur. At first, the inputs are multiplied by a set of weights. The number of weights is equal to the number of inputs. Then a bias value is added with the weighted inputs. At that stage, the inputs are called net input and they are ready to be fed through a function called the transfer function. Finally, the net inputs are processed using a transfer function which generates the output of the network. Mathematically, the output vector Y of a neuron can be expressed as function of the input vector X , the weight vector W and the bias vector B as shown in equation 2.9.

$$Y = f(WX + B) \quad (2.9)$$

The input data for ANN is organised in matrix form, and it can be categorised into two types, namely concurrent input, and sequential input. If all input data are fed together into a network, the input type is called concurrent input, and if input data are fed into the network in a particular sequence, then the input type is called sequential input. Concurrent input is used in static networks and sequential input is used in dynamic networks. However, there could be situations where the multiple sets of concurrent data are sequentially fed into the network. Similarly, output data in the output layer is delivered in matrix form. In general, the input and output layers contain the same number of neurons as the number data in the input and output matrix. The training process of ANN is an iterative process where each iteration is called an epoch. At the beginning of the training process an arbitrary value of weight and bias is assigned in each neuron. The weights and biases are updated after each iteration based on the gradient between the targets and the outputs generated in that iteration at an incremental rate. This incremental rate is called learning rate and the process of learning is known as back propagation technique. Generally, the iteration continues until the minimum gradient is reached, but there is provision to limit the number of epochs with a predefined value. Some networks, such as recurrent network, have provision of using feedback data with a specific time delay, while others do not use feedback data, and are usually called feedforward networks (Kuan, 2008). Feedforward neural network is suitable for regression classification and pattern recognition tasks (Gori, 2018). Recurrent neural network is suitable for sequential data analysis such as handwriting and speech recognition, machine translation and so on (Witten *et al.*, 2017). Dynamically driven recurrent neural network can be successfully applied to time series problems; however, there is a limitation of this method in terms of vanishing gradients i.e. the gradient become so small that it doesn't effectively change the weights and biases inside a neuron (Haykin, 2000). To overcome this limitation, a special type of recurrent neural network is developed by Hochreiter and

Schmidhuber (1997) which is called Long Short Term Memory (LSTM) network. LSTM network is provided with memory blocks which process information through different gates such as forget gate, peephole, input gate and output gate; and these gates facilitate the memory blocks to either remember or forget information selectively which allow LSTM network to overcome vanishing gradient problem (Witten *et al.*, 2017). Therefore, the LSTM network architecture is slightly different than other recurrent neural networks and it contains LSTM cells in the hidden layer instead of neurons.

ANN can predict the complex and nonlinear relationship among independent and dependent variables without involving formal statistical models because the neurons inside the ANN learn these features through the iterative training process; however, there is a risk of overfitting (Tu, 1996). To minimise overfitting, a simple way is to retrain the network for several times. As the network's initial weights and biases differ every time, the mean value of the network performance can give a generalised solution (Hudson Beale, Hagan and Demuth, 2017). The number of neurons on hidden layer(s) depend on the application and the desired performance level of the whole network. In generic sense, it could be speculated that more neurons in a layer will produce better output however, too many neurons may lead to the overfitting of output values. Therefore, it is necessary find out the optimum number of neurons required to perform a task smoothly and accurately. Unfortunately, there is no general rule for selecting optimum number of neurons. Rafiq, Bugmann and Easterbrook, (2001) suggested that the number of neurons sufficient for a particular network can be determined on the basis of root mean square (RMS) error and number of iterations required to reach at the desired acceptable error limit. The work of Yang, Yeo and Kim (2003) shows that for n neurons in the input layer, the least RMS value is obtained with $2n$ neurons in the hidden layer. However, Yang, Rivard and Zmeureanu, (2005) found the minimum RMS with $2n+1$ neuron in the hidden layer. Sheela and Deepa (2013) reported 10 different approaches

of determining optimum number of neurons; however, the authors could not finalise a single approach to be applicable in a generic level. Therefore, a sensitivity analysis before applying ANN would be useful to determine the optimum architecture. A network can be trained in two ways: incremental training and batch training. In incremental training, the weights and bias are updated at the rate of learning rate after every single input is fed into the network and generally it is used in recurrent neural networks. In batch training mode the weights and bias of the neurons are updated after all the input data are fed into the network. This technique is usually applied for feed forward neural networks. There are two types of learning processes, namely, unsupervised learning and supervised learning (Dalton and Deshmane, 1991). In the first process, the network constructs clusters of data with coherent statistical properties based on the network rules from the input training data sets and this knowledge is used to evaluate unknown input data; whereas in the second process, the network maps the relationship between input and target data sets, which is used to estimate output from an unknown input (Amin *et al.*, 2008). Among these two approaches, supervised approach is good for predicting energy consumption in buildings (Zhao *et al.*, 2019). ANN has been successfully used in many fields of study. In a review regarding the application of ANN, Abiodun *et al.* (2018) made a comprehensive list of ANN's use in different fields of study including system control, optimisation, robotics, manufacturing, forecasting, signal processing and so on. In the following section some applications of ANN regarding buildings' thermal and energy performances are reviewed from different literature.

2.5.1 Review of ANN's application

Ben-Nakhi and Mahmoud (2004) assess the feasibility of general regression neural network for predicting cooling load of three different office buildings with different occupancy type and orientation in Kuwait. The author considered hourly external temperature of previous day as input to the ANN and the output is the predicted hourly cooling load for the next day.

The authors use a building energy simulation software called ESP-r to validate the result and it shows a very good agreement with ESP-r estimation with a coefficient of determinant (R^2 value) around 0.95. The authors also point out the advantage of ANN over ESP-r as ANN requires far less inputs, such as weather data, compare to the ESP-r software. Neto and Fiorelli (2008) compared the performance of feedforward ANN with the energy simulation software, EnergyPlus, to predict the daily energy consumption of a building. The authors considered two different ANN models with dry bulb temperature as the input data for the first model and dry bulb temperature, relative humidity, global solar radiation and diffused solar radiation as the input of the second model. In both cases, the output is daily energy consumption. The results show that ANN models achieve around 90% mean accuracy when compared to the actual consumption data and EnergyPlus models achieve around 87% accuracy. Moreover, both the models of ANN produce very close result that support the findings of Ben-Nakhi and Mahmoud (2004) regarding the capability of ANN in terms of producing accurate prediction with less inputs. Naji *et al.* (2016) also found similar agreement in the performance ANN compare to EnergyPlus result. Martellotta *et al.* (2017) combine ANN with EnergyPlus to predict energy consumption of any given house combining weather data and monitoring data from low-cost sensors where the house is modelled using EnergyPlus to generate training data and the ANN estimation is validated using energy bills. The result shows that the prediction accuracy of ANN is above 95% in 92% cases. Similar approach of combining ANN with the software called TRNSYS also shows very good result in favour of ANN with R-square value of more than 0.92 (Wang, Lee and Yuen, 2018). Yokoyama, Wakui and Satake (2009) obtained similar performance of ANN as Neto and Fiorelli (2008), where the hourly cooling energy demand of a commercial building has been predicted with 90% accuracy using a simple feedforward neural network containing single hidden layer. A feedforward neural network with similar

architecture (i.e., with single hidden layer) has been used to predict heating demand in Turkish houses where the result shows the ANN achieves very high accuracy ranging from 94.83% to 98.51% (Ekici and Aksoy, 2009). Biswas, Robinson and Fumo (2016) showed that ANN is capable of predicting overall energy demand of a residential house with significant accuracy (R-square value between 0.87 to 0.91). Zhang *et al.* (2015) attempted to project the thermal performance of a pre-retrofitted office building to estimate the energy savings due to retrofitting using a similar ANN architecture used by Ben-Nakhi and Mahmoud (2004). The authors compared three other regression models namely: change-point regression model, Gaussian process regression model (GPM) and Gaussian Mixture Regression Model (GMM) with ANN. The result shows that significant accuracy is attained by all models. Although ANN's performance was slightly lower (2.35%) than the other three models, the accuracy of it is found to be within the acceptable limit of current industry practice and hence the author argued in favour of ANN as it is easier and simpler to construct ANN model than other models which offset the reduction of accuracy compared to other methods. Deb *et al.* (2015) compared the performance of feedforward neural network and Adaptive Neuro Fuzzy Interface System (ANFIS) to predict cooling load consumption in three buildings in Singapore and it found both methods showed very high performance with R-square value of 0.98 and 0.97 for ANN and ANFIS respectively. The extended study by the same authors shows that ANN achieves more than 97% accuracy and it is possible to successfully predict the cooling load for next 21 days utilizing five days previous data as input to the ANN (Deb *et al.*, 2016). Platon, Dehkordi and Martel (2015) compared the performance of ANN and Case Base Reasoning (CBR) for hourly electricity demand of up to 6 hours future span and it is found from the result that the ANN (7% error) is far better than CBR (13% error). The research of Chae *et al.* (2016) shows that feedforward neural network is capable of predicting electricity loads for 15 minutes future time span with an

accuracy of 90%. Farzana *et al.* (2014) use a recurrent neural network called Non-linear Auto Regressive neural network (NAR) to predict annual household energy consumption as well as annual household electricity consumption and compared the performance of neural network with the performance of different statistical model. The authors found that ANN has the best prediction accuracy with mean relative percentage error of 9% in both cases. Another use of recurrent neural network is found where a Nonlinear Auto Regressive neural network with exogenous input (NARX) is used to operate the control system of air handling units in an airport and the application of ANN reduces the energy consumption up to 28% a day and around 10% a month (Huang, Chen and Hu, 2015). Yildiz, Bilbao and Sproul (2017) conducted a comparative performance study among feedforward neural network, NARX, regression tree and Support Vector Machine (SVM) to predict hourly electricity demand. The result of the study shows that feedforward neural network achieves the best performance on daily peak load forecast and NARX neural network shows the best performance for hourly load forecast for one day in advance. Kim and Cho (2019) showed the successful use of LSTM neural network for predicting the household electricity consumption. Zheng, Chen and Luo (2019) showed that the use of LSTM neural network for predicting energy consumption by domestic electrical appliances could result in over 90% accuracy in some cases. Other than feedforward and recurrent models of ANN it also found some customized ensembled network capable of predicting electricity consumption with significant accuracy in buildings located in USA and China (Li *et al.*, 2018; Wang, Wang and Srinivasan, 2018). ANN has been successfully used in modelling heat transfer in supercritical fluids (Chang *et al.*, 2018) and estimating the thermal diffusivity coefficient of thermal insulating materials (Chudzik, 2012). The relationship between input variables and heating consumption is very complex and therefore, to estimate buildings' energy consumption, which is essential for energy supply strategy and capital investments, energy industry can benefit from using

neural networks' capability for this type of predictions (Jovanović, Sretenović and Živković, 2015).

2.6 Summary

The literature review on wall insulation shows that the wall insulation has a vital role on the energy performance of a building however, the effectiveness of the wall insulation depends on the type of insulation used, local climate and the geographical location of the building. Infrared thermography is an effective tool to rapidly evaluate the thermal performance of a building in a noncontact way which is further established through the review of literature on infrared thermography in this chapter. From literature review on the different approaches of U-value measurement, it is found that significant efforts have been made to estimate U-value under both laboratory condition and in-situ. There are mainly two methods found for in-situ U-value measurement. These are Heat flux meter (HFM) method governed by ISO 9869 and Infrared Thermovision Technique (ITT). Apart from that Sørensen (2010) developed U-value meter. All these methods have some limitations which is discussed at the end of relevant sections. The review on ANN shows that ANN is capable to map complex and nonlinear relationship among different parameters which is utilised to simulate the energy performance of buildings by many researchers. It is also found that ANN archives significant accuracy compared to the existing building simulation software in predicting the energy performance of buildings. However, there are limited research found in relation to integrating infrared thermography with neural networks. Therefore, there is a scope to develop a novel approach by combining thermography and ANN to overcome the limitation of existing U-value measurement methods.

Chapter 3: Methodology

3.1 Introduction

From previous chapter it is found that wall insulation has a positive impact on energy savings in buildings; however, the performance is not consistent. It is also revealed from the literature review that the existing U-value estimation methods have some limitations such as dependency on seasons, extended monitoring periods and so on. Moreover, there is a research gap that exists in relation to integrating thermography and Artificial intelligence for evaluating thermal performance of buildings as well estimation of U-value of buildings' wall. Artificial Intelligence based prediction requires less physical information about the building which in turns makes it a faster and more economical process than conventional methods. A review on Artificial Intelligence based buildings' energy consumption forecasting reports 25 case where ANN is used for building energy prediction which is 41% of the total study and hence ANN could be considered as the most widely used building energy prediction method (Wang and Srinivasan, 2017). Moreover, Deb *et al.* (2017) state that the ANN is more suitable in buildings' energy consumption prediction than conventional statistical methods because it has the capability of mapping complex relationship between inputs and outputs and it does not require any prior knowledge of input output relationship. In the current research the effect of wall insulation in the change in energy consumption due to working from home is mathematically modelled as well as the feasibility of integrating infrared thermography with ANN is investigated in relation to the development a novel evaluation tool to predict heat losses through buildings' wall and the development of a novel product to estimate U-value of buildings' wall. Considering the key limitations of the existing U-value estimation methods, the feasibility of the application of a point heat to create the necessary temperature gradient is also investigated. The following

two sections describe the detailed methodology to achieve the aim and objectives and the potential contribution to knowledge.

3.2 Methodology of the Research

The aim and objectives of the research is discussed in section 1.3 and 1.4 and the methodology adopted to achieve the objectives are discussed in this section. The methodology adopted for this research consists of three levels which is schematically presented in Figure 3.1. The first level includes the review of literature and evaluation of the influence of wall insulation in the household energy demand due to the Covid-19 pandemic situation where people are required to work from home.

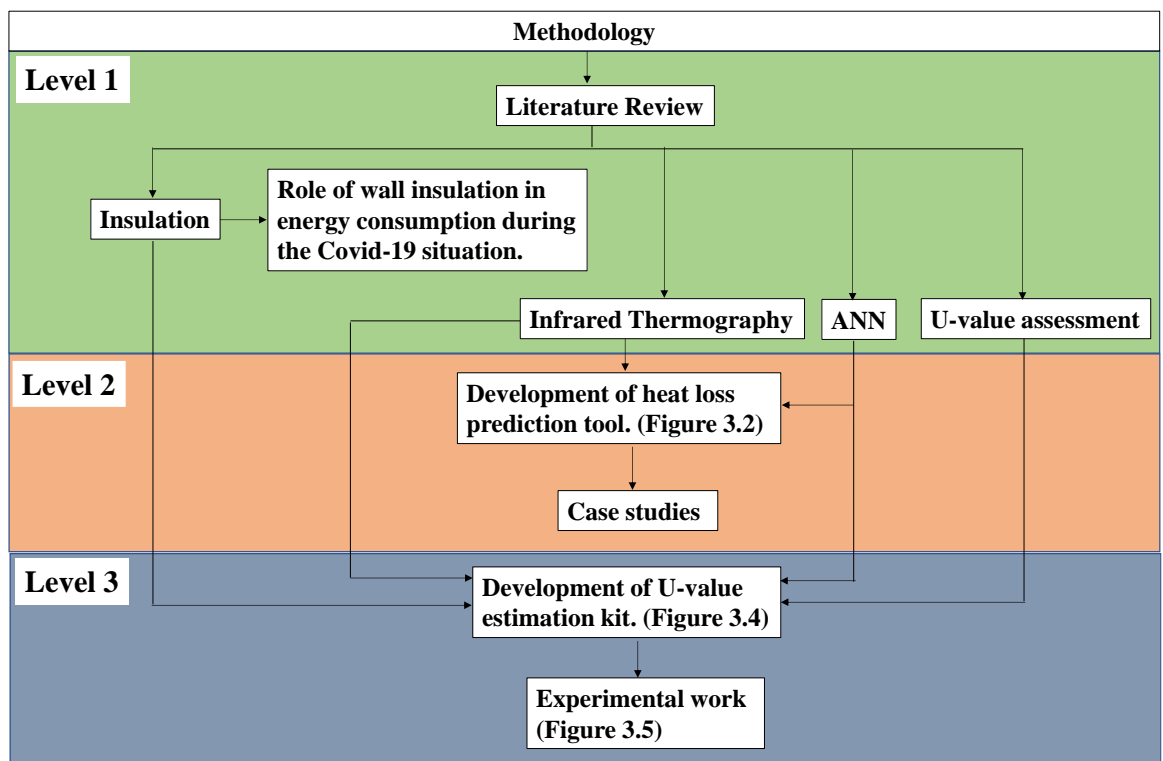


Figure 3.1: Schematic representation of the research methodology adopted for this PhD thesis.

The second level includes the development of a tool to predict heat loss through buildings' wall combining infrared thermography and ANN. The detailed steps of this level are shown

in Figure 3.2. The third and final level involves the development of a novel U-value estimation kit by combining infrared thermography and ANN with the application of a point heat and conduct experiments with this kit for the estimation of in-situ U-value in real buildings. The schematic arrangement of the U-value kit is shown in Figure 3.4 and the steps to conduct the experimental works are detailed Figure 3.5.

3.2.1 Literature Review

The literature review starts with review of wall insulation and its impact on heating and cooling energy savings, as wall insulation significantly lowers the U-value of buildings' wall as well as heat flow through the walls. Next, the basic principle of infrared thermography is reviewed with some of the uses of it in the evaluation of buildings' thermal performances. Afterwards detailed reviews on existing U-value measurements methods are conducted including the basic theory behind those methods and the common equipment used for those. The limitations of existing U-value measurement methods are summarised from these reviews so that these can be considered for the design and development of the novel U-value estimation kit. Finally, the basic principle of ANN, its application in the evaluation of building's energy performance and the performance of ANN compared to other energy simulation software are reviewed.

3.2.2 Role of Wall insulation in Energy consumption due to Covid-19 Situation

Wall insulation in buildings contributes to reduce the household heating energy consumption during winter by restricting heat loss through walls. In a building, heat loss through the walls can be estimated from the product of the U-value of the wall, the wall surface area exposed to the external environment and the temperature difference between indoor and outdoor environment as presented in equation 3.1 (Moran *et al.*, 2003).

$$Q = UA(T_{in} - T_{out}) \quad (3.1)$$

Here Q refers to the heat loss through a wall for an hour, U refers to the U-value of the wall, A is the surface area of the wall exposed to the external environment and T_{in} and T_{out} are the indoor and outdoor temperatures, respectively. Assuming a suitable indoor temperature, for instance 21°C for an occupied house and 15°C for an unoccupied house, the difference in heat loss E_h between an occupied and an unoccupied house can be estimated using equation 3.2.

$$E_h = \sum(Q_{21} - Q_{15}) \times 10^{-3} \text{ kWh} \quad (3.2)$$

The range of summation can be selected based on the period of interest. For example, in current research E_h has been calculated by summing up the difference in heat loss between 9.00 to 17.00 hours for the weekdays in a month. Assuming the heat loss through walls is equal to the heating demand, the heating energy bills can be estimated by multiplying E_h with the unit price of energy. Similarly, energy demand due to the use of electrical appliances E_e can be estimated from equation 3.3 and respective energy bills can be estimated by multiplying E_e with the unit price of energy.

$$E_e = P_e \times H \times D \times 10^{-3} \text{ kWh} \quad (3.3)$$

Here, P_e is the power required for an electric appliance, H is the hours of operation for an electrical appliance per day and D is the number of days the appliance is in use in a month. The increase in household energy demand for different dwelling types in England with different U-values has been evaluated and compared considering that the Covid-19 pandemic situation would be forcing people to work from home during next winter. Also, the increase in carbon emission due the production of these excess energy is estimated by multiplying E_h and E_e with the unit rate of CO₂ emission for the respective energy productions. The extended scenario of change in household budget and net carbon emission due to the

reduction in travelling is analyzed considering the drop in car milage, fuel cost and CO₂ emission rate per mile.

3.2.3 Development of heat loss prediction tool

Heat loss can be predicted by combining infrared thermography and ANN with reasonable accuracy in short period of time (Al-Habaibeh, Sen and Chilton, 2020). The steps involved in the development of heat loss prediction tool by combining infrared thermography and ANN is presented in Figure 3.2.

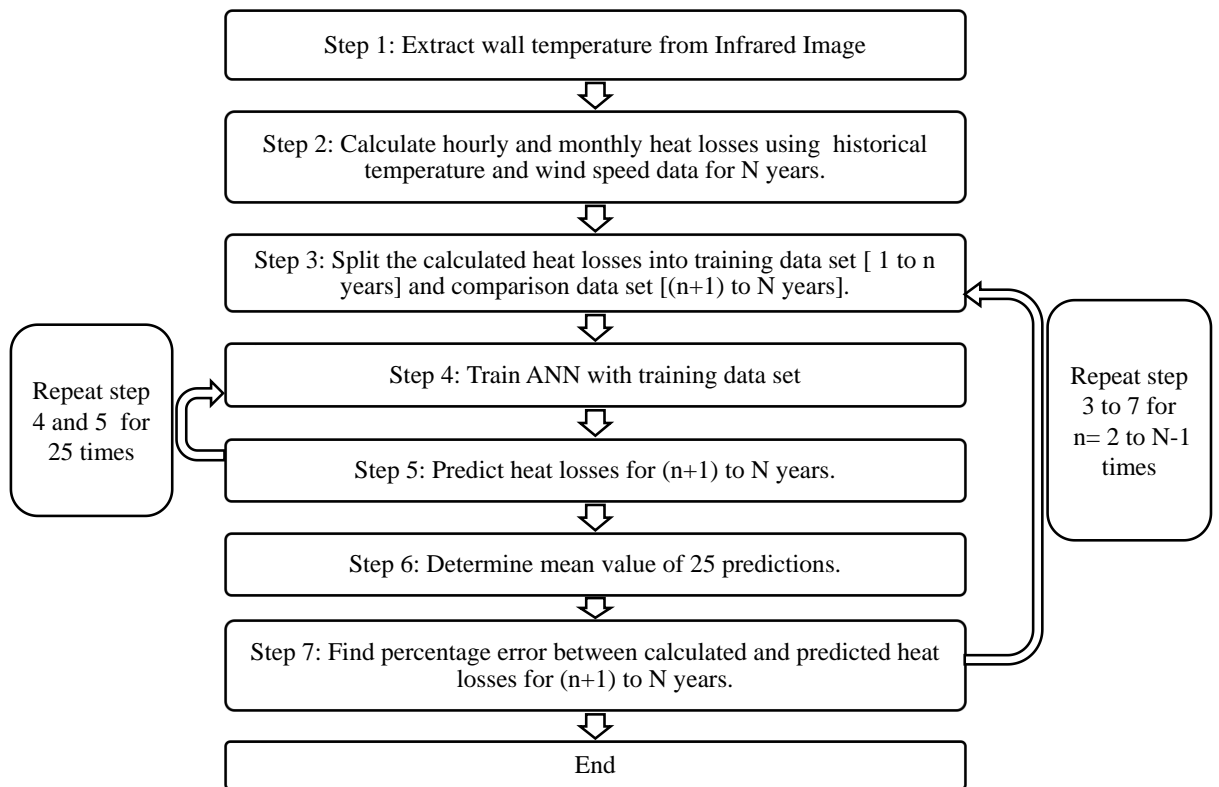


Figure 3.2: Schematic representation of the research methodology adopted for this PhD thesis.

To calculate the heat loss through per square meter of a building's wall, the thermal power approach developed by Albatici and Tonelli (2010) is considered which is discussed in Chapter 2 and presented using equation 2.8.

$$P = 5.67\varepsilon_{tot} \left(\left(\frac{T_s}{100} \right)^4 - \left(\frac{T_{ext}}{100} \right)^4 \right) + 3.8054v(T_s - T_{ext}) \quad (2.8)$$

In equation 2.8, which is presented above again, the outdoor temperature T_{ext} and the wind speed v are extracted from the weather station observations database of the UK Met Office, (2019) on hourly basis. The external wall surface temperature T_s is obtained from an infrared image captured using a high-resolution infrared camera. Assuming the indoor temperature to be constant, the external wall surface temperature will vary linearly with the outdoor temperature. If we consider the indoor temperature in a building is constantly maintained at 20°C throughout the year, the external wall surface temperature will be the same when the temperature in outdoor environment reaches at 20°C. Considering the external wall surface temperature with respect to the respective outdoor temperature at the time when the infrared image is captured as the first point and 20°C as the second point, a linear curve can be generated for any wall type as shown in Figure 3.3. The external wall surface temperatures required for the calculation of heat loss using equation 2.8 are extracted from this curve at different outdoor temperatures.

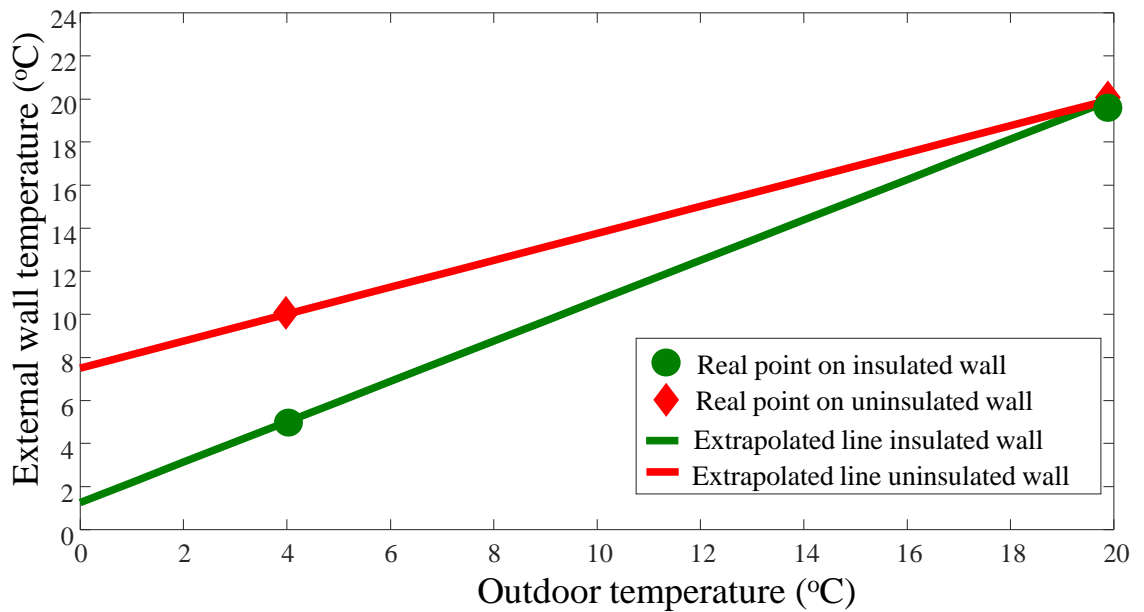


Figure 3.3: Relationship between outdoor temperature and external wall temperature

The emissivity, ε_{tot} , for plastered brick wall is considered as 0.93 (CIBSE, 2006). If 1 W/m^2 heat is radiated for one hour, it will be equivalent to 1 Wh/m^2 of heat energy transfer. Therefore, the value of P for each hour, calculated from equation 2.8, can be considered as the hourly heating energy loss through per square meter of a building's wall. The average heat loss in any given hour i in a given month j through per square meter of a wall, P_{ij} , can be expressed as:

$$P_{ij} = \frac{1}{n} \sum_{n=1}^D P_i \quad (3.4)$$

Where, $i = 00:00$ to $23:00$; and $j = \text{January to December}$.

Here, D represents the number of days in j^{th} month of a given year and P_i represent the heat loss at i^{th} hour of each day in j^{th} month obtained using equation 2.8. Similarly, the total heat loss in each calendar month in a year is the summation of hourly heat losses in that month and can be expressed as,

$$P_m = \sum_1^D \sum_1^{24} P \quad (3.5)$$

Here P_m is the total heat loss through a building's wall in a calendar month, D is the number of days in that month and P is the hourly heat loss obtained using equation 2.8. The hourly average heat loss and the monthly total heat loss for N years are calculated using the historical local weather data and these are split into training and test data sets respectively for the neural network analysis. The formation of training and test data set are made with different combinations starting from 2 years to $N-1$ years. For example, if the training data set is composed of 2 years' data, the test data set is composed of $N-2$ years' data; if the training data set contains 3 years' data, the test data set contains $N-3$ years' data and so on. The formation of different combinations of training and test data sets for ANN analysis facilitates to answer the fourth research question regarding the monitoring period required to evaluate the buildings' heat loss characteristics. A mathematical model in relation to that is also develop which is presented in chapter 5. The training data set is used to train the

neural network and the test data set is used to test the performance of neural network. The performance evaluation is conducted considering percentage errors. The error and percentage errors are calculated using equation 3.6 and 3.7, respectively.

$$e = \sum_{i=1}^n (Y_i - P_i) \quad (3.6)$$

$$e_p = \frac{|e|}{\sum_{i=1}^n P_i} \times 100 \quad (3.7)$$

Here e is error, e_p is percentage error (PE), Y is ANN predicted heat loss and P is calculated heat loss from equation 3.4 for hourly averaged heat loss and the same from equation 3.5 for monthly total heat loss, respectively. The value of n is 288 (24×12) in case of hourly average heat loss and 12 in case of monthly total heat loss. A sensitivity analysis is done at the beginning to look at the best ANN architecture in terms of number of layers and the number of neurons in each layer for both hourly average and monthly total heat loss predictions. Two case studies have been conducted applying this methodology to predict heat loss in an insulated building and an uninsulated building in England which are presented in Chapter 5.

3.2.4 Development of U-value Estimation Kit

The proposed U-value kit monitors a test wall using infrared camera with the application of a point heat source as presented in Figure 3.4. During the application of point heat, the heat transfer through an uninsulated wall with high U-value will be higher than the heat transfer through an externally insulated wall with low U-value. As a result, the heat dispersion on the internal surface of the externally insulated test wall will be higher than that of the uninsulated test wall. The infrared images, captured from the internal side of a test wall at a constant interval, could provide information about the heat dispersion and those can be related to the prediction of U-value of the test wall. However, the visual inspection may not provide reasonable information always. Therefore, a suitable thermal profile generated from

the series of infrared images can be analysed with ANN to estimate U-value. The detailed development process of the U-value kit is presented in Chapter 6.

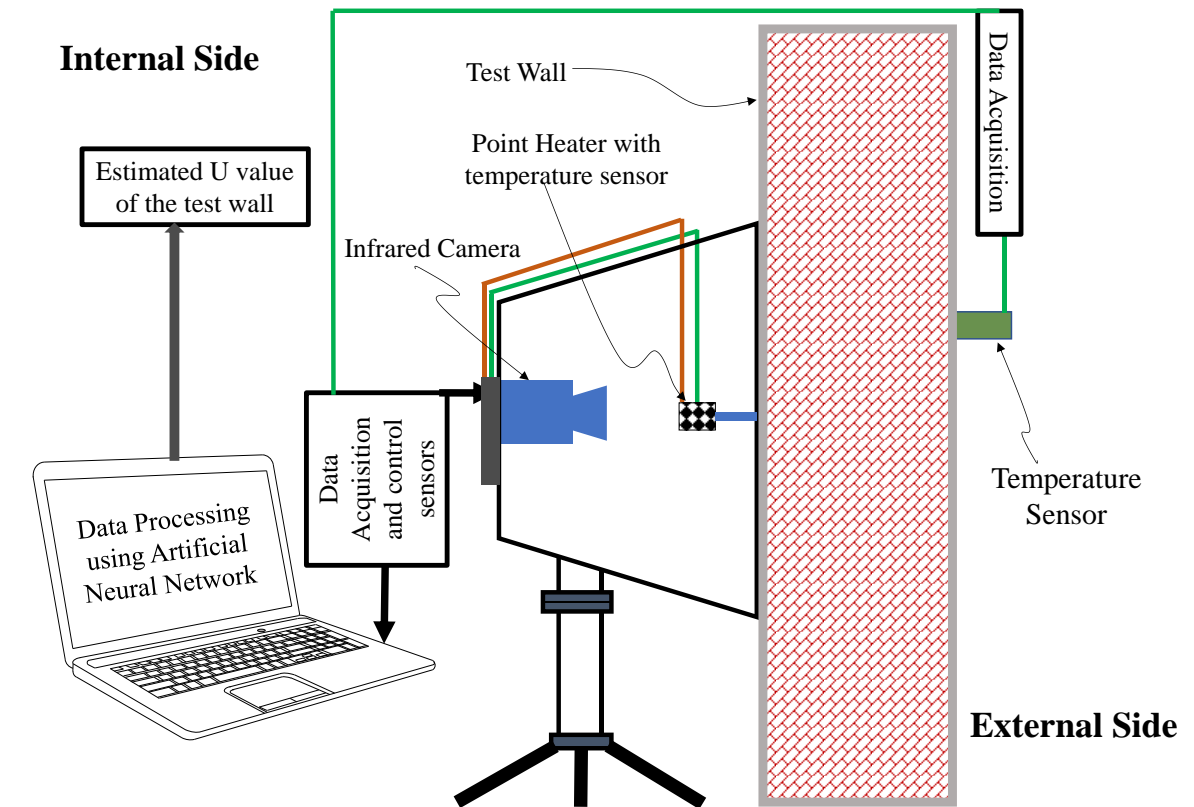


Figure 3.4: Schematic diagram of the experimental setup.

The steps followed for the experimental work are shown in Figure 3.5. The experimental works are conducted in two phases. In the first phase the experiments are conducted at laboratory on small scale test walls with different U-values. These data are used to train the neural network. The trained neural network is then used to analyse the infrared data obtained from the experiments conducted in real buildings' wall for the estimation of U-value of those walls. The performance of neural network is evaluated in terms of absolute percentage deviation as presented in equation 3.8.

$$e_d = \frac{|U_p - U_c|}{U_c} \times 100\% \quad (3.8)$$

Here e_d is the absolute percentage deviation, U_p is the ANN predicted U-value and U_c is the calculated U-value determined using equation 2.3. The results of the experimental works with detailed discussion are presented in Chapter 7.

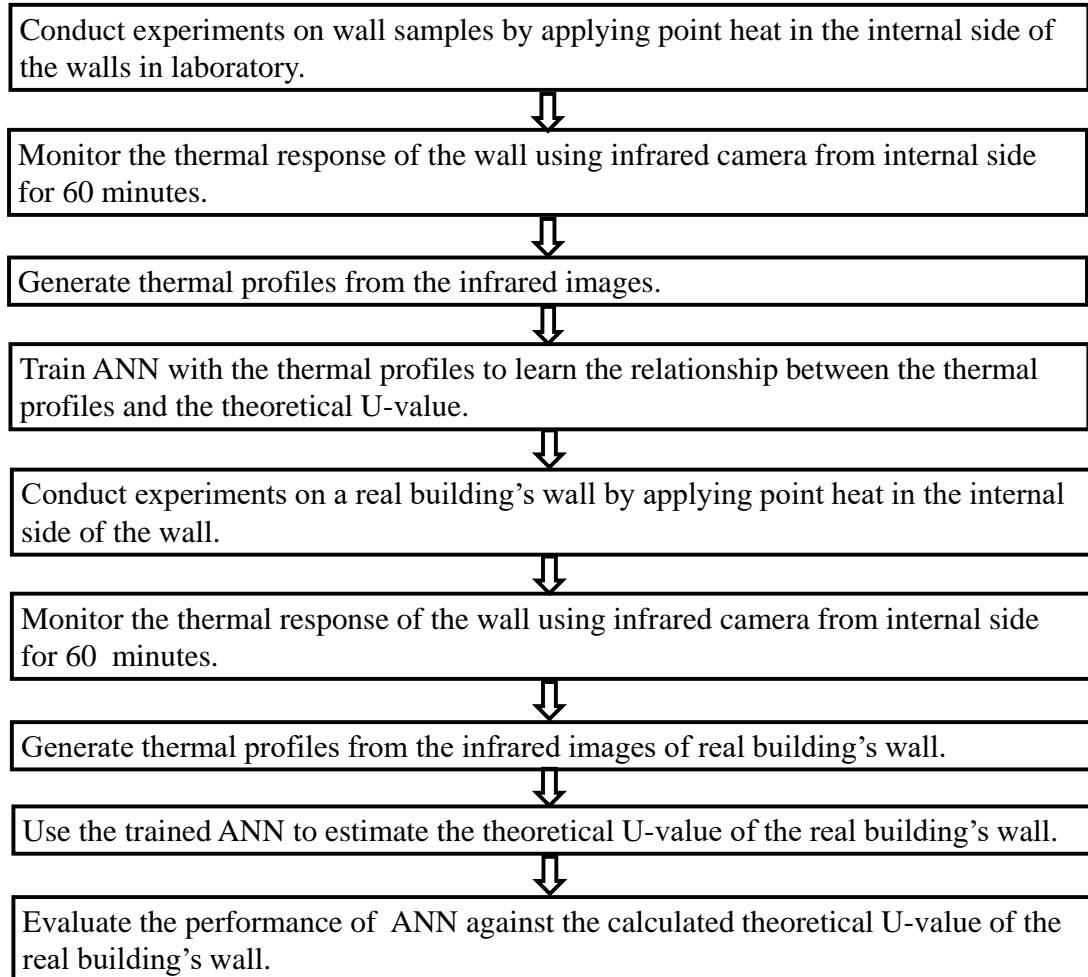


Figure 3.5: Schematic representation of the experimental work with the proposed U-value kit.

3.3 Potential Contribution to the Knowledge

The potential contribution to the knowledge is listed below:

1. A mathematical model to evaluate the influence of wall insulation on the change in household energy demand and related carbon emissions during winter where people are required to work from home due to Covid-19 pandemic situation.

2. A mathematical model to explain the monitoring period required for the successful prediction of heat loss through a building's wall.
3. Development of a tool to predict heat loss through a building's wall by combining infrared thermography and ANN.
4. Development of a novel U-value estimation kit combining infrared thermography and ANN with the application of a point heat.
5. Evaluation of the performance of the novel U-value estimation kit.

3.4 Summary

This chapter presents the detailed methodology developed for the current PhD research work. The research aims to develop novel techniques for the assessment of the benefits of thermal insulation in buildings with the help of mathematical models, integration of thermography and ANN and development of a product that can estimate U-value of buildings' wall by combining infrared thermography, ANN alongside the application of a point heat source. The methodology developed for the research contains three levels. The first level of the methodology includes a comprehensive literature review as well as evaluation of the change in household energy demand as a result of people working from home due to Covid-19 pandemic situation, its impact on household expenses and net carbon emission related to this. The second level explains the methodology of development of a prediction tool for heat loss through buildings' wall by combining infrared thermography and neural network. In the third and final level, the development of the novel U-value estimation kit using infrared thermography and ANN as well as the steps to carry out the experimental works are presented.

Chapter 4: The Role of Wall Insulation on Household Energy demand, Carbon Emission and Household Budget in English Dwellings due to Covid-19 Lock Down Situation During Winter

4.1 Introduction

The rapid spread of novel corona virus disease is forcing Governments in many countries to impose lock down restrictions at various levels, and as a result, majority of people are in a situation to work from home to some extent. In cold countries, the heating energy demand rises significantly during winter as space and water heating is responsible for very high energy consumption. Considering a lock down situation that confines people to work from home during winter would further increase the heating energy demand and result in excess carbon emission due to consumption of these excess energy. The literature review shows that wall insulation significantly reduces heating energy demand by limiting heat loss through buildings' wall. Therefore, people living in a well insulated house are expected to see minimum rise in energy demand and energy bills compared to those who are living in a poorly insulated house. However, the reduction in travelling to work would compensate the expenditure on energy bills as well as net carbon emission. As the new working pattern is still in its early stage, limited research has been conducted on the effect of household budget for energy consumption and carbon emission due to this. In this chapter, the change in household energy demand during winter in different English dwelling types with different U-values of wall is presented. Following that, the effect on household budget and net carbon emission due to the new work pattern has been analysed. The methodology adopted for this study is presented in Chapter 3. However, the assumptions and the equations associated with

the study are presented in next two sections. After that, the result and discussion are presented with a brief conclusion.

4.2 Assumptions and reference values

To estimate the heat loss through a building's wall for the winter of 2020-21, the outdoor ambient temperature distribution is assumed to be same as 2019. The next assumption is that the indoor temperature is constantly maintained at 15°C when the house is unoccupied and at 21°C when the occupants are working from home. It is also assumed that all the buildings are centrally heated with gas fired boiler and heat loss through walls represent the heating demand. In this study, only the reference U-values of buildings' walls presented in Table 4.1 from BRE (2016) are considered.

Table 4.1: Reference U-values of buildings' wall BRE (2016).

Wall Types	U-value (W/m ² K)
Solid wall in very old buildings (pre 1900)	2.30
Solid wall in old buildings (pre 1976)	1.70
Unfilled cavity wall	1.50
Solid wall with 100mm thick external insulation	0.32
Filled Cavity wall with 100 mm thick external insulation.	0.25

There are some reference values considered to facilitate the estimation process such as, unit prices of energy, CO₂ emission rate due to the production and consumption of energy, electricity consumption by some electrical appliances and fuel cost for a car. These references and their relevant sources are listed in Table 4.2. One of the key parameters that influence the overall heat loss through walls in a dwelling is the wall surface area exposed to the outdoor environment. The average wall surface area exposed to the external environment for different dwelling types and the number of uninsulated solid wall dwellings in England are collected from the study conducted by Loucari *et al.* (2016).

Table 4.2: The reference values used in for estimation and their sources.

Sl. no	Assumptions	Source
1.	The price of gas is 3.9 pence per kWh.	United Kingdom natural gas prices (no date).
2.	The price of electricity is 14.37 pence per kWh.	UK Power (no date).
3.	The CO ₂ emission due to electricity consumption is 0.277 kg/kWh.	Department for Business Energy & Industrial Strategy (2019).
4.	The CO ₂ emission due to domestic space heating by burning natural gas is 0.203 kg/kWh.	Campbell (2020)
5.	Fuel cost per mile for petrol is 12 pence and for diesel is 10 pence considering 1400 cc to 2000 cc engine.	HM Revenue & Custom (2020).
6.	Average CO ₂ emission by a newly registered car in the UK is 121.3 grams/ km which is equivalent to 0.195 kg/mile.	Department for Transport Statistics (2015).
7.	Electricity consumed by a TV (42-inch LCD) is 120 watts.	Energy Use Calculator (2020)
8.	Electricity consumption for a desktop computer is 150 watts.	Smarter Business (2019)
9.	Electricity consumption for a laptop is 50 watts.	Smarter Business (2019)
10.	Time required to boil 1litre water from room temperature with a 2-kW electric kettle is about 2 minutes and 45 seconds or 0.046 hours.	Shearman (no date)

4.3 Equation used for the estimation of energy demand

Equation 3.1, 3.2 and 3.3 from the methodology chapter are used to estimate the energy demands which are presented below:

$$Q = UA(T_{in} - T_{out}) \quad (3.1)$$

$$E_h = \sum(Q_{21} - Q_{15}) \times 10^{-3} \text{ kWh} \quad (3.2)$$

$$E_e = P_e \times H \times D \times 10^{-3} \text{ kWh} \quad (3.3)$$

Equation 3.1 is used to estimate the heat loss a buildings wall. The type of the buildings considered are end terraced, mid terrace, semi-detached, detached and bungalow with the wall surface area of 138 m², 103 m², 159 m², 257 m² and 152 m² exposed to the outdoor environment, respectively Loucari *et al.* (2016). The U-values considered in equation 3.1 are listed in Table 4.1. Equation 3.2 is used to work out the difference in heat loss if the indoor temperature of a building is maintained at 21°C and 15°C, respectively. Equation 3.3 is used to estimate the electrical power consumption due to the use of appliances such as TV, desktop, laptop, electric kettle and lighting a building. The reference values for the power consumption by those appliances are listed in Table 4.2. The average number of weekdays between 1st October and 31st March has been taken into consideration for the estimation of monthly average energy demand with 8 hours of working time each day between 9.00 to 17.00.

4.4 Effects on household energy demand and budget:

The increase in heating energy demand in different dwelling types with different U-values are presented in Table 4.3. It is noticed from Table 4.3 that the solid wall dwellings with high U-values of wall tend to consume high energy and the externally insulated dwellings with low U-values of wall consume less energy for space heating. A high U-value of wall represents poor wall insulation that results in high heat loss through the wall and therefore, responsible for the consumption of high heating energy. On the other hand, the dwellings with low U-values consume far less heating energy as the low U-value of a building's wall represents very good wall insulation.

Table 4.3: Increase in heating energy (gas) demand and energy bill per household because of working from home.

House Type		End terrace	Mid terrace	Semi detached	Detached	Bungalow
Surface area exposed to external environment (m ²)		138	103	159	257	152
Solid wall (U-value = 2.3 W/m ² K)	Average increase in energy demand (kWh/month)	415.47	310.10	478.70	773.74	457.62
	Average increase in energy bill (£/month)	£16.20	£12.09	£18.67	£30.18	£17.85
Solid wall (U-value = 1.7 W/m ² K)	Average increase in energy demand (kWh/month)	307.06	229.19	353.79	571.85	338.22
	Average increase in energy bill (£/month)	£11.98	£8.94	£13.80	£22.30	£13.19
Unfilled Cavity wall (U-value = 1.5 W/m ² K)	Average increase in energy demand (kWh/month)	270.94	202.22	312.17	504.57	298.43
	Average increase in energy bill (£/month)	£10.57	£7.89	£12.17	£19.68	£11.64
Solid wall with external insulation of 100 mm (U-value = 0.32 W/m ² K)	Average increase in energy demand (kWh/month)	57.80	43.14	66.60	107.64	63.66
	Average increase in energy bill (£/month)	£2.25	£1.68	£2.60	£4.20	£2.48
Filled Cavity wall with 100 mm of external insulation (U-value = 0.25 W/m ² K)	Average increase in energy demand (kWh/month)	45.16	33.70	52.03	84.10	49.74
	Average increase in energy bill (£/month)	£1.76	£1.31	£2.03	£3.28	£1.94

Among the dwelling types, detached houses tend to consume more heating energy compared to the other dwelling types of same U-value, because a detached house is exposed to the outdoor environment from all four sides. On the other hand, the mid terrace houses of all U-values are least energy consuming dwelling types because they are exposed to the outdoor environment from two sides only. Looking at the energy bills it is found that the household living in a very old solid wall building with U-value of 2.3 W/m²K will spend 9 times more on heating energy bills than the household living in a modern and well insulated detached house with U-value of 0.25 W/m²K and the difference is around £27 per month. Similarly, in mid terraced houses, the difference in heating energy bills between a very old house with U-value of 2.3 W/m²K and a modern well insulated house with U-value of 0.25 W/m²K is £11 which is again 9 times higher. The end terrace houses, semidetached houses and bungalows also show similar trend in heating energy consumption and the difference in heating energy bills between dwellings with above mentioned U-values are circa £14, £17, and £18, respectively. From the above discussion it is realised that solid wall houses have the highest contribution in terms of consuming excess energy; and considering all the solid wall houses of different dwelling types in England, it is found that these houses are responsible for consuming circa 1500 GWh of excess energy for space heating (Table 4.4). The average U-value of walls for these houses are considered as 1.7 W/m²K as this is the mean U-value of all solid wall houses in England (BRE, 2016). The household electricity demand would also rise due working from home as the occupant would use some electrical appliances, such as TV, desktop, laptop, and electric kettle, for longer hours than usual. Table 4.5 shows the excess electricity consumption due the use of these electrical appliances as well as lighting the house. It is found from Table 4.5 that the average increase in electricity consumption per household per month could be as high as 125 kWh.

Table 4.4: Increase in average monthly energy demand of dwellings with solid wall construction (U-value of 1.7 W/m²K) because of working from home.

House Type	Surface area exposed to external environment (m ²)	Number of dwellings with uninsulated solid brick walls	Average energy demand (GWh/month)
End terrace	138	874,000	268.37
Mid terrace	103	1,725,000	395.34
Semi detached	159	1,265,000	447.55
Detached	257	598,000	341.97
Bungalow	152	138,000	46.67
Total			1499.91

This increase in electricity consumption will be responsible for £17.97 increase in electricity bills per month per household. Considering 23.95 million households in England (Piddington *et al.*, 2020) the additional electricity demand per month would be as high as circa 2994.52 GWh per month as a result of people working from home due to the Covid-19 situation. The total increase in energy demand per month due to working from home will be sum of increase in heating energy demand and increase in electricity demand which is plotted in Figure 4.1-a. Figure 4.1-b shows the associated expenditure on energy bills.

Table 4.5: Increase in monthly electricity demand, electricity bills and CO₂ emission per household because of working from home.

Appliance	Quantity	Power (Watt)	Duration (hours)	Average electricity demand (kWh/month)	Average electricity bill (£/month)	CO ₂ emission (kg)
TV (42" LCD)	1	120	8	20.96	£3.01	5.81
Desktop	1	150	8	26.20	£3.76	7.26
Laptop	2	50	8	17.47	£2.51	4.84
Lighting	5 lights	60	8	52.40	£7.53	14.51
Electric Kettle	4 litres a day	2000	0.046	8.01	£1.15	2.22
Total				125.03	£17.97	34.63

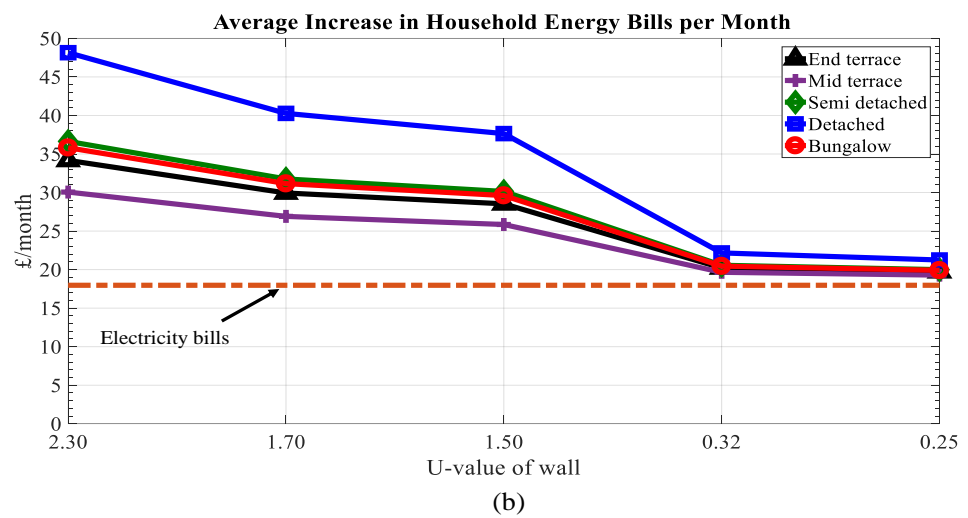
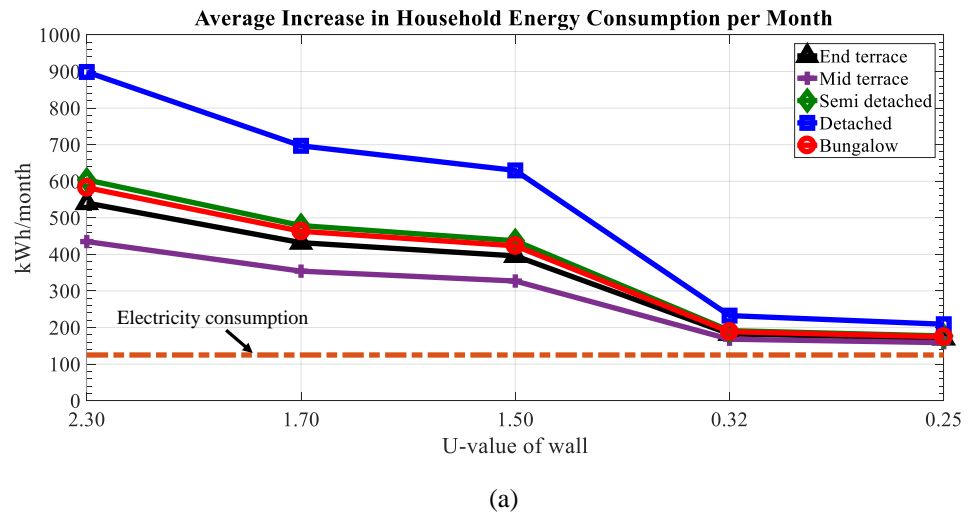


Figure 4.1: Average increase per month in (a) household energy consumption, (b) household energy bills due to working from home in winter.

The dotted line in Figure 4.1-a and 4.1-b represent the rise in electricity consumption and associated electricity bills, respectively. It is noticed from these two figures that for the family living in highly insulated houses, the major portion of the increase in total energy consumption as well as energy bills are due the rise in the electricity consumption. On the other hand, the family living in solid wall dwellings see that the significant portion of their energy bills rise is due to the increased heating energy consumption. The detached houses with solid wall and U-value of 2.3 W/m²K are the most severely affected houses in terms of energy bills with around £47 increase in energy bills per month. It is also noticed in Figure

4.1-a and 4.1-b that the households living in dwellings with externally insulated wall (U-value between 0.32 to .025 W/m²K) show similar pattern of energy demand and energy bills do not differ much based on the dwelling type. However, the pattern of energy demand and energy bills for the households living in dwellings with uninsulated wall (U-value between 2.3 to 1.5 W/m²K) vary widely based on the dwelling types. These point out the benefits of wall insulation particularly to those dwelling types which have higher wall surface area exposed to the outdoor environment. The increase in energy bills could be recovered from savings due to reduced travelling. During the complete lock down situation between 24th March and 24th April 2020, the reduction in car travelling was around 67% (Department for Transport, 2020). On the basis of average car mileage (Yurday, 2020), a typical household with a moderate car (1400 to 2000 cc engine) could see 413.17 miles reduction in car travelling in a month and this reduction in mileage travelled by a car would save £41.32 - £49.58 a month on travel expense depending on the fuel type i.e., petrol or diesel. Figure 4.2-a and Figure 4.2-b presents the net household savings for a family with 1 car and 2 cars, respectively. It is noticed from Figure 4.2-a that the family living in a very old detached house with U-value of 2.3 W/m²K and use one car for travelling spend almost all of their savings from reduced travelling to pay the energy bills. On the other hand, family living in modern externally insulated houses with U-value ranges between 0.32 to .025 W/m²K would experience net savings of £27-£30 due to reduced travelling from one car. If a family uses two cars for travelling, then the net savings ranges between £50-£70 for dwellings with wall U-value of 2.3 W/m²K and between £75-£80 for dwellings with wall U-value 0.32-0.25 W/m²K. It is also noticed that the difference in net savings in mid terraced houses of different U-values ranges between £20 - £30 if the family use one car and between £68 -£80 if they use two cars. On the contrary, for detached houses of different U-values the net savings ranges between £0 to £27 if the family uses one car and between £50 to £77 if the family use

two cars. As a result, the reduction in savings for the household living in a poorly insulated detached house would be 3 times more than the household living in a poorly insulated mid terrace house.

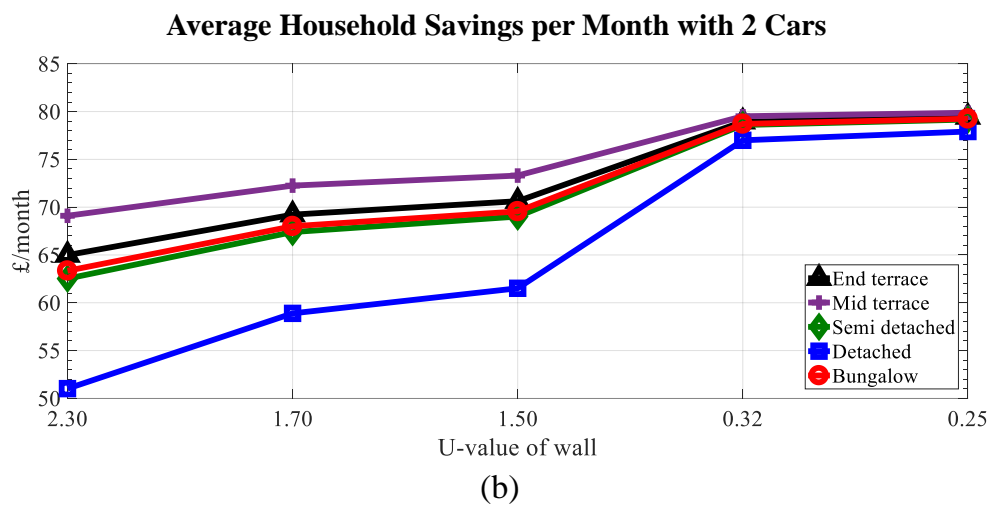
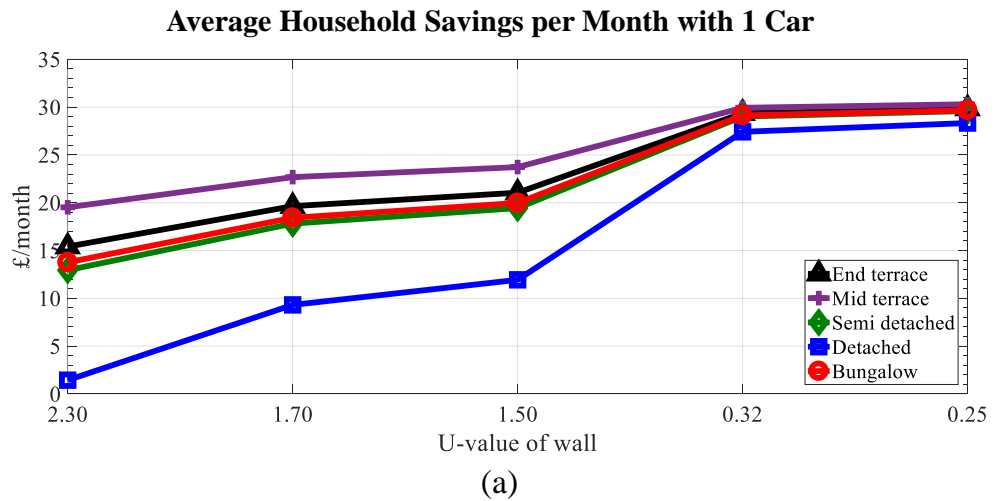


Figure 4.2: Average household savings per month for a family uses (a)1 car, (b) 2 cars for travelling.

4.5 Effects on CO₂ emission

The excess energy production to meet the increased household energy demand in winter due to work from home would result in increased carbon emission to the atmosphere. Figure 4.3

shows the CO₂ emission per month due to the consumption of excess energy among different households listed in Table 4.1.

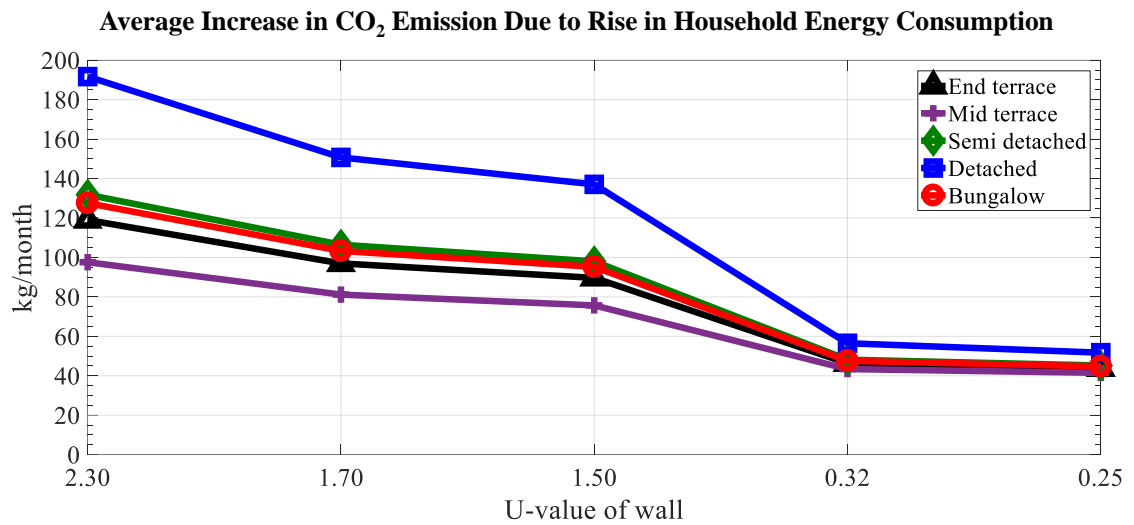


Figure 4.3: Average increase in CO₂ emission per month because of the excess household energy demand during winter

It is found from Figure 4.3 that uninsulated houses with U-value ranges from 2.3 to 1.5 W/m²K are responsible for releasing 80-195 kg of CO₂ per month per household. On the other hand, the insulated houses with U-values 0.32 to 0.25 W/m²K are responsible for releasing 40-60 kg of CO₂ per month per household. As mentioned in Table 4.2, the solid wall houses in England would be responsible for consuming 1500 GWh of excess heating energy per month, the additional heating energy consumption will release circa 304.48 Mt (million ton) of CO₂ in the environment. Similarly, the consumption of 2994.52 GWh excess electricity per month in English households would result in releasing circa 829.48 Mt of CO₂ in the environment. Therefore, the total increase in CO₂ emission per month is circa 1134 Mt. However, the 413.17 miles reduction in car travel per month contributes to 80.66 kg reduction in CO₂ emission; and considering the 32.88 million registered cars in the UK (Driver and Vehicle Licensing Agency, 2020), the estimated total reduction in CO₂ emission is 2652.30 Mt. Furthermore, the electricity consumption in commercial and industrial section

is reduced by circa 2457.85 GWh per month during the lock down situation from March to June (Department for Business Energy & Industrial Strategy, 2020). This reduction in electricity consumption results in the reduction of circa 680.83 Mt of CO₂ emission per month. Although working from home increases the CO₂ emission due to additional household energy consumption, the net CO₂ emissions is expected to be less than the normal working situation due to reduced energy consumption in industrial and commercial sector as well as reduced travelling by car. Figure 4.4-a and 4.4-b shows the net change in household CO₂ emission if a family uses one car and two cars, respectively.

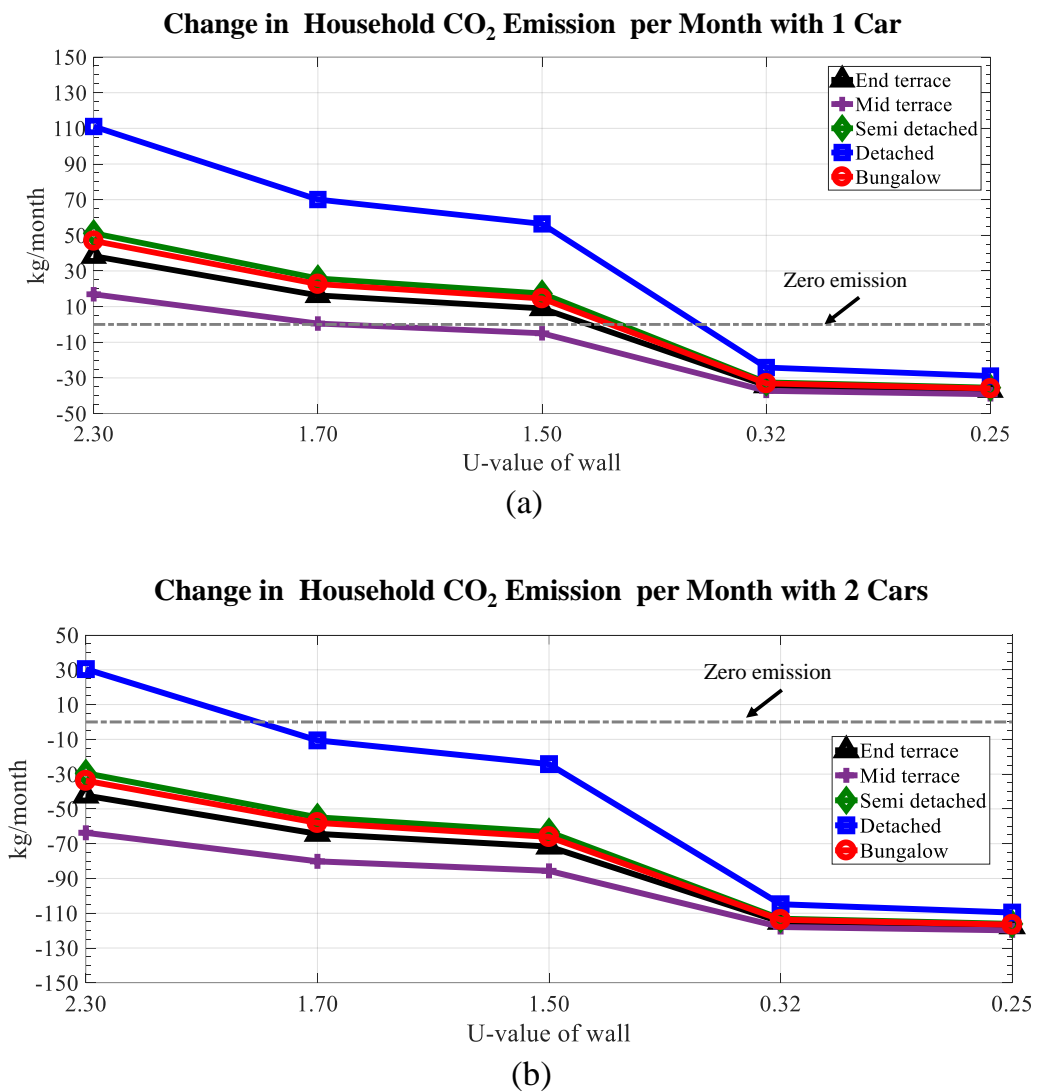


Figure 4.4: Net change in CO₂ emission per month per household that uses (a) 1 car for travelling and (b) 2 cars for travelling

It is found from Figure 4.4-a that end terraced, bungalow, semidetached and detached houses with uninsulated walls (U-value ranges from 2.3 to 1.5 W/m²K) do not contribute to net reduction of carbon emission and among them the detached houses are responsible for 50-110 kg of CO₂ release per month per household. Among the different wall U-values in mid terrace houses, only the very old house with U-value of 2.3 W/m²K is responsible to release CO₂ and at the rate of circa 15 kg per month per household. The externally insulated houses with U-value ranges from 0.32 to 0.25 W/m²K significantly contribute to the net reduction of carbon emission by releasing 15 to 40 kg less CO₂ per month per household than the normal working situation. From Figure 4.4-b it is found that the all the households using two cars for travelling contribute to the reduction in net carbon emission except the very old solid wall detached house with U-value of 2.3 W/m²K. The externally insulated houses with U-value ranges from 0.32 to 0.25 W/m²K show the major contribution by reducing more than 100 kg CO₂ per month per household.

4.6 Conclusion

Working from home due the present Covid-19 situation leads to rise in domestic energy demand; however, family living in externally insulated houses will not experience significant increase in energy bills. Instead, they will experience budget savings from reduced travelling. However, if people either walk or use bicycle for travelling to their workplace, then they will not experience any savings from travelling expenses. Among the different dwelling types, the household living in uninsulated detached houses will experience the highest increase in energy bills as well as these houses are responsible for significant amount of CO₂ emission in most of the cases. Modern and insulated homes will provide a much better financial advantage during lockdown situation (or during working from home) and the increase in heating bills will be as low as £1.31 for mid terrace houses and £3.28 for detached houses. The overall national energy demand may fall due the reduction in energy

consumption in commercial and industrial sectors. These as well as reduction in car travelling would result in a substantial amount of reduction in CO₂ emission. Therefore, the current working patterns could be continued to some extent even after the end of the pandemic situation in the UK as a part of the strategy to achieve net zero carbon emission by 2050. However, people living in uninsulated houses and already suffering from energy poverty will experience worse financial situation due to working from home hence require attention to their cases.

Chapter 5: Development of a Prediction Tool to Estimate Heat loss through walls using Infrared Thermography and Artificial Neural Network

5.1 Introduction

The energy consumption for space heating in a building largely depends on the thermal performance of the building's wall. In previous chapter, the role of wall insulation in reducing heating energy consumption and restricting heat loss through buildings' wall has been reviewed as well as the influence of insulation in energy consumption has been evaluated under the work from home condition. The need for retrofitting a building with improved wall insulation has been realised from those discussions. However, prior to that, the prediction of future energy savings due to retrofitting a building with improved insulation would be a key area of interest for the estimation of cost savings and payback periods. In this chapter, the development of a prediction tool for the estimation of heat loss through buildings' wall using infrared thermography and ANN is presented. Infrared thermography has been used in many studies for the rapid evaluation of thermal performance of buildings and some of those are reviewed in chapter 2. The suitability of ANN for the prediction of energy demand in buildings are also reviewed in chapter 2 and in most of the cases the performance of ANN is very close to other popular simulation software. There is limited research found regarding combining ANN with infrared thermography to predict future heat loss in a building. In a publication as a part of the current PhD study, the use of ANN in combination with infrared thermography to predict future heat loss through insulated and uninsulated building's wall has been established which is included in Appendix E (Al-Habaibeh, Sen and Chilton, 2020). In continuation with that study, the development of an evaluation tool by integrating infrared thermography and ANN is demonstrated in this

chapter with two case studies. Moreover, the performances of different neural network architecture are compared in case of hourly and monthly heat loss prediction in insulated and uninsulated buildings.

5.2 Implemented approach

The methodology used in this work has been discussed in chapter 3. Infrared thermography is used to evaluate the thermal characteristics of buildings with insulated and uninsulated wall and to estimate heat loss through those walls. The historical heat losses are calculated to train ANN which is later used to predict future heat loss through insulated and uninsulated wall. The ANN predicted heat loss is compared with the calculated heat loss to evaluate the performance of ANN. The equations used to for the heat loss calculation and evaluation of ANN performance are presented again in the section below.

5.2.1 Equations used for the study

The heat loss through per square meter of a building's wall is calculated using equation 2.8.

$$P = 5.67\varepsilon_{tot} \left(\left(\frac{T_s}{100} \right)^4 - \left(\frac{T_{ext}}{100} \right)^4 \right) + 3.8054\nu(T_s - T_{ext}) \quad (2.8)$$

The hourly heat loss in a given month is calculated using equation 3.4.

$$P_{ij} = \frac{1}{n} \sum_{n=1}^D P_i \quad (3.4)$$

The monthly total heat loss is estimated using equation 3.5.

$$P_m = \sum_1^D \sum_1^{24} P \quad (3.5)$$

The error and percentage errors are calculated using equation 3.6 and 3.7, respectively.

$$e = \sum_{i=1}^n (Y_i - P_i) \quad (3.6)$$

$$e_p = \frac{|e|}{\sum_{i=1}^n P_i} \quad (3.7)$$

5.2.2 Assumptions

The assumptions for this study are listed below.

1. The buildings' wall will behave as grey body and the emissivity of the wall is considered as 0.93 (CIBSE, 2006).
2. The emissivity value is constant within the range of working temperature of the camera as well as the spectral range of the thermal camera, which is 7.5-13 μm (Flir System, 2006).
3. It is assumed that there is no effect of thermal bridge as the area of thermal bridge in walls are very small compared to the whole wall area.
4. Heating is assumed to be switched on at any time throughout the year when the room temperature falls below 20°C.

5.2.3 Heat loss calculation

Equation 2.8 is used to calculate the heat transfer through the building's wall in W/m^2 for both case studies which is later converted into heat energy loss by multiplying with 1 as the amount of heat transferred in an hour through the building's wall represent the heat energy loss in Wh/m^2 . The wall surface temperature T_s is initially extracted from infrared image and then interpolated against the external temperature for the estimation of historical heat loss. The outdoor ambient temperature T_{ext} and wind speed v are obtained from weather stations observation. The historical hourly ambient temperature and hourly wind speed between year 2004 and 2019 for the locality of the case studies are extracted from the database of the Met Office (2019) in order to calculate the hourly average and monthly total heat losses. The hourly average heat loss for a given hour in given month has been calculated by taking the average heat loss for all days for the given hour in that month. For instance, the hourly average heat loss at 1.00 am in January 2004 will be the average of heat loss values calculated using equation 2.8 for 1.00 am each day from 1st January to 31st January 2004. Similarly, the

monthly total heat loss for a given month is the summation of hourly heat loss of each hour and each day and the total heat loss in January 2004, for example, will be the sum of hourly heat loss from 1st January to 31st January 2004. The hourly average heat losses in Wh/m² and monthly total heat losses in kWh/m² are calculated for both insulated and uninsulated buildings. The historical heat loss values for a building, calculated using equation 3.4 and 3.5, will represent the characteristics of heat loss for the building and ANN can learn those characteristics to predict future heat loss for that building. Although according to equation 2.8, the heat loss depends on the external temperature and wind speed, the advantage of predicting heat loss over temperature and wind speed is that it simplifies and speeds up the prediction process by reducing the number of parameters to be forecasted and the uncertainty related to the prediction of temperature and wind speed.

5.2.4 Mathematical model to determine the optimum monitoring period of a building

Weather condition and occupants' behaviour are responsible for the variation in heat loss in different years in a building. Therefore, it is necessary to determine the optimum period required to monitor a building for the accurate estimation of heat loss. A mathematical model is presented in the Al-Habaibeh, Sen and Chilton (2020) by the author of this thesis which is presented here again.

Let us consider, $E_i = f(w, b)$; where E_i is the energy consumption of a building in a year, w is the weather condition and b represent people's behaviour.

Let, $\sum_1^N E_i$ is the energy consumption over N number of years.

Hence, the average of annual energy consumption will be $\frac{\sum_1^N E_i}{N}$.

If we choose to take another number of years M such that $M = N + k$, where k is a positive

constant; then average of annual energy consumption will be $\frac{\sum_1^M E_i}{M}$.

When N reaches its optimum value then the addition of further years will not change the average annual energy consumption; or simply

$$\frac{\sum_1^N E_i}{N} = \frac{\sum_1^M E_i}{M} \quad (5.1)$$

$$\text{Hence, } \frac{M}{N} = \frac{\sum_1^M E_i}{\sum_1^N E_i} = \frac{(E_1+E_2+E_3+ \dots\dots\dots+E_M)}{(E_1+E_2+E_3+ \dots\dots\dots+E_N)} \quad (5.2)$$

Let, $M = N+k$, where k is the number of additional years, this gives:

$$\begin{aligned} \frac{N+k}{N} &= \frac{(E_1+E_2+E_3+ \dots\dots\dots+E_N+E_{N+1}+E_{N+2}+ \dots\dots\dots+E_{N+k})}{(E_1+E_2+E_3+ \dots\dots\dots+E_N)} \\ &= \frac{\sum_1^N E_i + \sum_{N+1}^k E_i}{\sum_1^N E_i} \end{aligned} \quad (5.3)$$

Simplifying equation (5.3) leads to:

$$1 + \frac{k}{N} = 1 + \frac{\sum_{N+1}^k E_i}{\sum_1^N E_i} \quad (5.4)$$

Subtracting 1 from each side in equation (5.4):

$$\frac{k}{N} = \frac{\sum_{N+1}^k E_i}{\sum_1^N E_i} \quad (5.5)$$

Re-arranging equation (5.5) leads to:

$$\sum_{N+1}^k E_i = \left(\frac{k}{N}\right) \sum_1^N E_i \quad (5.6)$$

As k and N are finite numbers, the equality in the equation 5.5 is highly unlikely. Because it is almost impossible to get identical weather condition and occupants' behaviour in successive years due to the stochastic and probabilistic natures of the variables to satisfy equation 5.5.

$$\text{Since by definition: } \frac{M}{N} = \frac{N+k}{N} \quad (5.7)$$

If $M \rightarrow \infty$ then $N \rightarrow \infty$ as k is a constant and hence,

$$\lim_{N \rightarrow \infty} \frac{N+k}{N} = \lim_{N \rightarrow \infty} \frac{\frac{N}{N} + \frac{k}{N}}{\frac{N}{N}} = \lim_{N \rightarrow \infty} \frac{1 + \frac{k}{N}}{1} = 1 \quad (5.8)$$

Hence from (5.7) and (5.8) this leads to $\frac{M}{N} = 1$

$$\text{or simply, } M = N \quad (5.9)$$

Equation 5.9 indicates that by monitoring the energy consumption of a building for finite number of years, it is impossible to reach to the equality of equation 5.3 given the changing nature of weather and people's behaviour. Therefore, from equation 5.3 the value of k should be equal to zero which implies that to guarantee the accuracy of estimation of the heat loss energy it requires to monitor a building for infinite number of years. The case studies presented in this chapter utilise 16 years heat loss data for the ANN analysis.

5.2.5 ANN Prediction

The successful use of feed forward neural network in predicting heat loss through insulated and uninsulated buildings is presented in Al-Habaibeh, Sen and Chilton (2020). The literature review in chapter 2 shows successful the use of some recurrent neural networks, such as NARnet, NARxnet and LSTM neural networks, for prediction of energy demand in buildings. In this chapter, these four neural networks are considered for ANN analysis using the hourly average and monthly total heat loss data. The historical heat losses calculated from 2004 to 2019 are divided into training and test data sets and these are done in different combinations ranging from 2 to 15 years. If the training data set contains 2 years data, for instance, heat loss data for the years 2004 and 2005, then test data set contains 14 years data

i.e., heat loss data for the years 2006 to 2019. On the other hand, if the training data set contains 15 years data i.e., heat loss data for the years 2004 to 2018 then the test data set will contain the heat loss data of the year 2019 only. Considering all other combinations between these two extreme cases, it is possible to construct 14 different combinations of training and test data sets. All these combinations are evaluated with the above mentioned four neural networks for both the hourly and monthly heat loss prediction. In each case the neural networks are used to predict the heat loss for the same length of data in test data set which is then compared against the test data to evaluate the performance of the neural network. In the training process of the hourly average heat loss prediction using feed forward neural network, hour, month, and year are the three parameters considered as inputs; and the hourly average heat loss obtained from equation 3.4 is considered as the output. In case of monthly heat loss prediction using feed forward neural network, month and year are the two input parameters to the neural network and monthly heat loss obtained from equation 3.5 is the output for the network. The recurrent neural network works slightly different than feed forward neural network where the output of previous time step is considered as additional input for the next time step. The training process of the recurrent neural network involves sequential training rather than batch training used by feed forward network. Time step is one of the default inputs for these networks and the hourly average heat loss (obtained from equation 3.4) for the previous time step is chosen as the other input in case of hourly average heat loss prediction. For monthly heat loss prediction monthly total heat loss, obtained from equation 3.5, is chosen as the second input instead of the hourly average heat loss. However, the NARxnet accepts additional inputs. Therefore, hour, month and years are chosen as the additional inputs in case of hourly average heat loss prediction and month and year are chosen as the additional inputs in case of monthly total heat loss analysis for NARxnet. The heat loss at the current time step is chosen as the output for all recurrent neural networks.

For hourly average heat loss prediction, it will be the heat loss value obtained from equation 3.4; and for monthly total heat loss prediction it will be the heat loss value obtained from equation 3.5.

5.3 Case study 1: Buildings in High Wycombe

The first case study includes the evaluation of thermal performance and prediction of heat losses in an insulated and an uninsulated building in High Wycombe, England. Figure 5.1 shows the infrared image of the insulated and uninsulated buildings that are considered for this case study.

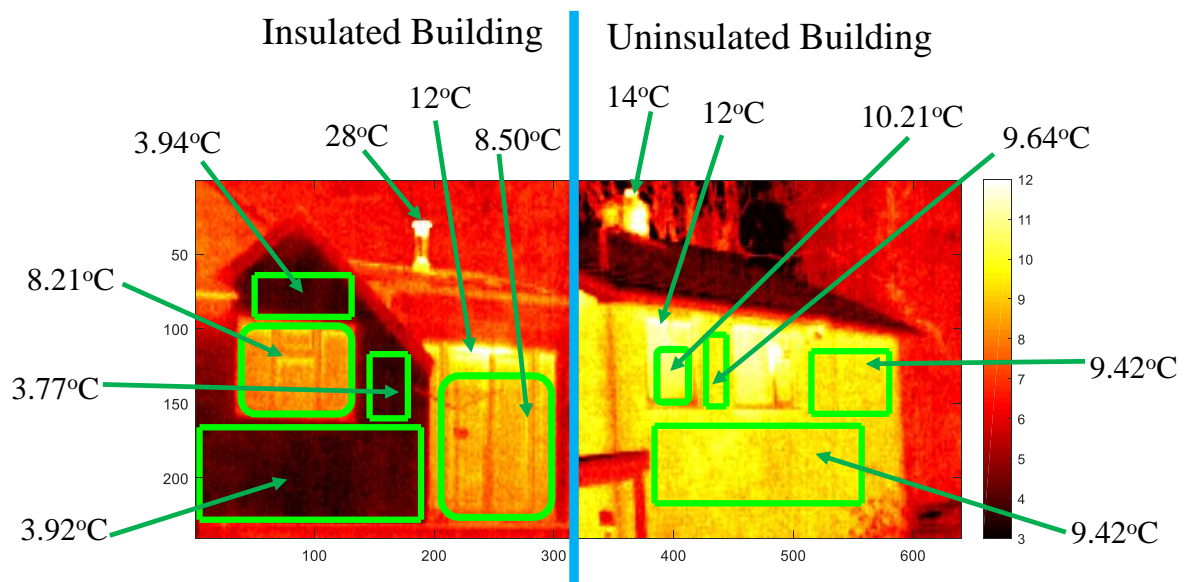


Figure 5.1: Infrared image of the insulated and the uninsulated house in High Wycombe.

The insulated building has been deep retrofitted with 200 mm thick external insulation, improved glazing area and solar photovoltaic panel on the roof prior to the study (Harrall, 2012). The material used for insulating the building is StyrofoamTMA which is a very good insulating material with R-value of circa 6.45 m²K/W (Accolade for *STYROFOAM as Greening-the-Box retrofit project wins Gold*, 2012). The uninsulated building in Figure 5.1 is a solid wall building near the insulated building. The infrared images of both the buildings

are taken using FLIR E25 thermal camera and then the pixel-by-pixel temperature values are extracted using ThermaCAM QuickReport software. Afterwards, the infrared images (in Figure 5.1) are reproduced in same scale from the temperature data using Matlab software. Several images of both the buildings were taken during the thermal survey of the buildings between 28th March 11.15 pm and 29th March 9.30 am. The ambient temperature at the start of the survey was 9°C and at the end of the survey was 7°C. The indoor temperature of the insulated building was 19°C at the start of the survey and 20°C at the end of the survey. These temperatures are measured with a thermocouple-based temperature sensor. The early morning temperature (at 6 am) on 29th March was around 4°C when the infrared images of Figure 5.1 were taken. The pixelwise temperature values from the infrared images of both insulated and uninsulated buildings are extracted using Thermacam quick report software from FLIR.

5.3.1 Infrared image analysis

Figure 5.1 also shows the temperatures of door, windows, chimneys, and different parts of wall for both insulated and uninsulated buildings where the temperature of the green boxes is the average temperature of the area covered by the box in all cases. The wall surface temperature in insulated building ranges between 3.77°C to 3.94°C at different parts whereas the chimney temperatures is 28°C. On the other hand, the wall surface temperature in uninsulated building ranges between 9.42°C to 9.64°C at different parts and the chimney temperature is 14°C. The high temperature of the uninsulated building's wall reflects the higher heat loss through the wall of the uninsulated building than the wall of the insulated building. The temperature of door gap in insulated building and the temperature in windows gap in uninsulated building is the same which is 12°C and therefore it can be inferred that the indoor temperatures in both the buildings are about same. The chimney temperature in insulated building is two times higher than that of the uninsulated building which points out

that there is very little heat loss through the walls of insulated building and therefore the temperature of the chimney is very high as most of the heat comes out of the building with the exhaust air and flue gas. On the other hand, a significant amount of heat loss occurs through the walls of uninsulated building and hence the chimney in that building is cooler than the chimney of the insulated building. The average temperatures of the door and the window in insulated building are 8.21°C and 8.50°C, respectively. Whereas the average temperature of the window in uninsulated building is 10.21°C. Therefore, the thermal performance of glazing area in the insulated building is better than that of the uninsulated building. Despite of the increase in overall glazing area due the retrofitting in insulated building, the overall thermal performance of the insulated building is better than that of the uninsulated building.

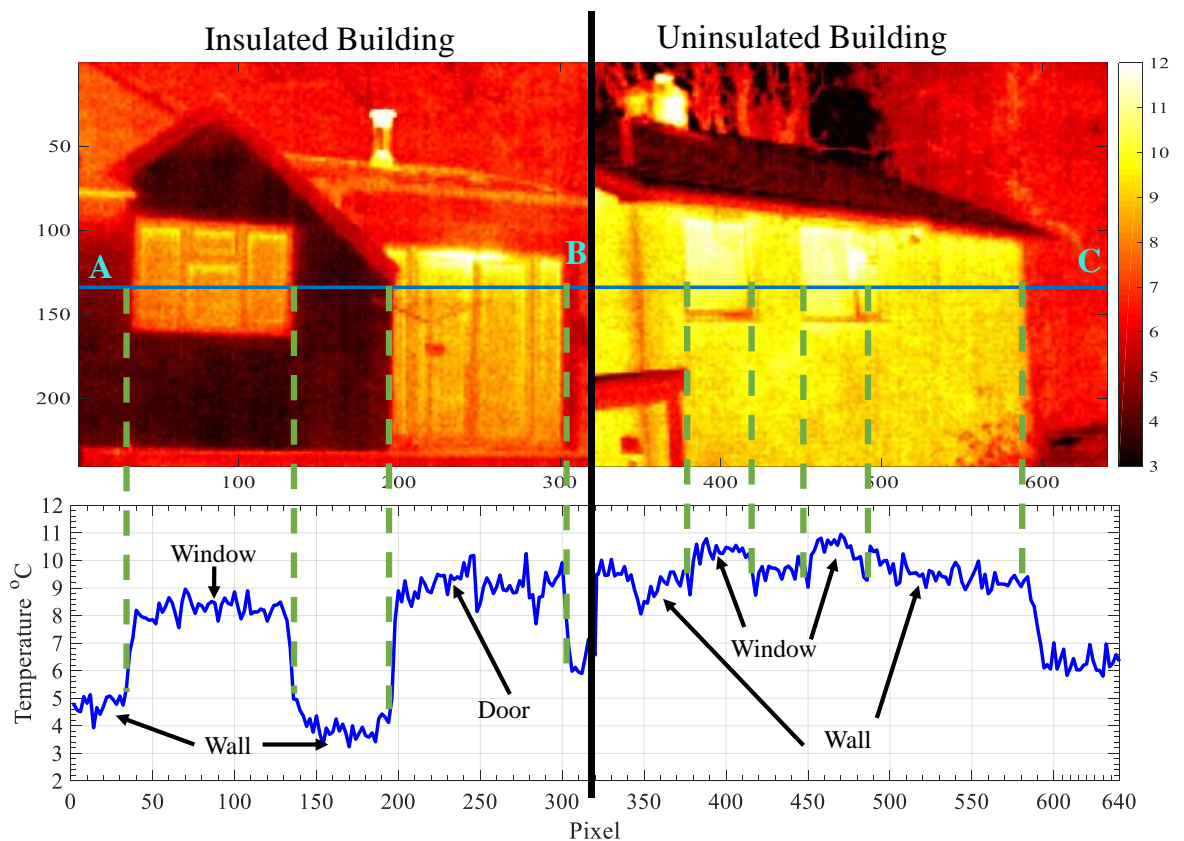


Figure 5.2: Temperature profiles generated from infrared images of the insulated and the uninsulated house in High Wycombe.

Figure 5.2 shows the temperature profile through line ABC on the infrared images of both insulated and uninsulated buildings. The temperature values along AB and BC are extracted to plot the thermal profile for the insulated and the uninsulated building, respectively. It is noticed in the temperature profile of line AB that the wall temperature varies between 3°C to 5°C, the window temperature varies between 7°C to 9°C, and the door temperature varies between 8°C to 10.5°C in insulated building. In uninsulated building, the variation in temperature on wall sections and windows along the line BC are between 8°C to 10°C and between 9°C to 11°C, respectively. Naturally, the temperature distribution will not be constant throughout the wall, door, and window sections. However, the ranges of variation in those sections along the line ABC (in Figure 5.2) confirms that consideration of average temperatures for those sections would be a reliable estimation for further quantitative analysis. Therefore, the average temperature values of the wall sections are considered as the wall surface temperature for the heat loss estimation using equation 2.8.

5.3.2 Hourly heat loss prediction:

A sensitivity analysis regarding the number of hidden layers and the number of neurons in each hidden layer have been conducted prior to the heat loss prediction as suggest by the literature review. First four years data of the whole data set (year 2004-2007) is chosen for training the neural network and next four years data (year 2008-2011) is chosen as the test data set. Heat loss data for both insulated and uninsulated walls are included and mean of the percentage error (APE) is considered as the measure of performance. The percentage error (PE) is calculated using equation 3.7. The feed forward neural network could have several hidden layers with multiple neurons in each layer. Therefore, it is necessary to evaluate the sensitivity of both parameters i.e., the number of hidden layers and the number of neurons in each hidden layer. Figure 5.3-a and 5.3-b show the result of sensitivity analysis for feed forward neural network regarding the number of hidden layers and the number of

neurons in each hidden layer, respectively. It is found from Figure 5.3-a that the average percentage error decreases as the number of hidden layers increases up to six hidden layers and then it slightly goes up with seven hidden layers. Figure 5.3-b shows that the minimum average percentage error is obtained with three neurons in each hidden layer. Therefore, feed forward network composed of six hidden layers and three neurons in each hidden layer is found to be the best network architecture and this configuration is set for the hourly heat loss analysis with feed forward neural network.

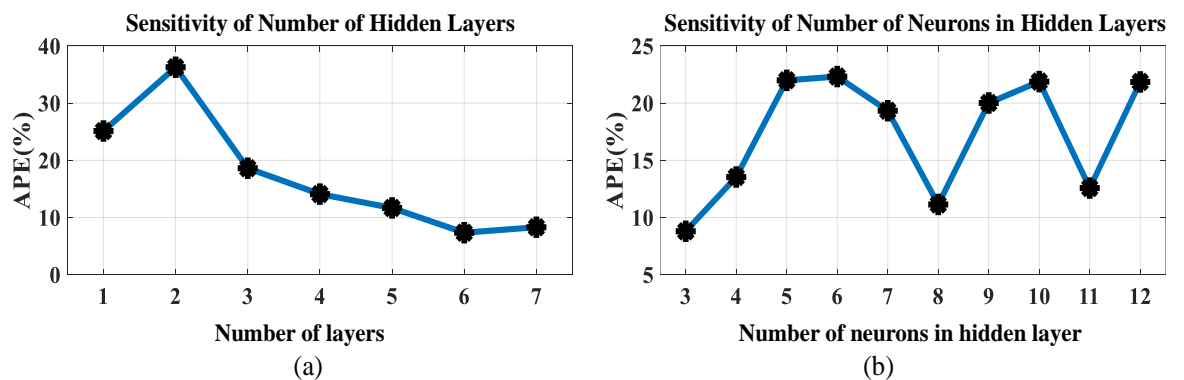


Figure 5.3: Sensitivity of feed forward neural network regarding (a) number of hidden layers and (b) number of neurons in each hidden layer for hourly heat loss prediction (case study 1).

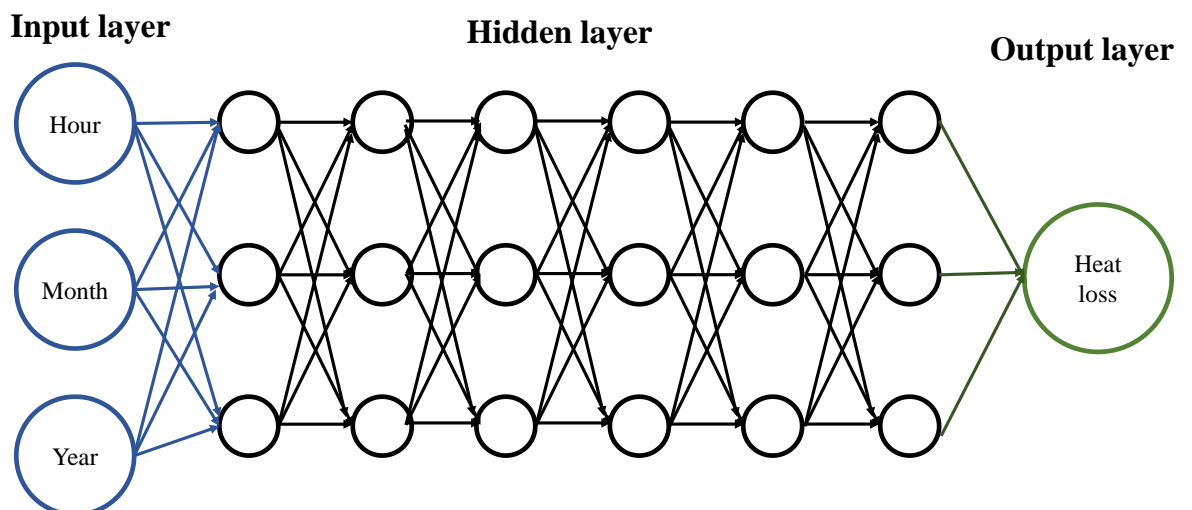


Figure 5.4: Architecture of feed forward neural network for hourly average heat loss prediction.

The schematic diagram of the feed forward neural network used for the hourly average heat loss prediction is presented in Figure 5.4. As, the recurrent neural networks follow incremental training process, those networks usually contain one hidden layer with several neurons in it. Therefore, the recurrent neural networks used in this study, namely NARnet, NARxnet and LSTM, are composed of only one hidden layer and the sensitivity analysis includes the sensitivity of number of neurons in the hidden layer which is presented in Figure 5.5.

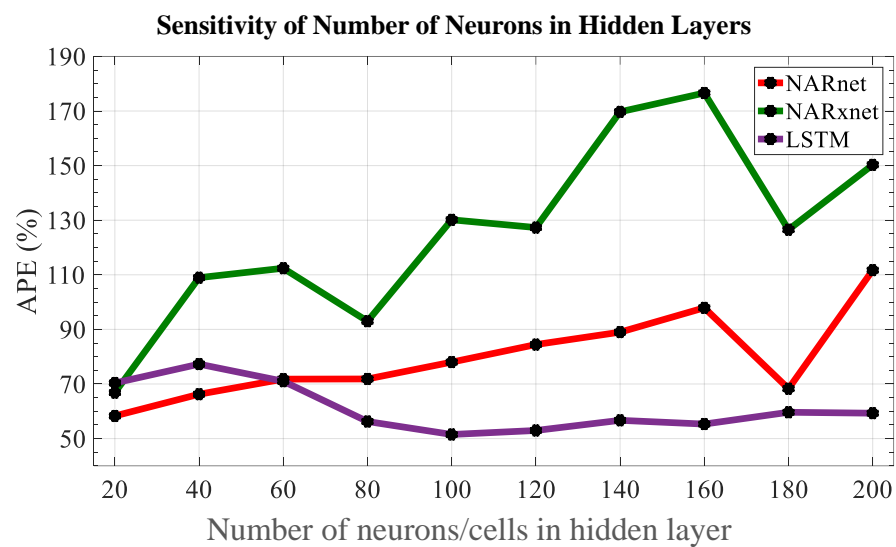
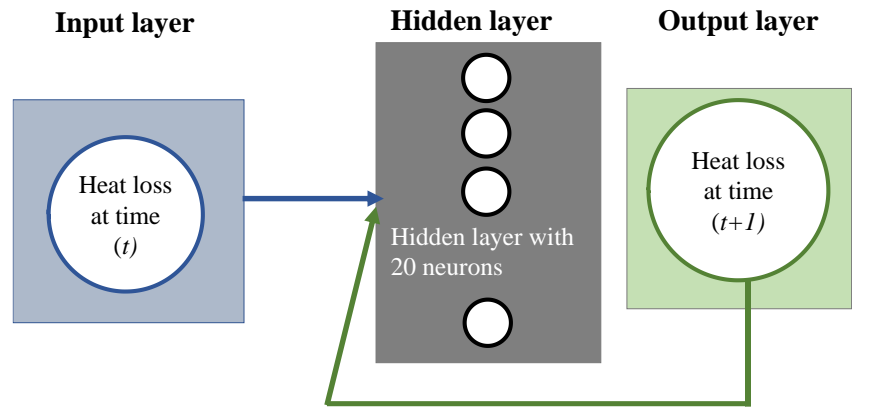
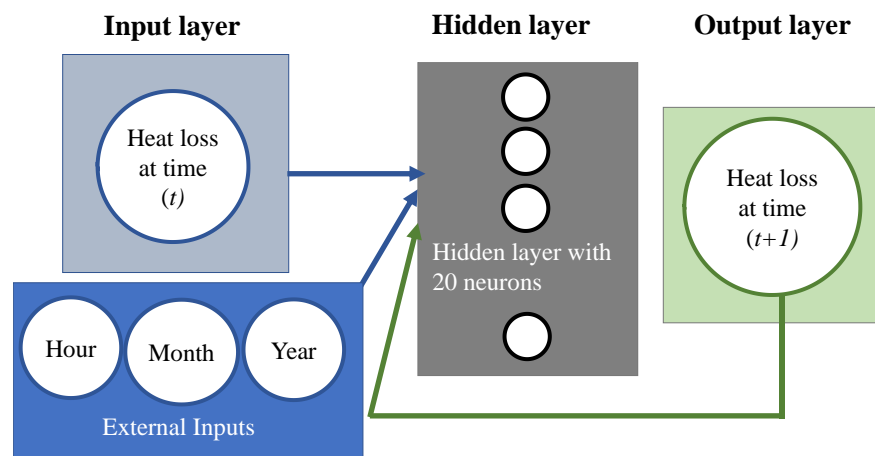


Figure 5.5: Sensitivity of NARnet, NARxnet and LSTM neural network regarding number of neurons in hidden layer for hourly heat loss prediction.

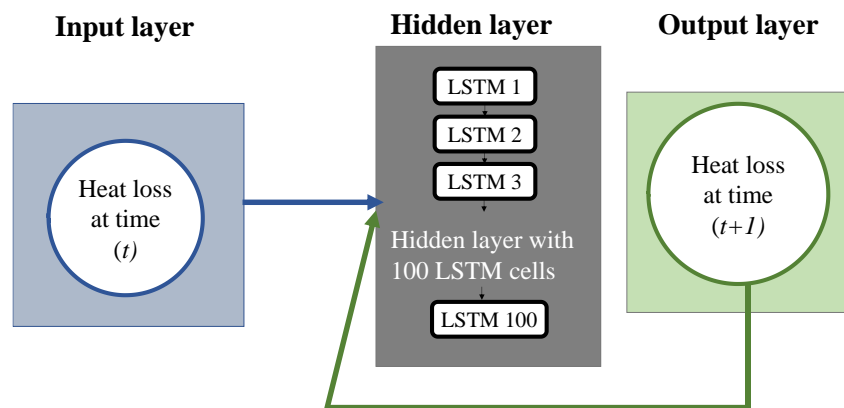
It is found from Figure 5.5 that the NARnet and the NARxnet shows the lowest APE with 20 neurons in the hidden layer and then the APE gradually goes up until 160 neurons in the hidden layer. There is drop in the APE at 180 neurons in the hidden layer; however, it starts rising afterwards. For LSTM network, the minimum average percentage error is found with 100 LSTM cells in the hidden layer. It is noted that the performances of all three recurrent neural networks are very poor compared to the performance of feed forward network. One reason could be small sample size of the training data set. Therefore, it would be worthy to look at the performance of those networks using the full data set.



(a)



(b)

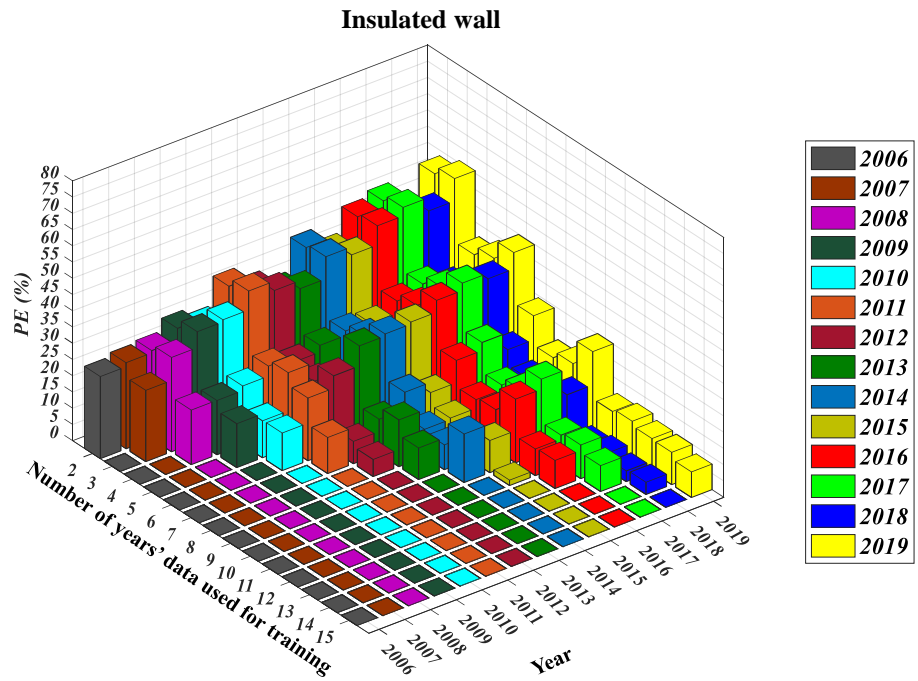


(c)

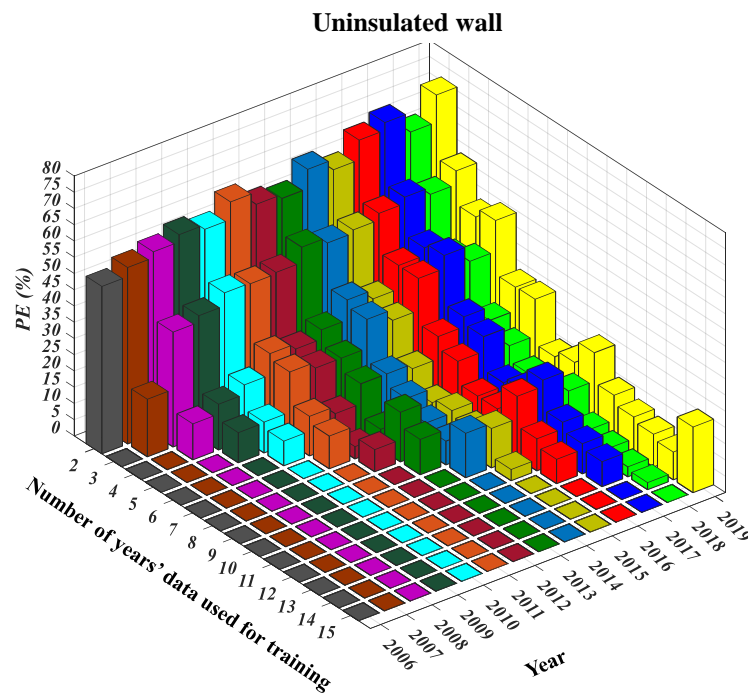
Figure 5.6: Architecture of recurrent neural networks used in this study (a) NARnet (b) NARxnet and (b) LSTM neural network.

Hence, the NARnet and NARxnet with 20 neurons in hidden layer is selected for the hourly heat loss prediction. For LSTM network, the network with 100 LSTM cells in hidden layer is selected for the hourly heat loss analysis. Figures 5.6-a, 5.6-b and 5.6-c show the configuration of NARnet, NARxnet and LSTM networks used in this study. The performance of feed forward neural network which is trained using two years to fifteen years data is presented in Figure 5.7-a and 5.7-b for the insulated wall and uninsulated wall, respectively. There are two significant facts observed from the bar charts in Figure 5.7 that the percentage error reduces with the increase in number of years' training data used and the heat loss prediction is more accurate for the near future than the remote future. ANN generalises the characteristics of heat loss through a building's wall from the iterative training process. As the number of data points in training data set increases, an ANN can map the relationship between input and output with more accuracy. It is noticed in both the bar charts of Figure 5.7 that the ANN trained with 8 years or more heat loss data achieves significant accuracy and the ANN trained with 11 years or more heat loss data archives very high accuracy. It is also noted that the variation in PE is higher in the uninsulated wall than in the insulated wall because the heat loss through an uninsulated wall is higher than the heat loss through an insulated wall. Similar bar charts showing the percentage error of NARnet, NARxnet and LSTM neural networks for both the insulated and the uninsulated walls are included in Appendix A. The average of the percentage errors (APE) for the ANN trained with two years to fifteen years heat loss data is shown in Figure 5.8; where Figure 5.8-a represents the APE in heat loss prediction through the insulated wall and Figure 5.8-b represents the APE in heat loss prediction through the uninsulated wall for feed forward, NARnet, NARxnet and LSTM neural network. The feed forward neural network shows the lowest APE compared to all other neural networks for insulated wall.

Case study 1: Performance of Feed Forward Neural Network



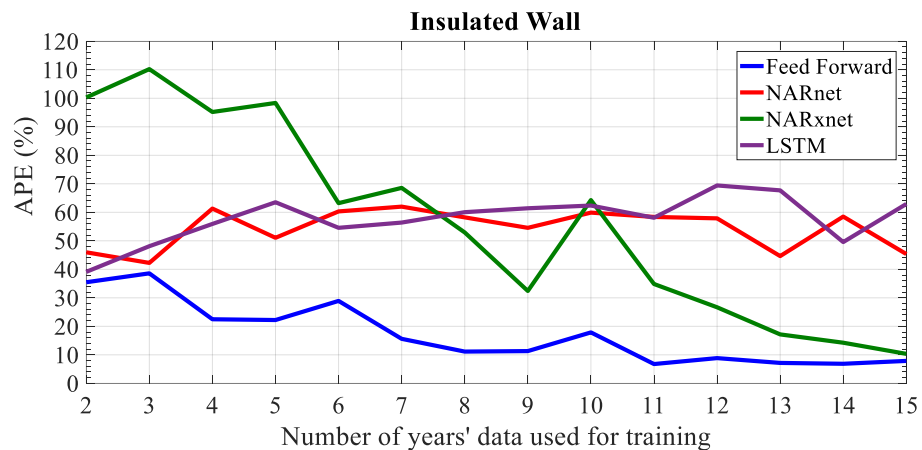
(a)



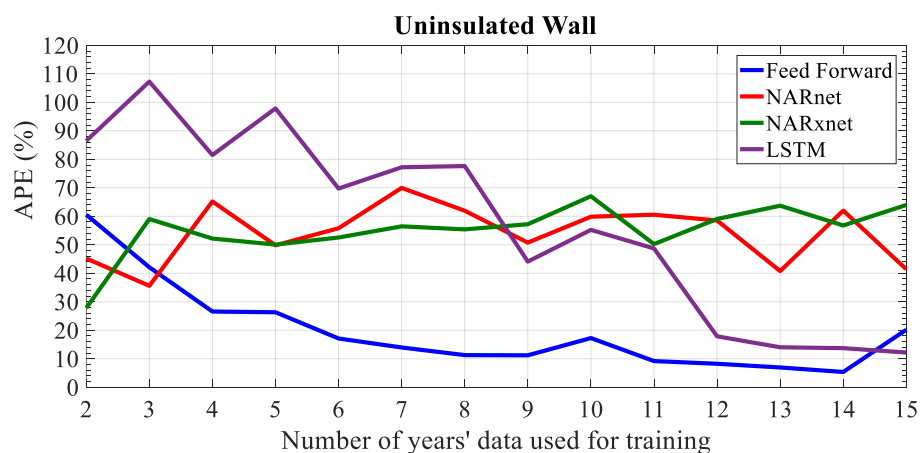
(b)

Figure 5.7: Performance of feed forward neural network to predict hourly heat loss (a) insulated building and (b) uninsulated building.

For uninsulated wall, the APE of feed forward neural network is lowest between 4 years to 14 years of training data. In both cases, the APE drops down to 10% with 8 years of training data and below 10% with 11 to 14 years of training data for feed forward neural network. With 15 years training data, the APE of feedforward neural network is below 10% for insulated wall; but close to 20% for uninsulated wall.



(a)



(b)

Figure 5.8: Comparison of performances among feed forward, NARnet, NARxnet and LSTM neural network for hourly heat loss prediction in (a) insulated building and (b) uninsulated building in case study 1.

The APE of all recurrent neural networks (NARnet, NARxnet and LSTM) never go below 10%. However, the APE of NARxnet is found to be below 20% with 13 to 15 years of

training data for insulated wall; and the APE of LSTM neural network is found to be below 20% for 12-15 years of training data for uninsulated wall. Therefore, it can be summarised from Figure 8.5 that NARnet, NARXnet and LSTM neural networks are not suitable for the hourly average heat loss prediction. Only feed forward neural network is able to predict the hourly average heat loss with acceptable accuracy if it is trained with 8 years or more heat loss data. The ANN predicted heat loss curve and the calculated heat loss curve for the years 2012-2019 is shown in Figure 5.9 for both the insulated and the uninsulated walls where the feed forward neural network is trained with 8 years of heat loss data from 2004 to 2011. It is found from Figure 5.9 that ANN predicted heat losses are very close to the calculated heat loss in most of the cases except few exceptions. For instance, the calculated heat loss is significantly higher in February and March of year 2013 and 2018.

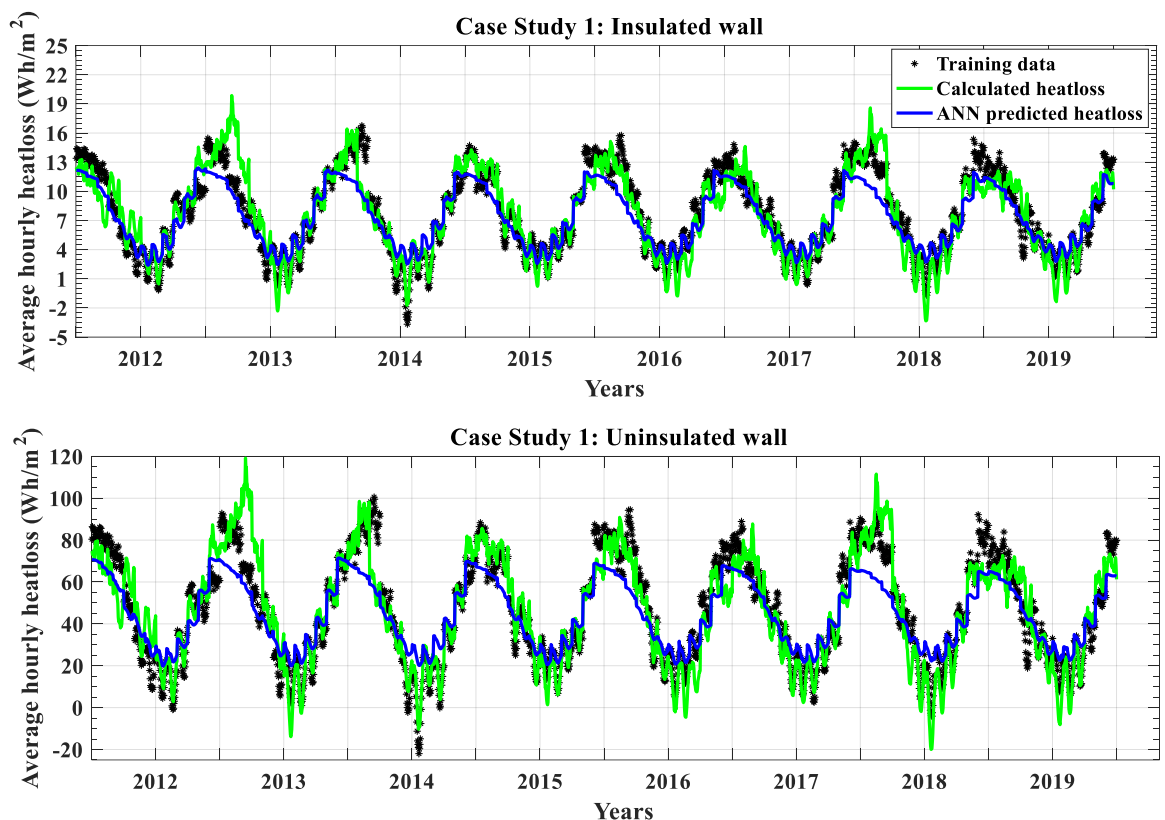


Figure 5.9: Comparison between the calculated heat loss and the ANN (feed forward) predicted heat loss for the years 2012 to 2019

The heatmap of average temperature in Figure 5.10 shows that the February and March in year 2013 and 2018 are cooler than the February and March in the other years. Similarly, the calculated heat loss is far less than the ANN predicted heat loss for the month of July in 2013 and 2018.

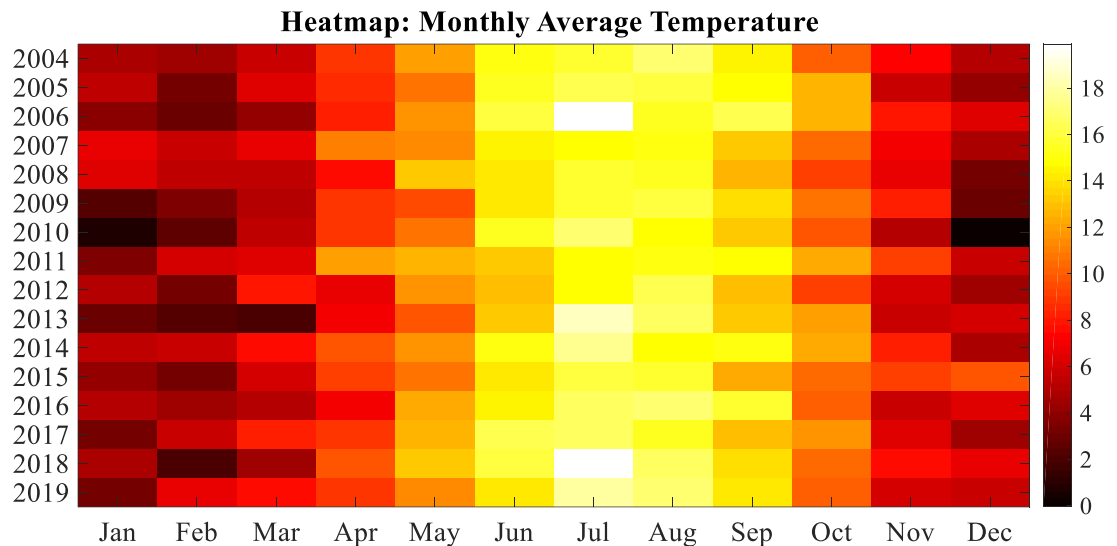


Figure 5.10: Heatmap representation of average temperature in each month from 2004 to 2019

Again, the heat map shows us a possible reason for the deviation is that in 2013 and 2018 the month of July is exceptionally warmer than the month of July in other years. In fact, the calculated heat loss curves show that there is negative heat loss or heat gain in the buildings due the solar irradiation during summer. ANN prediction does not capture the heat gain as the algorithm is developed to predict heat loss. This is more sensible because heat gain during the daytime in summer does not contribute to the heating energy savings which is a key aspect of estimating payback period of the investment for retrofitting a building with improved insulation.

5.3.3 Monthly heat loss prediction

Similar to the hourly average heat loss prediction, a sensitivity analysis is conducted to determine the best configurations for all four neural networks used in the case study. Monthly total heat loss calculated using equation 3.5 for the years 2004 to 2007 is chosen for training neural networks and monthly heat loss data for the years 2008 to 2011 is chosen to test the networks' performance. For feed forward neural network, the sensitivity of both the number of layers in the hidden layer and the number of neurons in each layer is evaluated which is shown in Figure 5.11-a and 5.11-b respectively.

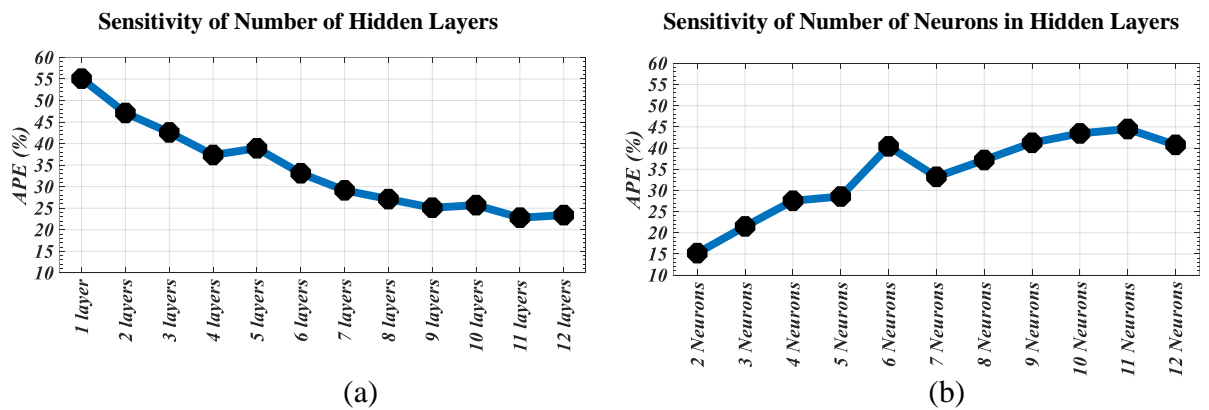


Figure 5.11: Sensitivity of feed forward neural network regarding (a) number of hidden layers and (b) number of neurons in each hidden layer for monthly heat loss prediction.

The APE gradually falls as the number of hidden layers increases; however, the APE rises with the increase in the number of neurons in hidden layer. At eleven layers in the hidden layer the APE is found to be minimum and it reaches in stable state. Regarding the number of neurons in each hidden layer, two neurons in a hidden layer shows the minimum APE. Therefore, feed forward network with eleven layers and two neurons in each hidden layer is selected for the monthly total heat loss prediction. Figure 5.12 shows the sensitivity of number of neurons in the hidden layer for NARnet and NARxnet and number of cells in the hidden layer for LSTM neural network. For NARnet and NARxnet, 12 neurons in hidden

layer shows the minimum APE; however, it is around 60% which is significantly high percentage of error. However, it is worthy to see the performances of those networks with full data set. Hence these two neural networks with 12 neurons in the hidden layer are considered for the heat loss prediction. The LSTM network shows very high accuracy with APE less than 10% in cases. The minimum APE is found as 5.21% with 12 cells in the hidden layer. The APE gradually increases to 8.48 % with 96 cells in the hidden layer and then fall slightly. Therefore, the LSTM network with 12 cells in the hidden layer is selected for the monthly total heat loss prediction.

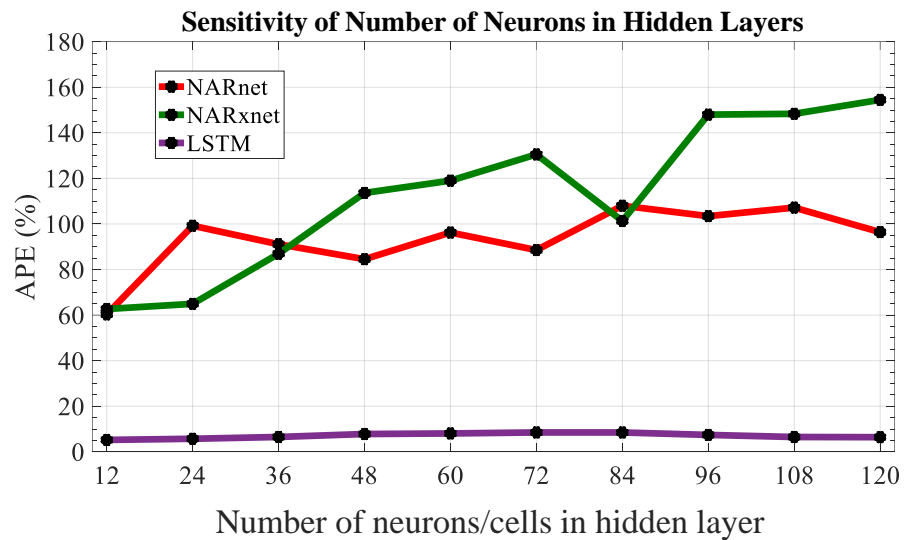
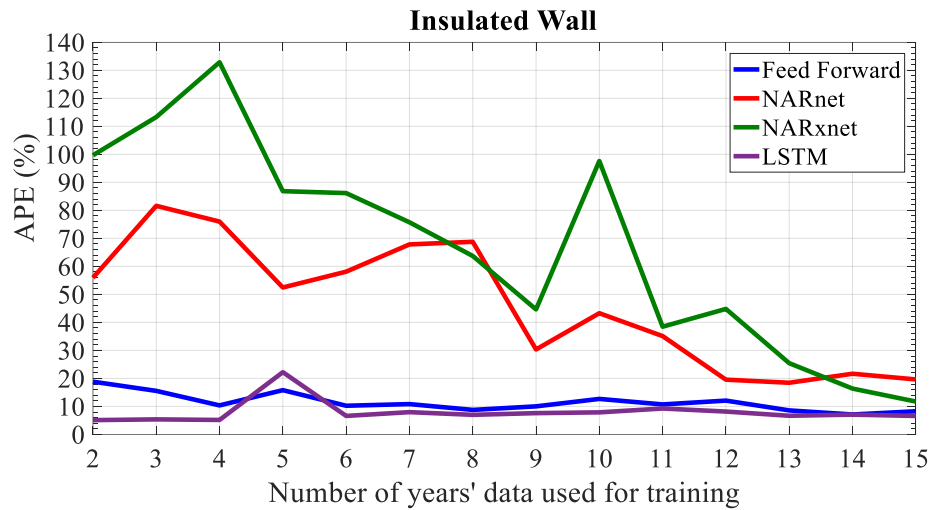


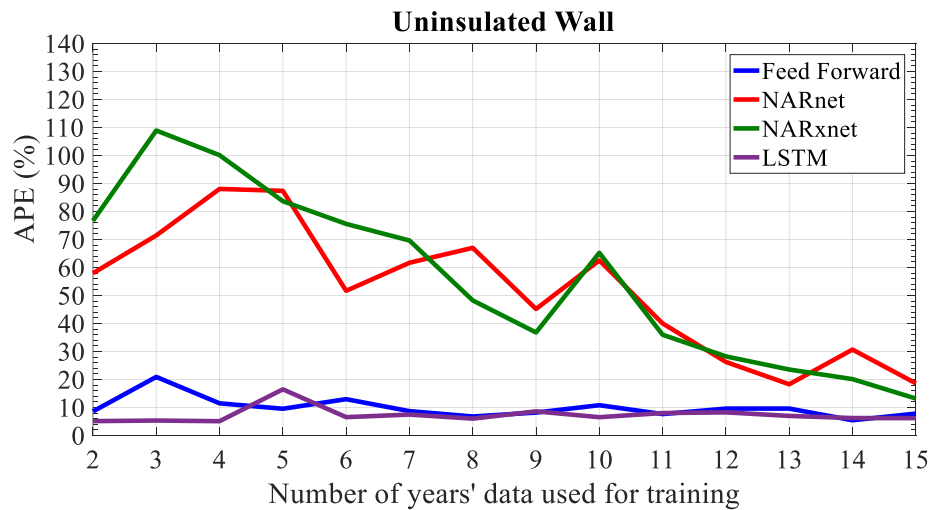
Figure 5.12: Sensitivity NARnet, NARxnet and LSTM neural network regarding number of neurons in hidden layer for monthly heat loss prediction.

The percentage errors of feed forward neural network, NARnet, NARxnet and LSTM neural networks trained with 2 to 15 years of heat loss data are included in Appendix B. The average percentage error (APE) for those neural networks for 2 to 15 years of training are presented in Figure 5.13, where Figure 5.13-a insulated wall and Figure 5.13-b includes uninsulated wall, respectively. It is found from Figure 5.13 that the LSTM neural network shows the best accuracy in both the insulated and uninsulated walls with APE less than 10%

for all combinations of training data set except with 5 years training data. The feed forward neural network also shows high accuracy with APE less than 20% with all combination of training data; however, the APE remains slightly higher than the LSTM neural network in all cases except for training with 5 years data.



(a)



(b)

Figure 5.13: Comparison of performances among feed forward, NARnet, NARXnet and LSTM neural network for monthly heat loss prediction in (a) insulated building and (b) uninsulated building in case study 1.

The NARnet and the NARxnet show very high APE which converges towards fifteen years training; however, the APE is still higher than the feed forward and LSTM networks.

Therefore, it can be concluded that NARnet and NARxnet are not suitable for the monthly total heat loss prediction as well. LSTM neural network show better accuracy over feed forward neural network and therefore, it is considered to compare the calculated heat loss and LSTM neural network predicted heat loss curves. Although using 2 to 4 years of training shows very high accuracy, there is a rise in APE with 5 years training for both the insulated and the uninsulated walls; and hence, the performance does not look consistent at this level. After that point, the next minimum APE is found with 8 years training data for both walls. It should be noted that a good consistency is also observed with 8 or more years of training in hourly average heat loss prediction.

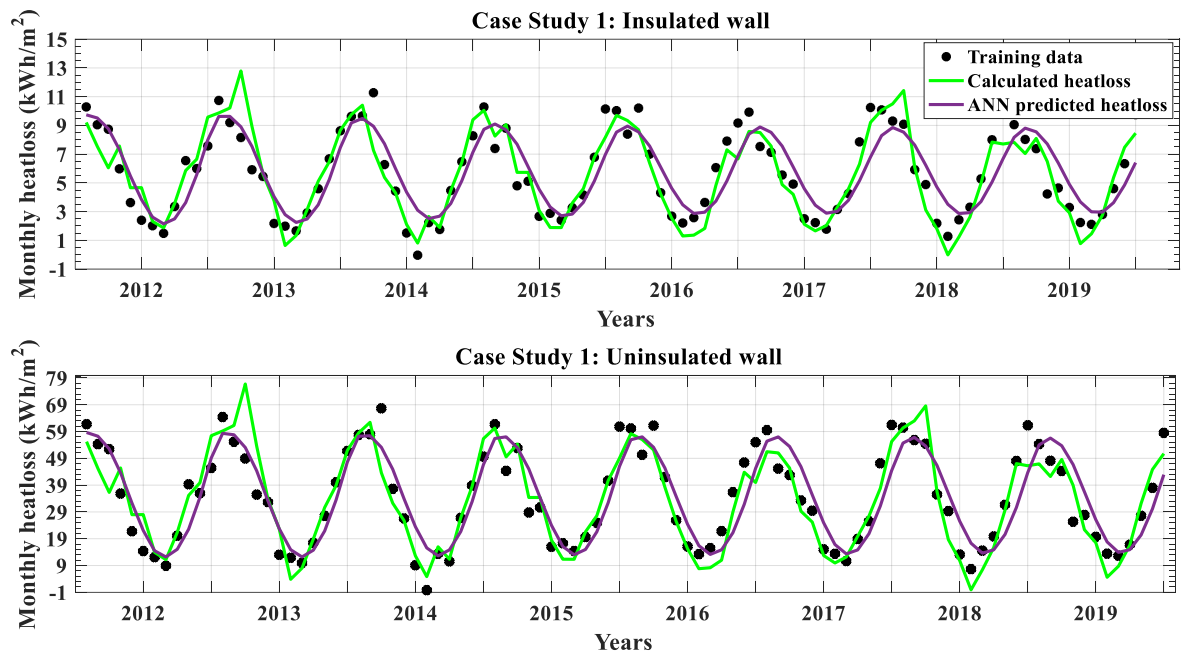


Figure 5.14: Comparison between the calculated heat loss and the ANN (LSTM) predicted heat loss for the years 2012 to 2019 in case of monthly heat loss prediction.

Figure 5.14 shows comparison between the calculated and ANN predicted heat loss for 8 years from 2012 to 2019 where the LSTM neural network has been trained with 8 years heat data from year 2004 to 2011. It is observed from the figure that LSTM neural network successfully generalised the characteristic of heat loss from training and the predicted heat

loss is close to the calculated heat loss in most of the cases. There are two instances where the calculated heat loss is notably higher in February-March of 2013 and 2018. This is because of very cold weather in February- March during those two years which is confirmed by the heatmap of historical average temperature in Figure 5.10. The heatmap in Figure 5.10 also shows that the month of July in year 2013, 2014 and 2018 are significantly warmer than other years and therefore the calculated heat losses in the month of July for those three years are notably lower than the ANN predicted heat losses. The similar deviation is observed for hourly average heat loss prediction in Figure 5.9.

5.4 Case study 2: Buildings in Nottingham

The second case study has been conducted in an externally insulated mid terraced and an uninsulated end terraced building in Nottingham, England. Figure 5.15 shows the infrared image of the insulated and uninsulated buildings where the two buildings are adjacent to each other. The infrared image of these two adjacent buildings is taken using FLIR T640 thermal camera during a thermographic survey on 12th February at around 8.30pm. The ambient temperature during the survey was 5°C. Again, Thermacam quick report software from FLIR is used to extract the pixelwise temperature values from the infrared image of the buildings.

5.4.1 Analysis of infrared image

Similar to the approach followed in the first case study, the average wall surface temperature at different section in the insulated and uninsulated buildings are marked in Figure 5.15. The average wall surface temperature at different section in the uninsulated building ranges from 8.19°C to 8.24°C. On the other hand, the wall surface temperature at different section in the insulated wall ranges from 6.55°C to 6.65°C. It is also noticed in Figure 5.15 that the insulated building is fitted with photovoltaic solar cell on the roof to make it more energy

efficient. The average wall surface temperature difference between the two buildings is circa 1.6°C. Figure 5.16 shows the temperature profile along line ABCD on the infrared image where the temperature values along AB represents the wall surface temperature of the uninsulated building, BC represent the wall surface temperature of the insulated building and CD present the wall surface temperature of another uninsulated building next to the insulated one.

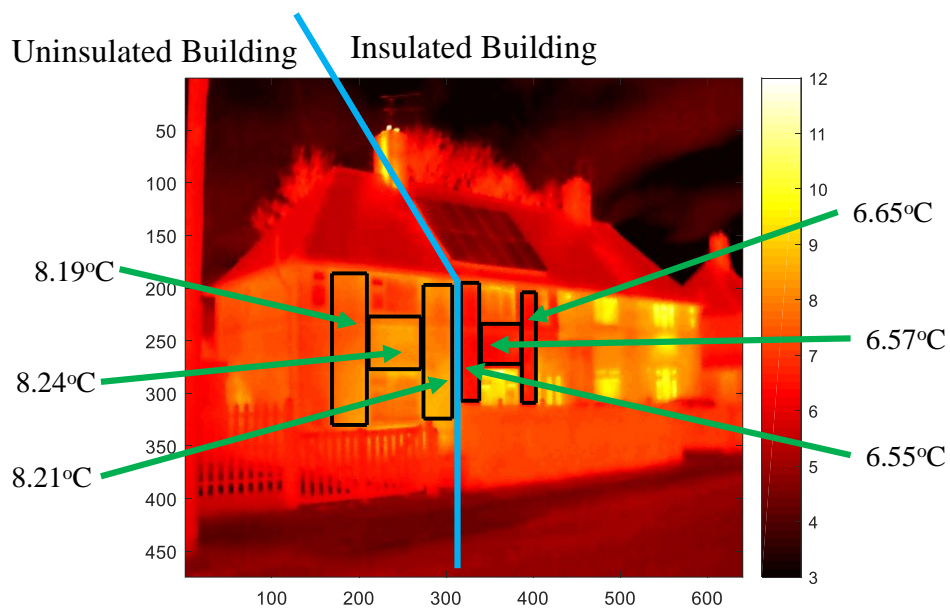


Figure 5.15: Infrared image of the insulated and the uninsulated house in Nottingham

The wall surface temperature in the uninsulated building along line AB ranges from 7°C to 8.5°C. There are two rooms noticed in the uninsulated building where the heating looks switched of in the left-hand side room with wall surface temperature ranges between 7°C to 7.5°C. The wall surface temperature in the right-hand side room ranges between 7.5°C and 8.5°C and warmest area represents the position of radiator behind the wall. The temperature profile along line BC shows that the wall surface temperature in the insulated building varies between 6.5°C and 7°C the position of radiator behind the wall is represented by the warmest area with a temperature of 7°C. Therefore, the infrared image in Figure 5.15 and the temperature profile in Figure 5.16 reveal similar information as the infrared images in the

first case study that the walls of uninsulated buildings always remain warmer than the walls of insulated buildings. Similar to the first case study, the mean value of wall surface temperature is considered for the heat loss calculation using equation 2.8.

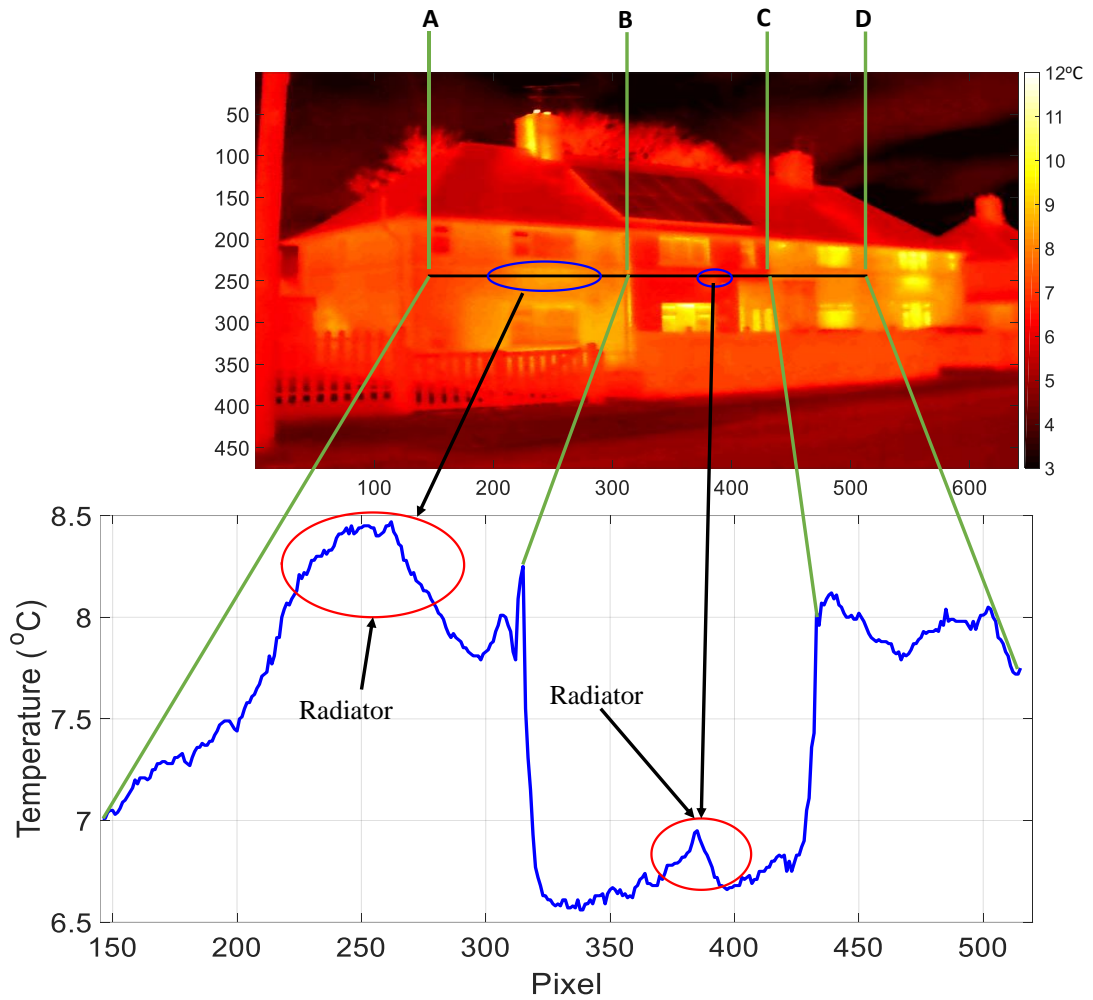


Figure 5.16: Temperature profiles generated from infrared images of the insulated and the uninsulated house in Nottingham.

5.4.2 Hourly average heat loss prediction

Prior to the heat loss prediction, a sensitivity analysis has been conducted following the same procedure as it is performed in the first case study. Figure 5.17-a shows the sensitivity of the number of hidden layers and Figure 5.17-b shows the sensitivity of number of neurons in each hidden layer for feed forward neural network. Both the figures show similar trend as it

is found in the sensitivity analysis for hourly average heat loss analysis in the first case study. The minimum APE is observed for six hidden layer and three neurons in each hidden layer. Therefore, the similar configuration of feed forward neural network (presented in Figure 5.4) used in the first case study is selected to use for the current case study. The sensitivity of number of neurons in the hidden layer for NARnet and NARxnet and the sensitivity of the number of cells in the hidden layer for LSTM neural network is presented in Figure 5.18.

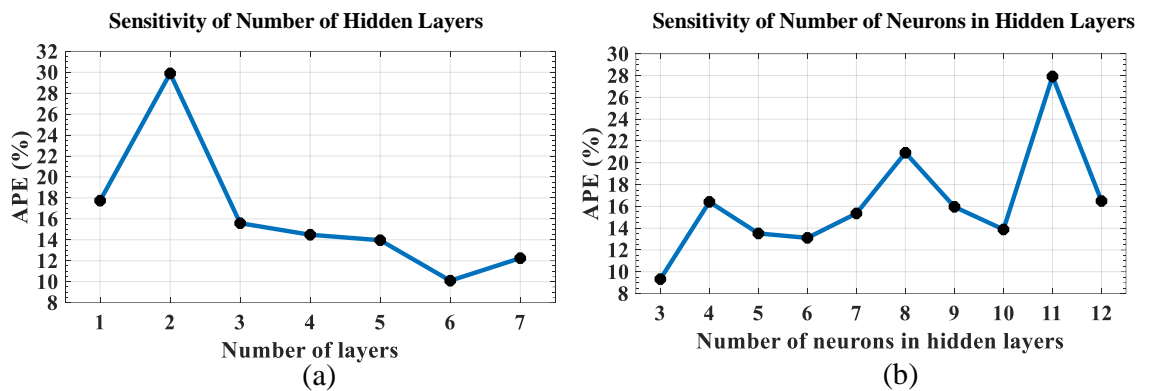


Figure 5.17: Sensitivity of feed forward neural network: (a) number of hidden layers and (b) number of neurons in each hidden layer for hourly heat loss prediction in case study 2.

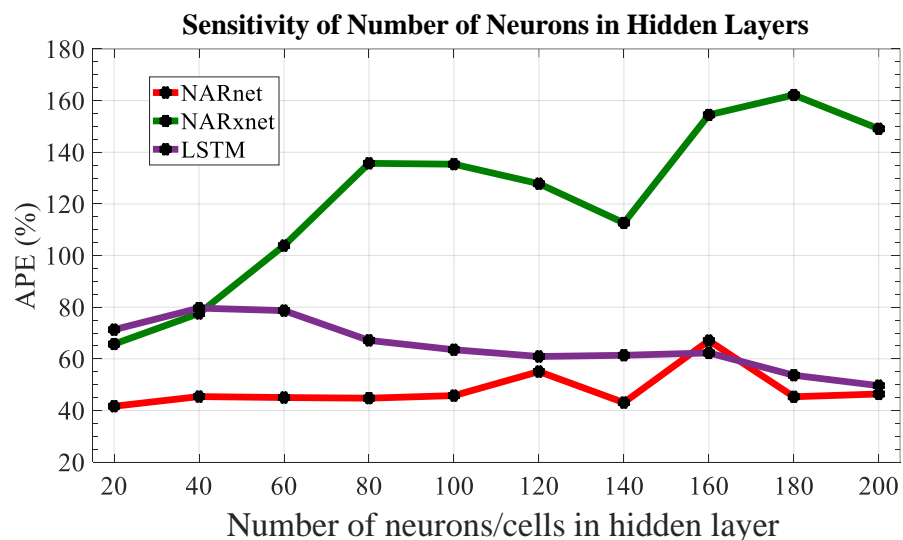


Figure 5.18: Sensitivity NARnet, NARXnet and LSTM neural network regarding the number of neurons in the hidden layer for hourly heat loss prediction in case study 2.

The NARnet and NARxnet shows minimum APE with 20 neurons in the hidden layer which is again similar to that of the first case study. However, APE is also found to be minimum with 140 neurons in hidden layer for NARnet which is not observed in first case study. For LSTM neural network the minimum APE is found with 200 LSTM cells in the hidden layer; however, with 100 to 160 LSTM cells in the hidden layer the APE remains almost constant. The APE slightly decreases with 180 cells in hidden layer and decrease again with 200 cells in the layer to reach at the minimum APE. This is different from the sensitivity analysis in the first case study where the APE started to increase after 100 cells in the hidden layer. Although, the minimum APE is found with 200 cells in the hidden layer, there is no significant improvement observed between 100 and 200 cells in the hidden layer. Moreover, the APE is significantly high for all configurations. Therefore, it is decided to choose the same configuration as it is used in the first case study for all three recurrent neural networks. The percentage error of all four neural networks for both the insulated and uninsulated walls are presented in Appendix C. Figure 5.19 shows the average of the percentage errors (APE) in hourly heat loss prediction with the feed forward, NARnet, NARxnet and LSTM neural networks trained using two years to fifteen years of heat loss data. Among all four neural networks, the feed forward neural network shows the lowest APE in all cases for the insulated wall except when it is trained with 15 year of heat loss data (shown in Figure 5.19-a). The APE reached around 10% when the feed forward network is trained with 7 and 11 years of heat loss data. For uninsulated wall, the APE of feed forward neural network is the lowest throughout all training cases (shown in Figure 5.19-b). The APE stays below 20% for both the walls when the feed forward network is trained with 7 years or more of heat loss data except with 10 years training. When the feedforward network is trained with 10 years of heat loss data the APE goes slightly over 20% in case of insulated wall however, for uninsulated wall it jumps to around 40%. Except this aberration in the uninsulated wall, the

feedforward network is able to achieve 80% accuracy in all cases when it is trained with 7 years or more of heat loss data. The APE of NARnet and NARxnet mostly stay above 50% except NARnet shows below 40% APE when it is trained with 13 years and 15 years of heat loss data, respectively.

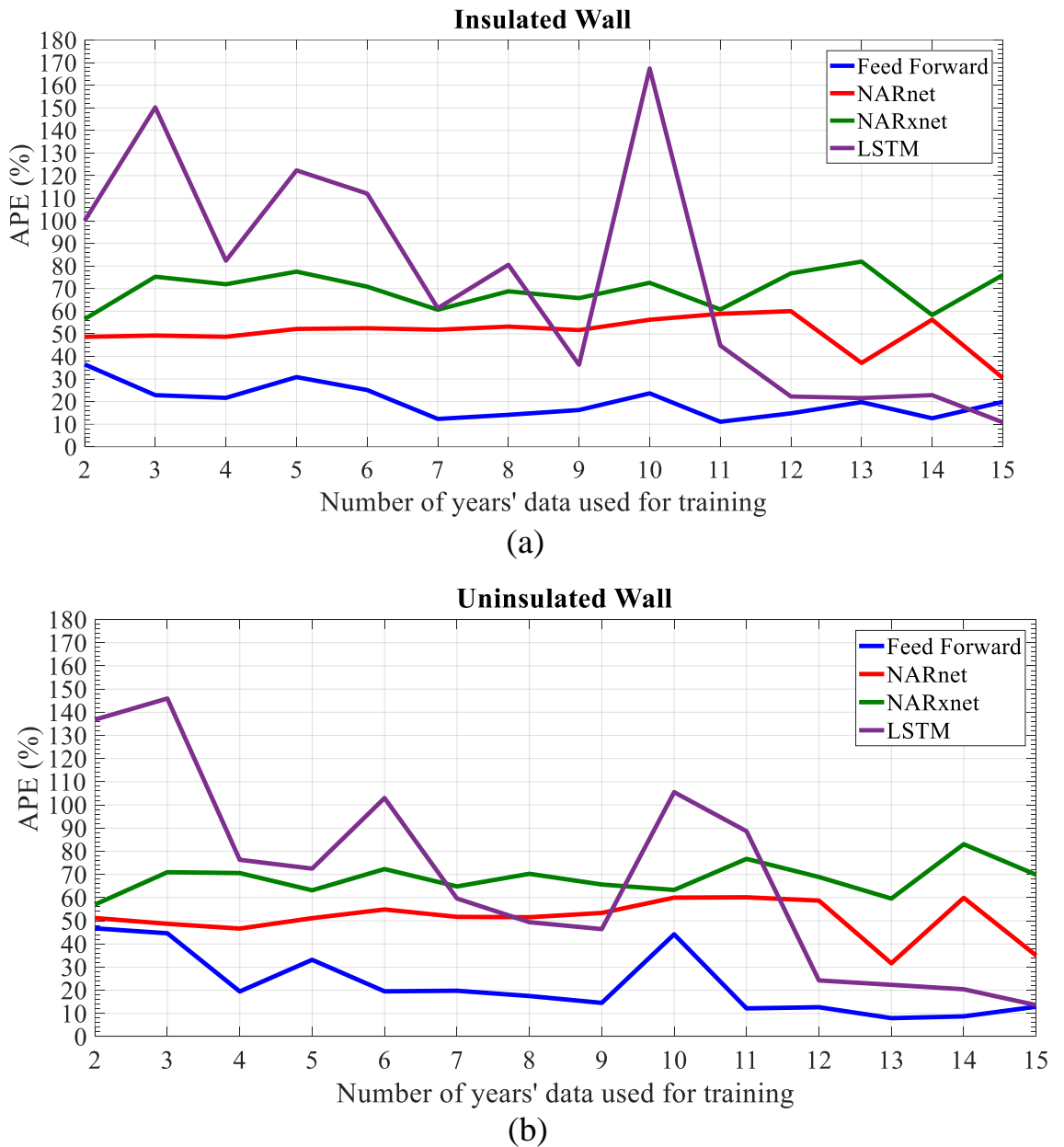


Figure 5.19: Comparison of performances among feed forward, NARnet, NARXnet and LSTM neural networks for hourly heat loss prediction in (a) insulated building and (b) uninsulated building in case study 2.

The LSTM neural network shows close to 20% APE when it is trained with 12 years or more of heat loss data with the lowest APE achieved by the network trained with 15 years of heat loss data. Therefore, similar conclusion as the first case study can be drawn based on the APE presented in Figure 5.19 which is NARnet, NARxnet and LSTM neural networks are not suitable for the hourly average heat loss prediction. The feed forward neural network is found to be capable of predicting the hourly average heat loss with more than 80% accuracy if it is trained with 7 years or more of heat loss data. Figure 5.20 shows the feed forward neural network predicted heat loss curve and the calculated heat loss curve for the years 2012-2019 for both the insulated and the uninsulated walls.

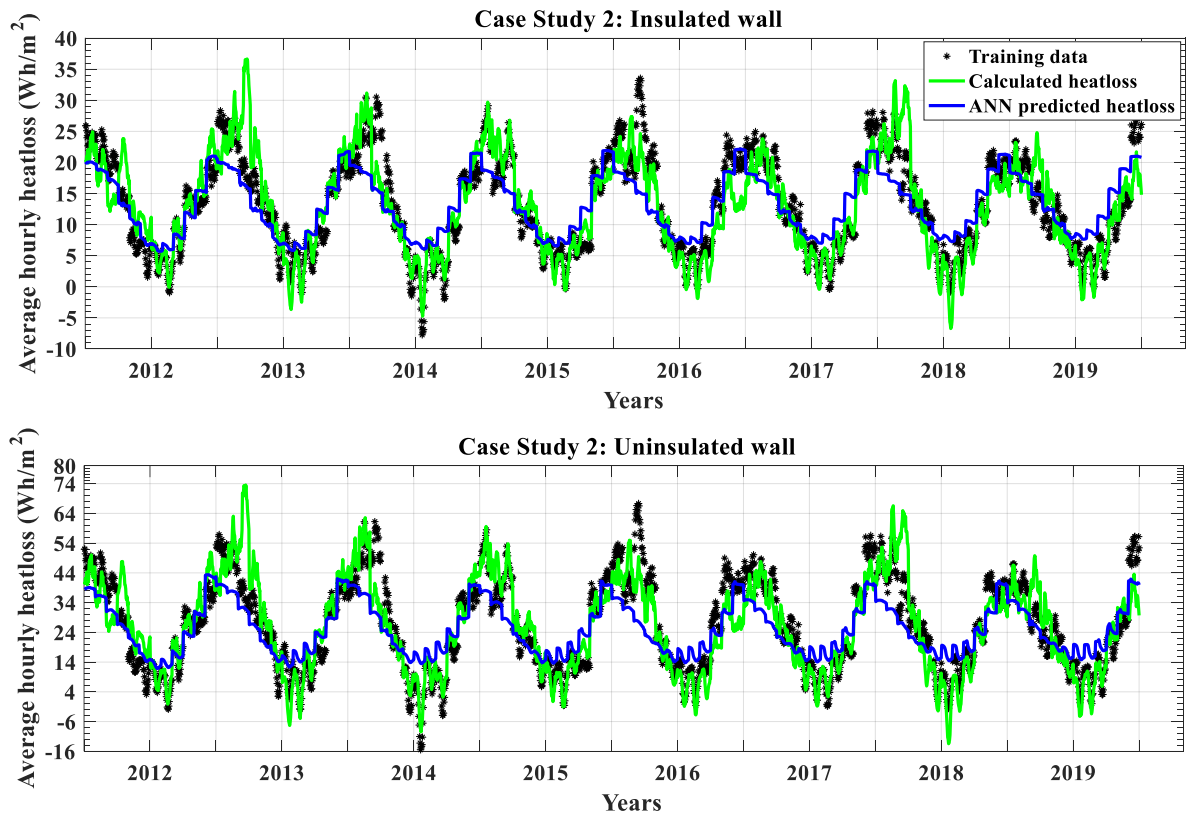


Figure 5.20: Comparison between the calculated heat loss and the ANN (feed forward) predicted heat loss for the years 2012 to 2019 in buildings of second case study.

Similar to the first case study, the feed forward neural network trained with 8 years of heat loss data from 2004 to 2011 is selected for the comparison. Again, the ANN predicted heat

losses are found to be very close to the calculated heat loss in most of the cases like in the first case study and similar type of deviations in the heat loss profile are observed as well. These deviations can be attributed to the variation in weather between the periods considered for training the ANN and predict the heat loss.

5.4.3 Monthly heat loss prediction

The result of sensitivity analysis regarding the number of hidden layers and the number of neurons in each hidden layer in a feed forward neural network for the monthly total heat loss prediction of this case is shown in Figure 5.21-a and 5.21-b, respectively.

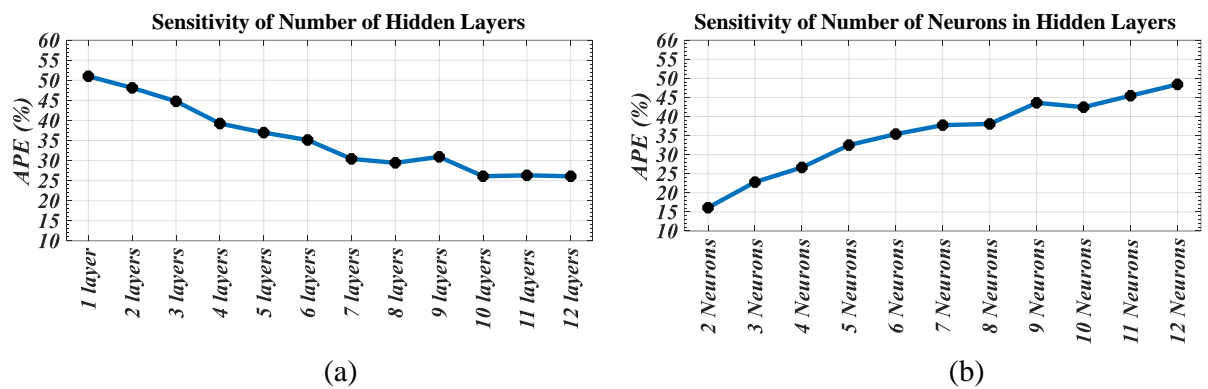


Figure 5.21: Sensitivity of feed forward neural network regarding (a) number of hidden layers and (b) number of neurons in each hidden layer for monthly heat loss prediction in the second case study.

Again, it is found that with the increase in number of hidden layers the APE decreases and with the increase in number of neurons in a hidden layer the APE increases. However, the APE reached the minimum and remain stable from 10 hidden layers. Regarding the sensitivity of number of neurons in a hidden layer, the minimum APE is obtained with two neurons in each hidden layer. Therefore, the feed forward network configuration used in the monthly heat loss prediction in the first case study can be adopted in this case study as well. Figure 5.22 shows the result of the sensitivity analysis regarding the number of neurons in

the hidden layer for NARnet and NARxnet and the number of cells in the hidden layer for LSTM neural network. Again, the APE of LSTM neural network is far lower than the APE of NARnet and NARxnet as found in the first case study. The minimum APE for NARnet and NARxnet is found to 60% with 12 neurons in the hidden layer, which is very poor prediction accuracy. However, these two networks are considered to use for the monthly heat loss prediction to further evaluate their performance with full data set. The APE of LSTM neural network is stable and remains below 10% with all different combinations of LSTM cells in the hidden layer. Therefore, the LSTM neural network with 12 cells in the hidden layer is selected for the current case study as the same configuration shows very good prediction accuracy in the first case study. Moreover, keeping the number of cells in the hidden layer as low as possible facilitates faster calculation in short time.

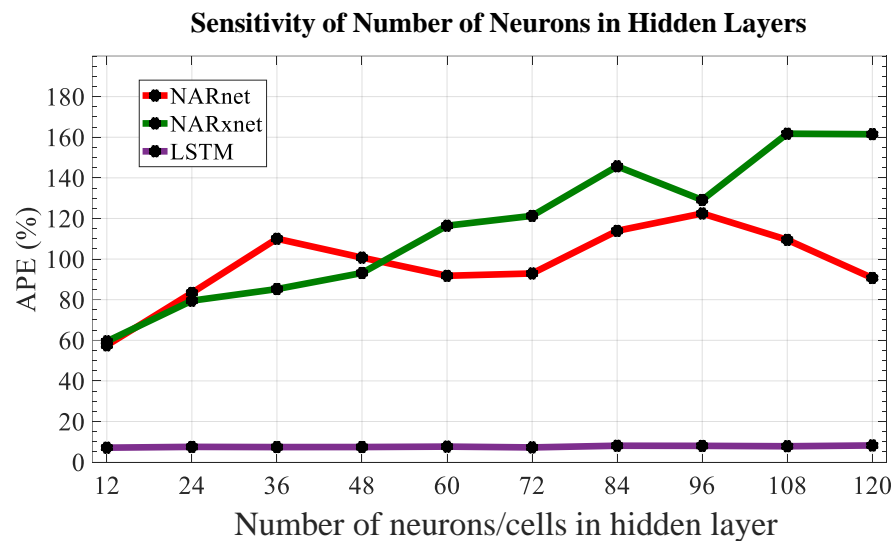
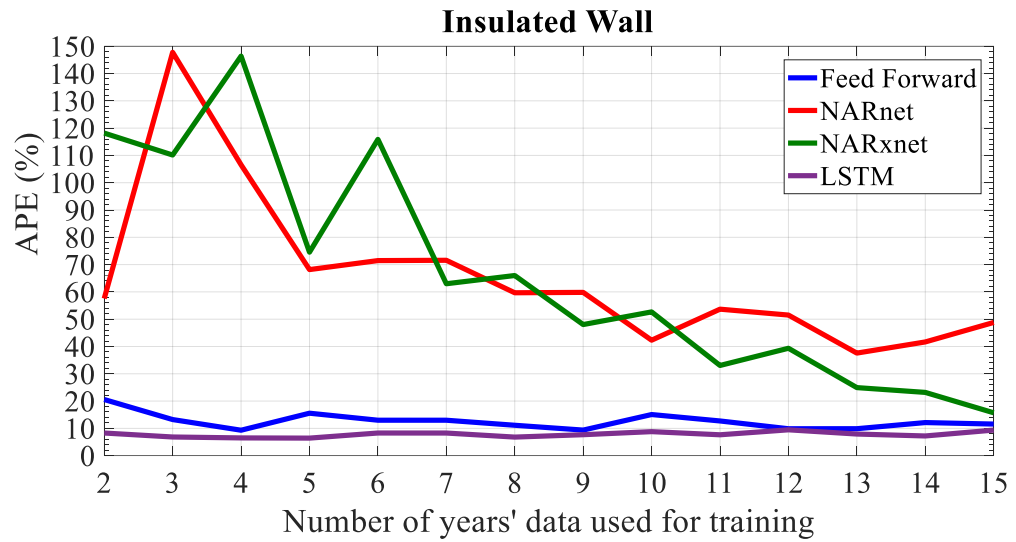


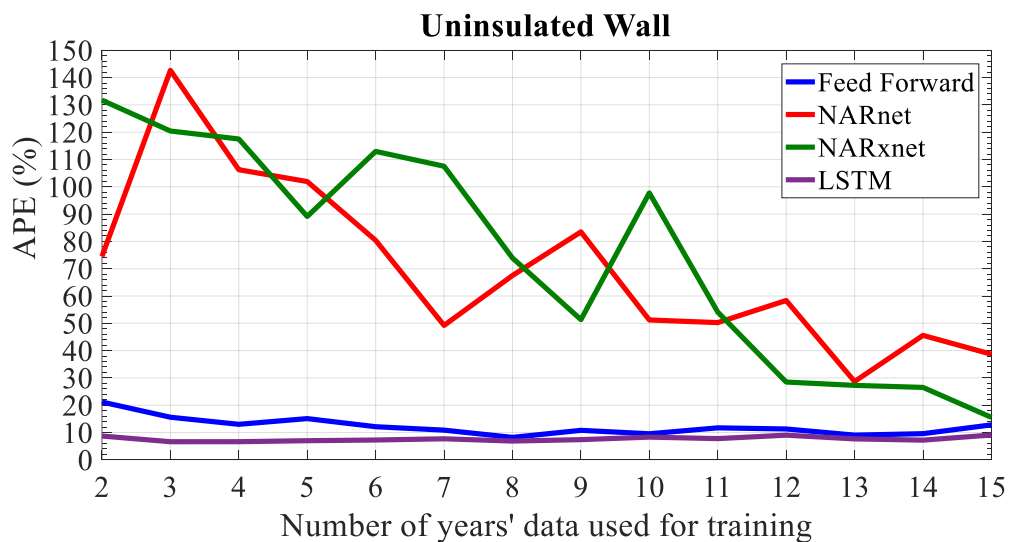
Figure 5.22: Sensitivity NARnet, NARxnet and LSTM neural network regarding number of neurons in hidden layer for monthly heat loss prediction in second case study.

The percentage error of all four neural networks used in the case study and trained with 2 years to 15 years of heat loss data are included in Appendix D for both wall types. Figures 5.23-a and 5.23-b show the mean value of percentage errors in the monthly heat loss

prediction for the insulated and the uninsulated wall for different networks where the networks are trained with 2 years to 15 years of heat loss data. Similar to the first case study, the LSTM neural network shows the best performance among all the neural networks used in the current case study. The APE of the LSTM neural network remains consistently less than 10% in all cases which is even better than that of the first case study.



(a)



(b)

Figure 5.23: Comparison of performances among feed forward, NARnet, NARxnet and LSTM neural network for monthly heat loss prediction in (a) insulated building and (b) uninsulated building in case study 2.

In first case study the APE of the LSTM network trained with 5 years of heat loss data jumps to 20% which does not occur here. The APE of the feed forward neural network remains slightly higher than that of the LSTM network and it ranges between 10% and 20%. However, in some cases for instance when the network is trained with 9 years and 12 years of heat loss data for insulated wall, the APE is same for both the feed forward networks and the LSTM network. Another similarity in the APE between the feed forward network and the LSTM network is observed in case of uninsulated wall when the network is trained with 8 years and 10 years of heat loss data. The performance of NARnet and NARxnet is far behind the performance of LSTM and feed forward neural network. Only the NARxnet shows below 20% APE when the network is trained with 15 years of heat loss data which also observed in the monthly heat loss prediction in the first case study. The NARnet shows the minimum APE when the network is trained with 13 years of heat loss data which is different than the first case study where NARnet achieves the minimum APE when trained with 15 years of heat loss data. As the NARnet and NARxnet show very high APE for most of the cases, they are considered unsuitable for monthly total heat loss prediction. It is decided to compare the LSTM neural network predicted heat loss curve with the calculated heat loss curve for the network that is trained with 8 years of heat loss data because the LSTM neural network shows the best prediction performance, and the first case study shows that the networks trained with 8 years of more of heat loss data are stable enough to learn the characteristics of training data with significant accuracy. Figure 5.24 shows the comparison between calculated heat loss and LSTM neural network predicted heat loss for both the insulated wall and the uninsulated wall; and it is found from the figure that both the actual and the ANN predicted heat loss curves show identical trend. Although there are some deviations noticed, for instance the higher calculated heat loss in February-March of 2013

and 2018, these are assignable to extreme weather as discussed in the first case study as well as in the hourly heat loss predictions.

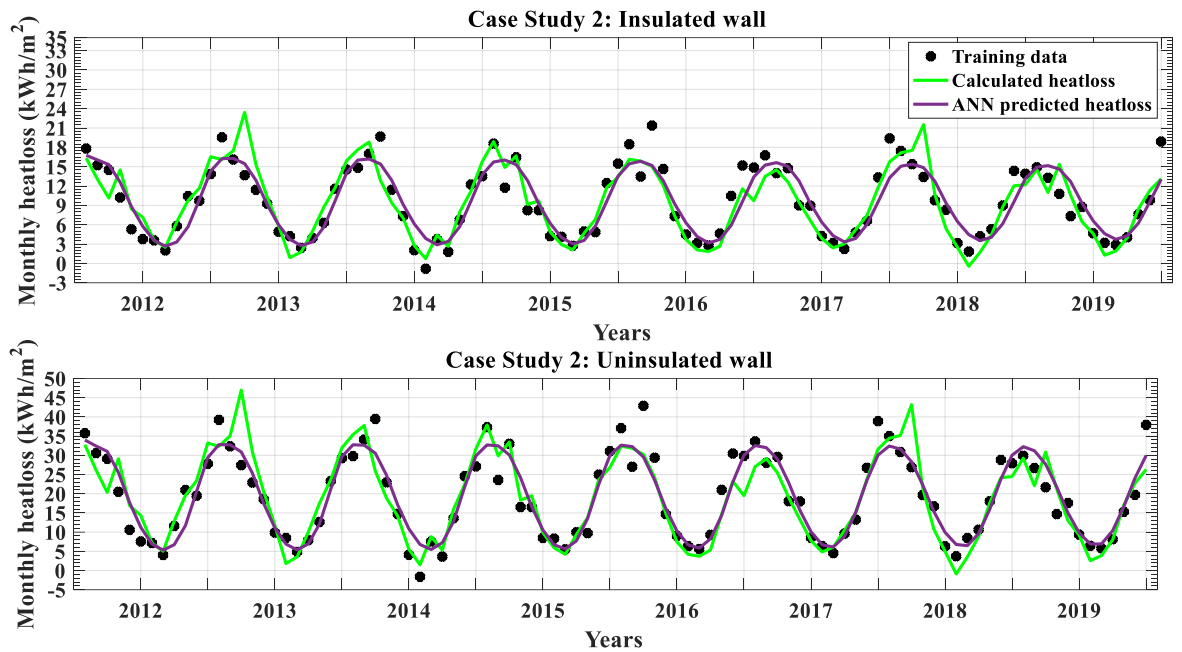


Figure 5.24: Comparison between the calculated monthly heat loss and the ANN (LSTM) predicted monthly heat loss for the years 2012 to 2019 in buildings of second case study.

5.5 Energy savings

The two case studies presented in this chapter demonstrate that feed forward neural network is suitable for hourly average heat loss prediction and LSTM neural network is suitable for monthly total heat loss prediction with a significant accuracy when the neural networks are trained with more than 8 year of heat loss data. However, it is worthy to look at the estimation of energy savings using the ANN predicted heat losses. Figure 5.25-a 5.25-b show the estimated energy savings in the insulated buildings for the first and second case study, respectively. The hourly average heat loss predicted by the feed forward network and the monthly total heat loss predicted by the LSTM neural networks are considered for energy savings estimation where all the networks are trained with 8 years of heat loss data. The difference in yearly total heat loss between the insulated building and the uninsulated

building represents the energy savings. The energy savings is calculated for the years 2012 to 2019 for both case studies. The calculated heat loss in the years 2012 to 2019 for both buildings in both case studies are considered to compare with the ANN results.

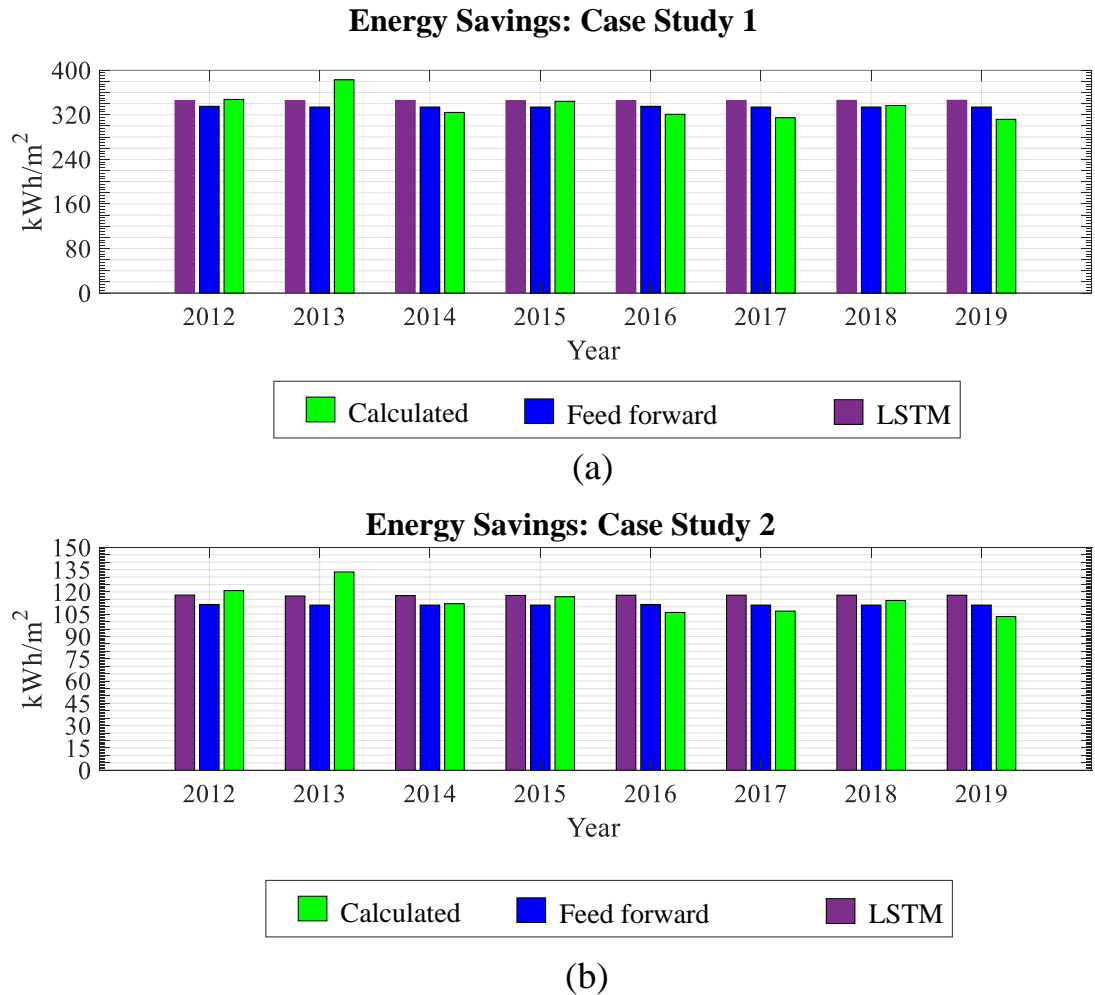


Figure 5.25: Comparison of energy savings among calculated heat loss, feed forward neural network predicted heat and LSTM neural network predicted heat loss: (a) case study 1 and (b) case study 2

It is found from Figure 5.25 that the difference between the ANN predicted energy savings and the calculated energy savings stays between $\pm 35 \text{ kWh/m}^2$ ($\pm 10\%$) in the first case study and between $\pm 15 \text{ kWh/m}^2$ ($\pm 10\%$) in the second case study for all the years except 2013. The deviation in 2013 is $\pm 49 \text{ kWh/m}^2$ ($\pm 12\%$) and $\pm 22 \text{ kWh/m}^2$ ($\pm 16\%$) for the first and

second case study, respectively. Looking at the heat map in Figure 5.10 it is found that the winter in 2013 is cooler than any other years in the heat map and the summer is warmer than any other years in the heat map. Therefore, the extreme weather in 2013 is responsible for the high deviation in the ANN energy savings. Therefore, the case studies confirm that the ANN can guarantee 84% accuracy to estimate energy savings despite the influence of extreme weather condition. It is highly unlikely to see extreme winter and summer like the year 2013 regularly and therefore, ANN is expected to achieve 90% prediction accuracy for estimation of energy savings in majority of cases. Figure 5.26 shows the payback periods which are estimated using the feed forward and LSTM neural network predicted heat loss as well the using the calculated heat loss for retrofitting an uninsulated building with improved insulation to achieve the performance of insulated building presented in the first case study. Considering the buildings are centrally heated using gas boiler and the price of gas is 3.9 pence/ kWh (United Kingdom natural gas prices, no date) the savings in energy bills can be calculated. According to that the average savings are listed in Table 5.1.

Table 5.1: Average savings in energy bills per year.

	Average savings per year (£/m ²)	Cost of Investment (£/m ²)
Actual calculation	13.08	100
Feedforward neural network prediction	13.04	
LSTM neural network prediction	13.48	

Assuming the cost of retrofitting is £100/m² (The Green Age, 2016), the payback period for the calculated heat loss is found to 7 years and 7 months. With the similar assumptions, the payback period estimated using the LSTM neural network predicted heat loss is 7 years 5 months and the payback period estimated using the feed forward neural predicted heat loss is 7 years 8 months. Therefore, the deviation in estimated payback period using the ANN predicted heat loss is within ±2 months and that shows the practicability of using ANN to

predict heat loss and estimate the payback period of the investment on retrofitting buildings with improved insulation.

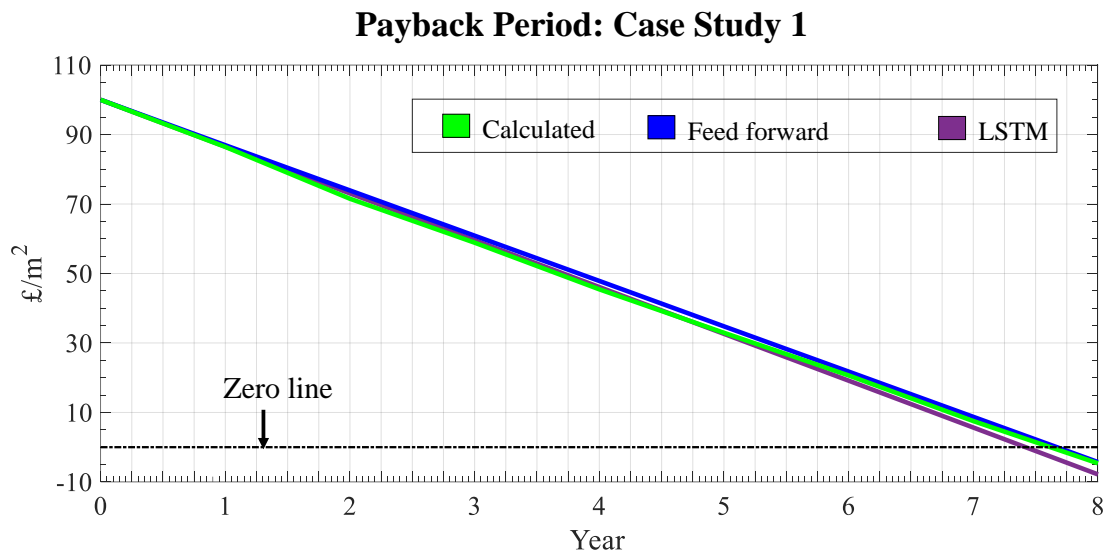


Figure 5.26: Estimation of simple payback period for the retrofitted house in case study 1.

5.6 Conclusion

Real buildings experience variable weather conditions and complex occupants' behaviour and therefore it is difficult to estimate exact energy savings in a building other than monitoring it for a long period. In fact, the mathematical model presented in this chapter confirms that the monitoring period is infinity. Hence, it is more practical to simulate the potential energy performance of a building using a simplified model with sufficient real data. In relation to that, a novel approach for predicting heat loss through a building's wall integrating thermography and ANN is presented in this chapter and its application is validated with two case studies. The infrared image analysis of the buildings in both case studies shows the rapidness and practicability in evaluating a building's thermal performance in a noncontact way. The sensitivity analysis of parameters regarding different ANN's configuration in both case studies shows identical responses and indicates that configuration of the different ANN presented in Figure 5.4 and Figure 5.6 would be ideal to use for heat

loss prediction. It is found from the result of the case studies that feed forward neural network with six hidden layers and three neurons in each hidden layer is the most suitable configuration for hourly average heat loss prediction and LSTM neural network with 12 LSTM cells in the hidden layer is the most suitable configuration for monthly total heat loss prediction. Although the mathematical model suggests that a building should be monitored for infinite number of years, the case study results demonstrate that 8 years monitoring data is sufficient for the ANN to predict heat loss with reasonable accuracy. Regarding estimation of energy savings in an externally insulated building, the approach to predict hourly average heat loss using feed forward and the approach to predict monthly total heat loss using LSTM neural network show similar performance. However, the monthly total heat loss prediction approach is faster than the hourly heat average heat loss prediction approach as it requires less calculation during the training process of ANN. The payback period analysis demonstrates that using ANN prediction for energy savings estimation in a retrofitted house with improved insulation would be able to determine the projected payback period which is accurate up to the quarter of a year. The application of this novel approach can facilitate architects and engineers to evaluate the thermal performance of a building's wall ahead of executing the building's retrofits. This will also allow the investors to realise the rate of return on the investments for retrofitting a building before the investment is made. Considering the complex and variable environmental parameters such as temperature, wind speed, solar irradiation and uncertain people's behaviour, monitoring a building for many years will not guarantee exact estimation of energy savings. Rather the use of the simplified approach presented in this chapter with some assumption would provide sufficient information about energy savings with reasonable accuracy.

Chapter 6: Development of U-value Estimation Kit

6.1 Introduction

The literature review points out the limitations of existing U-value measurement methods and there is a research gap in applying ANN integrated with infrared thermography for the estimation of U-value of a building's wall. In order to overcome the limitations of existing U-value estimation methods, the idea to develop a novel U-value estimation kit is presented in chapter 3. One of the key limitations of the current methods is the mandatory existence of a significant thermal gradient between indoor and outdoor environment and the novel product is designed to overcome this problem with the introduction of a point heat source from the internal side of a wall. Monitoring the walls during the application of point heat would provide significant information regarding the thermal characteristics of a wall. ANN can be employed to learn those thermal characteristics of a wall and identify the wall type based on that. In this chapter the development process of the novel U-value estimation kit is described. The next section describes the construction process of the proposed U-value kit followed by some initial experimental work with it. Section 6.3 includes the required modification made on the basis of the outcomes of those initial experiments. Section 6.4 discusses the visual inspection of the infrared images obtained from monitoring some sample materials with the U-value kit followed by the introduction of ANN to analyse these data in section 6.5. The monitoring of some sample walls made of the materials used in real buildings' construction are discussed in section 6.6. Section 6.7 includes the detailed process of developing key temperature profiles for ANN analysis based on the visual inspection of infrared images. In section 6.8 the categorisation of wall types using ANN based on the temperature profiles developed in section 6.7 is presented. A similar case study, as a part of

this PhD research, has been published in Sen and Habaibeh (2019) which is added in Appendix F.

6.2 Construction of the U-value kit

In order to construct the U-value estimation kit according to the schematic set up presented in chapter 3 (Figure 3.4), 3D CAD model of the major parts of it are developed using SolidWorks software.

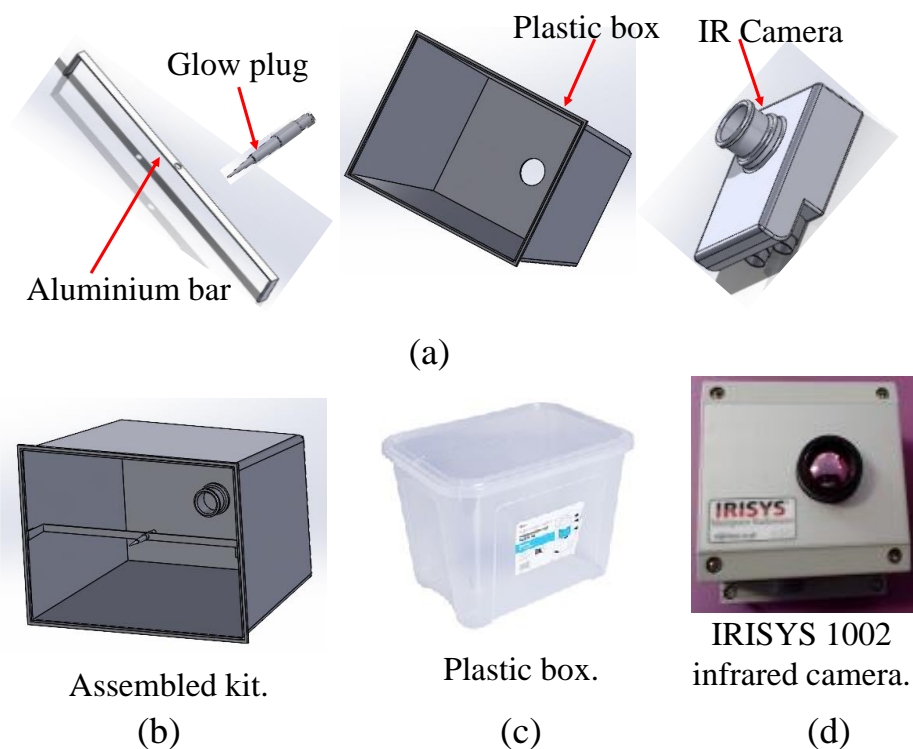


Figure 6.1: Schematic model of the proposed U-value kit with its major parts and assembly.

Figure 6.1-a shows the major parts of the U-value kit and Figure 6.2-b shows the assembled 3D model. A plastic box of dimension 37.7x27.7x27.8 cm is chosen as the main body of the U-value kit. IRISYS 1002 infrared camera is selected to capture infrared images at the initial phase of this product development as it is readily available in the laboratory. It is designed to fit the camera at the bottom of the plastic box. The plastic box and the infrared camera is

shown in Figure 6.1-c and 6.1-d, respectively. IRISYS 1002 infrared camera is a low-resolution infrared camera that is able to capture and save infrared images in 16x16 pixels format. A car engine glow plug is chosen to use as the point heater. The car engine glow plug operates with DC power supply and can generate very high heat at the tip of it. By controlling the input voltage, it is possible to control the amount of heat generated at the tip of the plug. The response of the glow plug is tested by supplying low voltage at different ranges using a variable DC power supply to determine the optimum operating voltage which is shown in Figure 6.2.

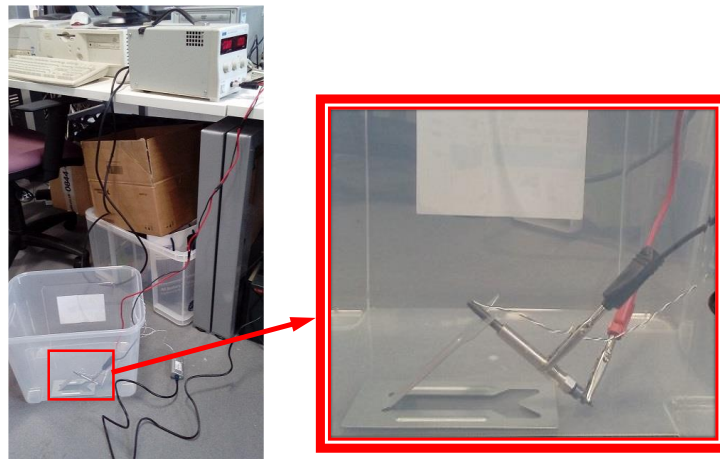


Figure 6.2: The test of glow plug performance of with the help of a variable power supply.

The tip temperature of the glow plug is measured by using a K-type thermocouple-based temperature sensor. It is found that at supply voltage 1V the tip temperature reaches at 70°C and at supply voltage 3V the tip temperature reaches at 150°C. This is a very high temperature, and it may risk burning of wall surface. However, the area of glow plug tip that comes in contact with the wall surface is very small. Therefore, it may not cause any damage to the wall surface. In order to find the effect of heating a surface with the glow plug, it is tested on a MDF board for about an hour (shown in Figure 6.3).

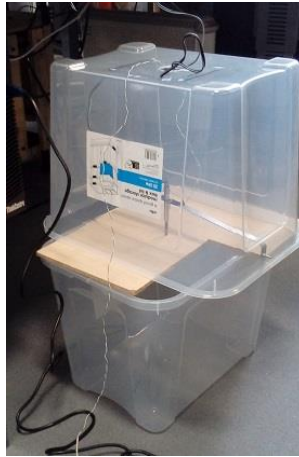


Figure 6.3: Test of the glow plug heating on MDF board for burning spot.

After an hour of heating, it is found from visual inspection that the MDF board does not have any burning marks or spot. The absence of any burning mark or spot signifies that glow plug is safe to use as heater in the test rig. The glow plug is fitted in the plastic box with the help of an aluminium bar. A K-type thermocouple is also attached at the tip of glow plug to measure the tip temperature. This is to ensure that if the tip temperature becomes dangerously high at any point during the experimentation due to any electrical fault, the power supply could be cut off before it catches fire.

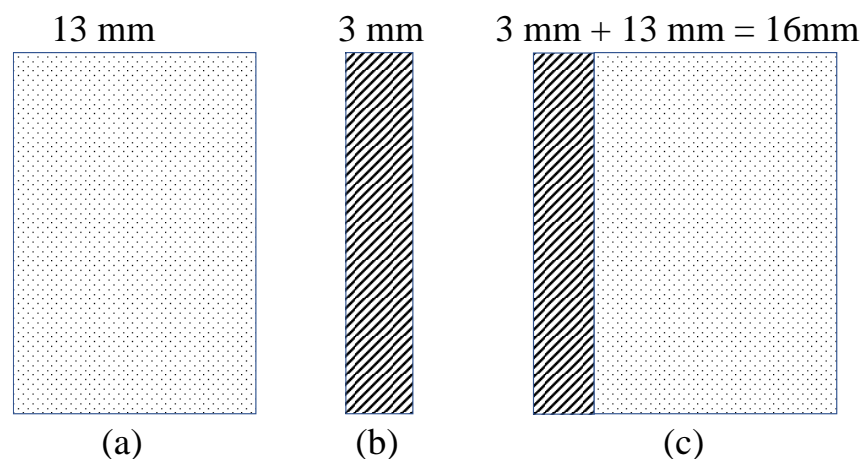


Figure 6.4: Schematic diagram of (a) sample A (MDF), (b) sample B (MS) and (c) sample C (MS and MDF clamped together).

For the initial experiment, it is planned to select two samples: one sample consists of a material with high thermal insulation and another sample consists of a with high thermal conductivity; so that their thermal responses after applying the point heat can be easily differentiated by visual inspection of respective infrared images. Afterwards, a third sample is added as combination of these two materials attached together. For that, a 13 mm thick Medium Density Fibre (MDF) board is selected as material with high thermal insulation which is named as sample A. A Mild Steel (MS) sheet of thickness 3 mm is selected as material with high thermal conductivity which is named as sample 'B'. Sample 'C' is constructed as the combination of A and sample B by clamping them together. The thermal conductivity of MDF is 0.18 W/m.K (ISO 10456, 2007), and the thermal conductivity of MS is 50 W/m.K (Anderson, 2006). The samples are schematically presented in the diagrams of Figure 6.4. The detailed properties of these three samples are included in Table 6.1. The U-values of these samples are calculated using equation 2.3. Equation 2.3 includes thermal resistances of air at internal and external wall surfaces. The layers of stagnant air near the wall surfaces limit the heat transfer to their resistance values. Hence, the air resistances at both sides need to be considered to avoid overestimation of the U-value. The heat generated by the glow plug is transferred through the wall from internal side to external side in two mechanisms. Firstly, direct conduction of heat at the point where the glow plug touches the wall. Secondly, the heat gained by the air in the internal side of the wall due to convection is conducted through the wall. In both cases, thermal resistance of the air in the external side needs to be considered for the U-value calculation due to the presence of stagnant air in the external side. For the first mechanism the thermal resistance of air in the internal side is not applicable as there is no gap between the glow plug and the wall. For the second mechanism the thermal resistance of air in the internal side needs to be considered as a stagnant layer of air present near the wall. In a 16x16 pixel infrared image, heat transfer by second mechanism

occurs at 255 points out of 256 and they require considering the thermal resistance of air in the internal side. The heat transfer by first mechanism occurs at only one point out of 256 where the thermal resistance of air is not considered. As a result, neglecting the exclusion of internal air resistance for one point would simplify the calculation process without affecting the result. Therefore, the thermal resistance of air at internal surface and external surface is considered as 0.13 and 0.04 respectively for the entire wall (Anderson, 2006).

Table 6.1: Properties of samples A, B and C

Sample No	Material	Thickness (mm)	Thermal Conductivity (W/m.K)	U-value (W/m ² K)
A	MDF	13	0.18	4.128
B	MS	3	50	5.880
C	MS and MDF clamped together	13 + 3 = 16	-	4.127

The initial experiments conducted on sample A and sample B are shown in Figure 6.5-a and Figure 6.5-b respectively. The infrared images are captured at 5 seconds interval. The tip temperature and external environment temperature are measured using a K-type thermocouple and the readings are logged with National Instrument's USB-TC01 data acquisition system with an interval of 1 second.



Figure 6.5: Initial test on (a) sample A (b) sample B.

During the experiments, the samples are monitored for about an hour, and the infrared images are then visually analysed. Figure 6.6 includes the infrared images after 1 minute, 10 minutes, 30 minutes and 50 minutes, respectively from the experiment on sample A and Figure 6.7 includes the infrared image at the same intervals from the experiment on sample B. The original low resolution images are enhanced to high resolution to facilitate visual inspection. In all infrared images, the bright area at the centre of the image represents the position of the glow plug heater. The bright area continuing from centre towards the left of the images represent only half portion of the aluminium bar that holds the heater. However, it is expected that the full aluminium bar to be represented in the infrared images because it is the same material in both sides and the glow plug is positioned at the centre of the aluminium bar. One possible reason for this unbalanced image is probably the presence of the wires that connects the heater with the power supply. As the wires are fixed on the left portion of aluminium bar, the heat coming out of the wires become prominent in the infrared images. Furthermore, because of these very bright areas at the centre of the images, the change in temperatures at the surrounding of the heater is difficult to detect.

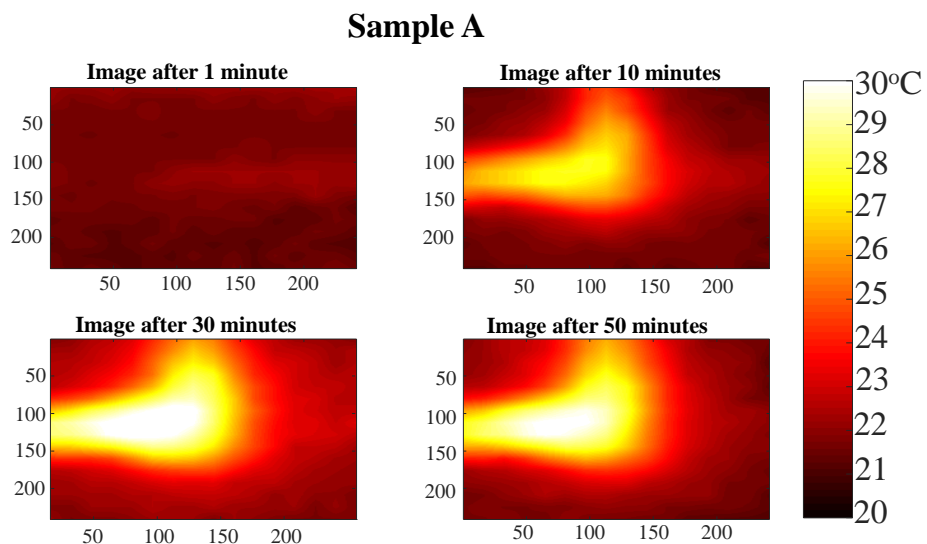


Figure 6.6: Infrared images of sample A from the initial test.

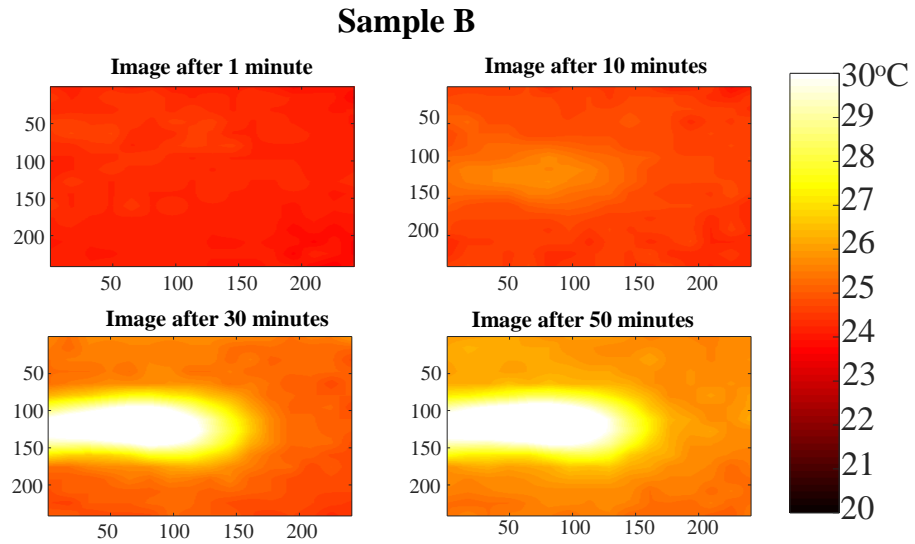


Figure 6.7: Infrared images of Sample B from the initial test.

To overcome this problem the aluminium bar and the rear portion of glow plug are insulated with rock wool. Figure 6.8-a shows the rock wool insulation on the aluminium bar and Figure 6.8-b shows the wrapping on the insulation.

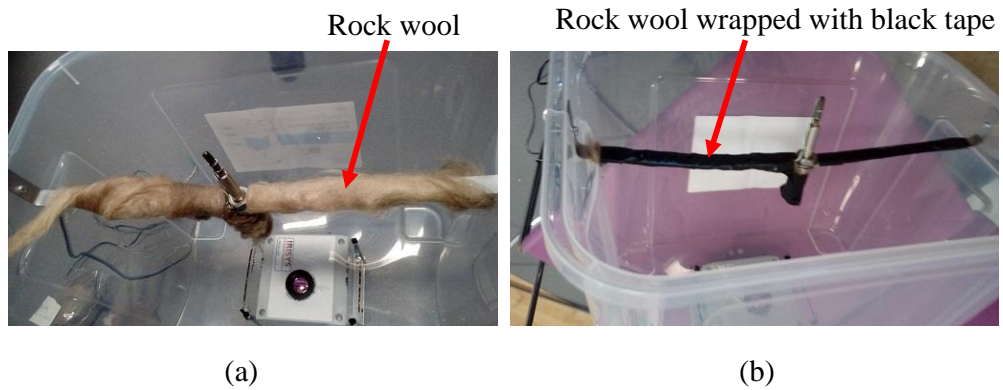


Figure 6.8: (a) rock wool insulation of aluminium bar and glow plug and (b) the wrapping on the insulation.

6.3 Experiment with the modified test kit

After modifying the test rig, the same experiments are conducted again on sample A and sample B. The experimental set up is shown in Figure 6.9 for sample A and in Figure 6.10 for sample B.

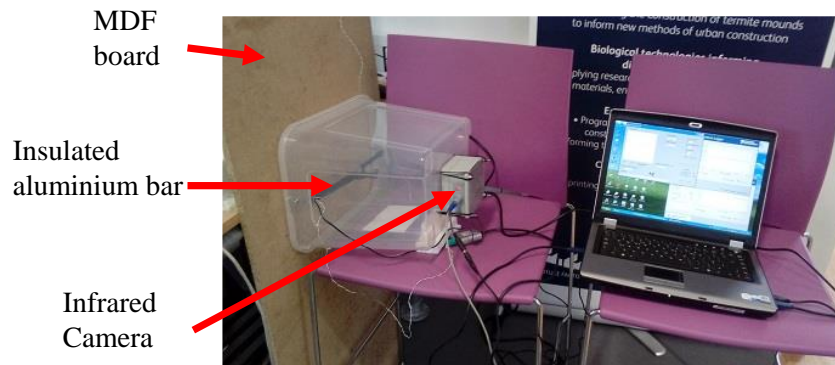


Figure 6.9: Test on sample A after modification

The previous experiments show that it is sufficient to monitor the samples for 50 minutes to obtain the distinguishable features in infrared images by visual inspection. Therefore, in this occasion, the samples are also monitored for about an hour to ensure that at least 50 minutes data would be available for analysis. The infrared images are saved at interval of 5 seconds, and the tip temperature and external environment temperatures are recorded at intervals of 1 second using K-type thermocouple and USB-TC01 data acquisition system. Figure 6.11-a, 6.11-b, 6.11-c and 6.11-d show the comparisons between infrared images of sample A and sample B after 1 minute, 10 minutes, 30 minutes and 50 minutes respectively from the experiments conducted with the modified test kit.

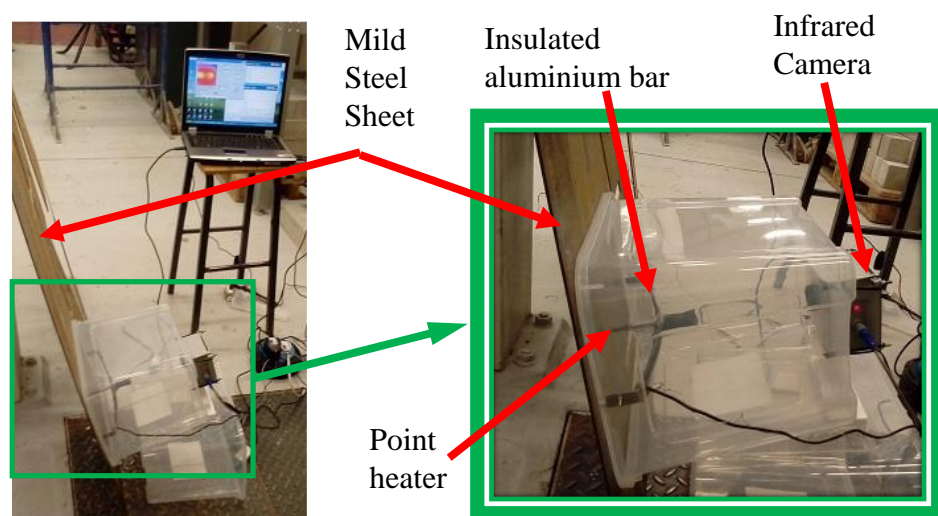


Figure 6.10: Test on sample B after modification

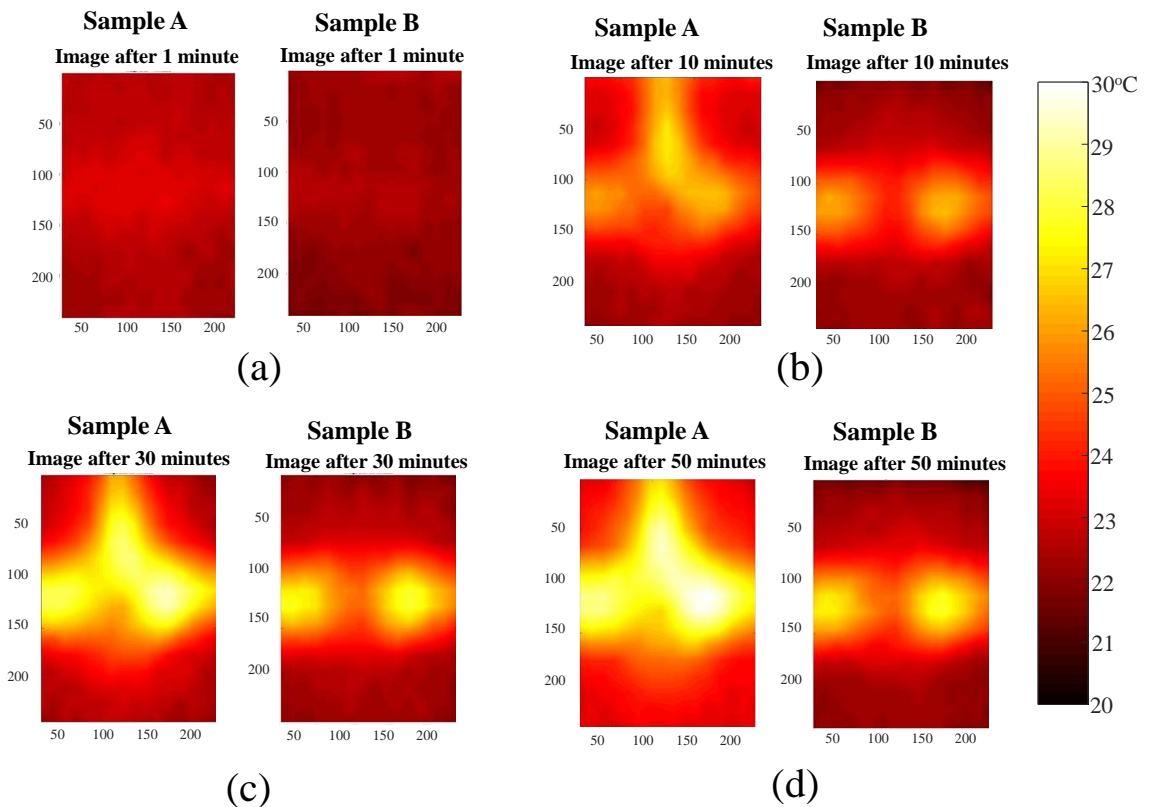


Figure 6.11: Infrared images of sample A1 and sample A2: (a) after 1 minute, (b) after 10 minutes, (c) after 30 minutes and (d) after 50 minutes.

It is noticed in the infrared images of Figure 6.11 that the glow plug heater is no more visible, and the aluminium bar is equally visible on both sides of the heater. As a result, the temperature changes in surrounding areas of heater are clearly detectable through visual inspection. The infrared images of sample A and B show that the surfaces get warm over the time due to application of point heat which is noticeable after 10 minutes. It is also observed from the infrared images that the temperature on the surface of sample A increases at a faster rate than that of the sample B which clearly reflects the difference in heat transfer through a highly conductive material and a highly insulated material. As sample A consists of a highly insulated material with low U-value, most of the applied heat could not pass through the surface which makes the surface very warm at the end of the monitoring period. On the other

hand, most of the applied heat passes through the surface of sample B as it is a highly conductive material leaving the surface cooler than that of the sample A. To evaluate the temperature distribution on the surface of a moderately conductive or moderately insulating material, the same experiment is repeated on sample C as shown in Figure 6.12. The infrared images obtained from this experiment are compared with the infrared images of sample A and sample B.

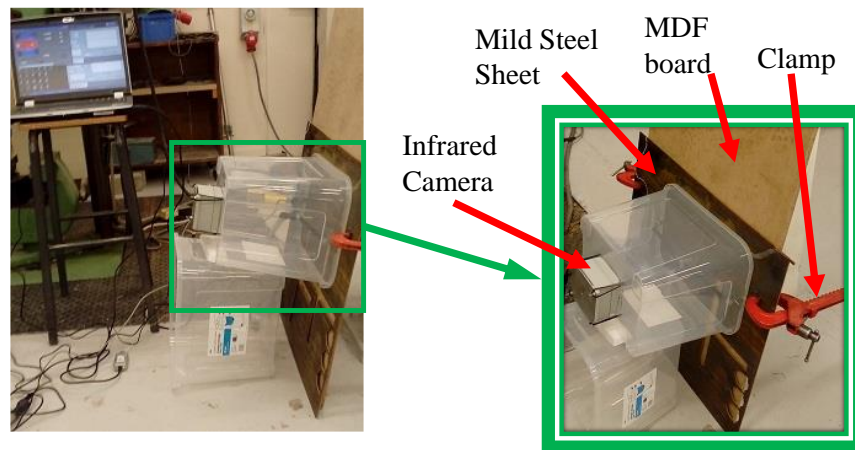


Figure 6.12: Test on sample A3 after modification of test rig.

6.4 Visual analysis of infrared images from samples A, B and C

The 16x16 pixel infrared images, obtained from the experiments conducted on samples A, B and C are reproduced to 241x241 pixel image in MATLAB for better visual representation. The images are then placed adjacent to each other in one frame to visually inspect the difference among them. Figure 6.13-a, 6.13-b and 6.13-c show the infrared images of sample A, sample B and sample C respectively. In each infrared image, three areas are spotted where the temperature differences among the similar areas in other images can be visually differentiated based on the characteristics of brightness. These areas are marked with black circle in the images of Figure 6.13. All the circled areas on the infrared image of sample A are brighter than same areas of two other infrared image.

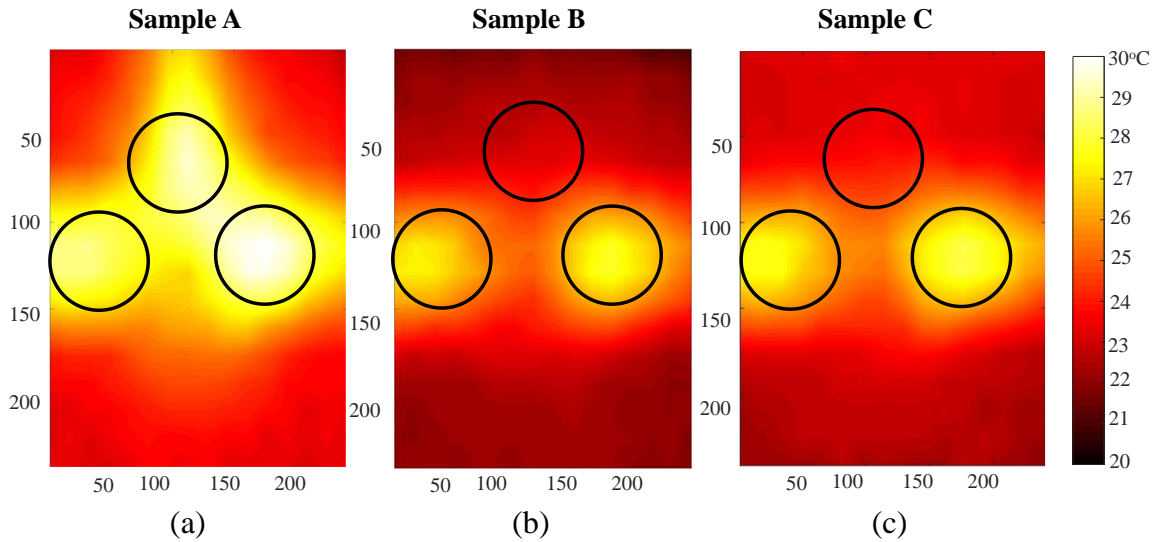


Figure 6.13: infrared image of (a) sample A, (b) sample B and (C) sample C.

The left and right circled areas on the image sample C are slightly brighter than the same areas of the image of sample B. However, the top-circled areas of these two images are not clearly distinguishable. MDF has a very low thermal conductivity compared to MS, and consequently less heat passes to the other side through the surface of the sample A than that of the samples B and C. Therefore, the surface temperature of sample A becomes higher than that of samples B and C, which is represented by high intensity of bright areas in the respective infrared image. The equivalent thermal transmittance or U-value of sample C is lower than that of sample B and but higher than the U-value of sample A. Therefore, intensity of brightness in the circled areas on the infrared image of sample C is higher than that of sample B but lower than that of sample A. In order to study the temperature profile through any point on an infrared image, the temperature values of a specific point on the first 600 images are extracted for all three samples. These temperature values are plotted in pairs to visually compare the temperature profiles. Figure 6.14 shows the temperature profiles through same points on infrared images of sample A and sample B. Figure 6.15 and 6.16 show the temperature profile comparison between the same points on infrared image of sample C vs sample B and sample A vs sample C, respectively.

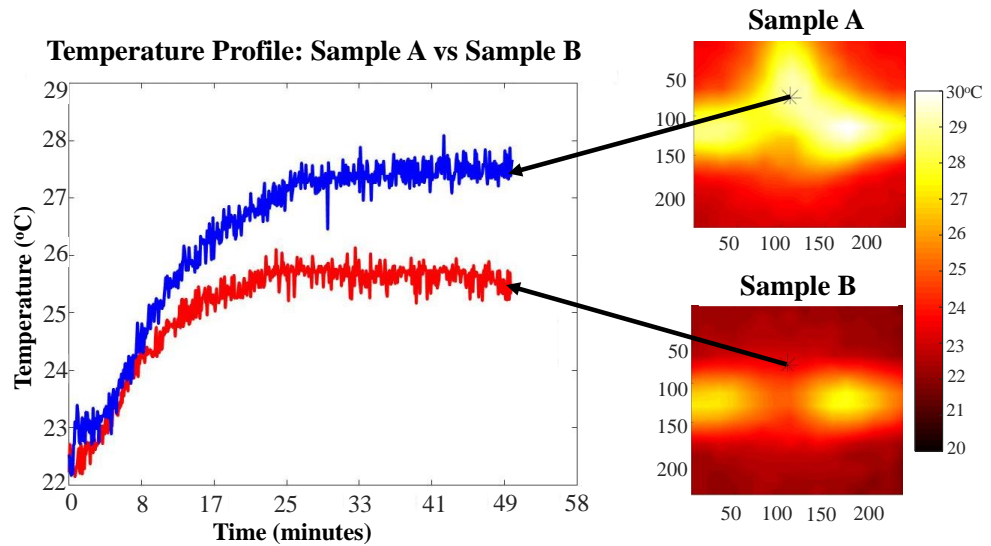


Figure 6.14: Comparison of temperature profile through a specific point on infrared images of sample A and sample B.

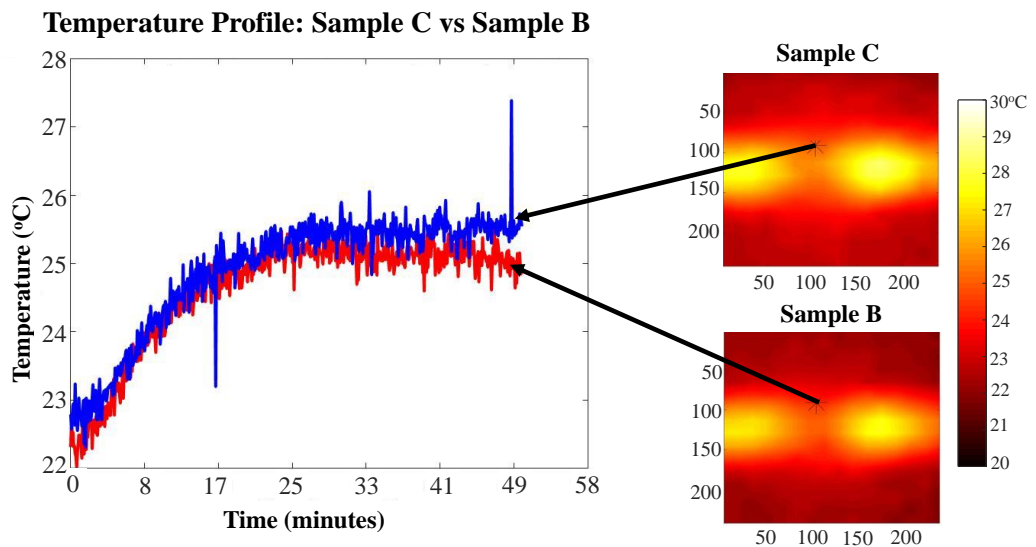


Figure 6.15: Comparison of temperature profile through a specific point on infrared images of sample C and sample B.

In all three cases it is found that the temperature profile of the sample with lower U-value remain higher than the temperature profile of the specimen with higher U-value. Similarly, the temperature profiles generated through some other points in left, right and bottom areas of infrared images for all three cases report identical outcomes and the sample or wall types are clearly recognised from the visual inspection of those temperature profiles. The above

method of visual inspection confirms that by analysing the temperature profile through some specific points on a series of infrared images acquired under the application of a point heat, it is possible to identify the wall type. Therefore, the use of ANN in relation to the analysis of the infrared images with the temperature profiles generated through each point could enhance the identification process.

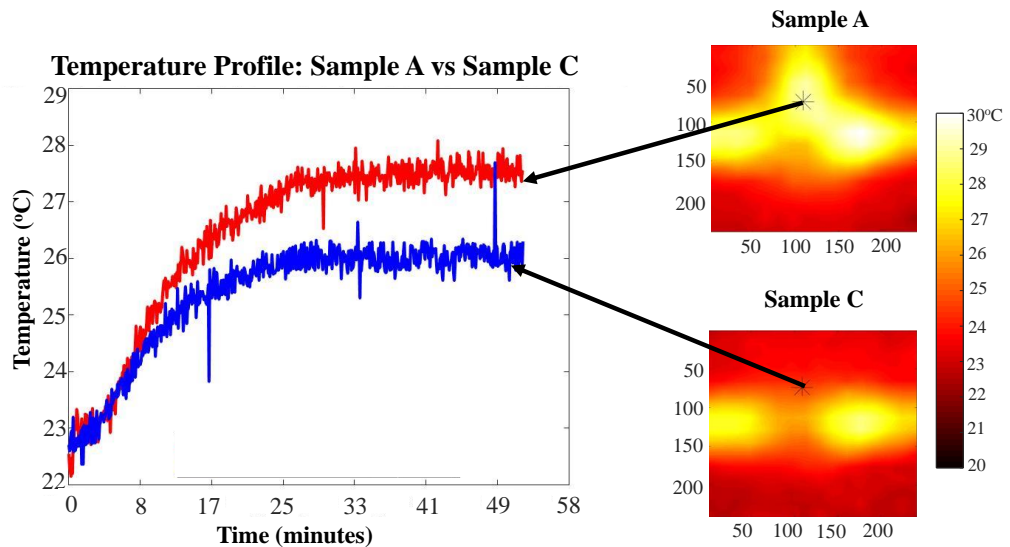


Figure 6.16: Comparison of temperature profile through a specific point on infrared images of sample A and sample C.

6.5 ANN analysis of data obtained from Samples A, B and C

Pattern recognition tool of Artificial Neural Network (ANN) is selected to analyse the series of infrared images obtained from the experiments on sample A, B and C. From a group of 600 infrared images captured at 5 second intervals, one image is selected for every minute to make a set of 50 image. At this interval rate there are 12 images captured in one minute. The first image captured at every minute is grouped together to form the first set of data; the second image recorded at every minute is grouped together to form the second set of data and so on. This process creates 12 sets of data for each type of material sample and three samples together make 36 set in total. Additional 12 sets of data are obtained by repeating

the experiment on sample A. Therefore, total 48 sets of data from three different samples are available for analysis using ANN, and each data set contains 12800 (16x16x50) input elements. Each sample is defined as a class which is the target or output of the network, and the network will be trained to identify the correct class. The network consists of one hidden layer, one softmax layer and one output layer as shown in Figure 6.17.

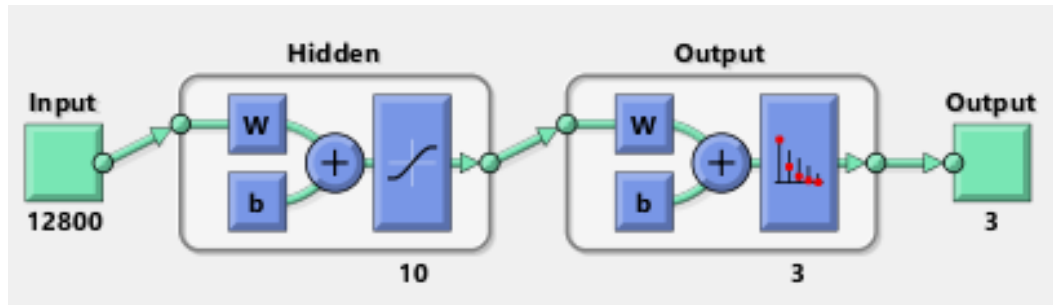


Figure 6.17: Neural Network Architecture for the classification of samples A, B and C

[Source: generated using Matlab software]

The hidden layer contains 10 neurons and the softmax layer contains three neurons. The 48 set of data is randomly divided into two parts with 34 sets of data (70%) is used for training the network and rest of the data (14 sets) are used to test and validate the network. The initial performance of the network shows that it attains 100% accuracy for class identification. The visual inspection shows that the temperature profiles are clearly distinguishable and hence the high accuracy by the ANN is justified. However, the outcome of the ANN analysis signifies the potential application of ANN for identifying wall types with high accuracy from set of infrared images captured during the application of point heat. In the next step the experimentation is extended to brick and concrete block walls to see the response of ANN.

6.6 Experiments on brick and concrete block walls

Up on achieving favourable outcome from the experiments on sample A, B and C, it is decided to study the performance of the test kit on sample walls consisting of real building materials. For this, sample walls made of hollow brick and concrete block are selected to

monitor in laboratory. The thickness of the brick wall is 100 mm, and the thickness of the concrete wall is 95 mm. EcoTherm board with a thickness of 100 mm is chosen as the external insulation material for these walls. EcoTherm is a Polyisocyanurate based insulation material and the thermal conductivity of the material is 0.022 W/mK (EcoTherm insulation, no date). Therefore, four combination of specimen walls are prepared namely: brick wall, concrete block wall, insulated brick wall and insulated concrete block wall. The schematic diagrams of these wall sections are shown in Figure 6.18 -a, 6.18 -b, 6.18 -c and 6.18-d respectively.

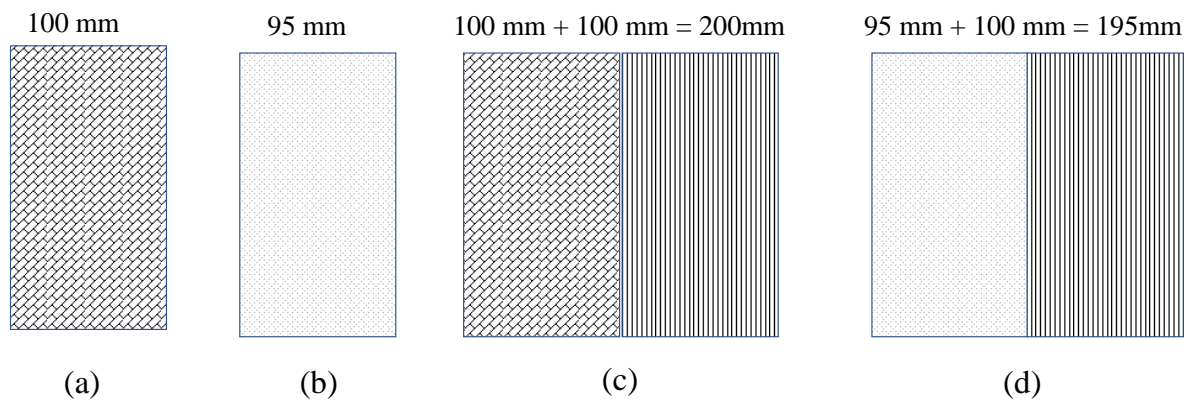


Figure 6.18: Schematic diagram of (a) sample D, (b) sample F (c) sample E and (d) sample G.

These sample walls are named as sample D, sample E, sample F and sample G. The detailed properties of these samples are tabulated in Table 6.2. The thermal conductivity of brick wall is taken as 0.27 W/m.K (Antoniadis *et al.*, 2012), and the thermal conductivity of concrete block is considered as 1.5 W/m.K (ISO 10456, 2007). Same as before the U-value of these samples are calculated using equation 2.8 considering the similar values of the thermal resistance of air at internal surface and external surface. Figures 6.19 and 6.20 show the experiment on sample D and F respectively. Same as previous experiments, the infrared images are captured at every 5 seconds, and the tip and external temperatures are recorded at every second using National Instrument's USB-TC01 data acquisition system.

Table 6.2: Properties of samples D, E, F and G.

Sample No	Material	Thickness (mm)	Thermal Conductivity (W/mK)	U-value (W/m ² K)
D	Brick	100	0.27	1.86
E	Brick insulated externally with Ecotherm	100+100 =200	0.27 & 0.22	1.01
F	Concrete block	95	1.5	4.29
G	Concrete block insulated externally with Ecotherm	95+100=195	1.5 & 0.22	1.45

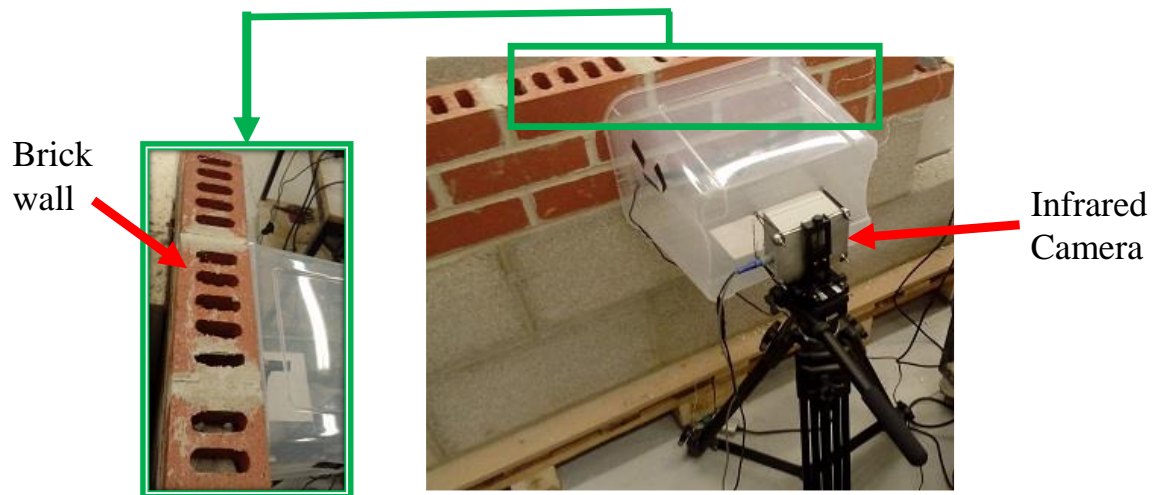


Figure 6.19: Experiment on sample D.

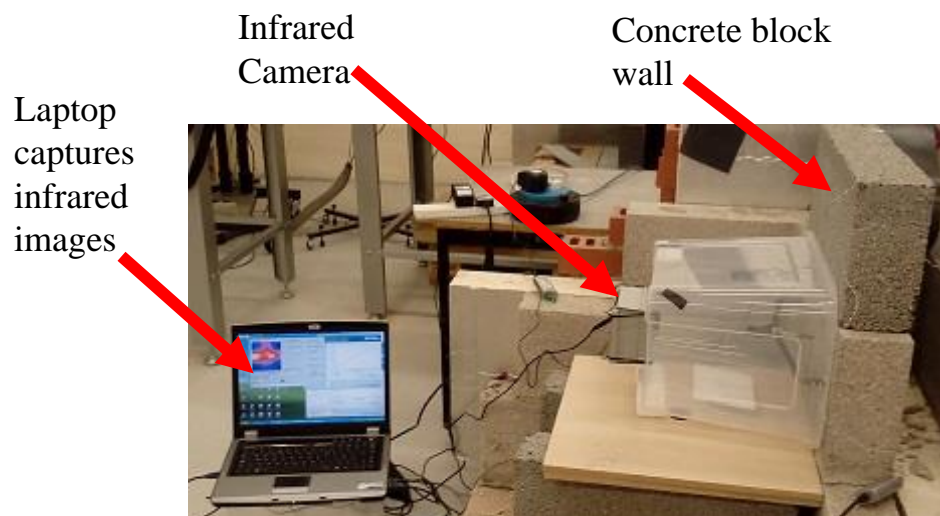


Figure 6.20: Experiment on sample F.

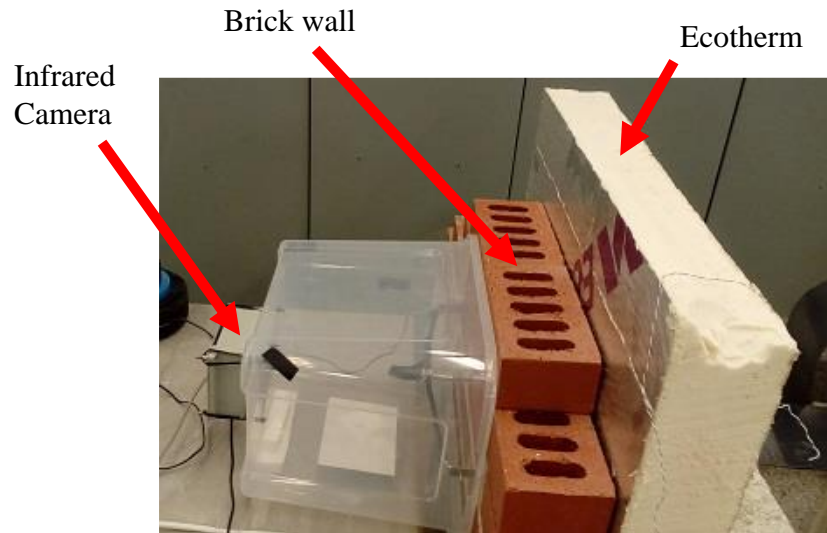


Figure 6.21: Experiment on sample E.

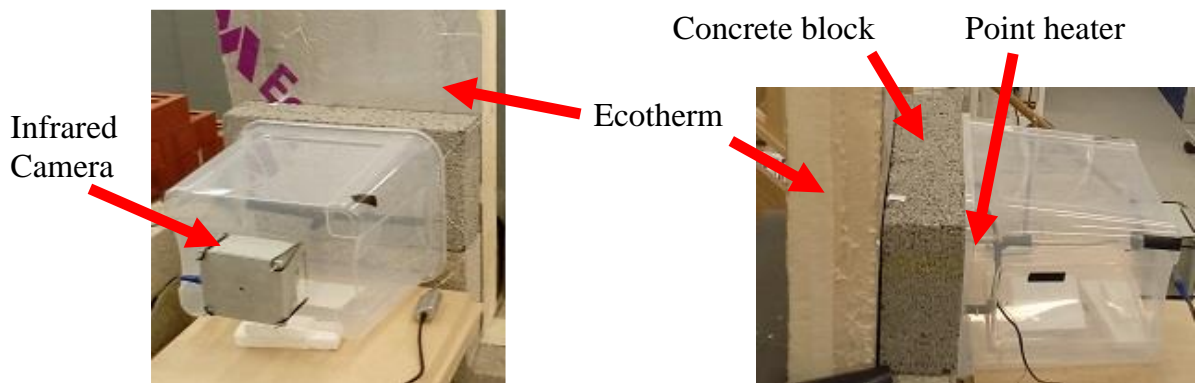


Figure 6.22: Experiment on sample G.

The experiments on insulated brick wall and insulated concrete block wall are shown in Figure 6.21 and 6.22 respectively. The same experiment on each wall is conducted again on different days so that the first set of data can be used to train artificial neural network and the second set of data can be used to test the performance of the neural network. The data obtained from the second experiments on each wall are tagged as sample D1 for brick wall, sample E1 for insulated brick wall, sample F1 for concrete block wall and sample G1 for insulated concrete block wall. The physical and thermal properties of sample D1, E1, F1, and G1 remains same as that of sample D, E, F and G as presented in Table 6.2. All infrared

image and temperature data are recorded at similar intervals as it is in the previous experiments conducted on samples A, B and C.

6.7 Visual analysis of infrared images obtained from samples D, E, F and G

According to the findings from the experiments on sample A, B and C, the insulated brick walls and insulated concrete block walls should have higher temperature distribution on the internal wall surface areas than that of uninsulated brick walls and uninsulated concrete block walls. This is because insulated walls have lower U-value and hence major portion of heat could not pass through the walls. However, visual inspections of the images obtained from the experiments conducted on sample D, E, F and G do not support that. In some cases, the surface of insulated walls looks cooler than that of uninsulated walls. This could happen because of the higher ambient temperature at the time of conducting the experiment on uninsulated wall samples than that of the insulated wall samples.

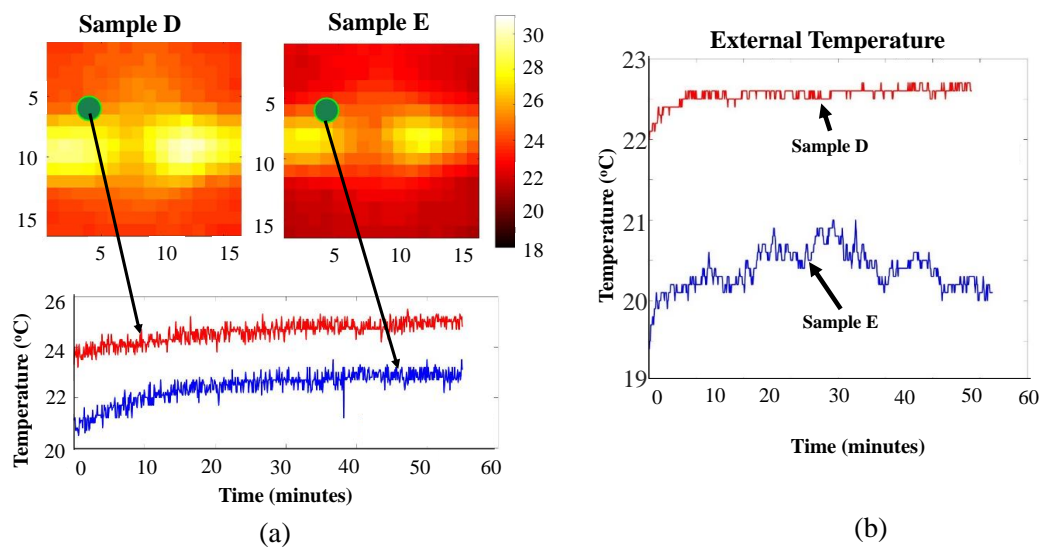


Figure 6.23: (a) Temperature profile of sample D and sample E through a specific point, (b) external temperature during the monitoring period of samples D and E.

Figure 6.23-a shows the temperature profiles through the same point on infrared image of an uninsulated brick wall (sample D) and an insulated brick wall (sample E), and Figure 6.23-

b shows the distribution of external (ambient) temperature during the time of those experiments. Figure 6.23-b clearly shows that the ambient temperature remains higher during the monitoring period of sample D than the external temperature during the monitoring period of sample E. Hence, the temperature profile of sample E is found to be higher than that of sample D. To eliminate the effect of ambient temperature, the respective external temperature values are subtracted from the temperature values obtained at each pixel of an infrared image which is represented in equation 6.1.

$$T_{(i,j,k)}^a = T_{(i,j,k)} - T_k^{ext} \quad (6.1)$$

Here, $T_{(i,j,k)}^a$ is the modified temperature value of pixel (i,j,k) on an infrared image, $T_{(i,j,k)}$ is the original temperature value at pixel (i,j,k) on an infrared image and T_k^{ext} is the external temperature when the infrared image is captured. Before calculating T^a according to equation 6.1, the infrared images are synchronised based on the time at which the point heater is switched on so that the effect of application of the point heat is clearly distinguishable. Figure 6.24 shows the modified temperature profiles T^a of sample D and sample E. From the visual inspection of temperature profiles in Figure 6.24, it is difficult to clearly identify the difference between temperature profiles of sample D and sample E; however, it gives closer representation to the outcomes of previous experiments than the temperature profiles of Figure 6.23-a. Similar analysis is conducted for samples F and G; and it is repeated at three other specific points on top, right and bottom of the infrared images to see the response of T^a in other areas of wall. The visual comparisons in those T^a profiles show that the temperature profile of an insulated wall is higher than that of an uninsulated wall in 55% cases, and the temperature profile of an insulated wall is lower than that of an uninsulated wall in 20% cases. In 25% cases, it is not possible to differentiate between insulated and uninsulated walls from the visual inspection of the T^a profiles.

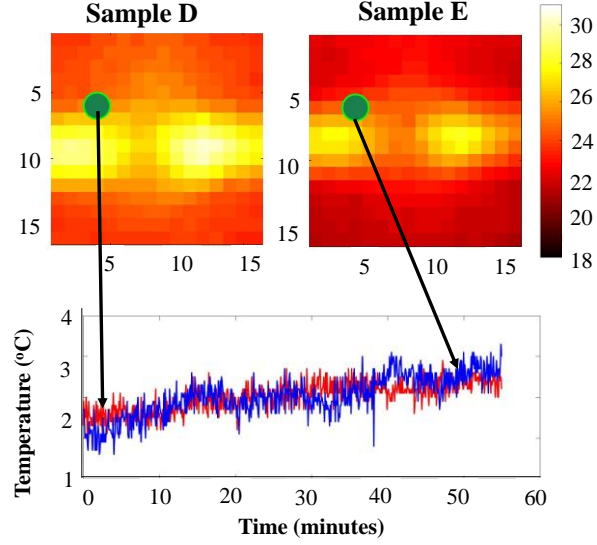


Figure 6.24: The profile T^a through a specific point on sample D and sample E.

It is also noticed in the profiles in Figure 6.24 that the start point of the T^a profile of sample E is slightly below the start point of the T^a profile of sample D; however, finish point of the T^a profile of sample E is higher than that of sample D. This points out the fact that there is a difference in the gradient of temperature profiles in insulated walls and uninsulated walls. To evaluate the effect of difference in gradient of thermal profiles, the cumulative temperature difference between same points on two successive infrared images are calculated as shown in equation 6.2.

$$T_{(i,j,k)}^b = \sum_1^k [T_{(i,j,k+1)} - T_{(i,j,k)}] \quad (6.2)$$

Here $T_{(i,j,k)}^b$ is the cumulative temperature difference at pixel (i,j,k) and $T_{(i,j,k)}$ is the original temperature value at pixel (i,j,k) on infrared image. Similarly, the cumulative difference of T^a between same points on two successive images can be calculated using equation 6.3.

$$T_{(i,j,k)}^{ab} = \sum_1^k [T_{(i,j,k+1)}^a - T_{(i,j,k)}^a] \quad (6.3)$$

Here $T_{(i,j,k)}^{ab}$ is the cumulative temperature difference of modified temperature obtained from equation 6.1. The profiles T^b and T^{ab} through a specific point on sample D and sample are shown in Figure 6.25-a and 6.25-b, respectively.

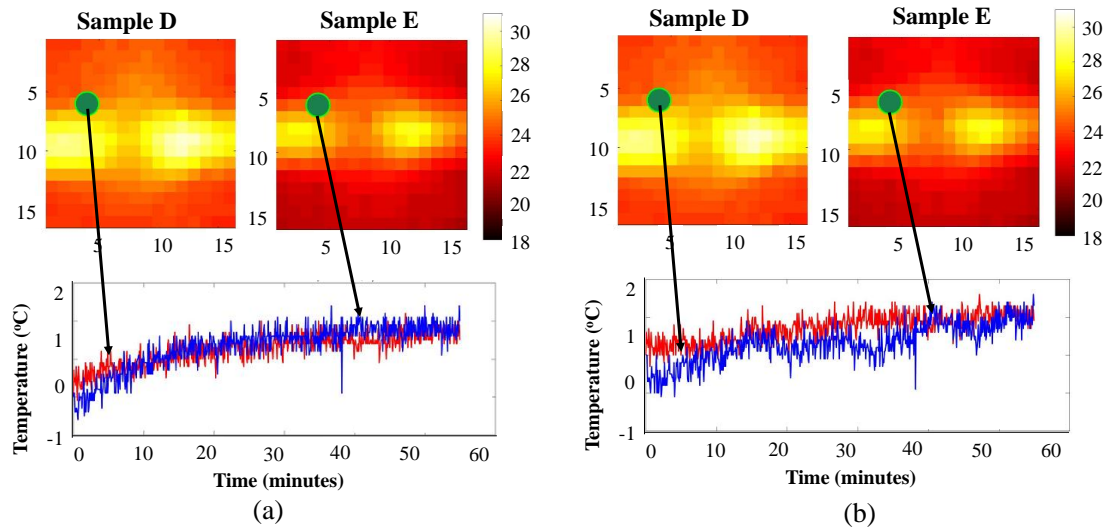


Figure 6.25: (a) Profiles of T^b and (b) profiles of T^{ab} through a point on a brick wall (sample D) and an insulated brick wall (sample E).

The profiles T^b do not convey any discernible information to differentiate between insulated and uninsulated wall, and the profiles in Figure 6.25-b indicates that profile T^{ab} of uninsulated wall is higher than that of insulated wall. To further analyse the variability of those temperature profiles, five periods moving range is generated for profiles T , T^a , T^b and T^{ab} , which are shown in Figure 6.26-a, 6.26-b, 6.26-c and 6.26-d respectively. None of the moving ranges produces noticeable differences that can be used to differentiate between insulated and uninsulated brick walls. Finally, the standard deviation of T , T^a , T^b and T^{ab} and the standard deviation of their five-period moving range are considered for analysis. The comparison of these standard deviations is shown in Figure 6.27-a and 6.27-b, respectively. Figure 6.27 points out that the standard deviations of those profiles of the insulated brick wall are higher than that of the uninsulated brick wall. The standard deviation of their moving range also expresses the similar information. From the different approaches of analysis

discussed above, three situations are observed. Firstly, profiles T and T^{ab} of uninsulated brick wall are higher than that of insulated brick wall. Secondly, profiles T^a , T^b and five periods moving range of all profiles are not clearly distinguishable.

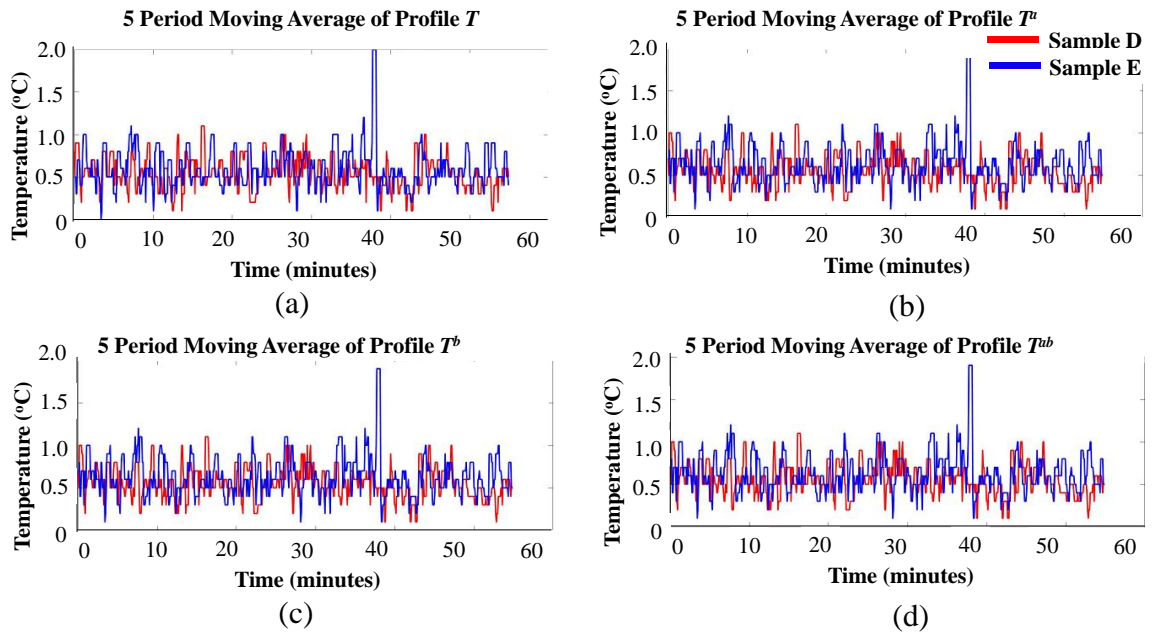


Figure 6.26: (a) Five periods moving range of T , (b) five periods moving range of T^a , (c) five periods moving range of T^b , and (d) five periods moving range of T^{ab} .

Finally, the standard deviation of all profiles of insulated brick wall is higher than that of uninsulated brick wall, as well as the standard deviation of five periods moving range of all profiles of insulated brick wall is higher than that of uninsulated brick wall.

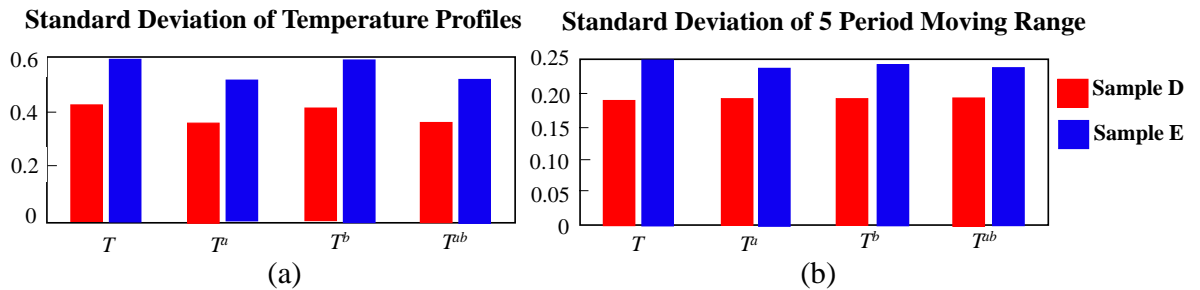


Figure 6.27: (a) standard deviation of T , T^a , T^b and T^{ab} (b) standard deviation of five periods moving range of T , T^a , T^b and T^{ab} .

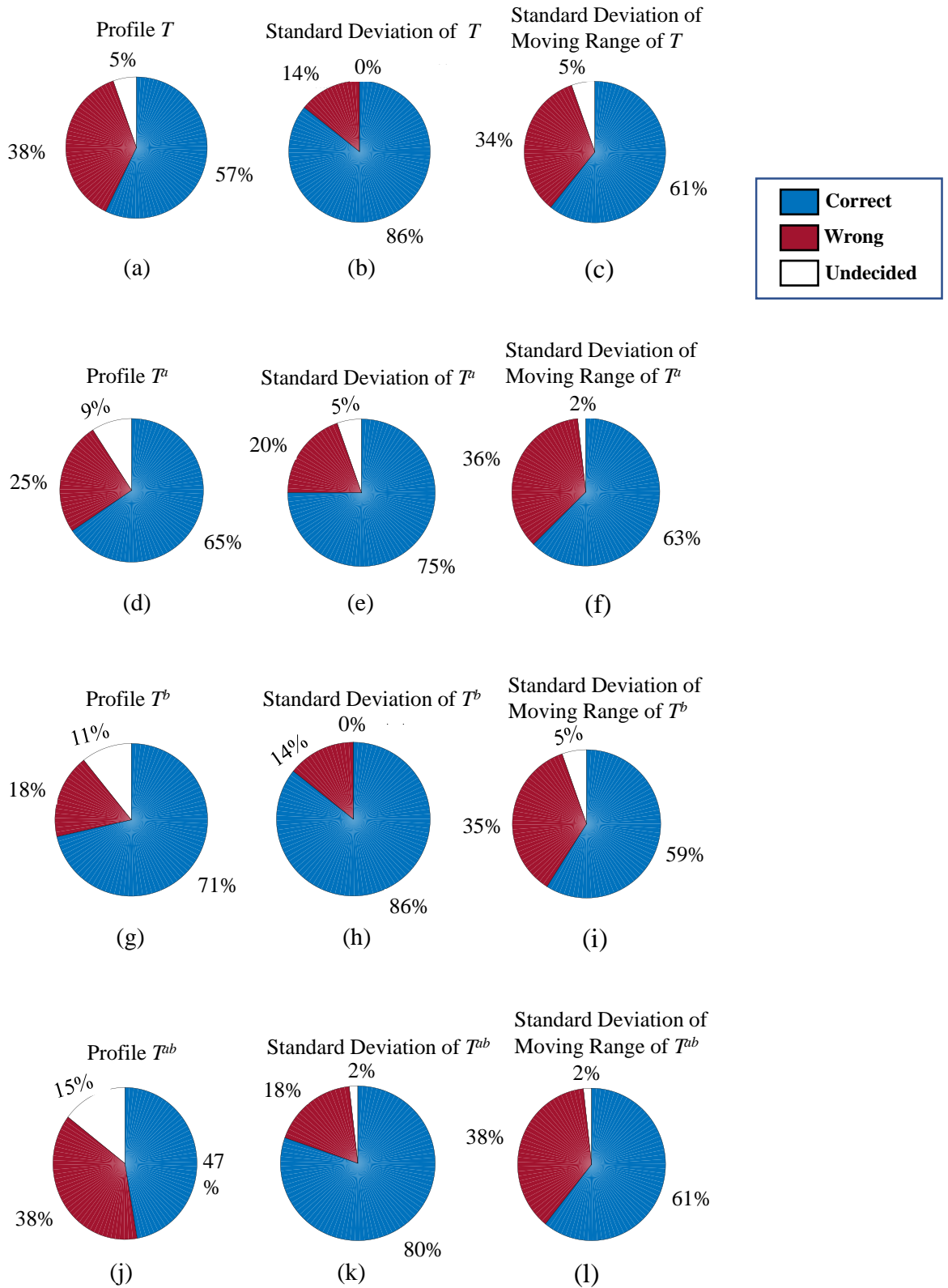


Figure 6.28: The result of visual inspection.

In each case, if the response of the profile or standard deviation of insulated wall is higher than that of uninsulated wall, it is considered as correct representation of profiles. If the profile or standard deviation of uninsulated wall is found higher than that of an insulated wall, it is considered as wrong representation; and the cases where it is not possible to differentiate between the two, is considered as undecided. The outcome of the visual analysis is summarized using pie charts in Figure 6.28. The pie chart shows that standard deviation of T and T^b provide the highest percentage of correct representations which is 86% as shown in Figure 6.28-b and 6.28-h. It is also observed during the visual inspection that the standard deviation of T and T^b are always same because T^b is the cumulative first derivative of T and hence the dispersion of data in both cases are identical. However, they may have different mean values. The standard deviation of T^{ab} provides second best correct representations which is 80% followed by the standard deviation of T^a which is 75% correct representations. Considering the two highest correct representation, standard deviation of T^b and standard deviation of T^{ab} are selected to analyse using pattern recognition tool of ANN. Other than the standard deviation of profiles, profile T^b has the highest percentage of correct representation among all four profiles, which is 71% as found in Figure 6.28-g. This is also the fourth highest percentage of correct representation. In cases of standard deviation of moving ranges, the percentage of correct representations ranges from 59% to 63%. Therefore, profile T^b is also included for the ANN analysis as it shows the best percentage of correct recognition among all different temperature profiles.

6.7.1 Readjustment of infrared images for accurate comparison

A further problem is noticed while observing the infrared images, which is illustrated in Figure 6.29-a and 6.29-b. The position of the aluminium bar that holds the heater is not same for the brick wall and the insulated brick wall on the infrared images in some cases. The position of the aluminium bar in infrared image of insulated brick wall is at the middle line

of the image, which is shown by black line in Figure 6.29-b. However, the infrared images in Figure 6.29-a shows that the position of aluminium bar is slightly below the middle line of the image. Here, a black line represents middle line of the image and a blue line represents the position of the aluminium bar.

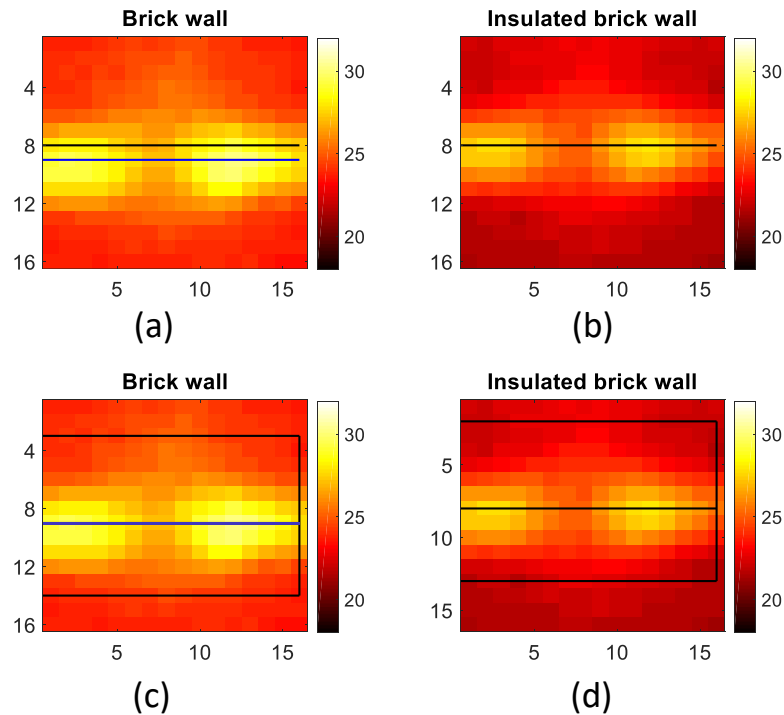


Figure 6.29: (a) Infrared image of brick wall, (b) infrared image of insulated brick wall, (c) infrared image of brick wall with crop boundary and (d) infrared image of insulated brick wall with crop boundary.

The aluminium bar is designed to be positioned at the middle of the test rig; however, the bar has been given some allowance to ensure that the point heater stays in continuous contact with the wall surface during the monitoring period. Sometimes the aluminium bar is displaced by the action of placing the test rig firmly against a wall surface. Therefore, it does not coincide with middle line in infrared image. The position of aluminium bar in infrared images can be considered as a reference line for the comparison of temperature profiles because the source of heating is located on this line and heat dispersion occurs on both side

of it. Consequently, this line contains the highest temperature values than any other lines in the infrared image. Therefore, it is necessary that the position of that bar should be identical on the infrared images in comparison. To overcome the problem the infrared images are cropped, keeping the position of aluminium bar at middle of the images, as shown in Figure 6.29-c and Figure 6.29-d. These cropped images are used for analysis using ANN which is discussed in the next section. Also, this procedure to adjust the images is followed later where it is necessary.

6.8 Categorisation of wall types using ANN

To develop an ANN that is able to identify the correct wall type from the temperature profiles of the samples D, E, F and G, the pattern recognition tool in MATLAB is selected. As mentioned in section 6.6, each sample has been monitored twice to ensure obtaining two sets of data. Of them, the data obtained from the first instance of monitoring are used to form the training data set and the second instance of monitoring data are considered for the test data set. Similar to the previous analysis with samples A, B and C, 600 infrared images captured at 5 seconds interval during the application of point heat are selected for each sample. Then those infrared images are divided in to 12 sets containing 50 images in each set and hence the time gap between two successive images in a set becomes one minute. Therefore, four different wall samples supplying 12 data set each produce 48 input data sets in total. Each input data set is composed of 9600 ($12 \times 16 \times 50$) input elements for profile T^b and 192 input elements for the standard deviations of profiles T^b and T^{ab} . The output data set contains 48 elements of four classes where each class represent a sample wall. These 48 data sets from the first instance of monitoring all the samples construct the training data set. Similarly, the test data set is formed with the data obtained from the second instance of monitoring. The AAN designed in this occasion also consists of four layers as it is used for samples A, B and C. Apart from input and output layers there are one hidden layer and one softmax layer. The

output and the softmax layer contain 4 neurons as there are only four classes. The input layer contains 9600 neurons when profile T^b is used as input because there are 9600 elements in each input data set.

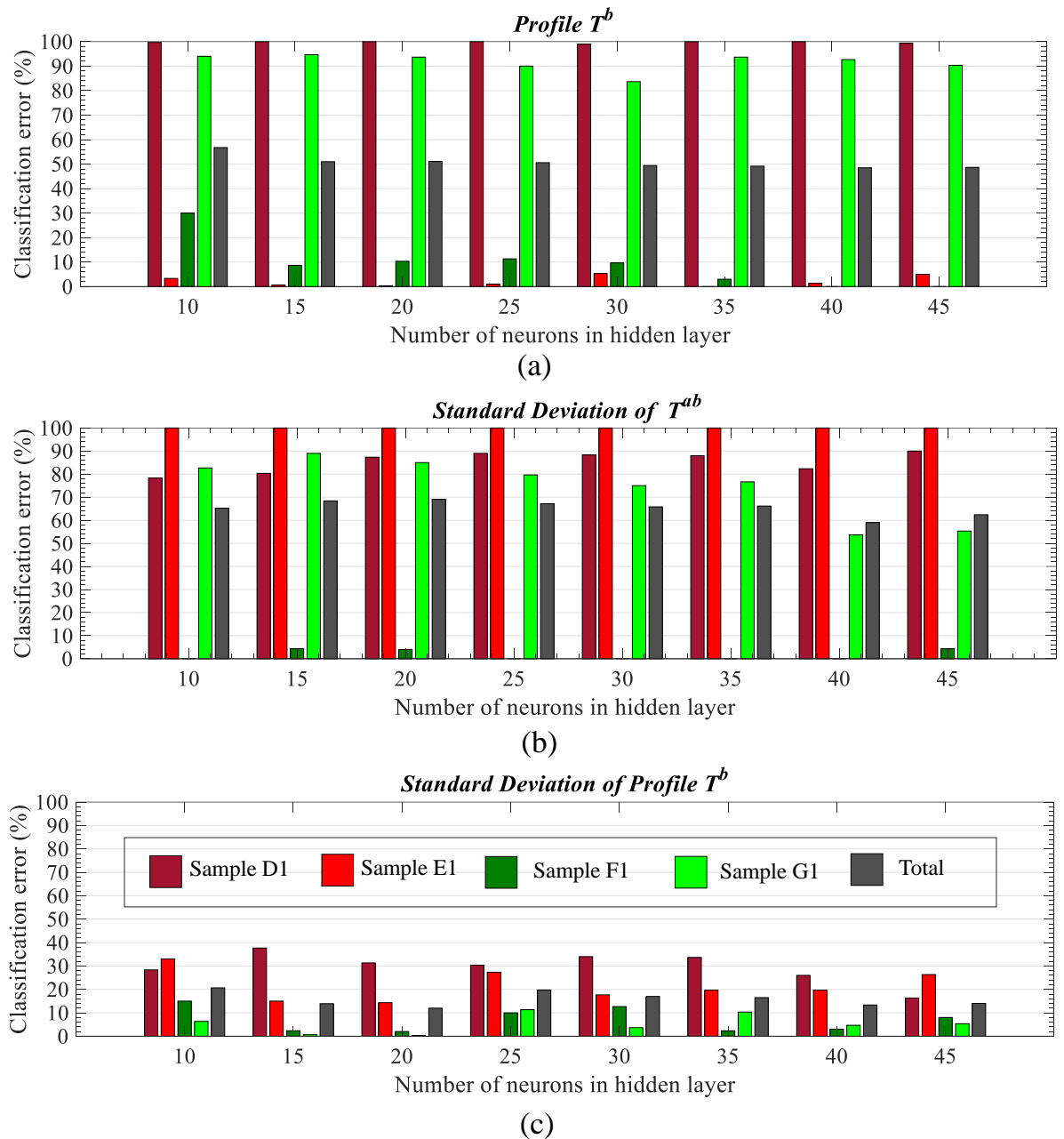


Figure 6.30: Percentage error in categorisation of wall samples (a) profile T^b , (b) standard deviation of profile T^{ab} and (c) standard deviation of profile T^b .

For the standard deviations of profiles T^b and T^{ab} as input, the input consists of 192 neurons as there are 192 elements in each input data set. The number of neurons in hidden layer is varied from 10 to 45 with a step of five neurons to evaluate the optimum configuration of hidden layer for this type of categorisation problem. As discussed in the previous chapters, the ANN is trained and tested 25 times to generalise the outcome of ANN analysis and the mean performance of ANN is considered which is presented in Figure 6.30. Figure 6.30-a, 6.30-b and 6.30-c show the percentage error in categorisation of wall samples using profile T^b , standard deviation of T^{ab} and standard deviation of T^b respectively as input to the ANN. It is found from Figure 6.30-a that the ANN achieves very high accuracy of categorising sample E1 with less than 10% classification error; however, the percentage error in categorising samples D1 and G1 are over 90%. The percentage error gradually goes down for categorisation of sample F1 when as the number of neurons in hidden layer increases. The overall classification error ranges between 48% to 57%. Figure 6.30-b shows that the ANN achieves more than 95% accuracy in categorising sample F1; however, the percentage errors in categorising samples E1 and D1 are significantly high. In fact, the ANN fails to identify sample E1 and predict wrong category for sample D1 in more than 80% cases. The percentage error in categorising G1 ranges from 55% to 90%. The overall percentage error considering all samples ranges between 59% to 70% where the least percentage error is found with the ANN contains 40 neurons in the hidden layer. In Figure 6.30-c, the ANN's performance is found to be far better than other two cases with percentage error remains less than 40% for all samples. The highest percentage error is 38% for categorising sample D1 with the ANN containing 15 neurons in the hidden layer. The best overall performance is found with the ANN containing one hidden layer with 20 neurons in it. For that case, the classification error for sample D1, E1, F1 and G1 are 31.33%, 14.33%, 2% and 0.33% respectively. It is noticed that similar performance is also available from the ANN with 40

neurons in the hidden layer. In that case, the percentage error for classification of sample D1, E1, F1 and G1 are 26%, 19.67%, 3% and 4.67% respectively. The overall classification error for the ANN with one hidden layer consisting of 20 neurons is 12% and the overall classification error for the ANN with 40 neurons in hidden layer is 13.33%. The ANN with 45 neurons in the hidden layer results in 16.33%, 26.33%, 8% and 5.33% error for categorisation of sample D1, E1, F1 and G1 respectively with the overall classification error of 14%. The range of variation in percentage errors among the samples D1, E1, F1 and G1 are more even in the ANN with 40 neurons and 45 neurons with one hidden layer compared to the ANN with 20 neurons in one hidden layer. The overall performance is slightly better with the ANN with one hidden layer consisting of 20 neurons. Moreover, ANN with less neurons in the hidden layer consume less computation power and produce faster result. Therefore, ANN with one hidden layer consisting of 20 neurons could be considered as the best configuration for categorising wall types. It is found from the bar charts of Figure 6.30 that using standard deviation of profile T^b as input to the ANN results in best classification performance among all three different inputs. The standard deviation of a profile represents the summary of variation in that profile and hence it is a key characteristic of that profile. As a result, the standard deviation of profile T^b represents the characteristic of variation more significantly than the profile itself. Moreover, when standard deviation of a profile is considered as input to the ANN, the ANN requires to handle 50 times less data compare to the original profile as input without losing the key characteristics of variations present in the data. T^{ab} is constructed from profile T^a and which is developed by subtracting external temperature from the initial temperature profile. This process may diminish the magnitude of variation in profile and therefore the standard deviation of profile T^{ab} does not represent meaningful characteristics for the ANN to learn.

6.9 Conclusion

The novel design of U-value estimation kit presented in this chapter demonstrates the successful use of infrared thermography and ANN with the application of point heat for the categorisation of wall types based on their U-values. The approach to visually inspect the infrared images and hence to develop the modified temperature profiles considering the effect of ambient temperature and gradient of the temperature profile is a key step for integrating ANN with infrared thermography. The visual inspection of temperature profiles at a specific point on infrared images enables to understand how human brain would differentiate the wall samples used in the study by analysing the temperature profiles of thermal images. As ANN mimics work patterns of a human brain, it would be able to categorise the wall samples by analysing the temperature profiles developed from the respective infrared images. The results of the ANN analysis presented in this chapter shows significant agreement with that. The ANN with one hidden layer consisting of 20 neurons, is able to categorise wall types with 88% overall accuracy and it is guaranteed to get 69% accuracy for any particular wall type. Two other important findings are the configuration of ANN and the choice of input elements. It is found that ANN with one hidden layer consisting of 20 neurons shows the best classification accuracy. In terms of input profiles, it is found that standard deviations of temperature profiles are much suitable to use as input to the ANN due to their capability of capturing the key characteristics of the input data comprising of minimum data elements. These outcomes are carried forward to apply in the U-value estimation of walls in a real building which is presented in the next chapter.

Chapter 7: Experimental Work on Real Building

7.1 Introduction

In the previous chapter (Chapter 6) the application of the novel U-value kit for categorising wall types based on their U-value has been investigated. In continuation to that, the estimation of the U-value in a real building's wall using the novel U-value estimation kit is presented in this chapter. The U-value kit is calibrated in laboratory environment by training the ANN with the data obtained from monitoring different wall samples in laboratory. Afterwards the calibrated device is used to monitor walls in a real building to estimate the U-value of the real building's wall. A case study related to the estimation of the U-value of a wall in a real building is also available in an accepted manuscript which is included in Appendix I. In this chapter the extended case study in the same building is presented with which investigate the U-value estimation in walls of four different rooms in that building.

7.2 Implemented approach

The methodology used to conduct the measurement using the novel U-value estimation kit is described in chapter 3 (Figure 5.3). The novelty in the methodology is that the U-value kit is calibrated in the laboratory by training an ANN with the temperature profiles generated from monitoring a wall sample of known U-value so that the U-value kit can estimate the U-value of an unknown wall from the temperature profile generated by the monitoring process of that wall. The four wall samples described in chapter 6, namely sample D, E, F and G, are considered for training the ANN. Another wall sample made of solid brick, tagged as sample H, is added with the set of above mentioned four samples for monitoring with the U-value kit in the laboratory environment. Therefore, five samples in together are prepared to monitor for the training of ANN. Four different walls in a three-bedroom flat are monitored with the U-value estimation kit between 7th and 21st February. All the experiments in the real building

are conducted between 8 pm and 11 pm as the effect of solar irradiation on the walls is minimum. The real building's walls are tagged as sample I. To generalise the estimation, ANN is trained and tested for 25 times and the mean value of those 25 iterations is considered as the ANN predicted U-value.

7.2.1 Equation Used

The equations used to conduct the study in this chapter are presented below

$$U = \frac{1}{R_T} \quad (2.3)$$

Where, $R_T = R_i + \frac{d_1}{\lambda_1} + \frac{d_2}{\lambda_2} + \frac{d_3}{\lambda_3} \dots \dots \dots + R_e$; with $R_i = 0.13$ and $R_e = 0.04$. Equation (2.3)

is used to calculate the U-value of sample walls.

$$T_{(i,j,k)}^a = T_{(i,j,k)} - T_k^{ext} \quad (6.1)$$

$$T_{(i,j,k)}^b = \sum_1^k [T_{(i,j,k+1)} - T_{(i,j,k)}] \quad (6.2)$$

$$T_{(i,j,k)}^{ab} = \sum_1^k [T_{(i,j,k+1)}^a - T_{(i,j,k)}^a] \quad (6.3)$$

Equation (6.1), (6.2) and (6.3) are used to generate profiles T^a , T^b and T^{ab} from the infrared images.

$$e_d = \frac{|U_p - U_c|}{U_c} \times 100\% \quad (3.8)$$

Equation (3.8) is used to evaluate the performance of neural network.

7.2.2 Wall Samples

Six wall samples are used in this study and five of them, namely sample D, sample E, sample F, sample G and sample H, are considered for monitoring in the laboratory. Samples D, E, F, and G have the similar composition as described in the previous chapter. Sample E is a solid brick wall of thickness 230 mm and sample I represents the real building's wall which

is a solid brick wall with mortar layer in both sides. The properties of the wall samples are listed in Table-7.1, The thermal conductivity of the materials in samples D, E, F and G remains the same as considered in the previous chapter. The thermal conductivities of the solid brick, the inner mortar layer and the outer mortar layers in samples H and I are selected from Anderson (2006). For solid brick it is 0.56 W/m.K for the inner leave and 0.77 W/m.K for the outer leave of the walls. For mortar layer the thermal conductivity is 0.88 W/m.K for inner layer and 0.94 W/m.K for the outer layer.

Table 7.1: Properties of sample wall used to train and test the ANN

Wall Sample	Material	Thickness (mm)	Thermal Conductivity (W/m.K)	U-value (W/m ² K)
D	Brick	100	0.27	1.86
E	Brick insulated externally with Ecotherm	100+100=200	0.27 & 0.22	1.01
F	Concrete block	95	1.5	4.29
G	Concrete block insulated externally with Ecotherm	95+100=195	1.5 & 0.22	1.45
H	Solid Brick Wall	230	Inner layer: 0.56 Outer layer: 0.77	1.91
I	Inner mortar layer + Solid Brick Wall + Outer mortar layer	15+230+20=265	Inner mortar layer: 0.88 Brick wall: 0.56 Outer mortar layer: 0.94	1.62

7.3 Experimental works

The U-value kit is slightly improved by replacing the IRISYS 1002 infrared camera with CHINO TP-L0260EN thermal camera. The new thermal camera is smaller in size and lighter in weight than the older one. As a result, the portability of the U-value kit has been improved. Moreover, CHINO TP-L0260EN thermal camera is better compatible with Windows10 operating system, and it can capture infrared images with higher resolution than the IRISYS

1002 infrared camera. This could enhance the quality of visual analysis; however, for ANN training the infrared images need to be downsized to 15 by 16 pixels. Similar to the previous case, the glow plug temperature and the ambient or room temperature are measured with thermocouples-based temperature sensor and NIUSB-TC01 data acquisition system is used to capture the temperature data. Figure 7.1 shows the monitoring of a solid brick wall (sample H) in the laboratory where the test kit is placed in the internal side of the wall.

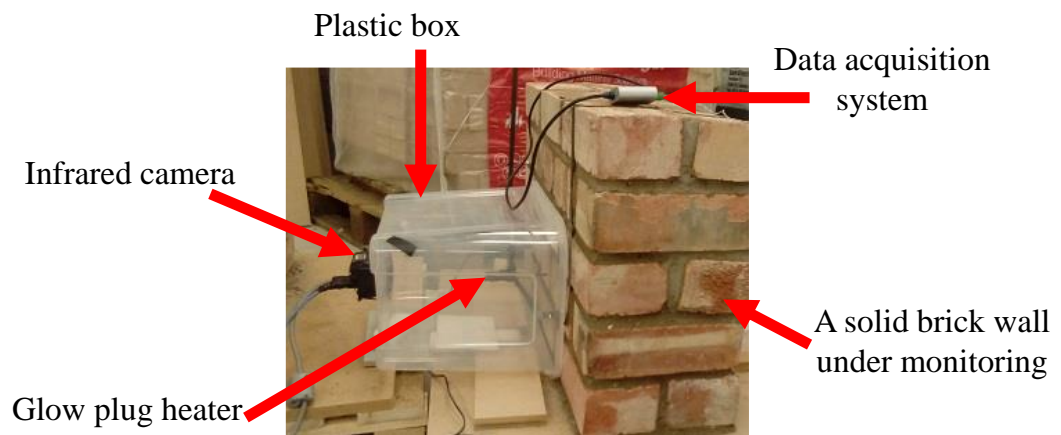


Figure 7.1: The monitoring of a sample wall in laboratory.

The interval to capture infrared images are also considered as five seconds. The monitoring period has been extended to one hour instead of 50 minutes in the study presented in chapter 6. As a result, 720 images per set up of the experiment are available for the ANN analysis. Figure 7.2-a shows the location of the building in Google map. The flat at which the monitoring of walls are conducted is situated on the first floor of the building. At the time of the experiments the ground floor was unoccupied. Figure 7.2-b shows the layout of the flat with locations where the monitoring is conducted. The flat consists of three bedrooms and a living room. The experiments are conducted in the master bedroom, near entrance, living room and bedroom 2, which are labelled in the layout of Figure 7.2-b with numbers 1, 2, 3 and 4 respectively. The wall in location 1 is a southwest facing wall, the wall in location 2 is south east facing wall and the walls in location 3 and 4 are north west facing

walls. The southeast facing walls of the bedroom 3 and the master bedroom were inaccessible due to position of the furniture in the room.

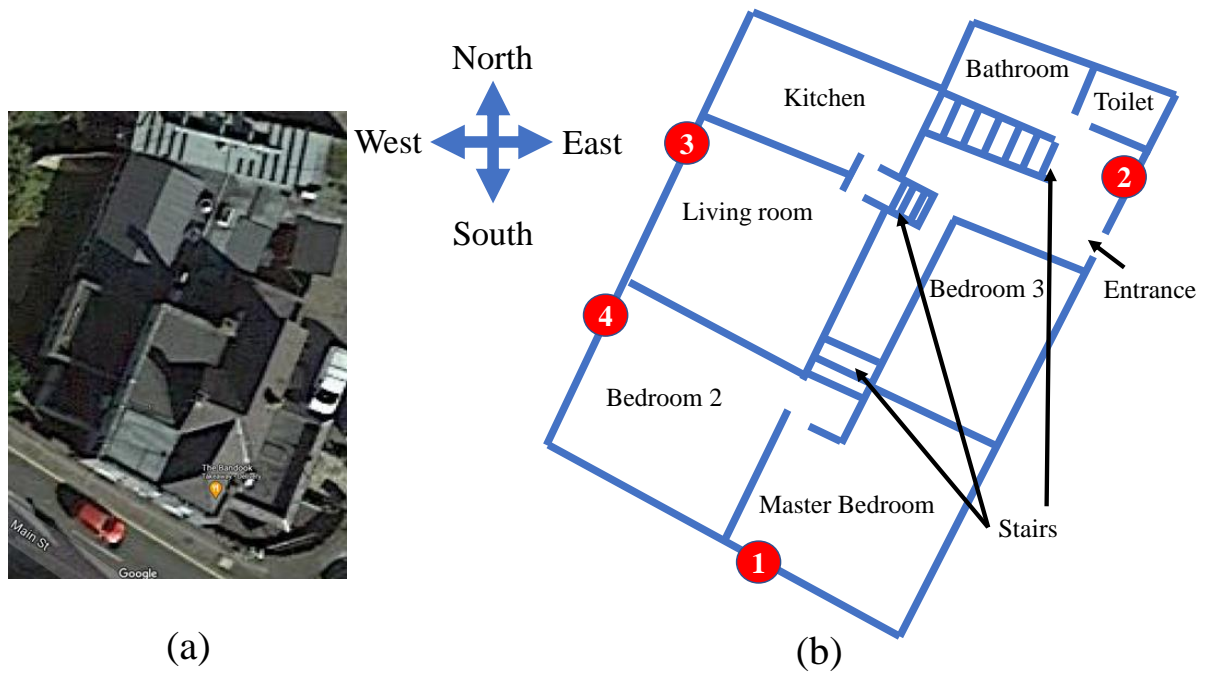


Figure 7.2: (a) Location of the building on Google Map (no date). (b) The schematic layout of the flat showing the location of monitoring the walls.

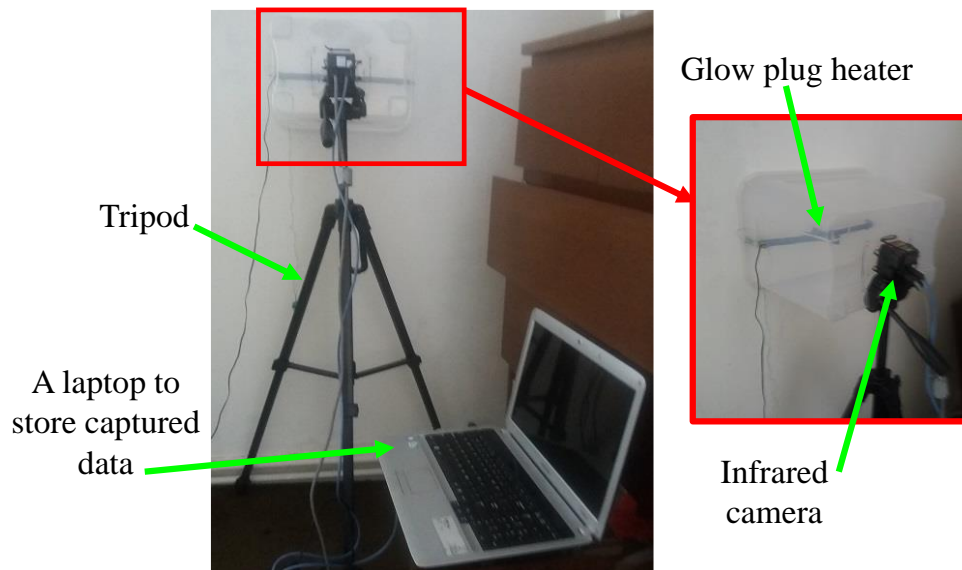


Figure 7.3: The experimental setup at one of the locations in the building.

Figure 7.3 shows the experimental arrangement in one of the locations inside the building. The U-value test kit is mounted on a tripod and the infrared images as well as the glow plug and room temperatures are stored in a laptop to be used later for ANN analysis. The room heating is switched off at least one hour before the monitoring starts to ensure that there would be no interference of heat from the radiator.

7.4 Results and Discussion

7.4.1 visual inspection of infrared images

Figure 7.4 represents the temperature profile and infrared image of samples E, H and I. It is noticed from the infrared images of Figure 7.4 that sample E has the warmest wall surface and sample I has the coolest wall surface. As sample E has the lowest U-value among the three samples shown in Figure 7.4, it is expected that there will be limited heat loss through the wall, instead most of the heat will be spread on the wall surface.

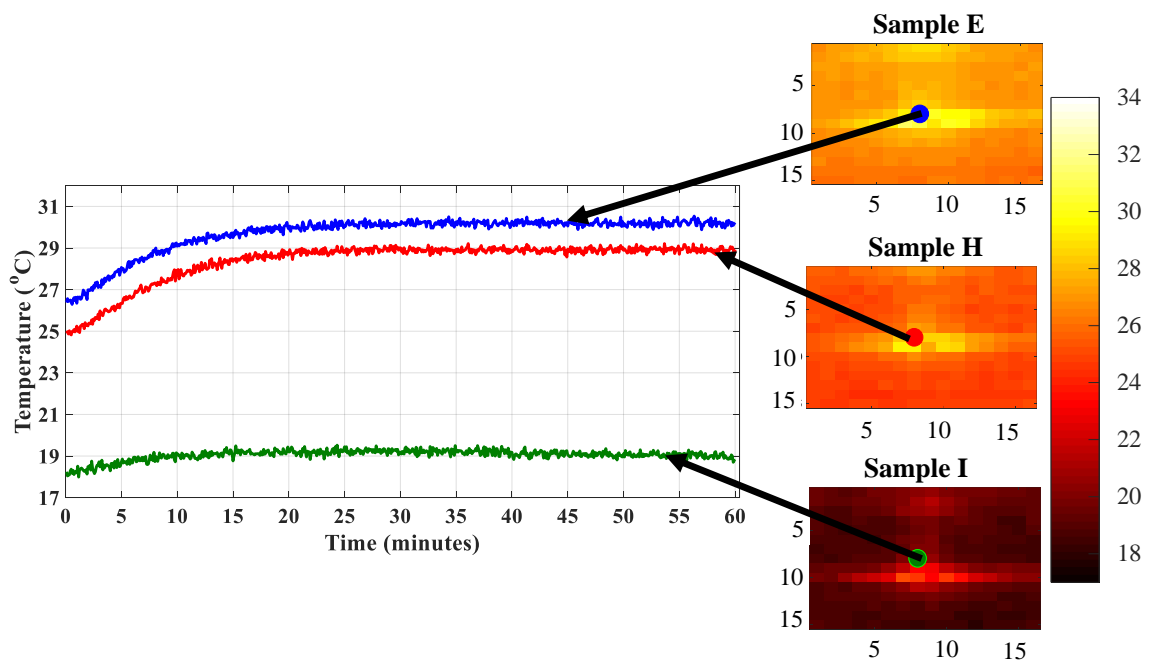


Figure 7.4: Visual inspection of temperature profiles from sample E, H and I.

On the other hand, sample H has the highest U-value among those three samples and therefore it is expected to have the warmest wall surface. The infrared images of Figure 7.4 represent the conflicting scenario. It is also found from Figure 7.4 that the temperature profile of sample E is located at the top followed by the temperature profiles of sample H and sample I. Based on the U-value of the wall samples, the temperature profile of sample H is expected to be located at the top followed by sample I and sample H. The primary reason behind this conflicting scenario seems to be the difference in ambient temperature during the monitoring periods of the wall samples. The start points of the temperature profiles in Figure 7.4 indicate that the ambient temperature during the monitoring period of sample E is 26.5°C and the ambient temperature during the monitoring period of sample I is 18°C. Hence it is justified to include the modified temperature profiles T^a , T^b and T^{ab} presented using equation 6.1, equation 6.2 and equation 6.3, for ANN analysis.

7.4.2 ANN prediction of U-value

It is observed in the categorisation analysis presented in chapter 6 that standard deviation of a profile provides some advantage if selected as the input to the ANN in terms of rapidness and accuracy of estimation. This is mainly because standard deviation of a profile represents the variations present in the profile with a single variable. Therefore, standard deviation of profiles T , T^a , T^b and T^{ab} are carefully chosen as input to the ANN. Figure 7.5 illustrates the configuration of the feed forward ANN used in this case.

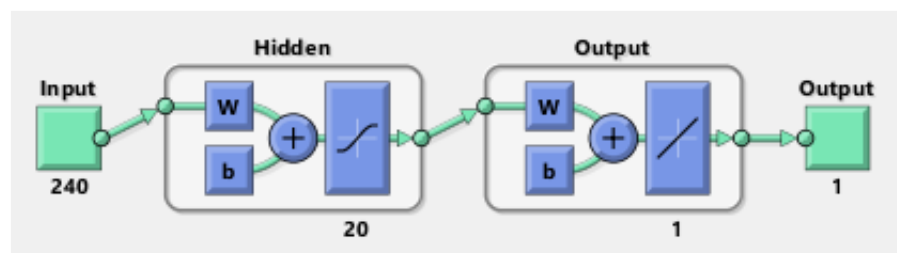


Figure 7.5: The ANN architecture used in this case study [Source: generated using Matlab software].

By following similar procedure as in chapter 6, 12 sets of input data are constructed from each monitoring task. As the monitoring period is 60 minutes in this case, each data set consists of 60 images. As the infrared images are downsized to 15 by 16 pixels, each input data set contains 240 (15x16) elements. Considering the monitoring of five wall samples, the training data set contains 60 sets of input data. For test data set there are 12 sets data obtained for each of the locations. The previous study also shows that neural network with single hidden layer containing 20 neurons is the most suitable configuration for this type of analysis. Therefore, a feed forward neural network with one hidden layer and 20 neurons in the hidden layer is constructed using MATLAB where sigmoid function is considered as the transfer function in neurons of hidden layer and Levenberg-Marquardt backpropagation algorithm is chosen as the learning algorithm. The target for the neural network is the calculated U-value of wall samples included in Table 7.1. The input layer has 240 neurons as each input data set has 240 elements and the output layer has one neuron as there is only one element in output data. Figure 7.6 presents the difference in training and test performance of the ANN.

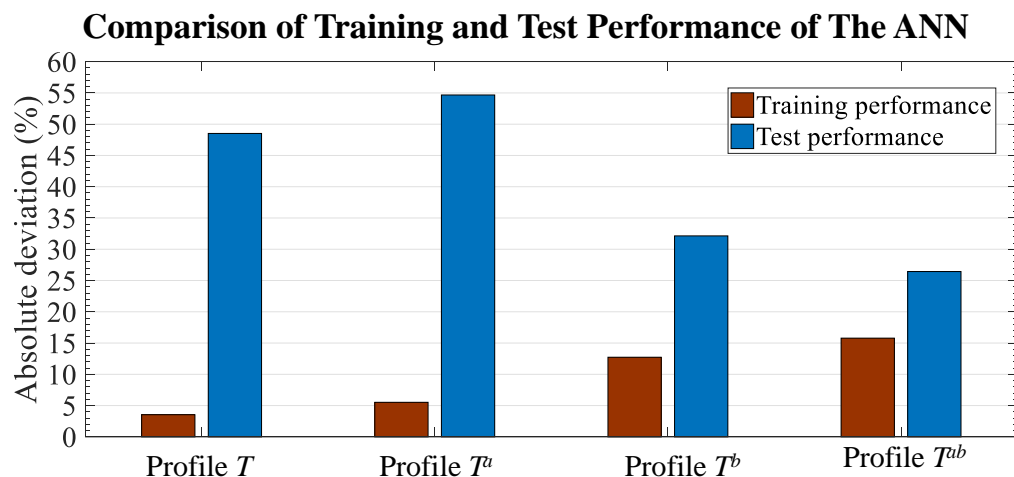


Figure 7.6: The comparison of training and test performance of the ANN.

It is found from Figure 7.6 that the training performances of the ANN that use the standard deviation of profile T and T^a as input are very high with less than 5% absolute deviation. On

the contrary the test performances of these networks are very high with more than 48% absolute deviation. This fact indicates that the ANN which use standard deviation of profile T and T^a as input tend to overfit and hence may not be suitable for estimation of U-value. The difference between the training performance and the test performance in ANNs which use standard deviation of profile T^b and T^{ab} as input much smaller than that of the ANNs use standard deviation of profile T and T^a as input. For the ANN that uses standard deviation of profile T^{ab} as input has 12.73% and 32.14% absolute deviation during training and test, respectively; and for the ANN that uses standard deviation of profile T^b as input has 15.78% and 26.44% absolute deviation during training and test, respectively. Therefore, these two networks are expected to show significant accuracy which is also reflected in the bar charts of Figure 7.7. It is found from Figure 7.7-a that use of profile T^a as input to the ANN results significantly underestimated U-value for all four locations. The ANN that uses profiles T as input significantly underestimate the U-value of wall in location 1 and overestimate the U-value of wall in location 4. For locations 2 and 3 it moderately overestimates the U-value of wall. This also reflected in the bar charts of Figure 7.7-b where the ANN with profile T^a as input shows over 60% of absolute percentage deviation for location 1,2 and 3. Although for location 4 the absolute percentage deviation is found 31.42 %, it is still a significant percentage of error. For the ANN with profile T as input shows over 70% absolute percentage error for location 1 and 4 however; it is 27.66% and 18.37% for location 2 and 3, respectively. The very high absolute percentage error of the ANN with profile T^a as input in 3 out of 4 locations indicates that profile T^a is not a suitable input for the ANN to estimate U-value of a building's wall. The ANN with profile T as input shows less than 30% absolute percentage deviation in two of the four locations; however, in the other two locations it is more than 70% which indicates the instability of the network performance. The key reason behind the poor performance of the ANN with profile T and T^a as input is overfitting. The

bar chart in Figure 7.6 supports the fact by presenting very high differences between training and test performance of the neural networks. The ANN that uses profiles T^b as input produce a highly accurate estimation for location 1 and it slightly overestimates the U-value of wall in location 2 and 3 (shown in Figure 7.7-a).

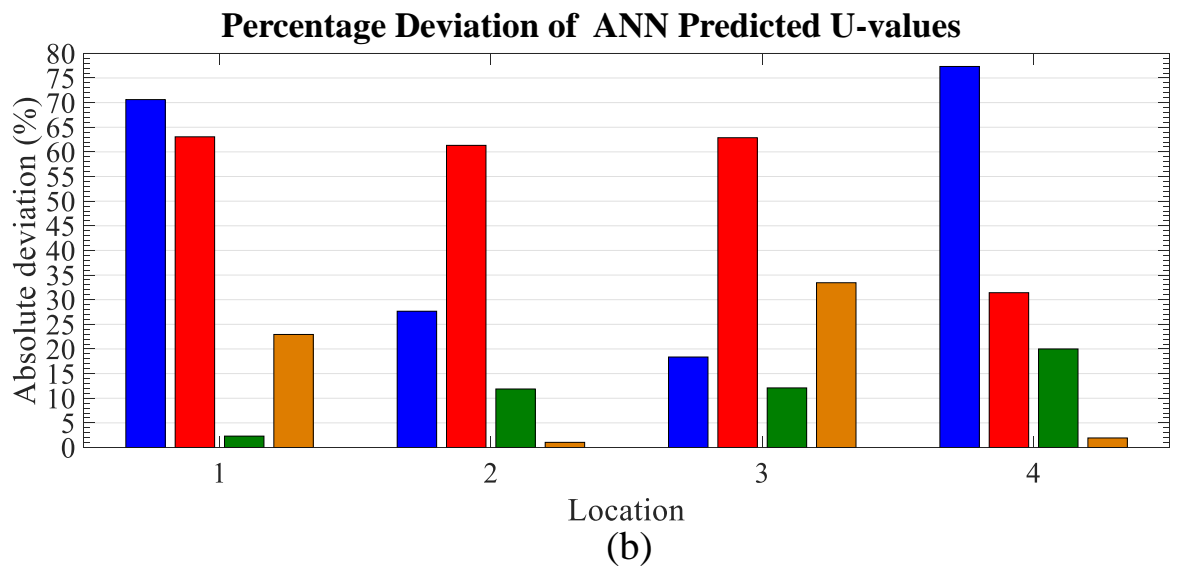
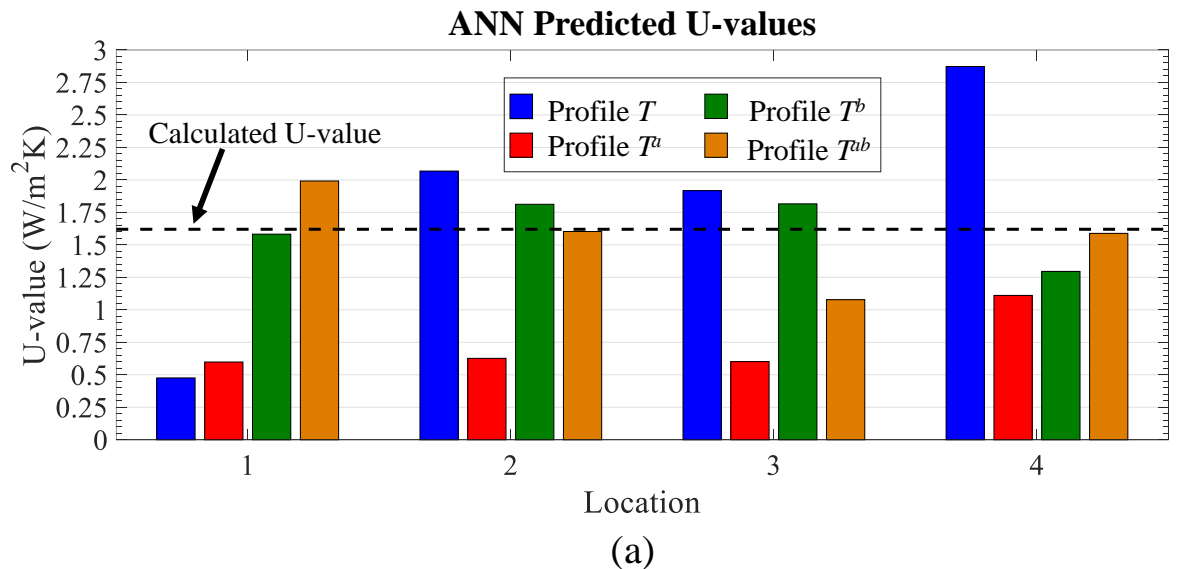


Figure 7.7: (a) ANN predicted U-values obtained using profiles T , T^a , T^b and T^{ab} as input to the ANN and (b) percentage deviation of ANN predicted U-values.

For location 4 it moderately underestimates the U-value of wall and therefore produce 20% absolute deviation (as in Figure7.7-b). The ANN that uses profiles T^b as input produce a

highly accurate estimation for location 2 and 4 (shown in Figure 7.7-a) with absolute percentage deviation of 1.04% and 1.93 %, respectively. For location 1 it moderately overestimates the U-value of wall and for location 3 it moderately underestimates the U-value of wall as shown in Figure 7.7-a. The absolute deviations are 22.94 and 33.45%, respectively. The comparison between the training performance and test performance for these two neural networks presented in Figure 7.6 indicates that there are fairly low differences exists between the training and test performances and therefore there is no overfitting occurred. Considering all these facts it can be claimed that the ANN that uses either profiles T^b or profile T^{ab} as input would be the most suitable to estimate U-value of a building's wall if the wall is monitored with the novel U-value estimation kit used in this case study. The case study presented in the accepted manuscript in Appendix I also reach to the similar conclusion. However, in that case study a wall in location 2 has been monitored which has shown identical absolute deviation for the ANNs with profile T^b and profile T^{ab} . The case study in this chapter includes similar monitoring process and analysis in four different locations. Considering the average of the absolute deviations of the four locations it is found that the ANN with profile T^b has 11.57% absolute deviation and ANN with profile T^{ab} has 14.84% absolute deviation from the calculated U-value of walls in a real building. Hence the ANN with profile T^b as input is slightly ahead of the ANN with standard deviation of profile T^{ab} as input. Similar observation is found in the study for categorisation of wall in chapter 6 where standard deviation of profile T^b as input to the ANN shows the best outcome. Combining these two studies, the feed forward neural network with standard deviation of profile T^b as input and 20 neurons with one hidden layer is the best approach to estimate U-value of walls in real buildings.

7.5 Conclusion

A novel approach of in-situ U-value measurement of wall in a real building using the novel U-value estimation kit is presented in this chapter where the U-value kit is calibrated by training an ANN with the help of infrared images obtained by monitoring material samples in the lab. It is found that the ANN trained with standard deviations in profile T^b achieves 88.43% accuracy and ANN trained with standard deviations in profile T^{ab} achieves 85.16% accuracy in predicting the U-value of multi-layered walls in a real building. As the performance of the ANN trained with standard deviation of profile T^b is slightly better than that of the ANN trained with the standard deviation of profile T^{ab} , standard deviation of profile T^b could be accepted as the best approach for training an ANN to calibrate the novel product. Literature review explains that there is no ideal procedure to determine the most suitable configuration of a neural network. Therefore, based on the outcome of the ANN analysis presented in this chapter it can be stated that the configuration of ANN used could be an appropriate configuration for the in-situ estimation of U-values in real buildings' wall. These results also show a good agreement with the previous case studies presented in Sen and Habaibeh (2019), in chapter 6 and in the accepted manuscript included in Appendix I. However, there are still scopes to research for the improvement of ANN's accuracy using different configurations and architecture of ANN as well as including more monitoring data for training an ANN. Literature review shows that existing U-value estimation systems are limited to use in winter only. Although the monitoring work in the real building is conducted during winter, monitoring of wall sample in laboratory has been conducted in summer. Hence the novel U-value estimation kit is expected to be applicable well in summer also. There is research opportunity in terms of monitoring a real building in summer.

Chapter 8: Discussion and Conclusion

8.1 Introduction

Retrofitting a building's wall with improved insulation is a key strategy in reducing energy consumption for space heating as well as cutting down carbon emission. However, it is sensible to evaluate the existing U-value of a building's wall and the potential future energy savings before the retrofitting work is commenced. The aim of this research work is to develop novel techniques for evaluating the benefits of thermal insulation in buildings by estimating heat losses and financial costs with the help of mathematical models, artificial intelligence, thermography and experimental works addressing the research scopes presented in chapter 1. A comprehensive review of literature has been conducted to summarise the limitations of existing U-value estimation methods as well to understand the effect of insulation in energy consumption in a building, infrared thermography as rapid tool to evaluate thermal performance of a building and the application of ANN in the evaluation of buildings' energy performance. A systematic methodology has been developed to accomplish the aim of the thesis with fulfilment of all objectives. The influence of wall insulation in terms of household expenditures, energy consumption and net change in carbon emission due to work from home is evaluated. In relation to the estimation of future energy savings and payback period of the investment for retrofitting, a prediction tool for estimating heat loss through a building's wall is developed by integrating infrared thermography and ANN with the use of historical temperature and wind speed data. Two case studies in buildings in High Wycombe and Nottingham are presented to demonstrate the application of the heat loss prediction tool. For in-situ U-value estimation, a novel product has been developed by integrating infrared thermography and feed forward neural network with the application of a point heat in the internal side of a wall where the product is calibrated in

laboratory by training the neural network with the help of the monitoring data obtained from some sample walls. In this chapter the objectives of the research works are compared against the achievements and the contribution to knowledge as well as the key findings are summarised. The chapter finishes with the limitations of this research work with future recommendation about further research on this topic.

8.2 Answer to the research questions with the achievement of the objectives

To accomplish the aim of developing a novel product for the in-situ U-value estimation of buildings' wall, the fulfilment of the objectives and answer to the related research questions presented in chapter 1 are established below.

Objective 1: A comprehensive literature review has been conducted on wall insulation, current U-value measuring systems, infrared thermography and how ANN is used for the evaluation of buildings' energy and thermal performance. The literature review on insulation points out that wall insulation significantly reduces energy consumption for space heat and cooling; however, the effectiveness of it depends on the geographical location, climate and the type of insulation applied in a building. The literature review on infrared thermography explains the working principle of infrared thermography as well as the rapidness of thermography in the evaluation of a building's thermal performance. The literature review regarding in-situ U-value assessment elaborately describes the procedures of existing in-situ U-value estimation methods with a summary of the limitation of each method. The literature review on ANN explains the working principle of ANN and its efficiency in predicting energy demands in building compared to other simulation software.

Objective 2: A methodology has been developed to estimate the change in household budget, energy demand and carbon emission due to work from home during winter in English dwellings. The study shows that people living in externally insulated house with low U-value

of wall do not experience significant increase in heating energy consumption as well as energy bills. Instead, those households enjoy significant savings from reduced travelling as well as they significantly contribute to cut down carbon emission. The family living in uninsulated solid wall houses with high U-value of walls suffer from increased energy bills as well as those households do not contribute to reduction in carbon emission unless they use more than one car for travelling.

Objective 3: A novel prediction tool to estimate future heat loss through buildings' wall has been developed by integrating infrared thermography and ANN where the ANN is trained with the heat loss data which is calculated using wall surface temperature obtained from infrared image and historical weather data.

Objective 4: Two case studies are conducted in buildings in High Wycombe and in Nottingham where the novel prediction tool is used to estimate future heat losses in buildings with the help of infrared images captured in thermographic surveys. A mathematical model in relation to the optimum monitoring period for a building to get exact heat loss information has been developed. According to the mathematical model a building is required to be monitored for infinite period to obtain exact information about the heat loss through wall; however, the case studies show that ANN trained with eight years of monitoring data could predict future heat loss with reasonable accuracy. The case studies also show that a feed forward neural network is the most suitable architecture for predicting hourly average heat loss and LSTM neural network is the most suitable architecture for predicting monthly average heat loss.

Objective 5: A novel U-value estimation kit is developed which can monitor wall using an infrared camera with the application of a point heat from the internal side of a wall as well

as record the ambient temperature and the temperature at the location of point heat source on the test wall surface.

Objective 6: Several wall samples with different U-values are monitored using the novel U-value kit and from the visual inspections of the infrared images obtained from the monitoring experiments, three modified temperature profiles have been developed to categorise the sample walls based on their U-values. A feed forward neural network is tested with different combination of neurons in its hidden layer to determine the optimum configuration for categorising the wall samples. The modified temperature profiles and their standard deviations are used as input to the ANN to select the best one among those. The result shows that ANN composed of 20 neurons in one hidden layer and trained with the standard deviation of the cumulative gradient of temperature profile produce best classification accuracy.

Objective 7: For in-situ estimation of U-value the experimental works in relation to monitoring walls have been conducted in four locations in a building. The result shows that a feed forward neural network consists of 20 neurons and one hidden layer is able to estimate U-value of walls in a real building with significant accuracy. It is also found from the outcomes of ANN analysis that the ANN trained with the standard deviation of the cumulative gradient of temperature profile produce the most accurate estimation of U-value in a real building's wall.

8.3 Contribution to knowledge

The key contribution to the knowledge obtained from this research work is presented below:

- The methodology to estimate the change in energy demand and carbon emission due to working from home during winter because of Covid-19 pandemic situation.

- The methodology to predict future heat losses through a building's wall using infrared thermography and ANN.
- A mathematical model showing the optimum the monitoring period of buildings for energy savings estimation.
- The neural network architecture and configuration for the prediction of heat loss through buildings' wall.
- A novel product to estimate U-value of buildings' wall combining infrared thermography and ANN with the application of point heat.
- The methodology to conduct U-value measurement with the novel U-value estimation kit.
- The neural network configuration for the U-value estimation with the novel U-value estimation kit.

8.4 Key findings

The main outcomes of the research are an evaluation tool for future heat loss prediction through walls in buildings and a novel product to estimate the U-value of a building's wall.

However, there are some key findings of this research which are presented below:

- The thesis establishes the method of integrating infrared thermography and ANN for predicting heat loss through buildings' wall and estimating U-value of buildings' wall.
- The wall insulation in a building has major impacts on household energy consumption and change in carbon emission due to working from home in winter.
- The family living in an uninsulated house would consume approximately nine times more energy for space heating than the family living in a modern insulated house due to working from home during winter.

- There are significant savings in household expenditure and reduction in carbon emission due to reduced travelling in pandemic situation. People living in modern insulated houses and use one car for travelling will contribute to reduce carbon emission by releasing 15 to 40 kg less CO₂ per month per household during winter because of working from home. On the other hand, family living in a poorly insulated detached house with wall U-value of 2.3 W/m²K and use two cars for travelling still release 30kg more CO₂ than the normal working situation.
- The mathematical model regarding the length of monitoring period for a building demonstrate that only lifelong monitoring of a building could provide exact information about the building's thermal performance.
- A feed forward neural network with six hidden layers and three neurons in each hidden layer is the most suitable configuration for hourly average heat loss prediction. The prediction accuracy of such neural networks ranges between 80% to 90% when the ANN is trained with eight years or more of heat loss data.
- LSTM neural network with twelve cells in the hidden layer is the best configuration to predict monthly total heat loss in buildings with over 90% prediction accuracy with two or more year of heat loss data required for training the ANN.
- The case studies show that ANN guarantee 84% prediction accuracy for the prediction of future energy savings in buildings.
- Payback period estimation considering ANN predicted energy saving for the investment on retrofitting could be accurate up to the quarter of a year.
- Infrared images obtained by monitoring sample wall with the application of point heat can be integrated with ANN to categorise wall samples based on their U-value.
- A feed forward neural network with softmax layer and one hidden layer consisting 20 neurons in it achieves 88% overall classification accuracy for categorising wall

samples with the minimum accuracy of 69% when the network is trained with the standard deviation of the temperature profile's cumulative gradient.

- Similar configuration of feed forward neural network can be used for the estimation of in-situ U-value in buildings' wall and when the network is trained with the standard deviation of the cumulative gradient of a temperature profile obtained from monitoring a real building's wall with the application of point heat, it would be able to estimate in-situ U-value of walls with more than 80% accuracy.
- The training of ANN by the monitoring of wall samples in laboratory has been conducted in summer; and therefore, the novel U-value estimation kit is expected to be operational during summer which will overcome one of the key limitations of existing U-value estimation methods.

8.5 Limitations and Future work

The limitations of the current research are:

- The payback period of the buildings in second case study could not be estimated as the payback period seems longer than 14 years which is beyond the size of weather data set available for this research work.
- Only feed forward neural network is considered for the estimation of in-situ U-value and only one building is monitored.
- The performance of the novel U-value estimation kit could not be compared with the performance of existing U-value estimation methods.

Based on the limitations of the current study the future work could involve:

- The ANN's prediction of heat losses in buildings can be extended with larger set of weather data to facilitate the estimation of longer pay back periods. Also, the

performance of ANN can be compared with the historical energy bills of the buildings that are monitored.

- The performance of other architecture of neural network can be investigated in relation to in-situ U-value estimation of buildings' wall using the newly developed U-value kit.
- The experimental work and the ANN training can be extended to monitor more wall samples on more buildings' walls.
- The performance of the novel U-value estimation kit could be compared with the performance of existing U-value estimation methods.
- The design of the U-value estimation kit can be further improved considering surface contact heating instead of point contact heating.

8.6 Summary

Exact simulation of the thermal performance as well as the U-value of buildings' wall require extensive data from prolonged monitoring of buildings. The simple realistic approach used in this thesis would facilitate the rapid estimation of the thermal performance and the U-value of buildings' wall with significant accuracy. This chapter summarises the discussion and conclusion of the thesis. The answers to the research questions with respect to the fulfilment of objectives are presented. Afterwards, the contribution to the knowledge and the key findings from the research work is summarised. Finally, the limitations of the current research work are discussed with the recommendations for future research works.

References

Abiodun, O. I. *et al.* (2018) ‘State-of-the-art in artificial neural network applications: A survey’, *Heliyon*, 4(11), p. e00938. doi: 10.1016/j.heliyon.2018.e00938.

Accolade for STYROFOAM as Greening-the-Box retrofit project wins Gold (2012). Available at: <https://www.egshpa.com/news-media/accolade-styrofoam-greening-the-box-retrofit-project-wins-gold/> (Accessed: 20 June 2017).

Adamczyk, J. and Dylewski, R. (2017) ‘The impact of thermal insulation investments on sustainability in the construction sector’, *Renewable and Sustainable Energy Reviews*, 80(December 2016), pp. 421–429. doi: 10.1016/j.rser.2017.05.173.

Aditya, L. *et al.* (2017) ‘A review on insulation materials for energy conservation in buildings’, *Renewable and Sustainable Energy Reviews*, 73(February), pp. 1352–1365. doi: 10.1016/j.rser.2017.02.034.

Akpan, U. F. and Akpan, G. E. (2012) ‘The Contribution of Energy Consumption to Climate Change: A Feasible Policy Direction’, *International Journal of Energy Economics and Policy*, 2(1), pp. 21–33. Available at: www.econjournals.com (Accessed: 12 June 2018).

Al-Habaibeh, A., Medjdoub, B. and Pidduck, A. (2012) ‘Investigating The Influence of Door Design on The Energy Consumption of Buildings Using Infrared Thermography’, in *4th. JIIRCRAC 2012, Amman-Jordan, Sept. 10th – 12th 2012*.

Al-Habaibeh, A., Sen, A. and Chilton, J. (2020) ‘Evaluation Tool For The Thermal Performance of Retrofitted Buildings Using An Integrated Approach of Deep Learning Artificial Neural Networks and Infrared Thermography’, *Energy and Built Environment*. doi: 10.1016/j.enbenv.2020.06.004.

Al-Habaibeh, A. and Siena, F. L. (2012) ‘The Application of Infrared Thermography for The

Evaluation of Insulation and Energy Performance of Buildings’, in *4th. JIIRCRAC 2012, Amman-Jordan*,.

Albatici, R. and Tonelli, A. M. (2010) ‘Infrared thermovision technique for the assessment of thermal transmittance value of opaque building elements on site’, *Energy and Buildings*, 42(11), pp. 2177–2183. doi: 10.1016/j.enbuild.2010.07.010.

Albatici, R., Tonelli, A. M. and Chiogna, M. (2015) ‘A comprehensive experimental approach for the validation of quantitative infrared thermography in the evaluation of building thermal transmittance’, *Applied Energy*, 141, pp. 218–228. doi: 10.1016/j.apenergy.2014.12.035.

Amin, I. J. *et al.* (2008) ‘Automated people-counting by using low-resolution infrared and visual cameras’, *Measurement*, 41(6), pp. 589–599. doi: 10.1016/j.measurement.2007.02.010.

Anderson, B. (2006) *Conventions for U-value calculations 2006 edition*. 2nd Editio. Scotland UK: BRE Press. Available at: www.bre.co.uk (Accessed: 3 January 2018).

Antoniadis, K. D. *et al.* (2012) ‘Improving the Design of Greek Hollow Clay Bricks’, *International Journal of Thermophysics*, 33(12), pp. 2274–2290. doi: 10.1007/s10765-012-1294-x.

Asdrubali, F., D’Alessandro, F. and Schiavoni, S. (2015) ‘A review of unconventional sustainable building insulation materials’, *Sustainable Materials and Technologies*, 4, pp. 1–17. doi: 10.1016/j.susmat.2015.05.002.

Baker, P. (2008) *In situ U-value measurements in traditional buildings –preliminary results*. Available at: <https://www.historicenvironment.scot/archives-and-research/publications/publication/?publicationId=7fc3d5f6-5992-4106-92bf->

a59400bf430c.

Baldinelli, G. *et al.* (2018) ‘A model for the improvement of thermal bridges quantitative assessment by infrared thermography’, *Applied Energy*, 211, pp. 854–864. doi: 10.1016/j.apenergy.2017.11.091.

Baldinelli, G. and Bianchi, F. (2014) ‘Windows thermal resistance: Infrared thermography aided comparative analysis among finite volumes simulations and experimental methods’, *Applied Energy*, 136, pp. 250–258. doi: 10.1016/j.apenergy.2014.09.021.

Ben-Nakhi, A. E. and Mahmoud, M. A. (2004) ‘Cooling load prediction for buildings using general regression neural networks’, *Energy Conversion and Management*, 45(13–14), pp. 2127–2141. doi: 10.1016/J.ENCONMAN.2003.10.009.

Berger, T. *et al.* (2016) ‘Impacts of external insulation and reduced internal heat loads upon energy demand of offices in the context of climate change in Vienna, Austria’, *Journal of Building Engineering*, 5, pp. 86–95. doi: 10.1016/j.jobbe.2015.11.005.

Biddulph, P. *et al.* (2014) ‘Inferring the thermal resistance and effective thermal mass of a wall using frequent temperature and heat flux measurements’, *Energy and Buildings*, 78, pp. 10–16. doi: 10.1016/j.enbuild.2014.04.004.

Bienvenido-Huertas, D. *et al.* (2019) ‘Influence of ICHTC correlations on the thermal characterization of façades using the quantitative internal infrared thermography method’, *Building and Environment*, 149, pp. 512–525. doi: 10.1016/j.buildenv.2018.12.056.

Biswas, M. A. R., Robinson, M. D. and Fumo, N. (2016) ‘Prediction of residential building energy consumption: A neural network approach’, *Energy*, 117, pp. 84–92. doi: 10.1016/J.ENERGY.2016.10.066.

BP (2018) *BP Statistical Review of World Energy*. Available at:

<https://www.bp.com/content/dam/bp/business-sites/en/global/corporate/pdfs/energy-economics/statistical-review/bp-stats-review-2018-full-report.pdf> (Accessed: 21 May 2019).

BRE (2016) *Review of default U-values for existing buildings in SAP*. Available at: https://www.bre.co.uk/filelibrary/SAP/2016/CONSP-16---Wall-U-values-for-existing-dwellings---V1_0.pdf (Accessed: 25 September 2020).

Byrne, A. *et al.* (2016) ‘Case studies of cavity and external wall insulation retrofitted under the Irish Home Energy Saving Scheme: Technical analysis and occupant perspectives’, *Energy and Buildings*, 130, pp. 420–433. doi: 10.1016/j.enbuild.2016.08.027.

Campbell, I. (2020) *Emissions from home energy use, Carbon Independent .org*. Available at: <https://www.carbonindependent.org/15.html#:~:text=The CO2 generated by burning,kg%2F kWh %5B8%5D> . (Accessed: 6 October 2020).

Campbell Scientific (2012) *Model HFP01 Soil Heat Flux Plate, Instruction Manual*. Available at: http://www.hukseflux.com/sites/default/files/product_manual/HFP01_HFP03_manual_v1620.pdf.

Chae, Y. T. *et al.* (2016) ‘Artificial neural network model for forecasting sub-hourly electricity usage in commercial buildings’, *Energy and Buildings*, 111, pp. 184–194. doi: 10.1016/J.ENBUILD.2015.11.045.

Chang, W. *et al.* (2018) ‘Heat transfer prediction of supercritical water with artificial neural networks’, *Applied Thermal Engineering*, 131, pp. 815–824. doi: 10.1016/J.APPLTHERMALENG.2017.12.063.

Chudzik, S. (2012) ‘Measurement of thermal diffusivity of insulating material using an

artificial neural network’, *Measurement Science and Technology*, 23(6), pp. 1–11. doi: 10.1088/0957-0233/23/6/065602.

CIBSE (2006) ‘CIBSE Guide A: Environment Design’. Elsevier, pp. 1–323. Available at: <http://www.cibse.org/getattachment/Knowledge/CIBSE-Guide/CIBSE-Guide-A-Environmental-Design-NEW-2015/Guide-A-presentation.pdf.aspx>.

Climate Change Act (2008). London: The Parliament of the United Kingdom. Available at: http://www.legislation.gov.uk/ukpga/2008/27/pdfs/ukpga_20080027_en.pdf (Accessed: 20 July 2017).

Committee on Climate Change (2016) *UK Climate Action Following the Paris Agreement*. London. Available at: <https://www.theccc.org.uk/wp-content/uploads/2016/10/UK-climate-action-following-the-Paris-Agreement-Committee-on-Climate-Change-October-2016.pdf> (Accessed: 19 July 2017).

Dall’O’, G., Sarto, L. and Panza, A. (2013) ‘Infrared Screening of Residential Buildings for Energy Audit Purposes: Results of a Field Test’, *Energies*, 6(8), pp. 3859–3878. doi: 10.3390/en6083859.

Dalton, J. and Deshmane, A. (1991) ‘Artificial neural networks’, *IEEE Potentials*, 10(2), pp. 33–36. doi: 10.1109/45.84097.

Danielski, I. and Fröling, M. (2015) ‘Diagnosis of Buildings’ Thermal Performance - A Quantitative Method Using Thermography Under Non-steady State Heat Flow’, *Energy Procedia*, 83(83), pp. 320–329. doi: 10.1016/j.egypro.2015.12.186.

Deb, C. *et al.* (2015) ‘Forecasting Energy Consumption of Institutional Buildings in Singapore’, *Procedia Engineering*, 121, pp. 1734–1740. doi: 10.1016/J.PROENG.2015.09.144.

Deb, C. *et al.* (2016) ‘Forecasting diurnal cooling energy load for institutional buildings using Artificial Neural Networks’, *Energy and Buildings*, 121, pp. 284–297. doi: 10.1016/j.enbuild.2015.12.050.

Deb, C. *et al.* (2017) ‘A review on time series forecasting techniques for building energy consumption’, *Renewable and Sustainable Energy Reviews*, 74, pp. 902–924. doi: 10.1016/J.RSER.2017.02.085.

Department for Business Energy & Industrial Strategy (2018) *Energy Consumption in the UK (ECUK) 2018, Energy Consumption in the UK*. Available at: https://assets.publishing.service.gov.uk/government/uploads/system/uploads/attachment_data/file/729317/Energy_Consumption_in_the_UK__ECUK__2018.pdf (Accessed: 14 March 2019).

Department for Business Energy & Industrial Strategy (2019a) *2019 GOVERNMENT GREENHOUSE GAS CONVERSION FACTORS FOR COMPANY REPORTING*. Available at: https://assets.publishing.service.gov.uk/government/uploads/system/uploads/attachment_data/file/904215/2019-ghg-conversion-factors-methodology-v01-02.pdf (Accessed: 6 October 2020).

Department for Business Energy & Industrial Strategy (2019b) *UK becomes first major economy to pass net zero emissions law - GOV.UK*. Available at: <https://www.gov.uk/government/news/uk-becomes-first-major-economy-to-pass-net-zero-emissions-law> (Accessed: 17 September 2019).

Department for Business Energy & Industrial Strategy (2020) *Energy Trends: UK electricity*. Available at: <https://www.gov.uk/government/statistics/electricity-section-5-energy-trends> (Accessed: 20 September 2020).

Department for Business Energy & Industrial Strategy and Waters, L. (2017) *ENERGY CONSUMPTION IN THE UK*. London. Available at: https://www.gov.uk/government/uploads/system/uploads/attachment_data/file/633503/EC_UK_2017.pdf (Accessed: 25 September 2017).

Department for Transport (2020) *Transport use during the coronavirus (COVID-19) pandemic*. Available at: <https://www.gov.uk/government/statistics/transport-use-during-the-coronavirus-covid-19-pandemic> (Accessed: 6 October 2020).

Department for Transport Statistics (2015) *New car carbon dioxide emissions*. Available at: <https://www.gov.uk/government/publications/new-car-carbon-dioxide-emissions> (Accessed: 6 October 2020).

Derradji, L. *et al.* (2017) 'A study on residential energy requirement and the effect of the glazing on the optimum insulation thickness', *Applied Thermal Engineering*, 112, pp. 975–985. doi: 10.1016/j.applthermaleng.2016.10.116.

Desogus, G., Mura, S. and Ricciu, R. (2011) 'Comparing different approaches to in situ measurement of building components thermal resistance', *Energy and Buildings*, 43(10), pp. 2613–2620. doi: 10.1016/j.enbuild.2011.05.025.

Doran, S. (2001) *DETR Framework Project Report : Prepared for : Safety and Health Business Plan Field investigations of the thermal performance of construction elements as built Approved on behalf of BRE*. Available at: <http://projects.bre.co.uk/uvalues/U-values.pdf> (Accessed: 17 February 2017).

Driver and Vehicle Licensing Agency (2020) *Licensed Cars by Keepership (private and company): Great Britain and United Kingdom*. Available at: <https://www.gov.uk/government/statistical-data-sets/veh02-licensed-cars>.

EcoTherm insulation (no date) *Rigid PIR Thermal Insulation Boards*. Available at: http://www.ecotherm.co.uk/rigid_insulation.aspx (Accessed: 29 April 2018).

Ekici, B. B. and Aksoy, U. T. (2009) 'Prediction of building energy consumption by using artificial neural networks', *Advances in Engineering Software*, 40(5), pp. 356–362. doi: 10.1016/J.ADVENGSOFT.2008.05.003.

Energy Use Calculator (2020) *Electricity usage of an LCD/LED Display or TV Screen*. Available at: http://energyusecalculator.com/electricity_lcdleddisplay.htm (Accessed: 29 September 2020).

Evangelisti, L. *et al.* (2015) 'In Situ Thermal Transmittance Measurements for Investigating Differences between Wall Models and Actual Building Performance', *Sustainability*, 7(8), pp. 10388–10398. doi: 10.3390/su70810388.

Fang, Z. *et al.* (2014) 'The effect of building envelope insulation on cooling energy consumption in summer', *Energy and Buildings*, 77, pp. 197–205. doi: 10.1016/j.enbuild.2014.03.030.

Farzana, S. *et al.* (2014) 'Multi-model prediction and simulation of residential building energy in urban areas of Chongqing, South West China', *Energy and Buildings*, 81, pp. 161–169. doi: 10.1016/J.ENBUILD.2014.06.007.

Ferrarini, G. *et al.* (2016) 'Thermal response measurement of building insulating materials by infrared thermography', *Energy and Buildings*, 133, pp. 559–564. doi: 10.1016/j.enbuild.2016.10.024.

Ficco, G. *et al.* (2015) 'U-value in situ measurement for energy diagnosis of existing buildings', *Energy and Buildings*, 104, pp. 108–121. doi: 10.1016/j.enbuild.2015.06.071.

Flir System (2006) 'ThermaCAMTM E25 User's manual'. Available at: <http://sti->

monge.fr/maintenancesystemes/wp-content/uploads/2013/06/FLIR-E25-Manual.pdf

(Accessed: 18 December 2018).

Fokaides, P. A. and Kalogirou, S. A. (2011) ‘Application of infrared thermography for the determination of the overall heat transfer coefficient (U-Value) in building envelopes’, *Applied Energy*, 88(12), pp. 4358–4365. doi: 10.1016/j.apenergy.2011.05.014.

Gaspar, K., Casals, M. and Gangoellis, M. (2016) ‘A comparison of standardized calculation methods for in situ measurements of façades U-value’, *Energy and Buildings*, 130, pp. 592–599. doi: 10.1016/j.enbuild.2016.08.072.

Gaspar, K., Casals, M. and Gangoellis, M. (2018) ‘Review of criteria for determining HFM minimum test duration’, *Energy and Buildings*, 176, pp. 360–370. doi: 10.1016/j.enbuild.2018.07.049.

Gong, Y. and Huang, K. (2006) ‘Comparison of Dynamic Data Analysis Methods for Thermal Property Measurement of a Building Wall’, *Envelope Technologies for Building Energy Efficiency*, 2(1–3). Available at: <https://oaktrust.library.tamu.edu/bitstream/handle/1969.1/5503/ESL-IC-06-11-41.pdf?sequence=4&isAllowed=y> (Accessed: 22 February 2017).

Google Map (no date) *No Title*. Available at: <https://www.google.com/maps/place/Main+St,+Calverton,+Nottingham+NG14+6FN/@53.036999,-1.0830091,59m/data=!3m1!1e3!4m5!3m4!1s0x4879c759398f7b5b:0x44fc4e6e94702a32!8m2!3d53.0370978!4d-1.0846771> (Accessed: 29 December 2020).

Gori, M. (2018) ‘Deep Architectures’, in *Machine Learning*. Elsevier, pp. 236–338. doi: 10.1016/B978-0-08-100659-7.00005-1.

Gori, V. *et al.* (2017) ‘Inferring the thermal resistance and effective thermal mass distribution of a wall from in situ measurements to characterise heat transfer at both the interior and exterior surfaces’, *Energy and Buildings*, 135, pp. 398–409. doi: 10.1016/j.enbuild.2016.10.043.

GreenTEG AG (2019) *Case Study on U-value Measurement of Building Using gSKIN® Measurement Kit Table of Content*. Available at: https://www.greenteg.com/template/userfiles/files/broschure_updated_January_2020.pdf (Accessed: 9 September 2020).

Harrall, J. (2012) ‘Building Adaptation Achieves 80% Reduction In Running Costs’, *Building Innovations*, pp. 68–69.

Hartig, K.W., Larson, S.L. and Lingle, P.J., G. I. C. (1996) ‘Low-E glass coating system and insulating glass units made therefrom’. U.S. Patent 5,514,476. Available at: <https://www.google.com/patents/US5514476> (Accessed: 8 December 2017).

Haslett, A. (2016) *HOUSING RETROFITS – A NEW START*. Available at: <https://d2umxnkyjne36n.cloudfront.net/insightReports/Housing-Retrofits-A-New-Start.pdf?mtime=20161111100257>.

Haykin, S. (2000) ‘Neural Networks: A Guided Tour’, in *Soft Computing and Intelligent Systems*. Elsevier, pp. 71–80. doi: 10.1016/B978-012646490-0/50007-X.

HM Revenue & Custom (2020) *Advisory fuel rates*. Available at: <https://www.gov.uk/guidance/advisory-fuel-rates> (Accessed: 6 October 2020).

Hong, S. H., Oreszczyn, T. and Ridley, I. (2006) ‘The impact of energy efficient refurbishment on the space heating fuel consumption in English dwellings’, *Energy and Buildings*, 38(10), pp. 1171–1181. doi: 10.1016/j.enbuild.2006.01.007.

Hoyano, A., Asano, K. and Kanamaru, T. (1999) ‘Analysis of the sensible heat flux from the exterior surface of buildings using time sequential thermography’, *Atmospheric Environment*, 33(24–25), pp. 3941–3951. doi: 10.1016/S1352-2310(99)00136-3.

Huang, H., Chen, L. and Hu, E. (2015) ‘A neural network-based multi-zone modelling approach for predictive control system design in commercial buildings’, *Energy and Buildings*, 97, pp. 86–97. doi: 10.1016/J.ENBUILD.2015.03.045.

Hudson Beale, M., Hagan, M. T. and Demuth, H. B. (2017) *Neural Network Toolbox™ User’s Guide*. Online 201. Natick: The MathWorks, Inc. Available at: https://www.mathworks.com/help/pdf_doc/nnet/nnet_ug.pdf.

Hulme, J. and Doran, S. (2015) *In-situ measurements of wall U-values in English housing*. Available at: www.bre.co.uk (Accessed: 17 February 2017).

IEA (2019) *World Energy Outlook 2019*, *World Energy Outlook 2019*. Available at: <https://www.iea.org/reports/world-energy-outlook-2019> <https://www.iea.org/reports/world-energy-outlook-2019> <https://webstore.iea.org/download/summary/2467?fileName=Japanese-Summary-WEO2019.pdf> (Accessed: 13 September 2020).

Incropera, F. P. *et al.* (2011) *Fundamentals of heat and mass transfer*. 7th edn. John Wiley & Sons, Inc.

International Thermal Instrument Company, I. (no date) *HT-50 Thermal Flux Meter*. Available at: <http://www.thermalinstrumentcompany.com/products/heatfluxtransducers/ht-50thermalfluxmeter> (Accessed: 28 April 2017).

ISO (2007) *ISO 6946. Building components and building elements—thermal resistance and thermal transmittance—calculation method*. Available at:

<https://www.iso.org/standard/40968.html> (Accessed: 29 August 2020).

ISO (2014) *ISO 9869-1. Thermal insulation — Building elements — In-situ measurement of thermal resistance and thermal transmittance — Part 1: Heat flow meter method*. Available at: <https://www.iso.org/standard/59697.html> (Accessed: 31 August 2020).

ISO (2018) *ISO 9869-2. Thermal insulation — Building elements — In-situ measurement of thermal resistance and thermal transmittance — Part 2: Infrared method for frame structure dwelling*. Available at: <https://www.iso.org/standard/67673.html> (Accessed: 31 August 2020).

ISO 10456 (2007) *ISO FDIS 10456:2007(E): Building materials and products — Hygrothermal properties — Tabulated design values and procedures for determining declared and design thermal values*. Available at: <http://www.superhomes.org.uk/wp-content/uploads/2016/09/Hygrothermal-properties.pdf> (Accessed: 14 May 2018).

Jovanović, R. Ž., Sretenović, A. A. and Živković, B. D. (2015) ‘Ensemble of various neural networks for prediction of heating energy consumption’, *Energy and Buildings*, 94, pp. 189–199. doi: 10.1016/J.ENBUILD.2015.02.052.

Kim, J. and Moon, J. W. (2009) ‘Impact of Insulation on Building Energy Consumption’, *Building Simulation* 2009, pp. 674–680. Available at: <http://citeseerx.ist.psu.edu/viewdoc/summary?doi=10.1.1.172.4791>.

Kim, T.-Y. and Cho, S.-B. (2019) ‘Predicting residential energy consumption using CNN-LSTM neural networks’, *Energy*, 182, pp. 72–81. doi: 10.1016/j.energy.2019.05.230.

Kolaitis, D. I. *et al.* (2013) ‘Comparative assessment of internal and external thermal insulation systems for energy efficient retrofitting of residential buildings’, *Energy and Buildings*, 64, pp. 123–131. doi: 10.1016/j.enbuild.2013.04.004.

Kossecka, E. and Kosny, J. (2002) 'Influence of insulation configuration on heating and cooling loads in a continuously used building', *Energy and Buildings*, 34(4), pp. 321–331. doi: 10.1016/S0378-7788(01)00121-9.

Kuan, C.-M. (2008) 'Artificial Neural Networks', in *The New Palgrave Dictionary of Economics*. Basingstoke: Nature Publishing Group, pp. 250–258. doi: 10.1057/9780230226203.0063.

'L1A Conservation of fuel and power in new dwellings' (2014). National Building Specification, pp. 1–46. Available at: https://www.gov.uk/government/uploads/system/uploads/attachment_data/file/540326/BR__PDF_AD_L1A_2013_with_2016_amendments.pdf (Accessed: 17 July 2017).

'L1B Conservation of fuel and power in existing dwellings' (2015). National Building Specification, pp. 1–31. Available at: https://www.gov.uk/government/uploads/system/uploads/attachment_data/file/540327/BR__PDF__AD_L1B_2013_with_2016_amendments.pdf (Accessed: 17 July 2017).

Lee, J. *et al.* (2017) 'Impact of external insulation and internal thermal density upon energy consumption of buildings in a temperate climate with four distinct seasons', *Renewable and Sustainable Energy Reviews*, 75(November 2016), pp. 1081–1088. doi: 10.1016/j.rser.2016.11.087.

Li, F. G. N. *et al.* (2015) 'Solid-wall U -values: heat flux measurements compared with standard assumptions', *Building Research & Information*, 43(2), pp. 238–252. doi: 10.1080/09613218.2014.967977.

Li, K. *et al.* (2018) 'A hybrid teaching-learning artificial neural network for building electrical energy consumption prediction', *Energy and Buildings*, 174, pp. 323–334. doi: 10.1016/J.ENBUILD.2018.06.017.

Lippmann, R. P. (1987) 'An Introduction to Computing with Neural Nets', *IEEE ASSP MAGAZINE*, (April 1987), pp. 4–22. Available at: <http://ieeexplore.ieee.org/stamp/stamp.jsp?tp=&arnumber=1165576>.

Loucari, C. *et al.* (2016) 'Retrofit solutions for solid wall dwellings in England: The impact of uncertainty upon the energy performance gap', *Building Services Engineering Research and Technology*, 37(5), pp. 614–634. doi: 10.1177/0143624416647758.

Lucchi, E. (2017) 'Thermal transmittance of historical brick masonries: A comparison among standard data, analytical calculation procedures, and in situ heat flow meter measurements', *Energy and Buildings*, 134, pp. 171–184. doi: 10.1016/j.enbuild.2016.10.045.

Marino, B. M., Muñoz, N. and Thomas, L. P. (2017) 'Estimation of the surface thermal resistances and heat loss by conduction using thermography', *Applied Thermal Engineering*, 114, pp. 1213–1221. doi: 10.1016/j.applthermaleng.2016.12.033.

Martellotta, F. *et al.* (2017) 'On the use of artificial neural networks to model household energy consumptions', *Energy Procedia*, 126, pp. 250–257. doi: 10.1016/j.egypro.2017.08.149.

Met Office (2019) 'MIDAS Open: UK hourly weather observation data, v201901', *Centre for Environmental Data Analysis*, 01 March 2019. doi: 10.5285/c58c1af69b9745fda4cdf487a9547185.

Moran, M. J. *et al.* (2003) *Introduction to thermal systems engineering*. John Wiley & Sons, Inc. Available at: [ftp://ftp.demec.ufmg.br/ema867/Bibliografia/Introduction to Thermal Systems Engineering Thermodynamics, Fluid Mechanics, and Heat Transfer/FM.pdf](ftp://ftp.demec.ufmg.br/ema867/Bibliografia/Introduction%20to%20Thermal%20Systems%20Engineering%20Thermodynamics,%20Fluid%20Mechanics,%20and%20Heat%20Transfer/FM.pdf).

Naji, S. *et al.* (2016) 'Application of adaptive neuro-fuzzy methodology for estimating

building energy consumption’, *Renewable and Sustainable Energy Reviews*, 53, pp. 1520–1528. doi: 10.1016/J.RSER.2015.09.062.

Nardi, I. *et al.* (2015) ‘Validation of quantitative IR thermography for estimating the U-value by a hot box apparatus’, *Journal of Physics: Conference Series*, 655, pp. 1–10. doi: 10.1088/1742-6596/655/1/012006.

Nardi, I. *et al.* (2016) ‘U-value assessment by infrared thermography: A comparison of different calculation methods in a Guarded Hot Box’, *Energy and Buildings*, 122, pp. 211–221. doi: 10.1016/j.enbuild.2016.04.017.

Nardi, I. *et al.* (2018) ‘Quantification of heat energy losses through the building envelope: A state-of-the-art analysis with critical and comprehensive review on infrared thermography’, *Building and Environment*, 146, pp. 190–205. doi: 10.1016/j.buildenv.2018.09.050.

Nardi, I., Sfarra, S. and Ambrosini, D. (2014) ‘Quantitative thermography for the estimation of the U-value: state of the art and a case study’, *Journal of Physics: Conference Series*, 547, pp. 1–8. doi: 10.1088/1742-6596/547/1/012016.

Neto, A. H. and Fiorelli, F. A. S. (2008) ‘Comparison between detailed model simulation and artificial neural network for forecasting building energy consumption’, *Energy and Buildings*, 40(12), pp. 2169–2176. doi: 10.1016/J.ENBUILD.2008.06.013.

O’Grady, M., Lechowska, A. A. and Harte, A. M. (2017) ‘Infrared thermography technique as an in-situ method of assessing heat loss through thermal bridging’, *Energy and Buildings*, 135, pp. 20–32. doi: 10.1016/j.enbuild.2016.11.039.

OECD (2011) *OECD Green Growth Studies Energy*. Available at: <https://www.oecd.org/greengrowth/greening-energy/49157219.pdf> (Accessed: 21 May

2019).

OMEGA Engineering, I. (no date) 'Thin Film Flux sensor User ' s Guide Benelux :', *Construction*. Available at: <http://www.omega.com/manuals/manualpdf/M1844.pdf>.

Papadopoulos, A. M. (2005) 'State of the art in thermal insulation materials and aims for future developments', *Energy and Buildings*, 37(1), pp. 77–86. doi: 10.1016/j.enbuild.2004.05.006.

Piddington, J. *et al.* (2020) *The Housing Stock of The United Kingdom*. Available at: https://files.bregroup.com/bretrust/The-Housing-Stock-of-the-United-Kingdom_Report_BRE-Trust.pdf (Accessed: 6 October 2020).

Platon, R., Dehkordi, V. R. and Martel, J. (2015) 'Hourly prediction of a building's electricity consumption using case-based reasoning, artificial neural networks and principal component analysis', *Energy and Buildings*, 92, pp. 10–18. doi: 10.1016/J.ENBUILD.2015.01.047.

Rafiq, M. ., Bugmann, G. and Easterbrook, D. . (2001) 'Neural network design for engineering applications', *Computers & Structures*, 79(17), pp. 1541–1552. doi: 10.1016/S0045-7949(01)00039-6.

Reilly, A. and Kinnane, O. (2017) 'The impact of thermal mass on building energy consumption', *Applied Energy*, 198, pp. 108–121. doi: 10.1016/j.apenergy.2017.04.024.

Rye, C. (2010) *U-Value Report, The SPAB U-value Report*. Available at: <https://www.spab.org.uk/downloads/TheSPABU-valueReportFINAL.pdf> (Accessed: 21 February 2017).

Sadineni, S. B., Madala, S. and Boehm, R. F. (2011) 'Passive building energy savings: A review of building envelope components', *Renewable and Sustainable Energy Reviews*,

15(8), pp. 3617–3631. doi: 10.1016/j.rser.2011.07.014.

Sassine, E. (2016) ‘A practical method for in-situ thermal characterization of walls’, *Case Studies in Thermal Engineering*, 8, pp. 84–93. doi: 10.1016/j.csite.2016.03.006.

Sen, A. and Al-Habaibeh, A. (2019) ‘The design of a novel approach for the assessment of thermal insulation in buildings using infrared thermography and artificial intelligence’, *International Journal of Design Engineering*, 9(1), p. 65. doi: 10.1504/IJDE.2019.104128.

Shearman, B. (no date) *Which is more energy efficient - boiling water using an electric kettle, a kettle on a gas hob or a microwave oven?* Available at: [https://www.theguardian.com/notesandqueries/query/0,5753,-2452,00.html#:~:text=Again%2C heating of 1 litre,\(0.091kWh\) of heat.](https://www.theguardian.com/notesandqueries/query/0,5753,-2452,00.html#:~:text=Again%2C heating of 1 litre,(0.091kWh) of heat.) (Accessed: 29 September 2020).

Sheela, K. G. and Deepa, S. N. (2013) ‘Review on methods to fix number of hidden neurons in neural networks’, *Mathematical Problems in Engineering*, 2013. doi: 10.1155/2013/425740.

Smarter Business (2019) *How Much Energy Do My Appliances Use? INFOGRAPHIC*. Available at: [https://smarterbusiness.co.uk/blogs/how-much-energy-do-my-appliances-use-infographic/#:~:text=A laptop typically uses about,of 12.5 p%2FkWh\).](https://smarterbusiness.co.uk/blogs/how-much-energy-do-my-appliances-use-infographic/#:~:text=A laptop typically uses about,of 12.5 p%2FkWh).) (Accessed: 29 September 2020).

Sørensen, L. (2013) ‘Heat Transmission Coefficient Measurements in Buildings Utilizing a Heat Loss Measuring Device’, *Sustainability*, 5(8), pp. 3601–3614. doi: 10.3390/su5083601.

Sørensen, L. S. (2010) ‘Energy Renovation of Buildings Utilizing the U-value Meter, a New Heat Loss Measuring Device’, *Sustainability*, 2(2), pp. 461–474. doi: 10.3390/su2020461.

Staszczuk, A., Wojciech, M. and Kuczyński, T. (2017) ‘The effect of floor insulation on

indoor air temperature and energy consumption of residential buildings in moderate climates’, *Energy*, 138, pp. 139–146. doi: 10.1016/j.energy.2017.07.060.

Tabrizi, T. B., Hill, G. and Aitchison, M. (2017) ‘The Impact of Different Insulation Options on the Life Cycle Energy Demands of a Hypothetical Residential Building’, *Procedia Engineering*, 180, pp. 128–135. doi: 10.1016/j.proeng.2017.04.172.

TESTO (no date) *Temperature probe for calculating U value: 0614 1635*. Available at: <https://static-int.testo.com/media/44/01/2e792781772d/testo-U-value-probe-Application-Information.pdf> (Accessed: 9 September 2020).

The Construction 2025 (2013) *Industrial Strategy: government and industry in partnership*. Available at: https://www.gov.uk/government/uploads/system/uploads/attachment_data/file/210099/bis-13-955-construction-2025-industrial-strategy.pdf (Accessed: 20 July 2017).

The Green Age (2016) *How much does external wall insulation cost?* Available at: <https://www.thegreenage.co.uk/how-much-does-external-wall-insulation-cost/> (Accessed: 22 December 2020).

The Sustainable Energy Association (b) (2017) *Energy Efficiency – A Policy Pathway Addressing the Able to Pay Sector*. Available at: http://www.sustainableenergyassociation.com/wp-content/uploads/2017/03/SEA_Energy-Efficiency-A-Policy-Pathway_Final.pdf (Accessed: 20 September 2017).

Tu, J. V. (1996) ‘Advantages and disadvantages of using artificial neural networks versus logistic regression for predicting medical outcomes’, *Journal of Clinical Epidemiology*, 49(11), pp. 1225–1231. doi: 10.1016/S0895-4356(96)00002-9.

Tzifa, V. *et al.* (2017) ‘Uncertainty and method limitations in a short-time measurement of

the effective thermal transmittance on a building envelope using an infrared camera’, *International Journal of Sustainable Energy*, 36(1), pp. 28–46. doi: 10.1080/14786451.2014.982119.

U.S. Energy Information Administration (2016) *International Energy Outlook 2016*. doi: [www.eia.gov/forecasts/ieo/pdf/0484\(2016\).pdf](http://www.eia.gov/forecasts/ieo/pdf/0484(2016).pdf).

UK Green Building Council (2017) ‘Delivering Low Carbon Infrastructure’, pp. 1–32. Available at: [http://www.ukgbc.org/sites/default/files/Delivering Low Carbon Infrastructure.pdf](http://www.ukgbc.org/sites/default/files/Delivering_Low_Carbon_Infrastructure.pdf) (Accessed: 19 July 2017).

UK Power (no date) *Compare energy prices per kWh*. Available at: https://www.ukpower.co.uk/home_energy/tariffs-per-unit-kwh (Accessed: 29 September 2020).

United Kingdom natural gas prices (no date). Available at: https://www.globalpetrolprices.com/United-Kingdom/natural_gas_prices/ (Accessed: 29 September 2020).

United Nations Framework Convention on Climate Change (2015) ‘ADOPTION OF THE PARIS AGREEMENT - Paris Agreement text English’. Paris : United Nations, pp. 1–27. Available at: https://unfccc.int/files/essential_background/convention/application/pdf/english_paris_agreement.pdf (Accessed: 19 July 2017).

Usamentiaga, R. *et al.* (2014) ‘Infrared Thermography for Temperature Measurement and Non-Destructive Testing’, *Sensors*, 14(7), pp. 12305–12348. doi: 10.3390/s140712305.

Wang, D. *et al.* (2016) ‘The influence of thermal insulation position in building exterior walls on indoor thermal comfort and energy consumption of residential buildings in

Chongqing’, *IOP Conference Series: Earth and Environmental Science*, 40, p. 012081. doi: 10.1088/1755-1315/40/1/012081.

Wang, L., Lee, E. W. M. and Yuen, R. K. K. (2018) ‘Novel dynamic forecasting model for building cooling loads combining an artificial neural network and an ensemble approach’, *Applied Energy*, 228, pp. 1740–1753. doi: 10.1016/j.apenergy.2018.07.085.

Wang, Z. and Srinivasan, R. S. (2017) ‘A review of artificial intelligence based building energy use prediction: Contrasting the capabilities of single and ensemble prediction models’, *Renewable and Sustainable Energy Reviews*, 75, pp. 796–808. doi: 10.1016/J.RSER.2016.10.079.

Wang, Z., Wang, Y. and Srinivasan, R. S. (2018) ‘A novel ensemble learning approach to support building energy use prediction’, *Energy and Buildings*, 159, pp. 109–122. doi: 10.1016/j.enbuild.2017.10.085.

Waters, L. (2019) *Energy Consumption in the UK (ECUK) 1970 to 2018*. Available at: https://assets.publishing.service.gov.uk/government/uploads/system/uploads/attachment_data/file/820843/Energy_Consumption_in_the_UK__ECUK__MASTER_COPY.pdf (Accessed: 13 September 2020).

Witten, I. H. *et al.* (2017) ‘Deep learning’, in *Data Mining*. Elsevier, pp. 417–466. doi: 10.1016/B978-0-12-804291-5.00010-6.

Yang, I.-H., Yeo, M.-S. and Kim, K.-W. (2003) ‘Application of artificial neural network to predict the optimal start time for heating system in building’, *Energy Conversion and Management*, 44(17), pp. 2791–2809. doi: 10.1016/S0196-8904(03)00044-X.

Yang, J., Rivard, H. and Zmeureanu, R. (2005) ‘On-line building energy prediction using

adaptive artificial neural networks’, *Energy and Buildings*, 37(12), pp. 1250–1259. doi: 10.1016/j.enbuild.2005.02.005.

Yildiz, B., Bilbao, J. I. and Sproul, A. B. (2017) ‘A review and analysis of regression and machine learning models on commercial building electricity load forecasting’, *Renewable and Sustainable Energy Reviews*, 73, pp. 1104–1122. doi: 10.1016/J.RSER.2017.02.023.

Yokoyama, R., Wakui, T. and Satake, R. (2009) ‘Prediction of energy demands using neural network with model identification by global optimization’, *Energy Conversion and Management*, 50(2), pp. 319–327. doi: 10.1016/j.enconman.2008.09.017.

Yurday, E. (2020) *Average Car Mileage UK 2020*. Available at: <https://www.nimblefins.co.uk/average-car-mileage-uk#:~:text=Commuting mileage has held steady,by 700 miles a year.> (Accessed: 6 October 2020).

Zhang, Y. *et al.* (2015) ‘Comparisons of inverse modeling approaches for predicting building energy performance’, *Building and Environment*, 86, pp. 177–190. doi: 10.1016/J.BUILDENV.2014.12.023.

Zhao, Y. *et al.* (2019) ‘A review of data mining technologies in building energy systems: Load prediction, pattern identification, fault detection and diagnosis’, *Energy and Built Environment*. doi: 10.1016/j.enbenv.2019.11.003.

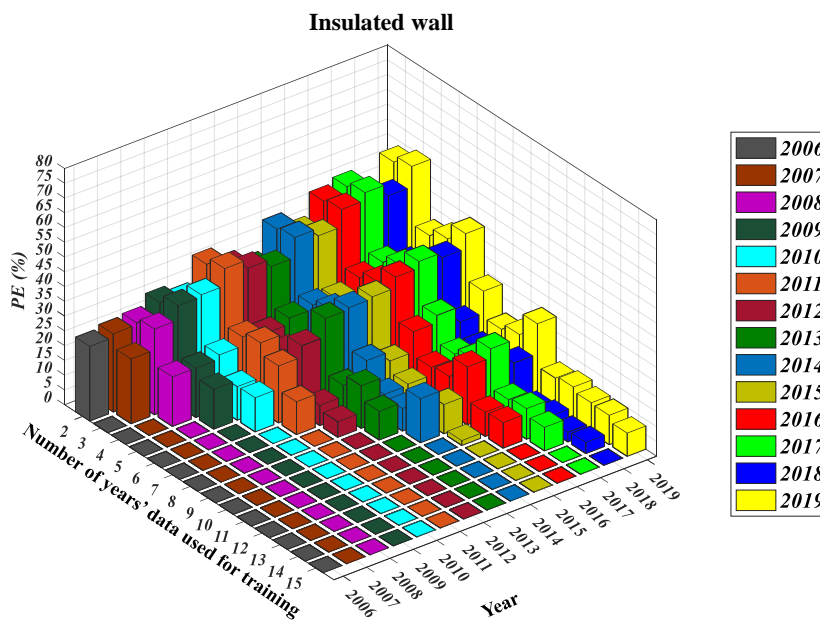
Zheng, Z., Chen, H. and Luo, X. (2019) ‘Spatial granularity analysis on electricity consumption prediction using LSTM recurrent neural network’, *Energy Procedia*, 158, pp. 2713–2718. doi: 10.1016/j.egypro.2019.02.027.

Appendix: A

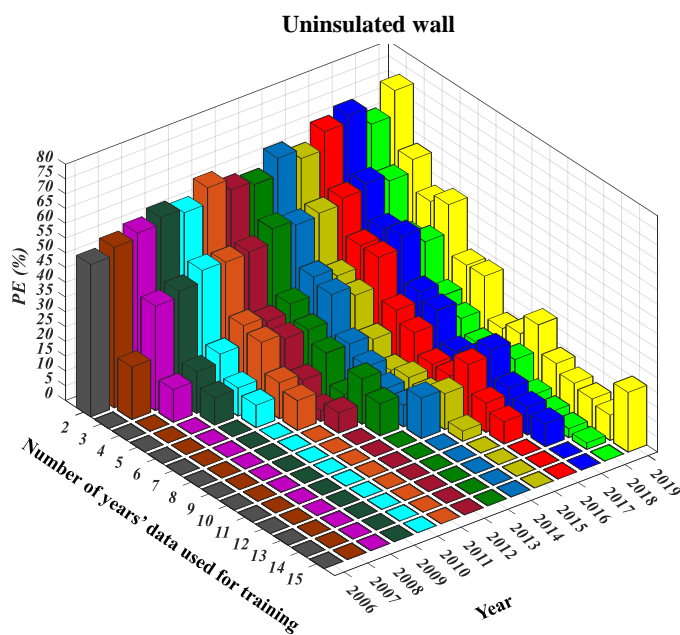
Performance of different Neural Network Architecture for Hourly Heat

Loss Prediction (Case Study 1)

Case study 1: Performance of Feed Forward Neural Network

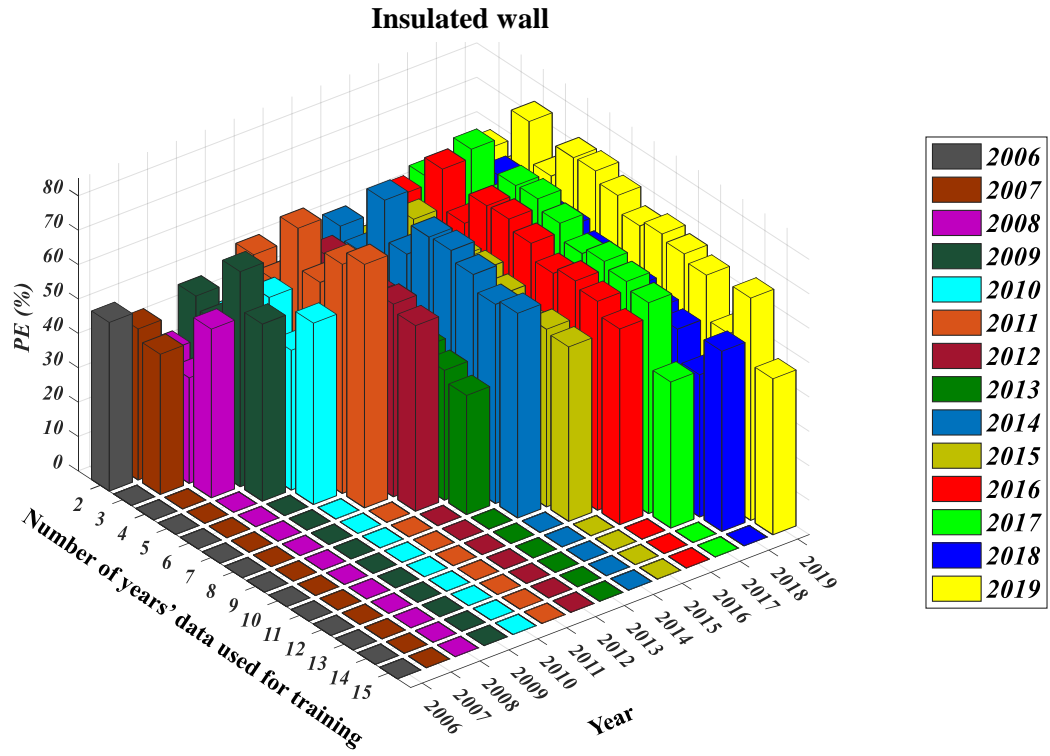


(a)

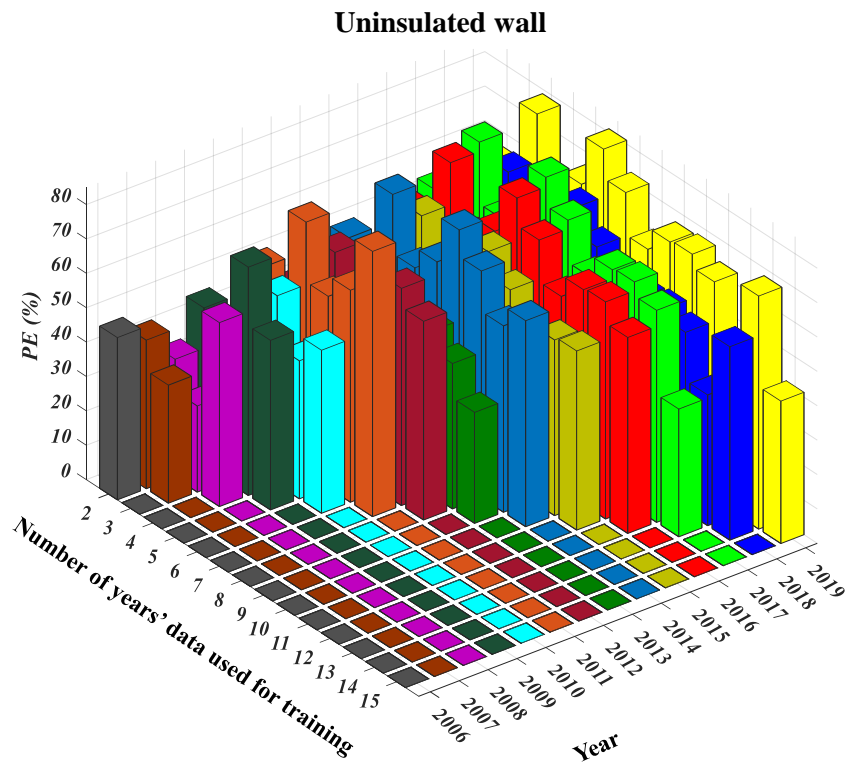


(b)

Case study 1: Performance of Nonlinear Auto Regressive Neural Network (NARnet)

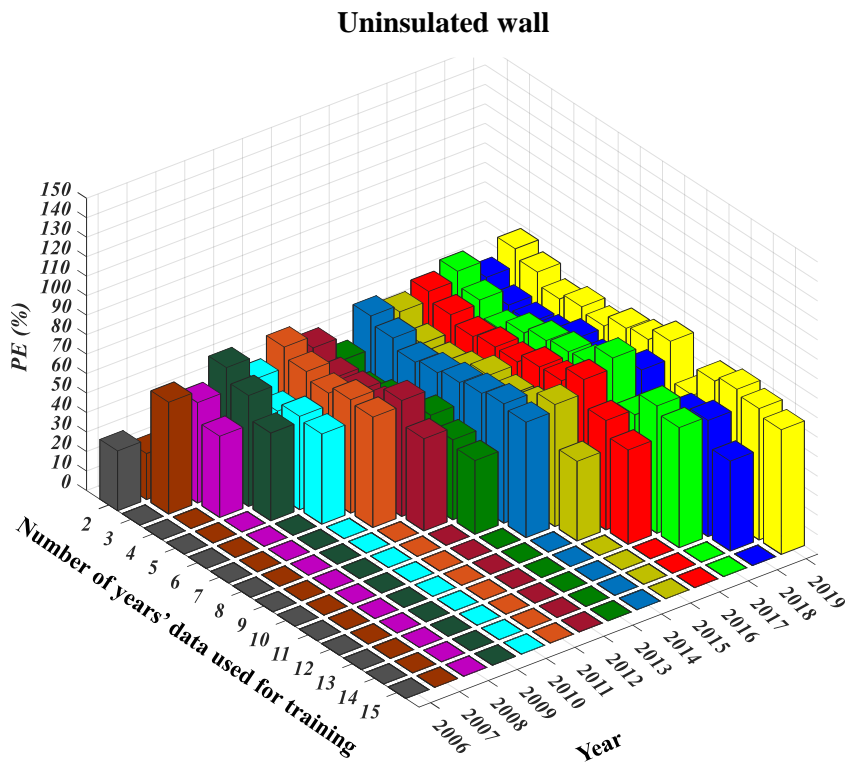
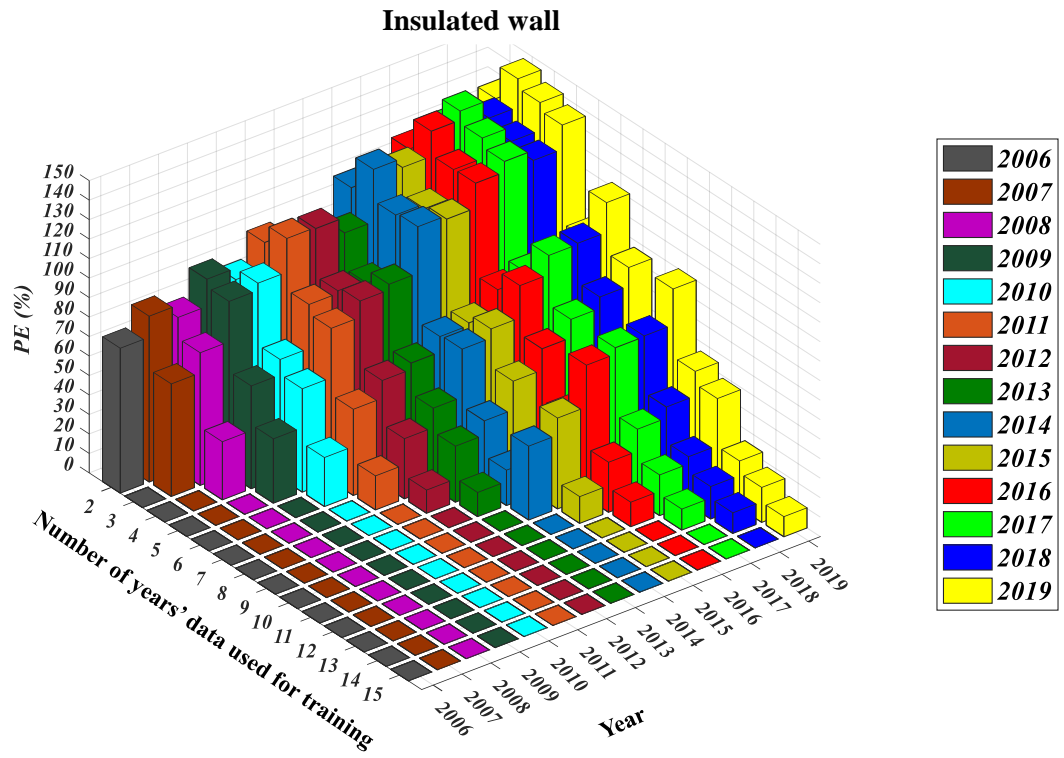


(a)



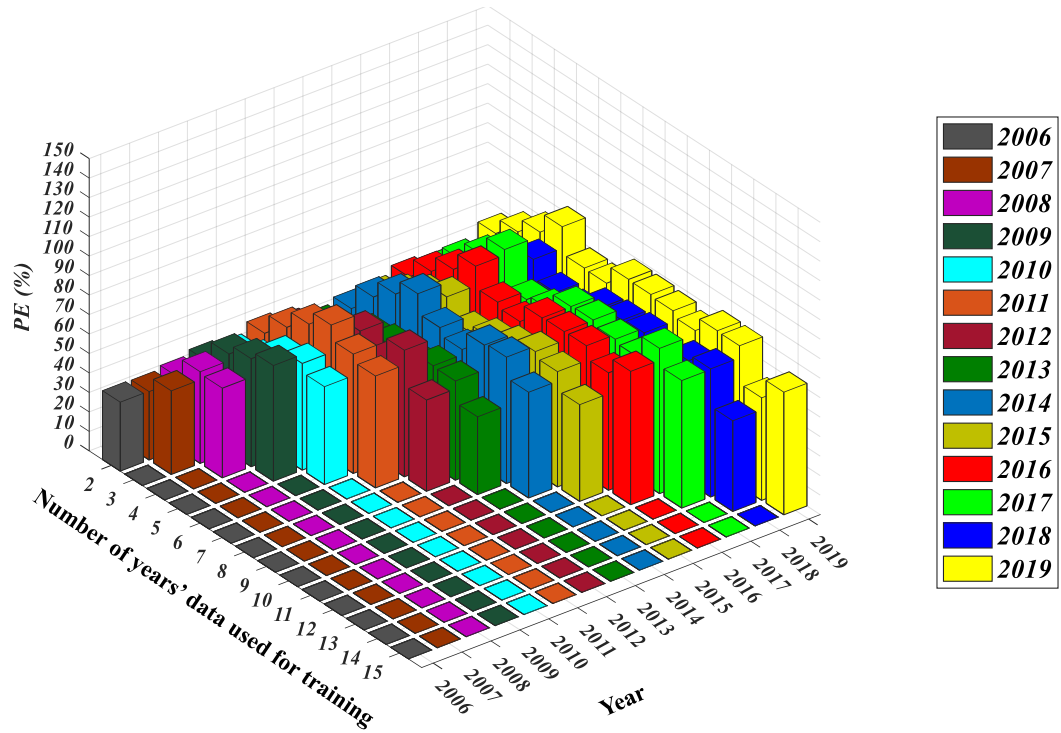
(b)

Case study 1: Performance of Nonlinear Auto Regressive Neural Network with External Input (NARxnet)



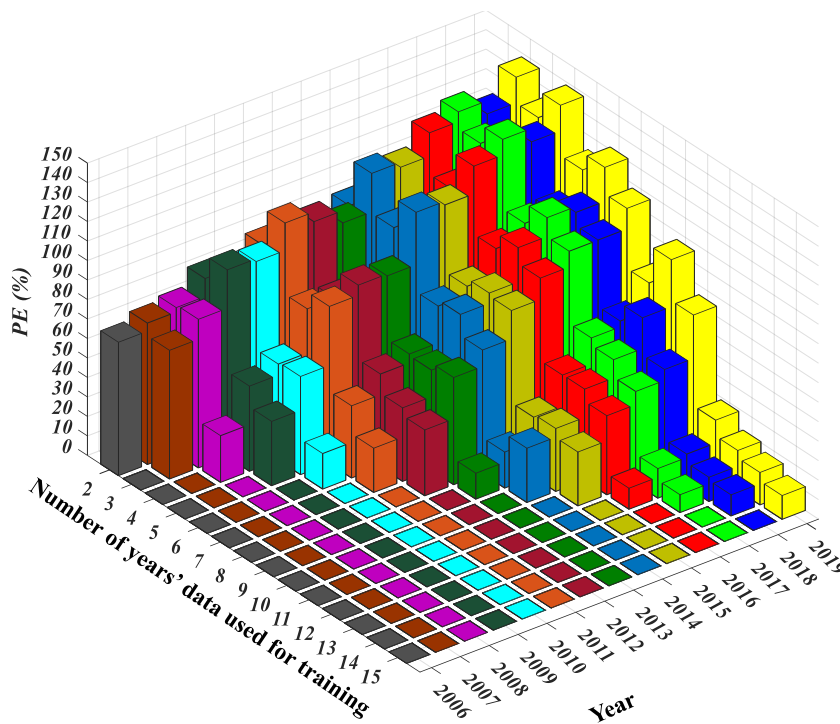
Case study 1: Performance of Long Short Term Memory Network (LSTM)

Insulated wall



(a)

Uninsulated wall



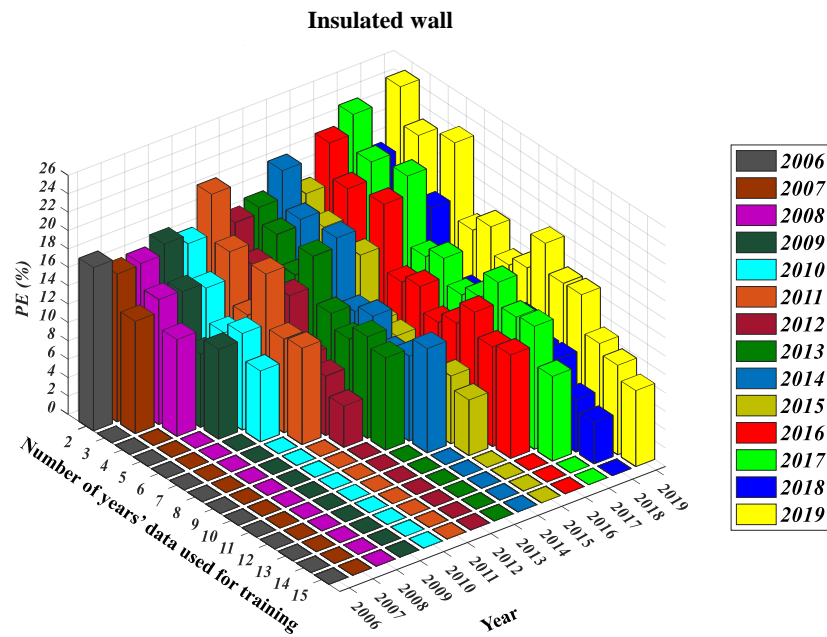
(b)

Appendix: B

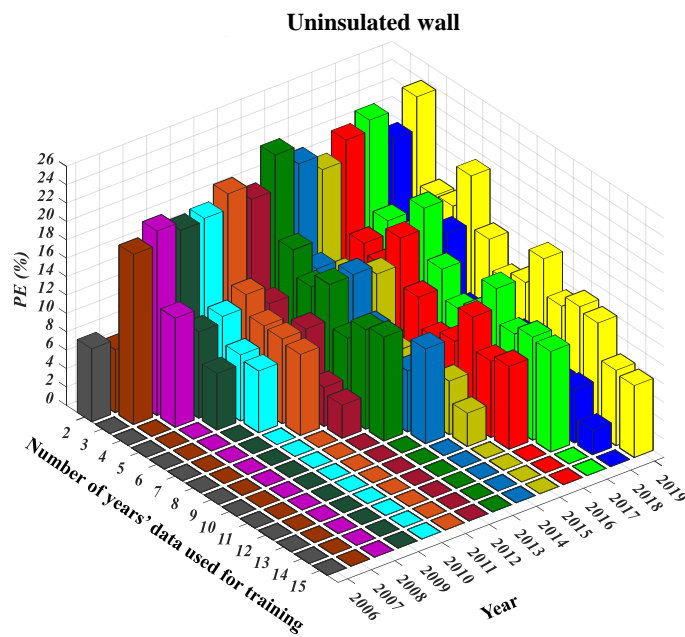
Performance of different Neural Network Architecture for Monthly Heat

Loss Prediction (Case Study 1)

Case study 1: Performance of Feed Forward Neural Network

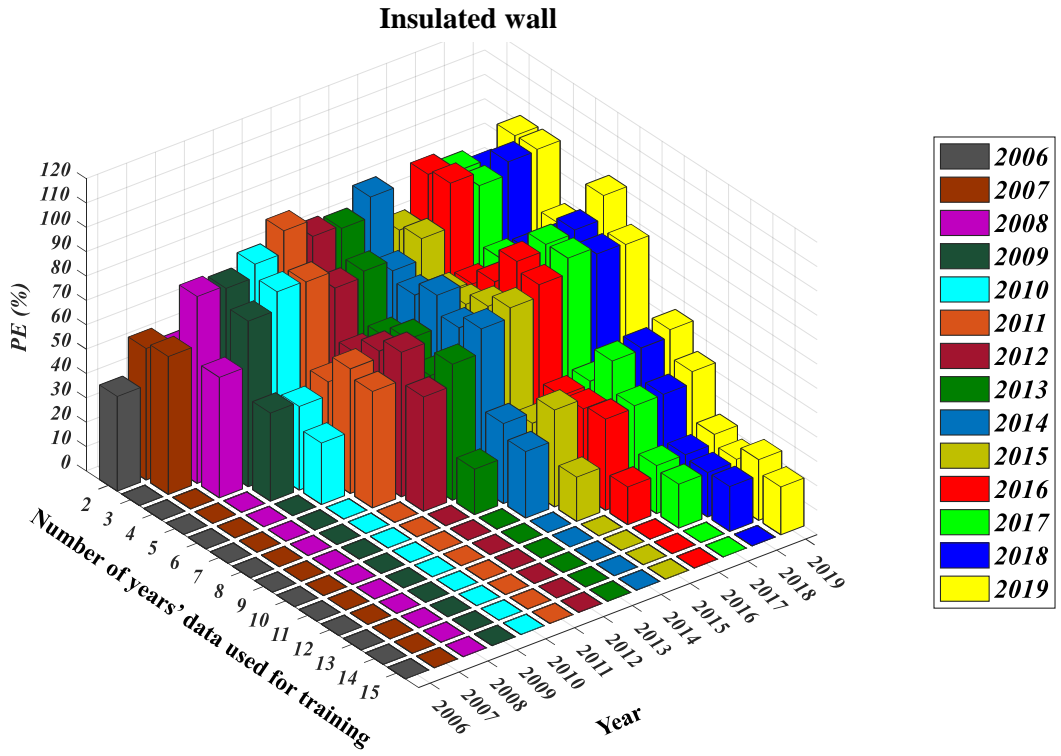


(a)

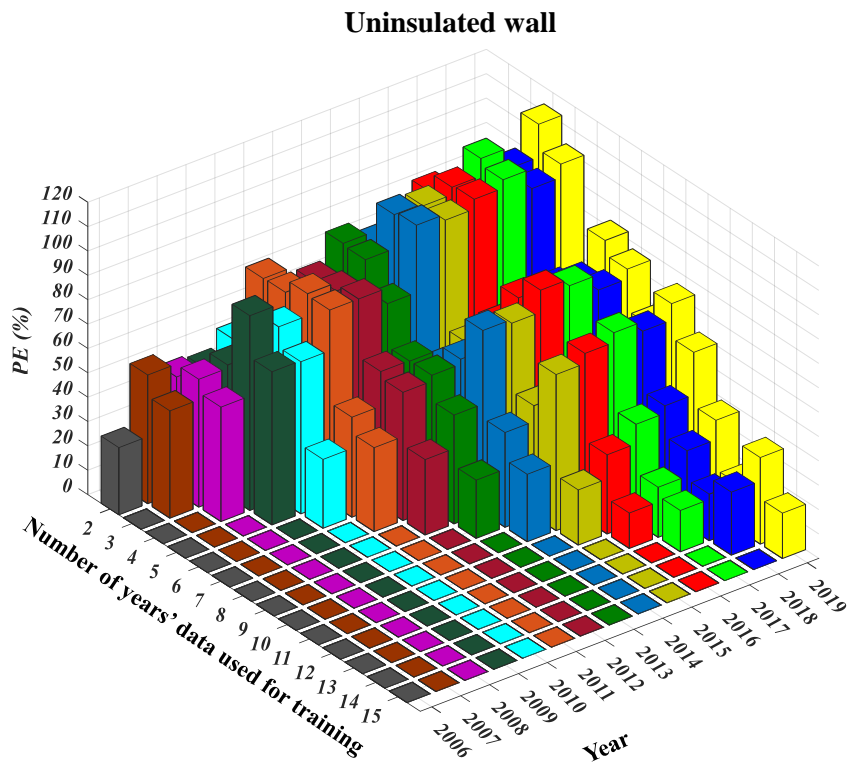


(b)

Case study 1: Performance of Nonlinear Auto Regressive Neural Network (NARnet)

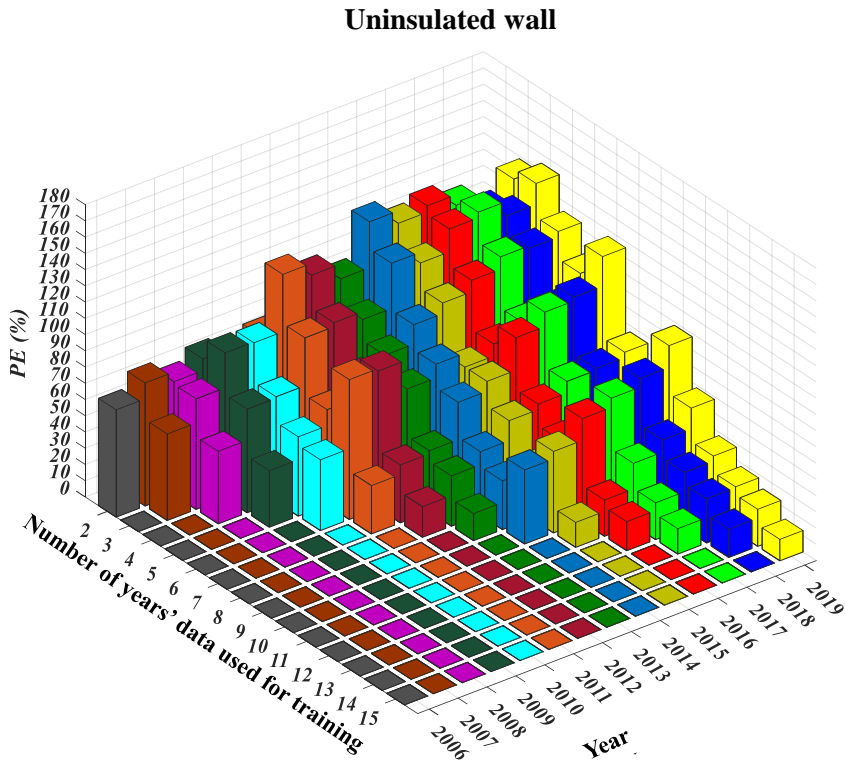
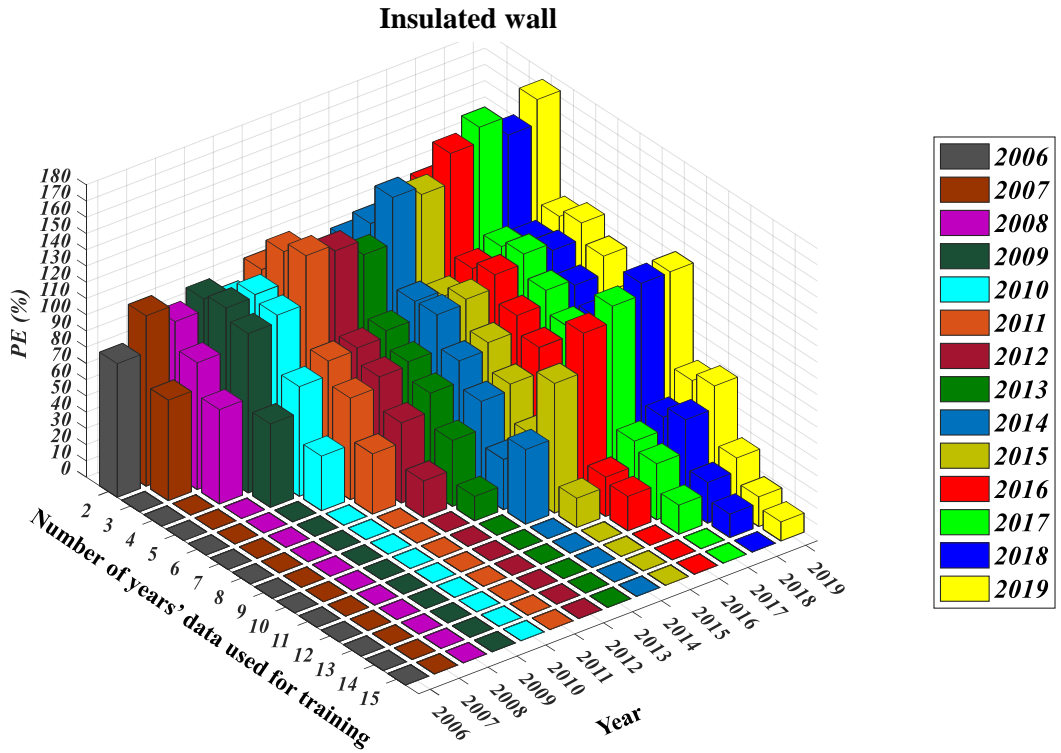


(a)



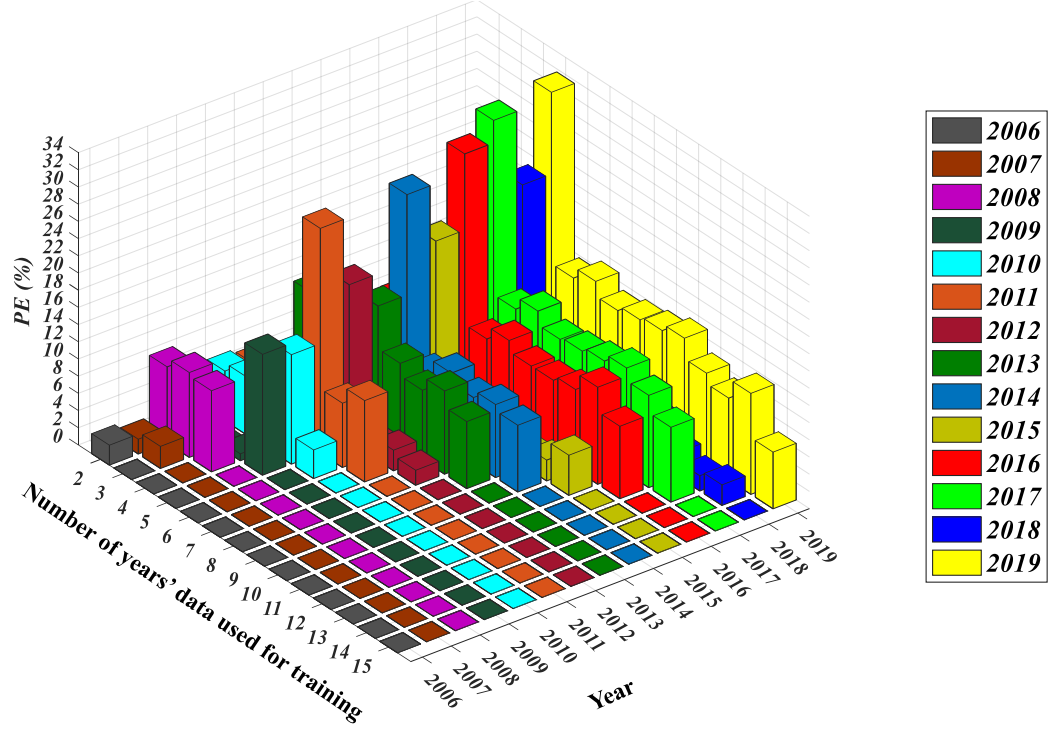
(b)

Case study 1: Performance of Nonlinear Auto Regressive Neural Network with External Input (NARxnet)



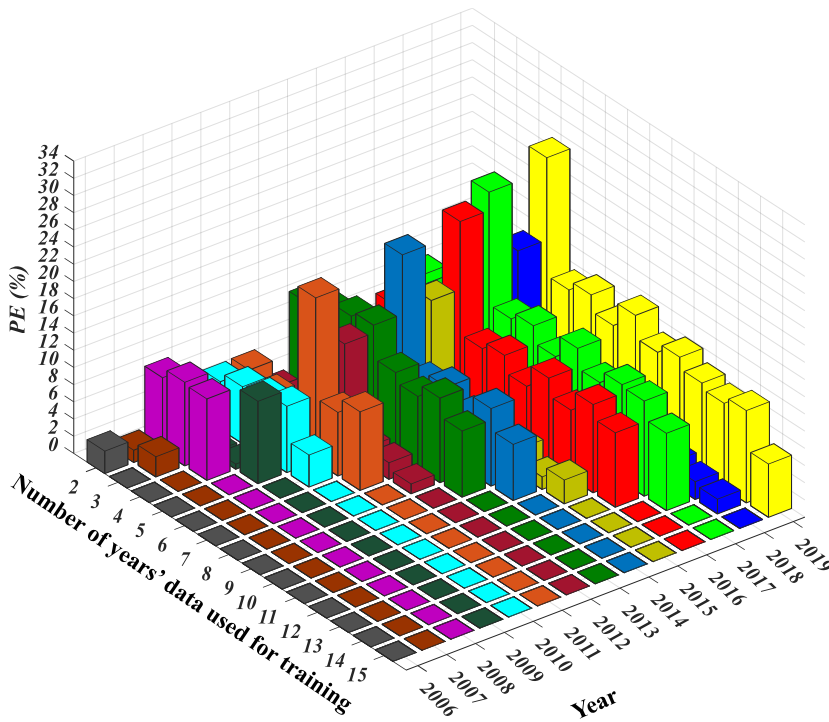
Case study 1: Performance of Long Short Term Memory Network (LSTM)

Insulated wall



(a)

Uninsulated wall



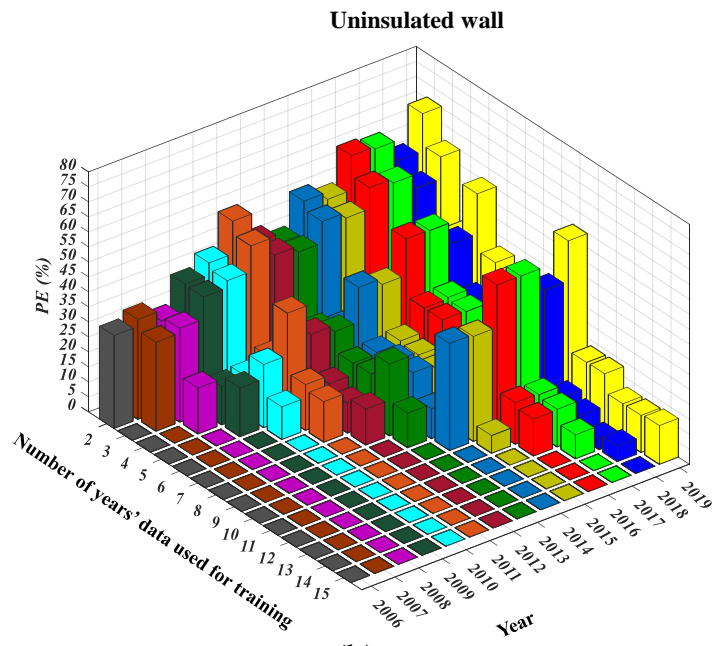
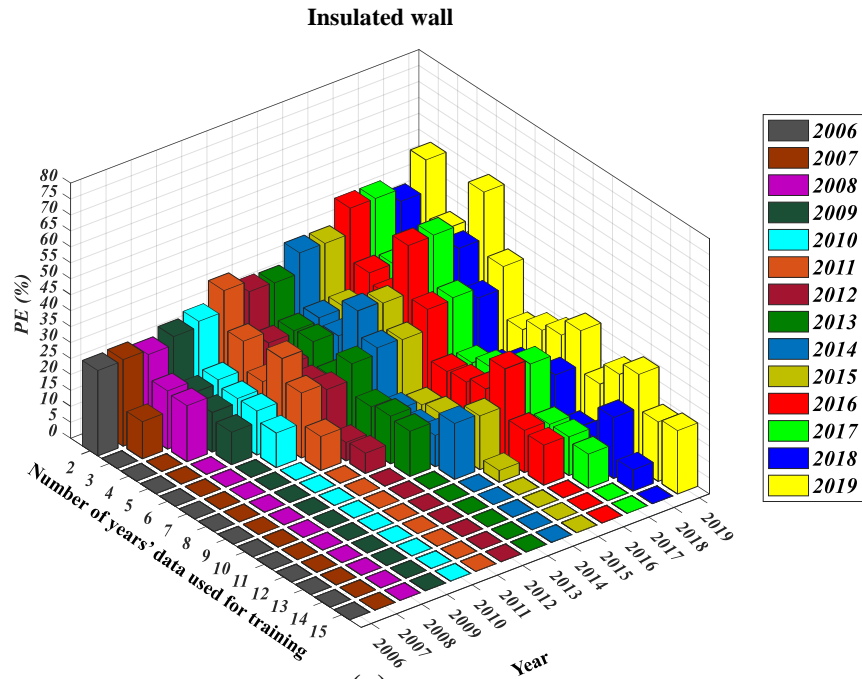
(b)

Appendix: C

Performance of different Neural Network Architecture for Hourly Heat

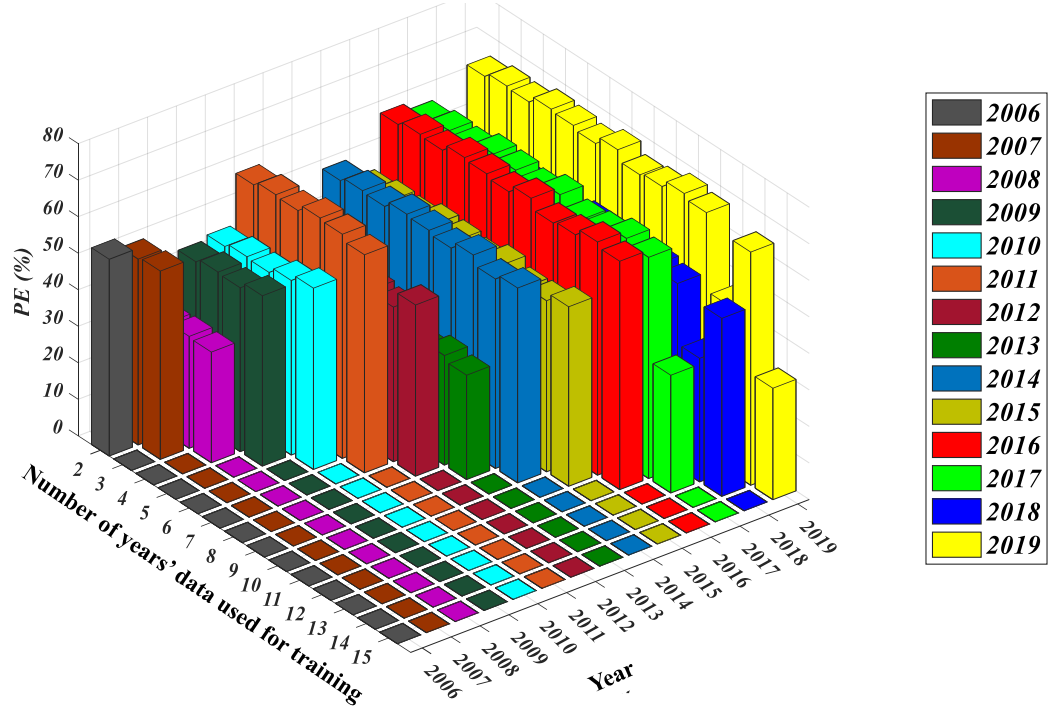
Loss Prediction (Case Study 2)

Case study 2: Performance of Feed Forward Neural Network



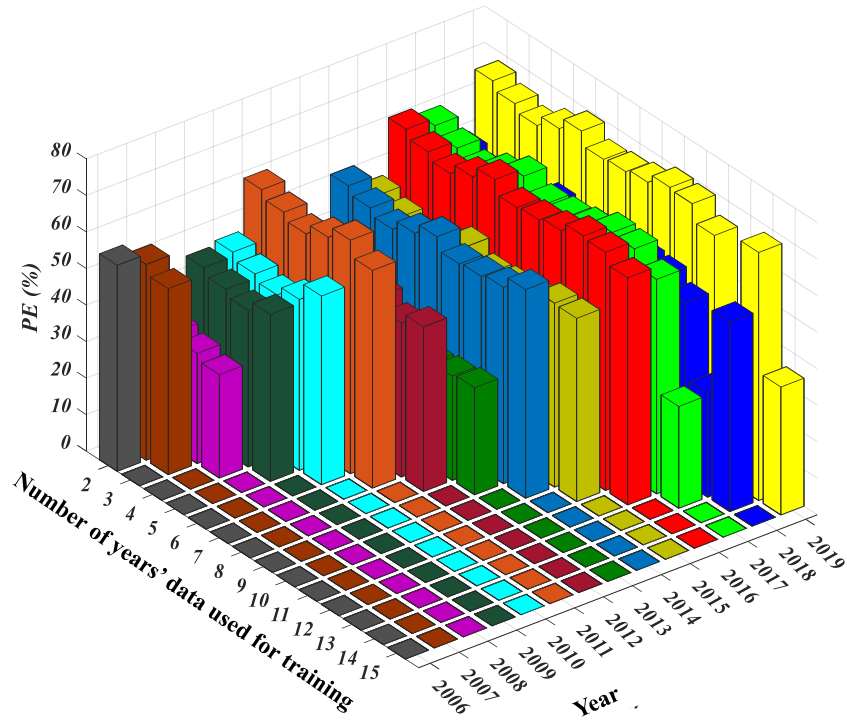
Case study 2: Performance of Nonlinear Auto Regressive Neural Network (NARnet)

Insulated wall



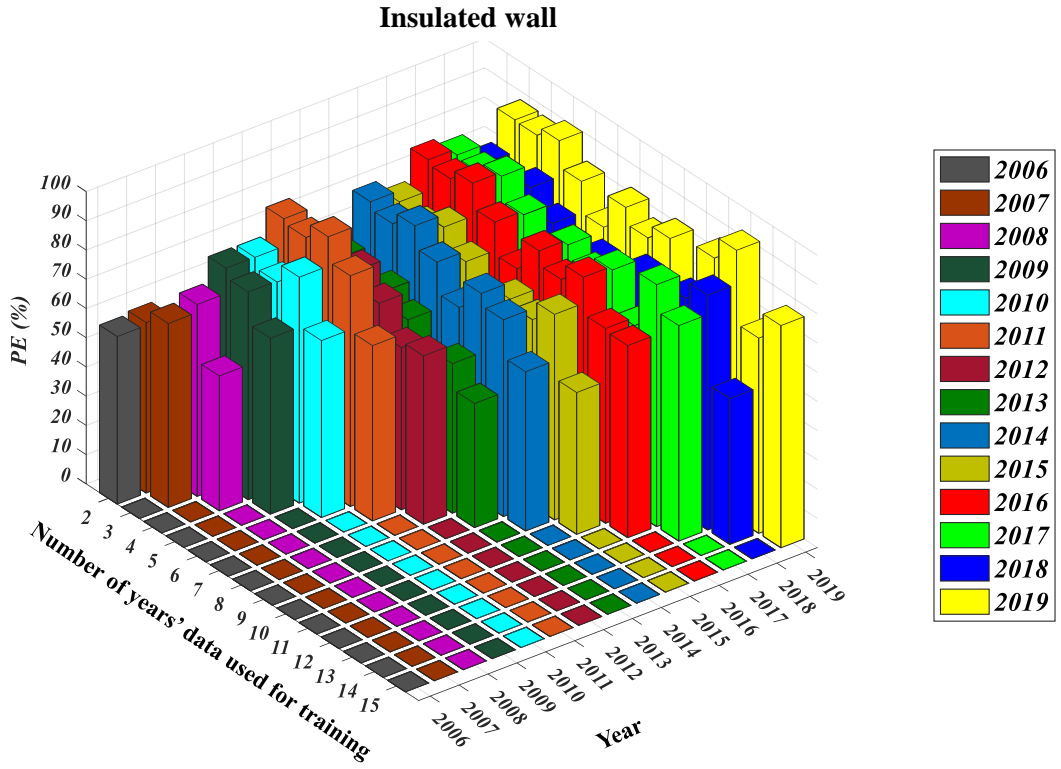
(a)

Uninsulated wall

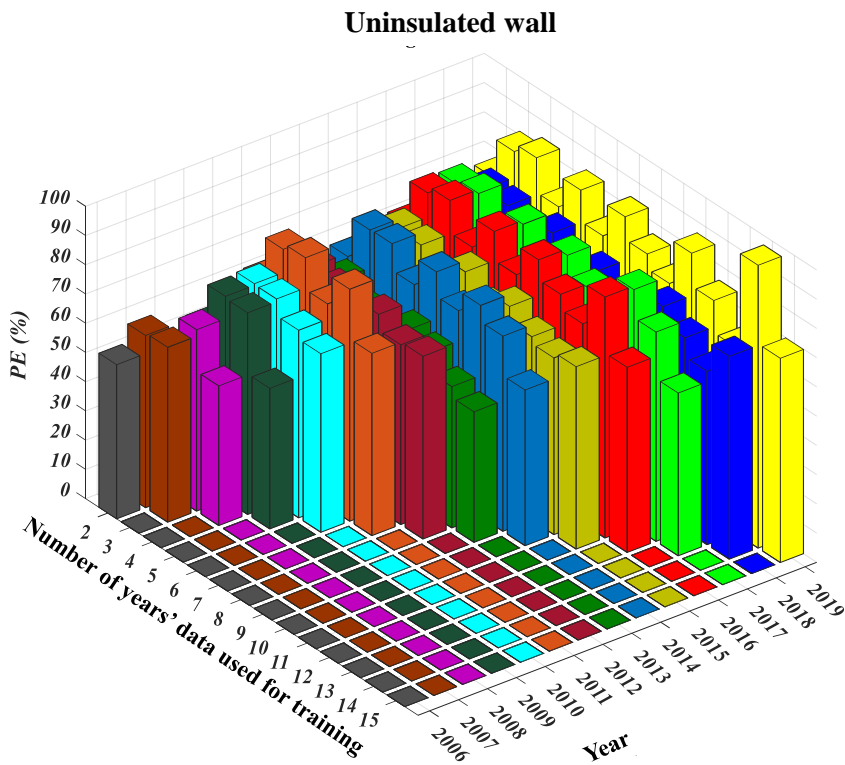


(b)

Case study 2: Performance of Nonlinear Auto Regressive Neural Network with External Input (NARxnet)



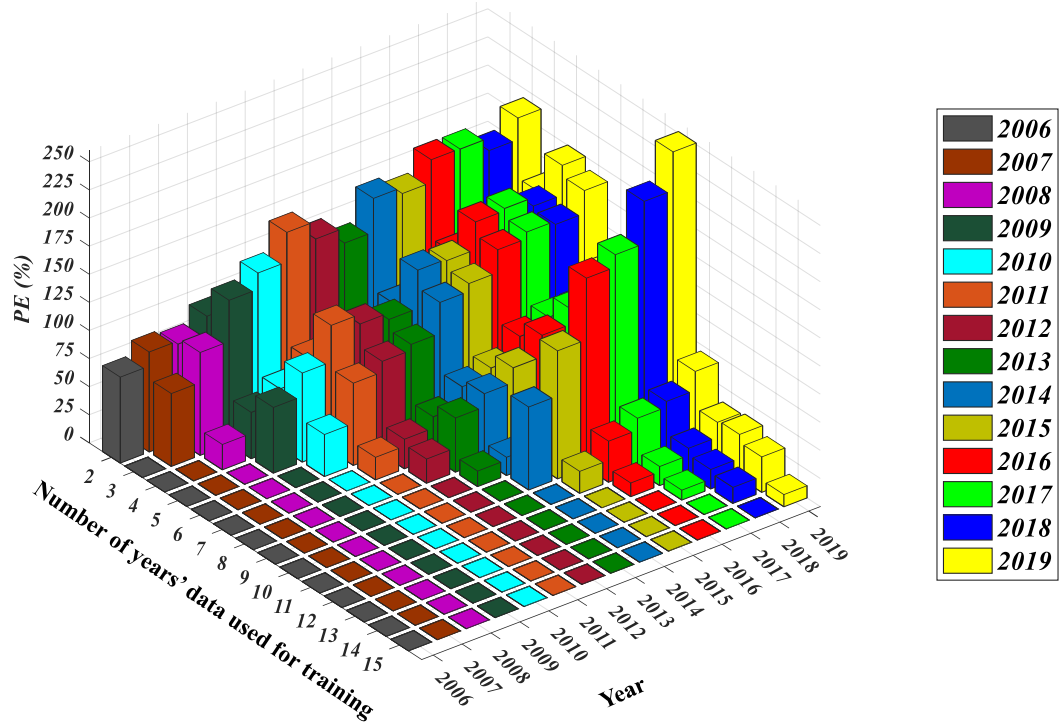
(a)



(b)

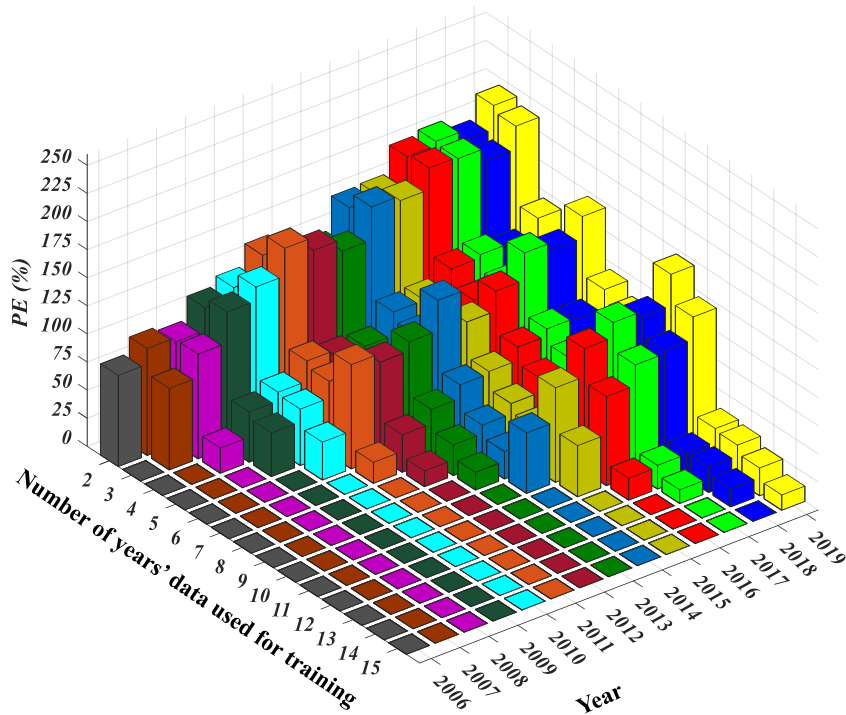
Case study 2: Performance of Long Short Term Memory Network (LSTM)

Insulated wall



(a)

Uninsulated wall

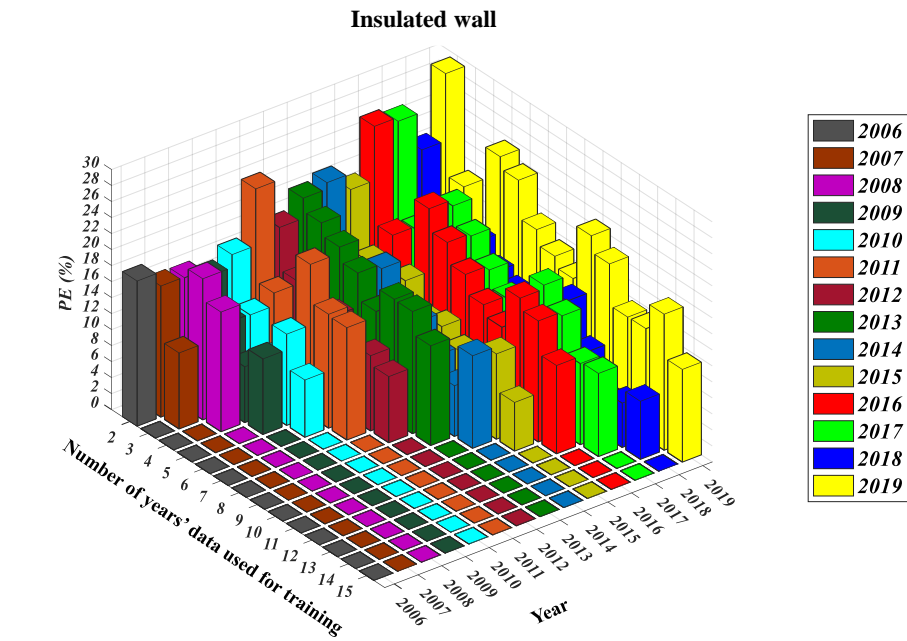


(b)

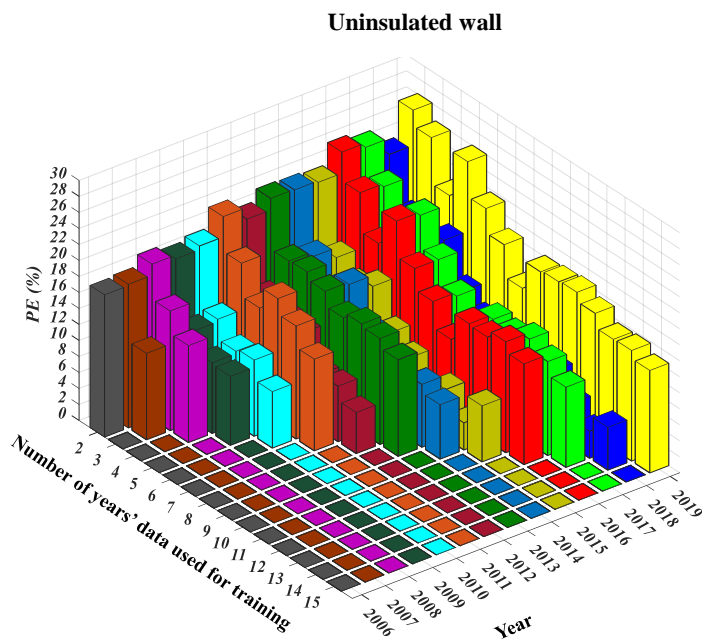
Appendix: D

Performance of different Neural Network Architecture for Monthly Heat Loss Prediction (Case Study 2)

Case study 2: Performance of Feed Forward Neural Network

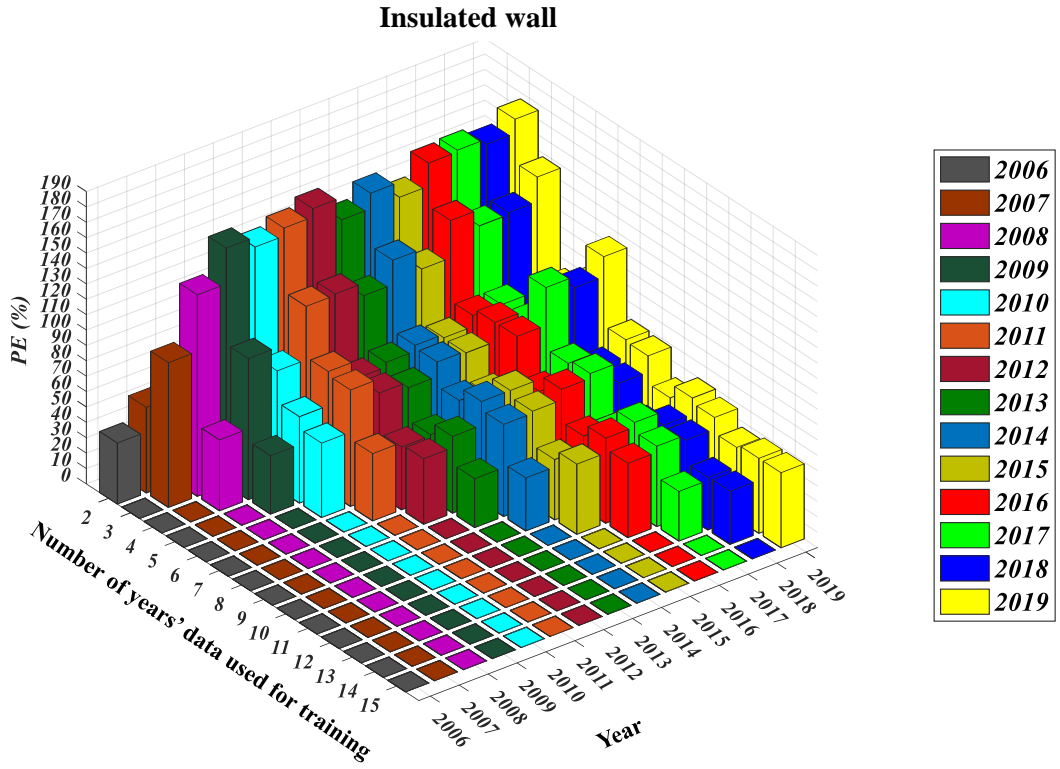


(a)

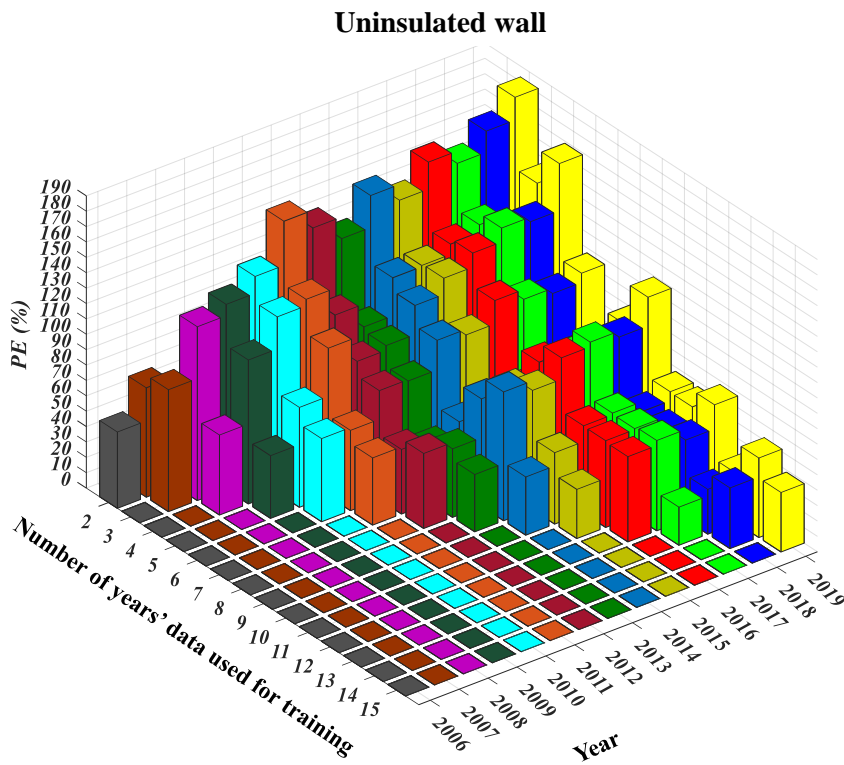


(b)

Case study 2: Performance of Nonlinear Auto Regressive Neural Network (NARnet)

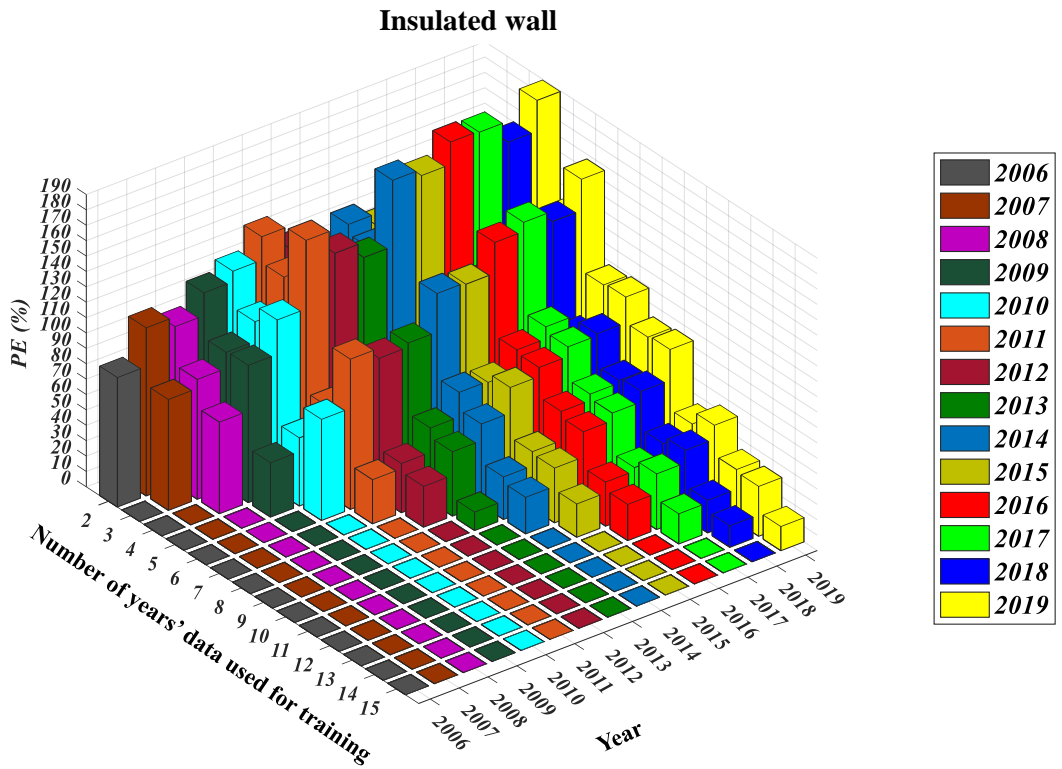


(a)

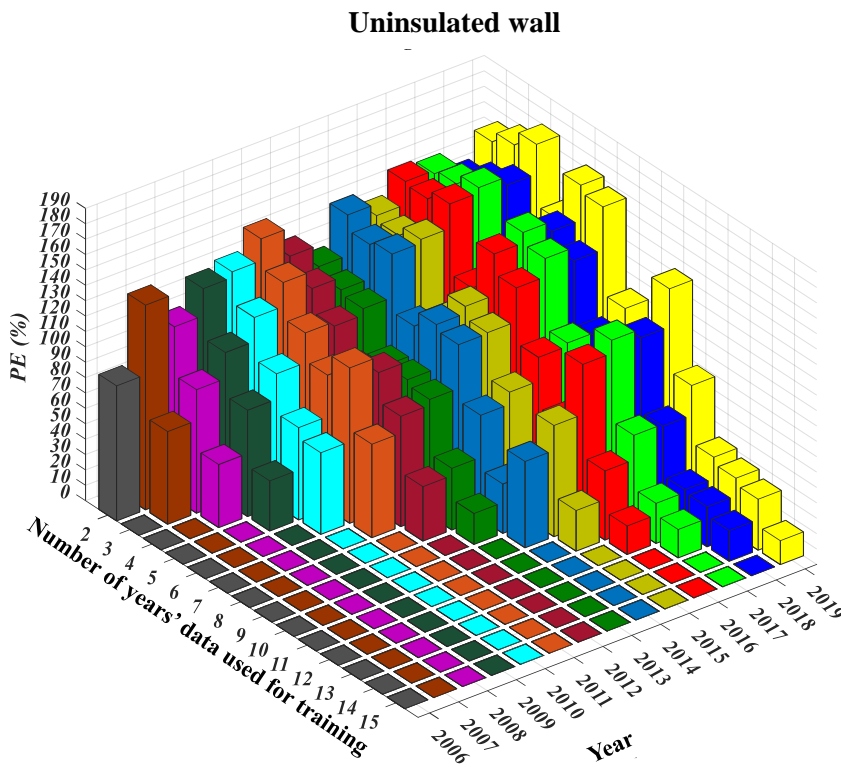


(b)

Case study 2: Performance of Nonlinear Auto Regressive Neural Network with External Input (NARxnet)

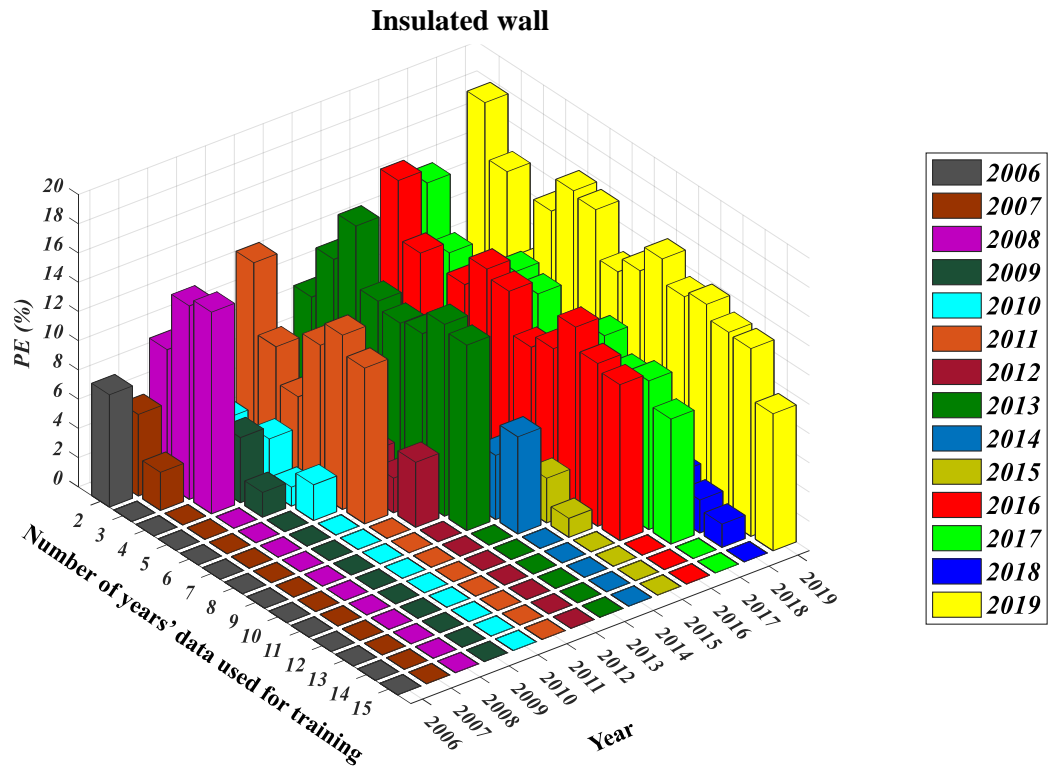


(a)

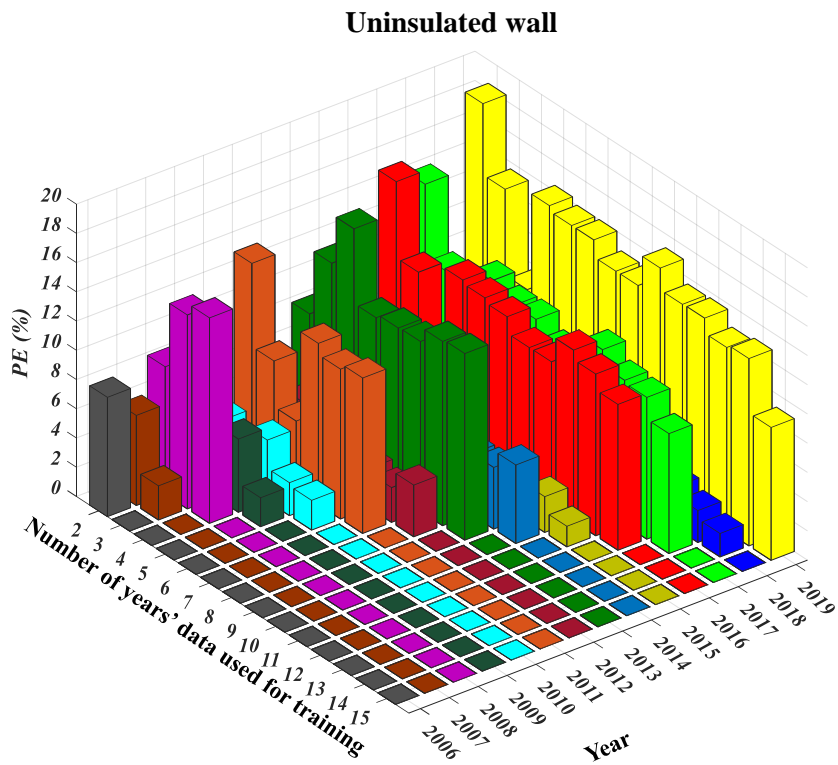


(b)

Case study 2: Performance of Long Short Term Memory Network (LSTM)



(a)



(b)

